Technical Report Documentation Page

1. Report No. FHWA/TX-12/0-5974-2	2. Government Accession No.	3. Recipient's Catalog No.
4. Title and Subtitle Estimating Texas Motor Vehicle Operating Costs: Final Report		5. Report Date November 2011 6. Performing Organization Code
7. Author(s) Dr. Ronald Matthews, Dan Seedah, Murat Ates, Kyung Jin Kim, Garrett Anderson, James Vaughn, Dimitrios Dardalis, Dr. Hao Lijun, Robert Harrison		8. Performing Organization Report No. 0-5974-2
9. Performing Organization Name and Address Center for Transportation Research The University of Texas at Austin 1616 Guadalupe St, Suite 4.202 Austin, TX 78701		10. Work Unit No. (TRAIS) 11. Contract or Grant No. 0-5974
12. Sponsoring Agency Name and Address Texas Department of Transportation Research and Technology Implementation Office P.O. Box 5080 Austin, TX 78763-5080		13. Type of Report and Period Covered Technical Report September 2007–August 2011 14. Sponsoring Agency Code
15. Supplementary Notes Project performed in cooperation with the Texas Department of Transportation and the Federal Highway Administration.		

16. Abstract

This report and its appendices summarize the findings of a 2-year extension to the TxDOT-sponsored study 0-5974 entitled "Estimating Texas Motor Vehicle Costs" undertaken by a Center for Transportation Research (CTR) team of mechanical engineers and economists at The University of Texas at Austin. The work was conducted in two phases over a 4-year period beginning in 2007 and this report details the second phase conducted over the period 2009–2011. It reports results in three areas: 1) total operating costs for the major vehicle classes currently seen on Texas highways, 2) engine models for hybrid light vehicles, and 3) results from examining the impact of transmission types through gearbox and differential sub-models. This second phase is the focus of this report but the reader interested in why this work was undertaken should peruse technical report 0-5974-1. This second, and final, report contains several detailed appendices on mechanical engineering sub-models and a product—a Vcost model and manual—for TxDOT use in highway and freight planning, economics and departmental revenue estimation. (Note: Traditionally vehicle operating costs were termed VOCs but the current use of this acronym to represent volatile organic compounds in emission studies encouraged the authors to adopt a different term—Vcost.)

17. Key Words Vehicle operating costs, Texas, light duty vehicles, fuel experiments, fuel consumption model, rolling resistance, Texas vehicle composition	18. Distribution Statement No restrictions. This document is available to the public through the National Technical Information Service, Springfield, Virginia 22161; www.ntis.gov.

19. Security Classif. (of report) Unclassified	20. Security Classif. (of this page) Unclassified	21. No. of pages 274	22. Price

Form DOT F 1700.7 (8-72) Reproduction of completed page authorized

Estimating Texas Motor Vehicle Operating Costs: Final Report

Dr. Ronald Matthews
Dan Seedah
Murat Ates
Kyung Jin Kim
Garrett Anderson
James Vaughn
Dimitrios Dardalis
Dr. Hao Lijun
Robert Harrison

CTR Technical Report:	0-5974-2
Report Date:	November 2011
Project:	0-5974
Project Title:	Estimating Texas Motor Vehicle Operating Costs
Sponsoring Agency:	Texas Department of Transportation
Performing Agency:	Center for Transportation Research at The University of Texas at Austin

Project performed in cooperation with the Texas Department of Transportation and the Federal Highway Administration.

Center for Transportation Research
The University of Texas at Austin
1616 Guadalupe St, Suite 4.202
Austin, TX 78701

www.utexas.edu/research/ctr

Disclaimers

Author's Disclaimer: The contents of this report reflect the views of the authors, who are responsible for the facts and the accuracy of the data presented herein. The contents do not necessarily reflect the official view or policies of the Federal Highway Administration or the Texas Department of Transportation (TxDOT). This report does not constitute a standard, specification, or regulation.

Patent Disclaimer: There was no invention or discovery conceived or first actually reduced to practice in the course of or under this contract, including any art, method, process, machine manufacture, design or composition of matter, or any new useful improvement thereof, or any variety of plant, which is or may be patentable under the patent laws of the United States of America or any foreign country.

Engineering Disclaimer

NOT INTENDED FOR CONSTRUCTION, BIDDING, OR PERMIT PURPOSES.

Project Engineer: Dr. Ronald Matthews
Professional Engineer License State and Number: Texas No. #52561
P. E. Designation: Researcher

Acknowledgments

The team wishes to acknowledge and thank the consistent leadership and support provided by the Project Director Don Lewis (GSD) and Dr. Duncan Stewart (RTI), ably supported by the project advisors Janie Temple (TPP), Jackie Ploch (ENV), Jo Woten (GSD), Paul Campbell (FIN), and Peggy Thurin, P.E. (TPP). The experimental work relied on the assistance of many GSD staff who are thanked as a group. Finally, the rolling resistance experiments for heavy trucks could not have been completed without the commitment of both Bruce Merrill, P.E. (AUS), who reserved the highway for the test and the trucks, and the fleet manager and drivers from HEB who worked over a test weekend.

The HEB effort was led by Kenneth Allen, V.P. of Supply Chain and Logistics, and Mike Moynahan, Fleet Manager; this work was crucial in determining future heavy truck technologies, the impact of extra-wide tires, and the rolling resistance tests. Technical assistance was also provided by David Higbie, Ram Chandrasekaran, and Mohamed Gouda (AVL); Stephen Allen and Steve Stillman (Antx Inc.); Herman Masse, Roger Van Elslander, and Mike Bartkowiak (Dearborn Group Technology); Vitaliy Maksimov and Mike McBeath (ScanTool.net); Lee Butler (Greatwide Logistics Services); Lance Shillingburg and Les Findeisen (TMTA); Dennis Beale (FedEx Freight); and Brad Bryant (Wal-Mart); and Bob Davie (Vanguard Trucks). Finally, David Schwarz (Consultant) and Emre Meric (Microsoft) assisted on software issues. Our thanks are extended to all these individuals and companies that helped frame the study and address key issues.

Products

Accompanying this report is a CD containing the Vcost software and a user manual.

Table of Contents

List of Figures

List of Tables

Chapter 1. Summary of Initial Results and Deliverables

1.1 Background

This report and appendices summarize the findings of a 2-year extension to the TxDOT sponsored study 0-5974 entitled "Estimating Texas Motor Vehicle Costs" undertaken by a Center for Transportation Research (CTR) team of mechanical engineers and economists at The University of Texas at Austin. The work was conducted in two phases over a 4-year period beginning in 2007 and this second report details the second phase conducted over the period 2009–2011. It reports the results in three areas: 1) total operating costs for the major vehicle classes currently seen on Texas highways, 2) engine models for hybrid light vehicles, and 3) research results from examining the impact of transmission types through gearbox and differential sub-models. This second phase is the focus of this report but the reader interested in why this work was undertaken should peruse technical report 0-5974-1. This second and final report contains several detailed appendices on mechanical engineering sub-models and a product—a Vcost model[1] and manual—for TxDOT use in highway and freight planning, economics, and departmental revenue estimation.

As noted, Report 0-5974-1 records the justification for undertaking this work and reports the results from the first phase. The primary motivation was a lack of current Vcost data precisely at a time when vehicle designs—both autos and large trucks—were undergoing fundamental changes to their engines, transmissions, and overall vehicular design[2]. Originally a 2-year study, 0-5974 was designed to produce an array of results that would allow TxDOT planners to make improved estimates of the economic consequences of various engineering strategies and permit the Department to accurately estimate future revenues—an important benefit given its constrained budget. Fuel was to receive significant attention through development or calibration of the latest mechanistic models, corroborated by trucker surveys and interviews. This process represented a major step forward in developing a fuel model capable of predicting consumption over the decade to 2020.

Report 0-5974-1 also noted the history of Vcost research through 2007. Essentially, only two fundamental experimental Vcost studies have contributed to the estimation of U.S. vehicle operating costs in the last three decades[3]. The Texas Research and Development Foundation (TRDF) contributed to both—the first being the World Bank Highway Design and Maintenance Model (HDM III), which was then updated in the late 1990s by an Asian Development Bank team incorporating an earlier mechanistic fuel model and adjustments for congestions and social costs[4]. The second TRDF study was the FHWA-RD-80 study completed in early 1982 and whose results still form elements, some critical, of several highway planning models. These include modeling both work zone Vcost impacts (QUEWZ) and highway cost-benefit analysis (MicroBencost and HERS). In 2006, the National Cooperative Highway Research Program (NCHRP) awarded a new Vcost study (01-45) that, although beginning before the CTR study,

[1] Traditionally vehicle operating costs were termed "VOCs" but the current use of this acronym to represent volatile organic compounds in emission studies encouraged the authors to adopt a different term—Vcost.

[2] These include alloys and metals to reduce mass, tires that reduced rolling resistance, and aerodynamic designs to reduce air resistance.

[3] This refers to aggregate economic cost estimation in the public domain; Report 0-5974-1 notes many technical reports on individual components from engineering companies and vehicle manufacturers.

[4] See World Bank products at http://www.worldbank.org/transport/roads/tools.htm

has not yet published a full report[5]. The TxDOT 0-5974 study was therefore broadly consistent with the national interest and the first report showed that by 2009 the results were capable of determining free-speed Vcost estimates for Texas conditions. TxDOT then decided to address a further set of questions to enable estimates of and insight into the rapidly changing world of automotive design (hybrids, emissions, and fuels) and TxDOT revenues by extending the work by 2 years.

The basic study outline is given in Figure 1.1 and shows the sequencing of research tasks developed at the outset. NCHRP 01-45 results were not available at the time this report was drafted, and thus could not be used for comparative purposes. The central products were a comprehensive Vcost model that could be easily used by all TxDOT planners and two fuel consumption models: one for gasoline-powered light-duty vehicles, of which over 190 million are registered in Texas, and one for diesel-fueled heavy trucks, the vehicles most critical to the Texas economy. The next section describes the tasks completed in the second phase of the work, which forms the basis of this report.

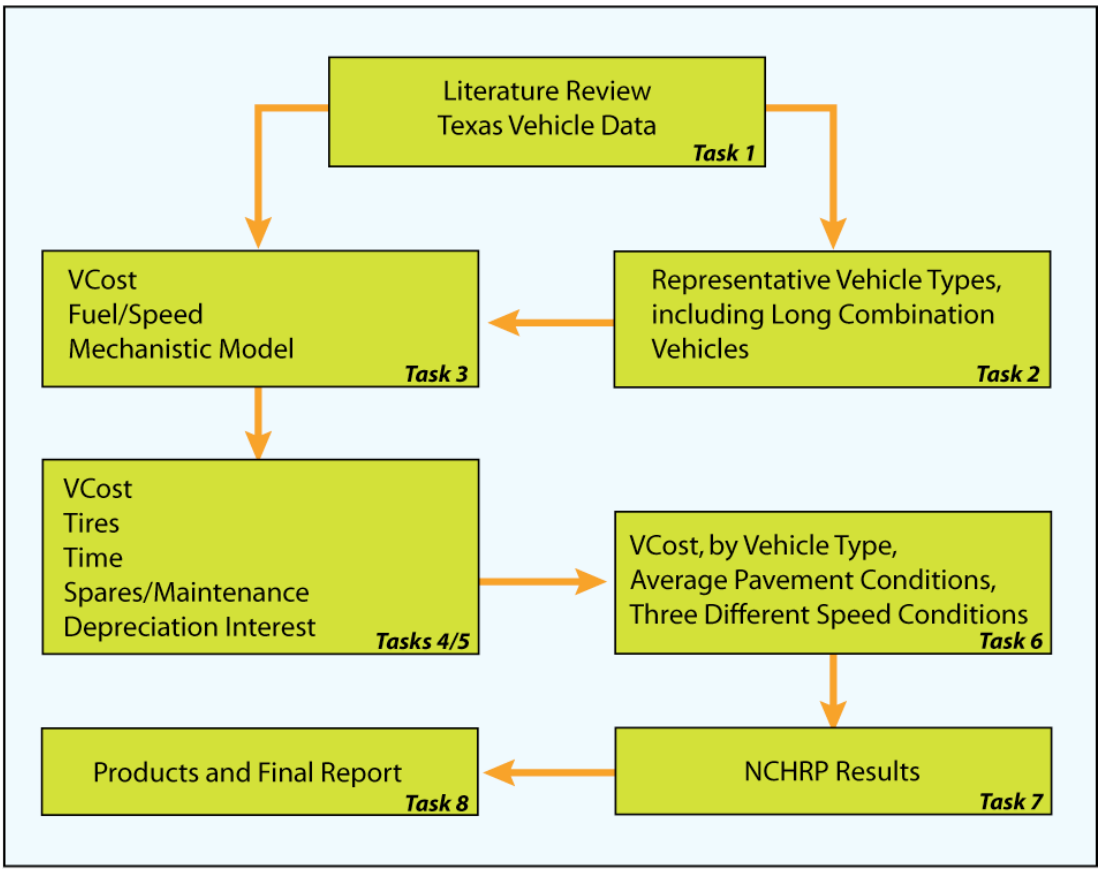

Figure 1.1: 0-5974 Study Task Outline

[5] http://apps.trb.org/cmsfeed/TRBNetProjectDisplay.asp?ProjectID=231

1.2 Enhanced Tasks

The 2007 basic report study task outline, shown in Figure 1.1, was retained but enhanced in five of the seven original task areas—representative vehicles (particularly heavy trucks and hybrids), fuel consumption, other costs like depreciation, speed and congestion levels by vehicle type, and their aggregation into an enhanced Vcost model. Final products include improved fuel consumption and Vcost models, relative to the models reported in 0-5974-1. The two key areas that absorbed much of the team effort were fuel and the Vcost model and enhancements are now described.

1.2.1 Estimation of Fuel Consumption

The CTR team improved the fuel consumption model developed during the initial phase of TxDOT Project 0-5974 in three key areas. The first improvement incorporated the effects of the various types of hybrids—both light-duty and heavy-duty—in the model. Hybrids have established a foothold in Texas auto ownership and this will impact the relationship between vehicle miles of travel (VMT) and aggregate state fuel consumption. The benefits to air quality and other social costs, while positive, create a challenge for agencies such as TxDOT, for whom fuel taxes represent a substantial revenue resource.

The second improvement was to continue development of the engine sub-model, especially to include the effects of the new heavy-duty diesel engines that were mandated beginning in calendar year 2010. These low-emission units perform differently, operators run them differently, and their technical wizardry raises the purchase price—and therefore the depreciation—when calculating their aggregate operating costs. Trucking accounts for over 70% of the freight ton-miles in Texas and so has a direct impact on economic efficiency and competitiveness. This improvement included the development of new transmission and differential sub-models that could form the basis of further enhancements in future projects updating this work.

The third improvement was to generate data that would allow the research team to develop standardized driving schedules, to be incorporated in the vehicle operating costs model in Task 6. Three speed conditions were proposed in each vehicle class: 1) free flow, 2) moderate to heavy use where speed cycles are present, and 3) congested, where speed is low with numerous speed cycles. This data would allow the user to estimate the impacts of congestion—and the benefits from its mitigation—when incorporated into the updated Vcost model.

1.2.2 Aggregate Operating Costs by Vehicle Type

The model was to be modified during the second phase to produce aggregate and disaggregated costs in a manner familiar to TxDOT staff. The team also proposed running a series of pilot tests, under the guidance of the project advisory team, to ensure that early feedback from TxDOT staff was incorporated into the model development.

The work was undertaken during the similar time period as a federally sponsored study and it was hoped that results from this work could be incorporated into the Texas modeling. The 2006 NCHRP 01-45 study report was to specifically address the relationship between user costs and highway conditions—especially roughness—and was scheduled to be published during the 2-year extension. It was therefore hoped that some broad classes of conditions, such as roughness, could be included into the enhanced Vcost model. The team proposed that if the NCHRP team found that U.S operating costs were sensitive to the ranges of roughness found on

typical highways, the CTR team would undertake further coastdown tests on different pavement types and conditions. However, when it became obvious that the NCHRP study results would not be available in time for this study, it was agreed that this aspect of the project extension would not be necessary because of the similarity of pavement conditions on those key Texas highways carrying the most traffic[6]. Second, it was proposed that the research team perform coastdown tests on long combination vehicles (LCVs). Ultimately, no LCVs were available for coastdown testing during the study period. However, the research team found another source for the coastdown coefficients.

Finally, the Vcost model itself was continuously refined during the second phase, both to make it more reliable and to capture the work developed by the team. Inevitably, however, the engineering team reported refinements that could not be captured in the model within the specified contract. Where relevant, this material is reported in the appendices to be considered at a future time when the model is updated.

1.3 Report Outline

The report summarizes the work undertaken, major findings, and the products produced by the research team in the second phase of the study. Chapter 3 describes the latest version of the study product—the Vcost model. Chapter 4 presents the enhanced fuel models for both light and heavy duty vehicles while Chapter 5 summarizes results and recommends further research topics. Finally, six appendices support the main text and complete the report by covering two types of engine models, two types of transmissions (manual and automatic), five different differential models, a light-duty electric vehicle, a heavy-duty hybrid electric vehicle (Prius), and a heavy-duty hydraulic hybrid truck model. This report is submitted with the study product—the Vcost model—and a user manual available online to TxDOT staff.

[6] As an example, the 2010 TxDOT-sponsored 2030 study estimated that less than 20% of the state "on-system" carried over 70% of the truck ton-miles. See http://texas2030committee.tamu.edu/documents/final_022609_execsummary.pdf

Chapter 2. Improved Vehicle Operating Costs Model

Improvements were made to the first generation vehicle operating cost model developed during the initial part of TxDOT Project 0-5974. The improved application (called CT-Vcost) utilizes an object-oriented programming structure where modules are developed to perform particular tasks.

The following sections of this chapter discuss the modules and data used for this case study. The toolkit's default data is based on verified secondary vehicle cost data and certified vehicle databases such as the Environmental Protection Agency's (EPA) Fuel Economy database and Annual Certification Test Results databases. The toolkit also allows users to change parameters so that cost calculations are specific to any particular situation, and can be updated as the economic or technological landscape changes. Cost categories in the CT-Vcost toolkit include the following:

- depreciation,
- financing,
- insurance,
- maintenance costs,
- fuel cost,
- driver costs,
- road use fees (e.g., tolls), and
- other fixed costs, such as annual vehicle registration and inspection fees.

Analysis types that can be performed with CT-Vcost include single vehicle analysis, multi-vehicle comparisons, fleet vehicle analysis, growth rate and market penetration simulation, and route cost analysis. CT-Vcost is compatible with the sophisticated fuel economy prediction models also developed in this study and discussed in Chapter 3. The fuel economy models have the ability to predict fuel consumption for default or custom drive cycles specified by the user. Output from the fuel economy models can be used within the toolkit to perform route cost analyses. CT-Vcost is also updatable and can be effortlessly calibrated for any state or region. In summary, CT-Vcost was designed to be intuitive and flexible enough for simulating different scenarios and situations that planners may envision.

In the following sections the overall structure of the model, CT-Vcost, is discussed beginning with the two data types, Default and User Data, in Section 2.1. The Share modules, which are utilized by the different analysis modules, are discussed in Section 2.2. Section 2.3 discusses all the different types of analyses: Single Vehicle, Multi-Vehicle, Fleet, Route Cost, Light-Duty, and Heavy-Duty Drive Cycles. Section 2.4 presents the formulas and the main algorithms used in developing CT-Vcost, and Section 2.5 reviews the different output types such as bar charts, pie charts, line graphs, and data tables that are packaged with CT-Vcost.

2.1 Default Data vs. User Data

Default Vcost data is stored in the ***DefaultData*** folder and user-generated data is stored in the ***UserData*** folder. The two separate folders enable users to easily distinguish between default data prepackaged with Vcost and data generated by others. Default data is stored in four Extensible Markup Language (XML) files:

I. *DefaultVehicles.xml:* This database file stores specific default vehicle data such as vehicle make, model, class, EPA city fuel economy in miles per gallon (mpg), EPA highway mpg, manufacturer's suggested retail price (MSRP), axle ratio (differential gear ratio), target coastdown coefficients, vehicle weight, and transmission type. Each vehicle is assigned a unique ID starting with the prefix *veh*. For example, the first vehicle is referenced by the unique ID *veh001*. Vcost uses this ID for data storage, cost calculations, and user interactions via the Graphical User Interface (GUI). The unique ID property also enables vehicles to retain their unique identities and data values when dealing with multiple vehicles, vehicle classes, and vehicle fleets. If the vehicle is missing a certain data requirement, e.g., MSRP, the data value is represented as -1 in the database, and the vehicle class average value is used in the calculations.

II. *DefaultParameters.xml:* This file stores default parameter values for various vehicle classes. Default parameter values stored by vehicle class include average annual miles traveled, annual insurance cost, annual percentage rate[7] (APR), finance term (in years), average first year depreciation, subsequent year depreciation, and other fixed costs such as vehicle registration. Further details on the default values are discussed in Section 2.2.5 (Vehicle Parameters) of this report.

III. *DefaultValues.xml:* This file stores miscellaneous default data used in various aspects of the toolkit. Following are examples of information stored in this file:

- Default scenario values such as 2011 Texas average fuel price and fuel tax values, analysis period, combined fuel economy weights, fuel price and tax projections, and the time value of money.
- Default light-duty and heavy-duty utilization ratios.
- Default fleet size value of 100 vehicles.
- Default speed constraint values for congested, moderate, and highway conditions.

For further notes on the different modules that use the above-listed data, please refer to their specific subsections: 2.2.1. Scenario Module, 2.2.2 Vehicle Utilization Module, 2.3.3 Vehicle Maintenance Module, and 2.3.5 Default Vehicle Parameters.

IV. *DefaultMaintenance.xml:* This file stores default maintenance cost data by vehicle class and by individual vehicles when available. The database stores the following parameters:

[7] Annual percentage rate (APR) describes the interest rate for a whole year (annualized) as applied on a vehicle loan.

vehicle name/class, vehicle make, vehicle model, begin year and end year[8], maintenance item description, frequency of work performed, and cost associated with the item

Cost data for light-duty vehicles (LDVs) was collected from RepairPal.com® and TxDOT's Fleet Maintenance Database. For additional information on vehicle maintenance data and calculations, please refer to Subsection 2.2.3, Vehicle Maintenance Module.

2.2 Shared Modules

Shared modules are modules utilized by more than one analysis type. They are accessible to users when performing certain types of analysis. The shared modules in Vcost are the Scenario Module, the Vehicle Utilization Module, and the Vehicle Maintenance Module, each of which is discussed in the following subsections.

2.2.1 Scenario Module

The Scenario Module enables users to input general parameters which influence vehicle operating costs but are not specific to any given vehicle (see Figure 2.1). All the parameters have default values; however, users can modify these values based on their specific needs.

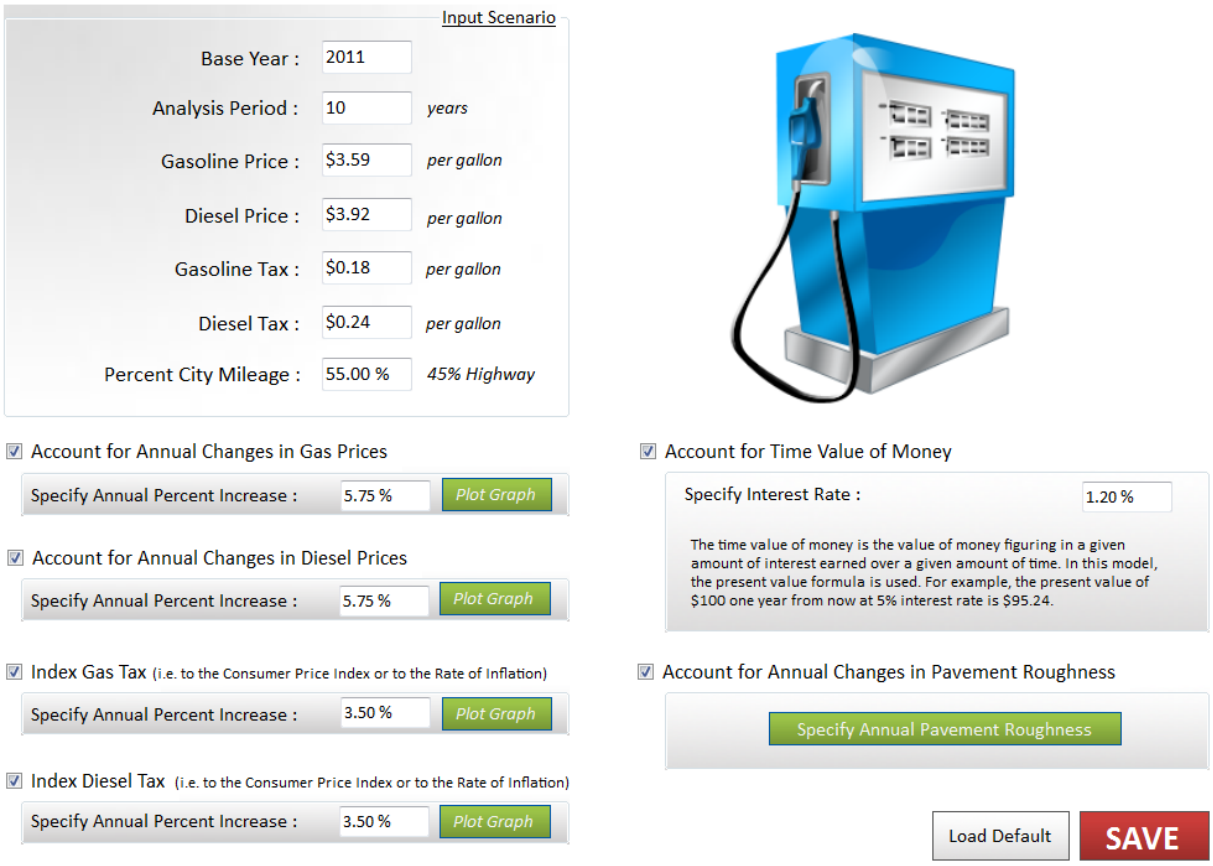

Figure 2.1: Screenshot of the Scenario Module.

[8] This parameter is used for maintenance schemes that are similar for vehicle models of different years.

Parameters that can be altered include the following:

Base Year: This value sets the year from which analyses are to be performed. This value is mainly used by the Fleet Analysis Module when accounting for different vehicle ages.
Analysis Period: This value sets the number of years involved in a particular analysis. Projections and calculations are made using this value.

Gasoline Price: The user specifies the base gasoline fuel price. Using the **Account for Annual Changes in Gas Prices** option, users can specify a percent change in gasoline prices over the analysis period.

Diesel Price: Similar to the Gasoline Price input, users can specify the base diesel fuel price. With the **Account for Annual Changes in Diesel Prices** option, users can input the percent change in diesel prices over the analysis period.

Gasoline Tax and Diesel Tax: Users can specify the current tax rate on a gallon of gasoline or diesel fuel. The **Index Gas Tax** and **Index Diesel Tax** options are used for projections based on a user-specified annual percentage increase.

Percent City Mileage: This value is used in calculating the combined fuel economy of vehicles. Combined fuel economy is used in determining fuel consumption when performing Single, Multi-Vehicle, and Fleet Analyses.

Account for Time Value of Money: This option enables users to capture any changes in the value of money over the analysis period. As presented in Equation 2.1, it uses the Present Value formula:

$$PV = \frac{FV}{(1+i)^n} \quad (2.1)$$

where Present Value (*PV*) is the value at time 0, Future Value (FV) is the value at time n, *i* is the interest rate at which the amount will be compounded each period, and *n* is the number of years. For each annual cost item, *PV* is calculated to reflect its current value. This is essential to accurately capture future tax revenues and other cost items.

Account for Annual Changes in Pavement Roughness: This option utilizes fuel consumption percentage increases due to the effect of pavement roughness as reported by Zaabar and Chatti (2010), using the calibrated Highway Development and Management Software (HDM-4). When this option is selected, the *Specify Annual Pavement Roughness* button is displayed and users can click on it to access the Pavement Roughness Module (see Subsection 2.2.4 for further details).

2.2.2 Vehicle Utilization Module

As vehicles age, they tend to be driven less than newer vehicles. The Vehicle Utilization Module was developed to capture this change in vehicle use over time. Default data correlating vehicle utilization with age is taken from the *Transportation Energy Data Book* (U.S. Department of Energy, 30th Edition).

Users, however, have the option of changing the utilization curve. To alter a vehicle utilization curve, the user may click on either the Utilization Curve button or link (available when performing an analysis) and the **Utilization Curve Generator** will pop up (see Figure 2.2). Utilization is represented as a ratio of the specified *Base Annual Mileage*. The ratios can be edited in the *Utilization Factor* column. To view how changes compare with default utilization values, the user should click on the *Plot Graph* button.

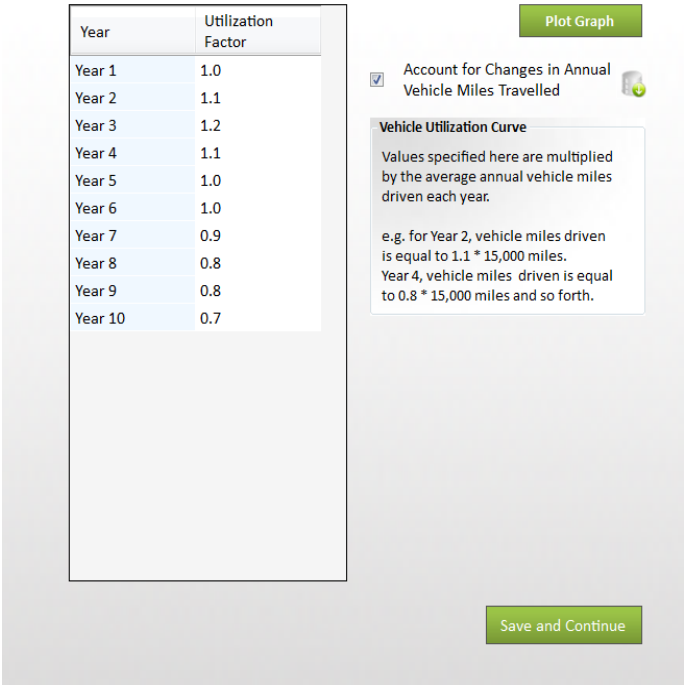

Figure 2.2: The Utilization Curve Generator.

If users decide not to account for changes in utilization with vehicle age, the *Account for Changes in Annual Vehicle Miles Traveled* check box should be unchecked.

Users can also load default data after any edits by clicking on the *Load Data* button.

2.2.3 Vehicle Maintenance Module

The Vehicle Maintenance Module seeks to simulate the actual maintenance activities of a vehicle. Vehicle data from RepairPal.com and TxDOT's fleet database are used as default values. The module can be accessed via the *Edit Maintenance* button or link. Once accessed, the module displays the *Annual Maintenance Cost* of the vehicle through each year of the analysis period (see Figure 2.3). The *Average Annual Maintenance Cost* and *Average Per Mile Maintenance Cost* are also calculated and displayed. Annual repair costs can be graphed by clicking on the *Plot Graph* button.

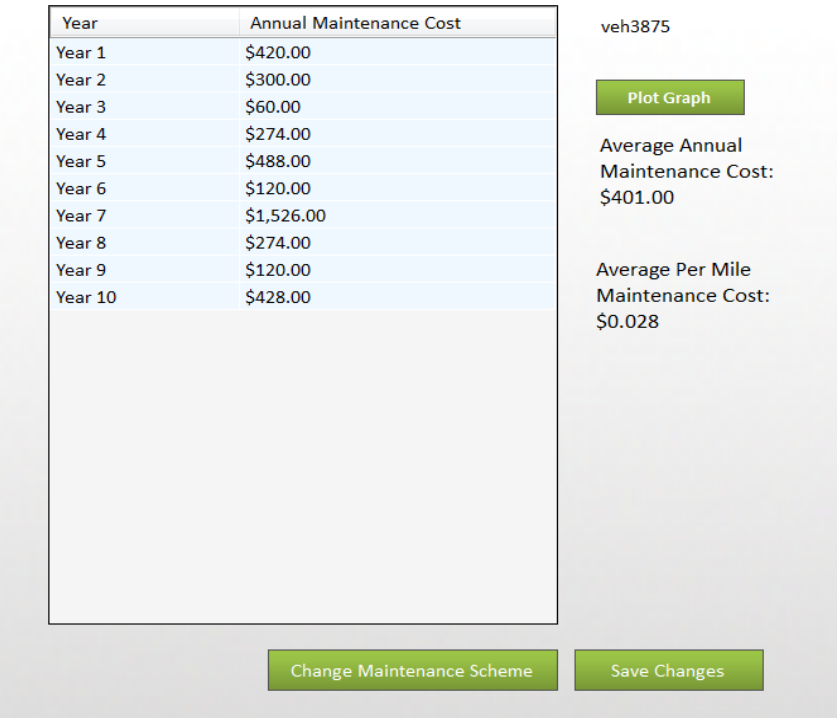

Figure 2.3: Vehicle Maintenance Module—annual maintenance cost display.

If a user chooses to alter the maintenance scheme of the vehicle, the *Change Maintenance Scheme* button should be clicked; this opens up the vehicle's maintenance scheme page (see Figure 2.4). Users have a variety of options to specify the maintenance activity of a vehicle. Using the *Item Name* column, a maintenance activity can be described and set to either *Exact* or *Range* (in the *Schedule Interval* column) to determine if the activity occurs at a fixed mileage or within a certain mile range. For example, oil changes usually occur every 3,750 miles but tire replacement varies between 40,000 and 80,000 miles depending on the type being purchased.

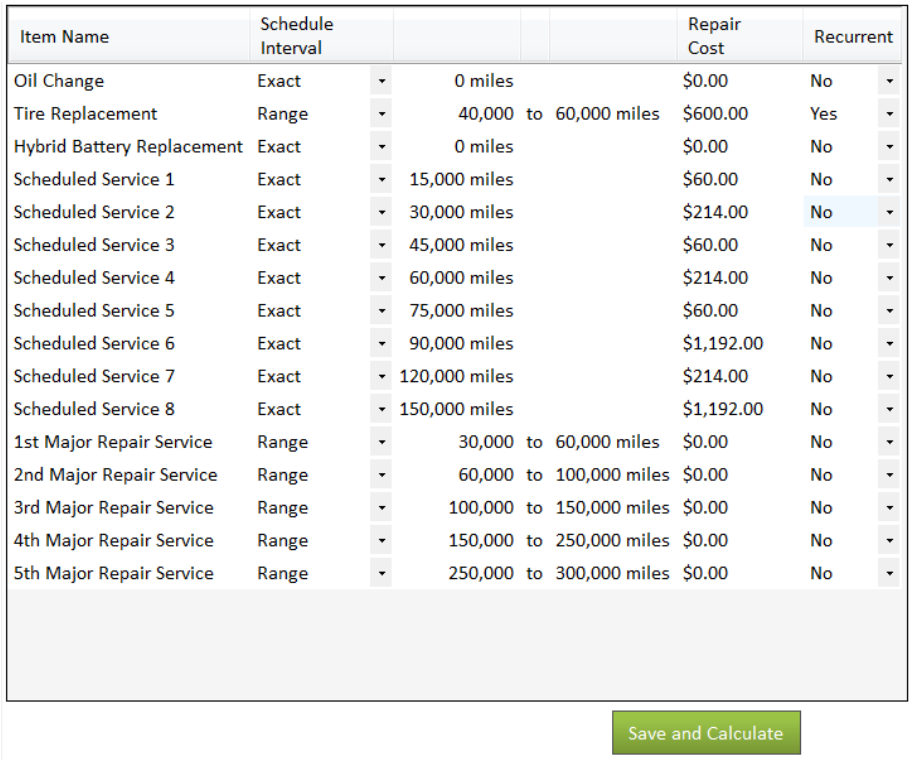

Item Name	Schedule Interval				Repair Cost	Recurrent
Oil Change	Exact	0 miles			$0.00	No
Tire Replacement	Range	40,000	to	60,000 miles	$600.00	Yes
Hybrid Battery Replacement	Exact	0 miles			$0.00	No
Scheduled Service 1	Exact	15,000 miles			$60.00	No
Scheduled Service 2	Exact	30,000 miles			$214.00	No
Scheduled Service 3	Exact	45,000 miles			$60.00	No
Scheduled Service 4	Exact	60,000 miles			$214.00	No
Scheduled Service 5	Exact	75,000 miles			$60.00	No
Scheduled Service 6	Exact	90,000 miles			$1,192.00	No
Scheduled Service 7	Exact	120,000 miles			$214.00	No
Scheduled Service 8	Exact	150,000 miles			$1,192.00	No
1st Major Repair Service	Range	30,000	to	60,000 miles	$0.00	No
2nd Major Repair Service	Range	60,000	to	100,000 miles	$0.00	No
3rd Major Repair Service	Range	100,000	to	150,000 miles	$0.00	No
4th Major Repair Service	Range	150,000	to	250,000 miles	$0.00	No
5th Major Repair Service	Range	250,000	to	300,000 miles	$0.00	No

Figure 2.4: Vehicle Maintenance Module—maintenance scheme.

The difference between the two calculations is that with the *Exact* interval, the repair cost is included in the cost calculation at the exact time the vehicle reaches the specified mileage. However, with the *Range* interval, the repair cost is distributed between the start and end of the mileage range. For example, if the tires need to be replaced somewhere between 40,000 and 60,000 miles as shown in Figure 2.5, once the accumulated mileage falls within that range, the tire replacement cost is included in the vehicle's repair cost for that year.

If the repair occurs over multiple years within that range, the repair cost is divided by the number of occurrences and evenly distributed over the years of occurrence (see Figure 2.6).

NOTE: Ranges should be used only if the range is greater than the **base annual mileage** (e.g., 15,000 miles).

In addition, a repair may be set to be recurrent (select *Yes),* which means that at the specified schedule interval, the repair item will occur again. Using the tire replacement repair as an example, the tire repair cost will be calculated again when the vehicle mileage reaches between 80,000 and 120,000 miles (see Figure 2.6).

Item Name	Schedule Interval				Repair Cost	Recurrent
Oil Change	Exact	0 miles			$0.00	Yes
Tire Replacement	Range	40,000	to	60,000 miles	$600.00	Yes
Hybrid Battery Replacement	Exact	0 miles			$0.00	No
Scheduled Service 1	Exact	15,000 miles			$0.00	No
Scheduled Service 2	Exact	30,000 miles			$0.00	No
Scheduled Service 3	Exact	45,000 miles			$0.00	No
Scheduled Service 4	Exact	60,000 miles				
Scheduled Service 5	Exact	75,000 miles				
Scheduled Service 6	Exact	90,000 miles				
Scheduled Service 7	Exact	120,000 miles				
Scheduled Service 8	Exact	150,000 miles				
1st Major Repair Service	Exact	30,000 miles				
2nd Major Repair Service	Exact	60,000 miles				
3rd Major Repair Service	Exact	100,000 miles				
4th Major Repair Service	Exact	150,000 miles				
5th Major Repair Service	Exact	250,000 miles				

Year	Annual Maintenance Cost
Year 1	$0.00
Year 2	$0.00
Year 3	$600.00
Year 4	$0.00
Year 5	$0.00
Year 6	$0.00
Year 7	$600.00
Year 8	$0.00
Year 9	$0.00
Year 10	$0.00

Figure 2.5: Tire replacement between 40,000 and 60,000 mile with "recurrent" turned on and corresponding Annual Maintenance Cost.

Item Name	Schedule Interval				Repair Cost	Recurrent
Oil Change	Exact	0 miles			$0.00	Yes
Tire Replacement	Range	30,000	to	60,000 miles	$600.00	No
Hybrid Battery Replacement	Exact	0 miles			$0.00	No
Scheduled Service 1	Exact	15,000 miles			$0.00	No
Scheduled Service 2	Exact	30,000 miles			$0.00	No
Scheduled Service 3	Exact	45,000 miles				
Scheduled Service 4	Exact	60,000 miles				
Scheduled Service 5	Exact	75,000 miles				
Scheduled Service 6	Exact	90,000 miles				
Scheduled Service 7	Exact	120,000 miles				
Scheduled Service 8	Exact	150,000 miles				
1st Major Repair Service	Exact	30,000 miles				
2nd Major Repair Service	Exact	60,000 miles				
3rd Major Repair Service	Exact	100,000 miles				
4th Major Repair Service	Exact	150,000 miles				
5th Major Repair Service	Exact	250,000 miles				

Year	Annual Maintenance Cost
Year 1	$0.00
Year 2	$300.00
Year 3	$300.00
Year 4	$0.00
Year 5	$0.00
Year 6	$0.00
Year 7	$0.00
Year 8	$0.00
Year 9	$0.00
Year 10	$0.00

Figure 2.6: Tire replacement between 30,000 and 60,000 miles with "recurrent" turned off and corresponding Annual Maintenance Cost.

2.2.4 Pavement Roughness Module

Studies have shown that pavement conditions have an effect on a vehicle's fuel consumption. In 2010, Zaabar and Chatti published a paper on the fuel consumption of five different vehicle classes under different operating, weather, and pavement conditions using a

calibrated version of the HDM-4 model. The vehicle classes in the study included a medium-sized passenger car, an SUV, a van, a light truck, and an articulated truck. Vcost integrates the results of the HDM-4 calibration study into the toolkit by enabling users to specify an annual pavement condition rating for each year of the analysis period (see Figure 2.7).

The five available pavement roughness options available to users are listed in Table 2.1. Depending on the option selected by the user, Vcost multiplies the percentage change in fuel consumption (by vehicle class) by the vehicle's fuel consumption in that year (see Figure 2.7). This results in slightly higher fuel consumption values for smooth to very rough pavement conditions.

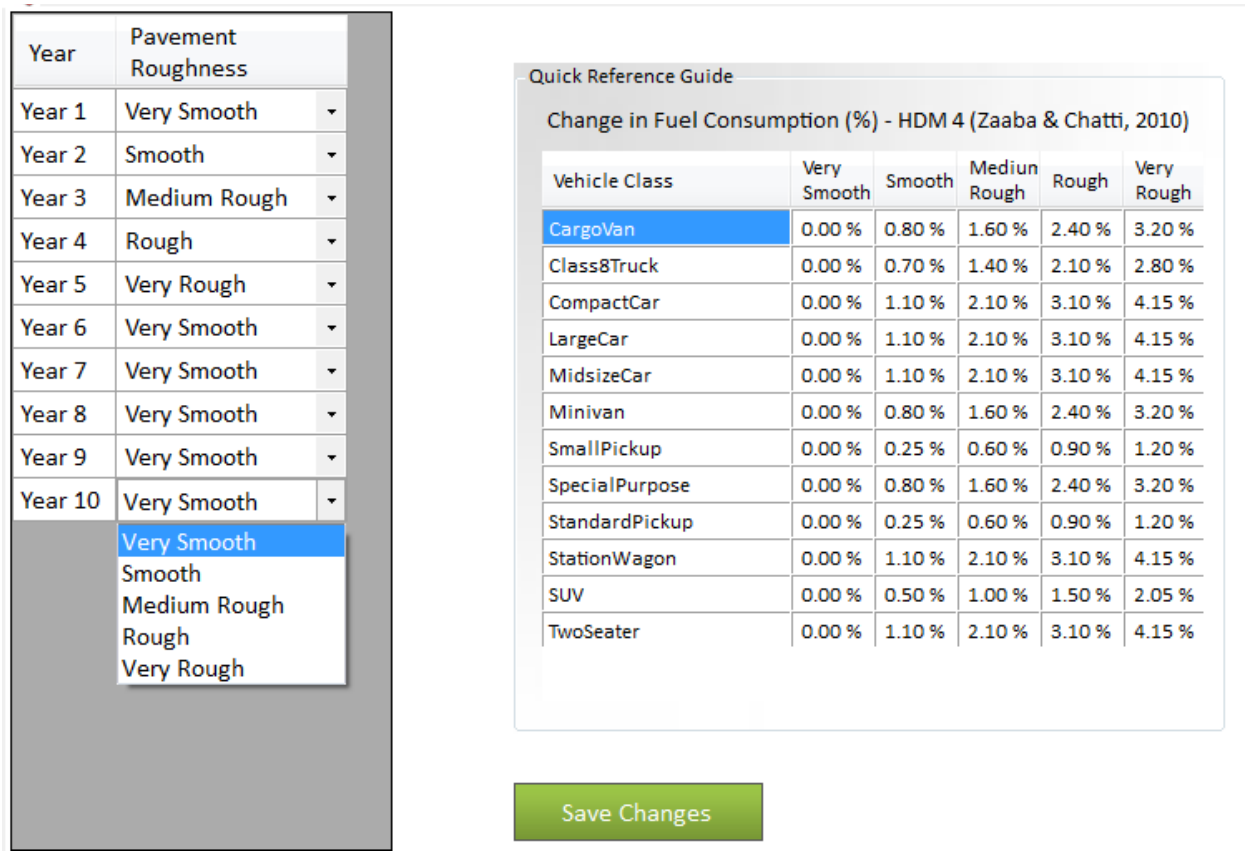

Figure 2.7: The Pavement Roughness Module.

Table 2.1: Pavement Roughness Descriptions and Their Corresponding International Roughness Index (IRI) Score.

Description	Corresponding IRI (inches per mile)
Very Smooth	1–59
Smooth	60–95
Medium Rough	96–130
Rough	131–169
Very Rough	170–950

2.2.5 Default Vehicle Parameters

As discussed earlier, default vehicle parameters are stored in the DefaultParameters.xml file. Parameters stored by vehicle class include average annual miles traveled, annual insurance cost, annual percentage rate (APR), finance term (in years), average first year depreciation, subsequent year depreciation, and other fixed costs such as vehicle registration. Further discussion of the cost categories and default data are presented in this section.

2.2.5.1. Depreciation

New vehicles are known to depreciate more in the first year of ownership than in subsequent years. Typical vehicle depreciation for LDVs was found to be around 20% the first year and 15% for the subsequent years. For heavy-duty vehicles (HDVs), a constant 15% depreciation value is used as the default, although this may vary substantially for different truck models and miles driven annually. The values for both first year and subsequent yearly depreciation can be edited by the user if empirical values are available.

2.2.5.2. Financing

For LDVs, as discussed in the final report for the initial part of this project (Welter et al., 2009), the cost of financing is dependent on the cost of the new vehicle, the interest rate, the down payment amount, the term of the loan, and the credit score of the individual or group financing the vehicle (Welter et al., 2009). According to HSH® Associates, the average auto loan interest rates for Dallas and Houston in March 2011 were 5.42% and 5.27% respectively (HSH, 2011). CT-Vcost uses the higher Dallas value as a default for passenger vehicles and light trucks. A default loan term of 60 months is also used, and financing is based on a 10% down payment (AAA, 2011). For HDVs, a 48-month lease term is used as large trucking companies tend to heavily utilize their new trucks (they can accumulate between 140,000 miles and 300,000 miles annually[9]) before selling them to smaller carriers.

2.2.5.3. Insurance

The LDV insurance cost was taken from the 2007 National Association of Insurance Commissioners report and adjusted for annual inflation of 2.09% from 2007 to 2011 (NAIC, 2007). The default value for Texas was determined as $877 per year. The AAA national average for full-coverage insurance for LDVs ranged between $853 and $1,006 annually. The HDV insurance cost was based on industry estimates, which ranged from $4,000 to $7,500 annually. A value of $5,500 is used by default.

2.2.5.4. Other Costs

Other costs include registration and permit fees. For LDVs, annual fees including vehicle registration renewal and inspection fees are assigned an average default value of $93.00, which can be changed by the user. Registration and permit fees for HDVs were back-calculated using industry estimates from the American Transportation Research Institute (ATRI) study (ATRI, 2011), and an annual value of $2,300 was assigned.

[9] Depending on the utilization (sleeper cab, day cab, sleeper cab team, day cab with terminal switching).

2.3 Performing Analyses

CT-Vcost integrates all the models (or modules) developed in this study. The toolkit enables users to perform various types of analyses, as summarized in the following section.

2.3.1 Single Vehicle Analysis Module

This module enables users to select a single vehicle, and alter parameters such as vehicle value, annual mileage driven, insurance rates, maintenance cost and schedules, and other fixed costs. It is the simplest of the Vcost applications. It enables users to select a particular vehicle and alter parameters such as vehicle price (MSRP), average annual mileage driven, insurance premium, interest rate (APR), down payment, finance term, first year depreciation, subsequent years depreciation, fixed annual costs, and maintenance costs (see Figure 2.8).

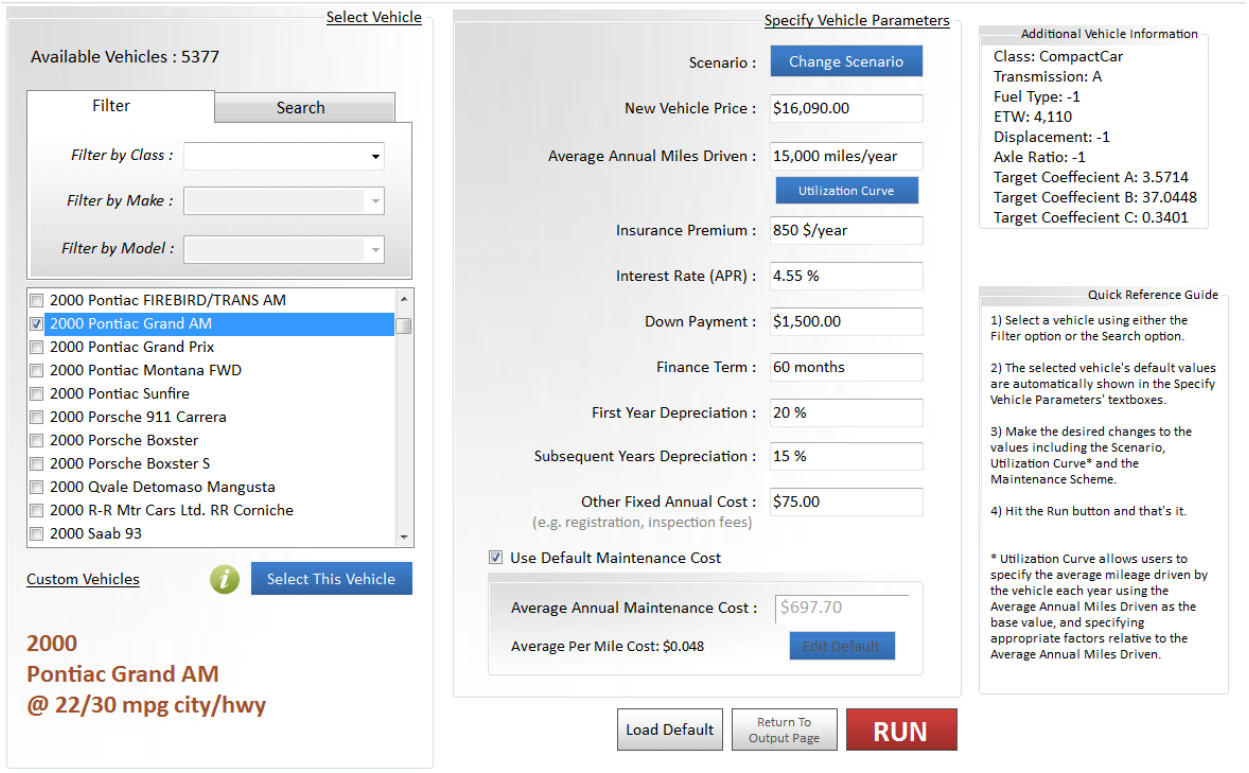

Figure 2.8: Single Vehicle Analysis example.

2.3.2 Multi-Vehicle Analysis Module

This module is similar to the Single Vehicle Analysis module in that users can alter vehicle parameters. In addition, users are allowed to select two or more vehicles to make cost comparisons. Outputs such as total operating cost, fuel consumption, and others can be analyzed for multiple vehicles simultaneously. A screenshot of the Multi-Vehicle Analysis module is provided as Figure 2.9.

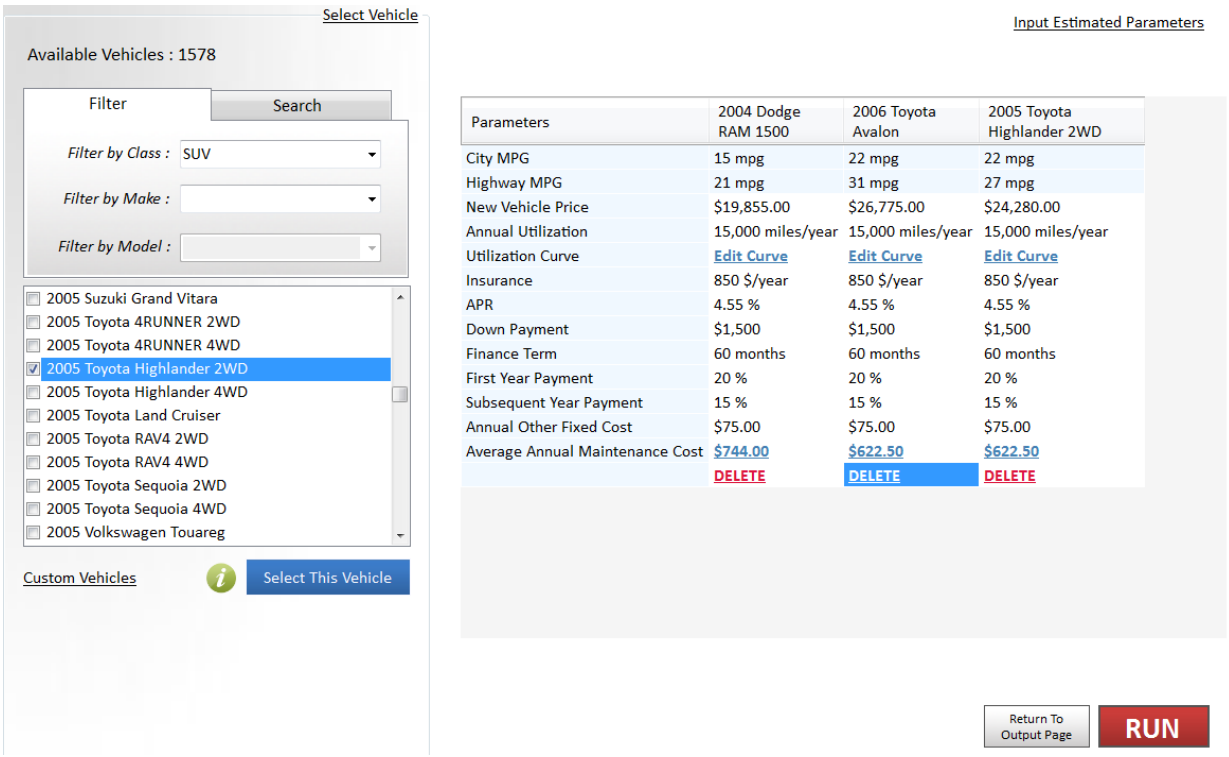

Figure 2.9: The Multi-Vehicle Analysis module.

2.3.3 Fleet Analysis Module

This module builds on the single vehicle and multi-vehicle analyses by enabling users to perform analyses involving a fleet of vehicles. Users can build fleets from a wide selection of LDVs and HDVs and specify their compositions and parameters. The Fleet Analysis window has five main sub-modules that can be accessed via their respective buttons, and a data summary sheet for each sub-module (see Figure 2.10).

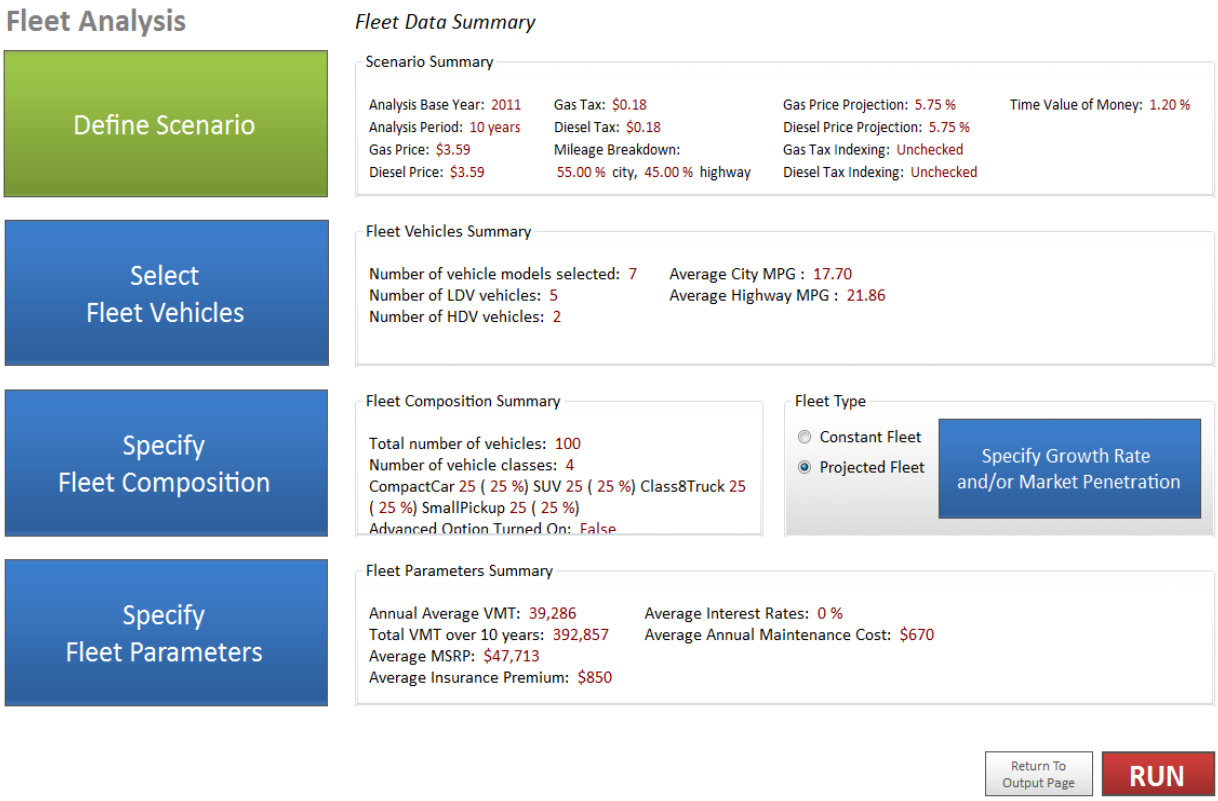

Figure 2.10: A Fleet Analysis screenshot.

2.3.3.1 Define Scenario

The Define Scenario button takes the user to the Scenario Module where base year, analysis period, fuel prices, fuel taxes, etc., can be specified by the user.

2.3.3.2 Fleet Vehicles

Multiple LDV and HDV models can be selected by the user via this sub-module.

2.3.3.3 Fleet Composition

The Fleet Composition module allows users to specify the total number of vehicles in a fleet and the number of vehicle models in each class by altering the percentages. Vehicle composition can also be specified by vehicle model.

2.3.3.4 Fleet Parameters

Users are able to specify vehicle parameters, such as vehicle price (MSRP), average annual mileage driven, insurance premium, interest rate (APR), etc., either by Vehicle Class or by Individual Vehicles.

2.3.4 The Growth Rate and Market Penetration Module

This sub-module, which forms part of the Fleet Analysis module, enables planners to examine how various vehicle types (such as hybrids and pure electric vehicles) and fleet growth

rates may influence fuel tax revenues, fuel consumption, and carbon emissions over a projected time period.

On the Growth Rate/Market Penetration page, users can input the expected vehicle growth rate (in percentages) into the Growth Rate column and the number of years that this growth rate will occur in the *No. of Years* column. The Initial Count is equal to the specified Total Number of Vehicles in the Fleet Composition module and the default number of years is equal to the length of the analysis period.

Users can also input the market penetration as a percentage of the total fleet and the number of years the change is expected to occur. CT-Vcost then calculates the number of vehicles of that model over the years specified. Using these numbers, the appropriate calculations such as the vehicle fuel economy values are utilized in determining fuel consumption and fuel cost.

2.3.5 The Route Analysis Module

This module enables users to simulate the cost of moving a vehicle or a fleet of vehicles via certain routes. Multiple route lengths and characteristics such as speed, congestion level, driver costs, etc., can be defined by the user and the vehicle operating cost via each route is calculated and presented for comparison.

It builds on the Fleet Analysis module by enabling users to simulate the movement of vehicles over specified routes. Route characteristics that can be stated are distance, speeds, congestion level, road use charge (toll), driver delay cost, and driver per-mile cost.

2.3.5.1. Fuel Consumption

CT-Vcost is packaged with three different algorithms to calculate fuel consumption as a function of vehicle speed: 1) a slope-based approach, 2) a lookup table approach, and 3) the ability to run any selected light-duty vehicle, from the ~5,000 in the data set, over the "speed cycle" using the UT Fuel Economy Model. The UT Fuel Economy Model, which was developed as part of this study, provides fuel consumption versus speed data via the lookup table algorithm. The UT Fuel Economy Model provides a very accurate prediction of fuel consumption over a vehicle's drive cycle and its output data is synthesized and used in CT-Vcost.

Each of the fuel consumption algorithms is briefly described in the following sections and further details on the Fuel Economy Model can be found in the next chapter of this report.

<u>*Slope-Based Approach*</u>: Fuel consumption is calculated as a function of speed using at least two known points: city fuel economy (FE_{city}) and highway fuel economy (FE_{hwy}). This approach assumes that city mpg and highway mpg are achieved at average cycle speeds, respectively, of 21.2 mph ($\bar{V}_{\text{city}}$) and 48.3 mph ($\bar{V}_{\text{hwy}}$), according to EPA tests results (EPA, 2011). The user specifies a vehicle speed that yields optimum fuel economy (V_0). Then, using Equations 2.2 and 2.3, the possible mpg estimates are derived. As illustrated in Figure 2.11, the slope-based approach, though simple and replicable for most vehicles, is not entirely accurate, as the vehicle speed that yields optimum fuel economy varies between 25 to 55 mph when using actual fuel economy data (West, 1997)[10].

[10] Additional resources: www.fhwa-tsis.com

$$FE(\mathrm{V})=\begin{cases}\mathrm{mV}+FE_{\mathrm{city}} & \text{if } \mathrm{V} \le \mathrm{V}_0 \\ FE(\mathrm{V}_0)-2(\mathrm{V}-\mathrm{V}_0) & \text{if } \mathrm{V}>\mathrm{V}_0\end{cases} \tag{2.2}$$

where the slope (m) is defined as

$$\mathrm{m}=\frac{FE_{\mathrm{hwy}}-FE_{\mathrm{city}}}{\bar{\mathrm{V}}_{\mathrm{hwy}}-\bar{\mathrm{V}}_{\mathrm{city}}} \tag{2.3}$$

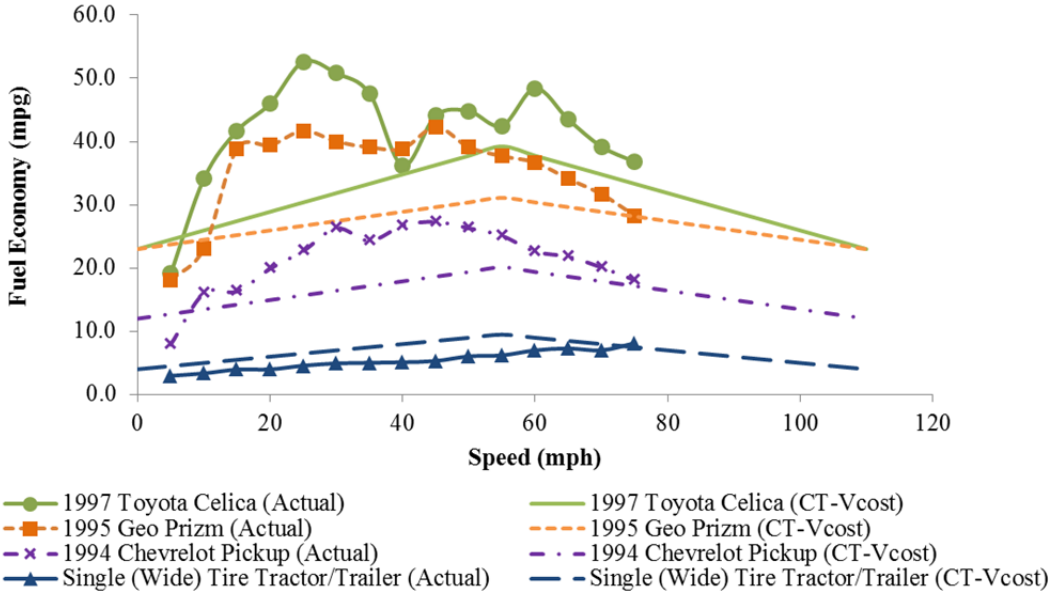

Figure 2.11: Comparison of slope-based approach with reported fuel economy data.

Lookup Table Approach: The lookup table approach provides a much better estimate of fuel economy as a function of speed by utilizing actual mpg values (see Table 2.2). This approach, though more accurate, is dependent on the availability of accurate data. For each speed (V) on the specified route profile, CT-Vcost iterates through each row of the column matching the vehicle model, and returns the vehicle's fuel economy $FE(\mathrm{V})$ in mpg. When the vehicle speed falls within the range of two successive speeds (V_i and V_{i+1}), the fuel economy of the successive speeds ($FE(\mathrm{V}_i)$ and $FE(\mathrm{V}_{i+1})$) are used in determining the vehicle's instantaneous fuel economy $FE(\mathrm{V})$ using Equation 2.4.

$$FE(\mathrm{V})=\frac{FE(\mathrm{V}_{i+1})-FE(\mathrm{V}_i)}{\mathrm{V}_{i+1}-\mathrm{V}_i}\left(\mathrm{V}-\mathrm{V}_i\right)+FE(\mathrm{V}_i) \tag{2.4}$$

Table 2.2: Sample Lookup Table

Speed (Vi) [mph]	1994 Chevrolet Pickup[11]	1994 Jeep Grand Cherokee[11]	1997 Toyota Celica[11]	Single Wide Tire Tractor —Dual Tire Trailer[12]	Single Wide Tire Tractor— Single Wide Tire Trailer[12]	Sample HDV FEM Output[13]
5	7.9	8.2	19.1	3	2.96	
10	16	11.2	34.1	3.3	3.35	
15	16.3	17.5	41.7	3.9	3.95	
20	19.9	24.7	46	4	3.98	
25	22.7	21.8	52.6	4.6	4.57	
30	26.3	21.6	50.8	5	4.93	9.8
35	24.3	25	47.6	5.2	5.02	9.2
40	26.7	25.5	36.2	5.3	5.1	8.5
45	27.3	25.4	44.1	5.6	5.31	7.8
50	26.3	24.8	44.8	6.2	6.04	7.3
55	25.1	24	42.5	6.2	6.2	6.5
60	22.6	23.2	48.4	6.9	6.99	5.8
65	21.8	21.3	43.5	7.1	7.29	4.9
70	20.1	20	39.2	7	7	4.2
75	18.1	19.1	36.8	7.9	8.11	

A comparison of sample lookup table output (based upon the UT Fuel Economy Model for an HDV) and reported data from other studies (West, 1997; Capps 2008) is presented in Figure 2.12. This graph shows significant differences in the results from the two experimental studies, especially at speeds greater than 50 mph. It should be noted that the exact configurations of the trucks/trailers in the fuel economy versus speed data is unknown, so a direct comparison of the experimental results to the model predictions is difficult. More importantly, the experimental trends, at least for the bottom two curves, are highly suspect because the aerodynamic drag increases with the square of vehicle speed, so the fuel economy should not increase with vehicle speed past 70 mph. The final experimental curve, which does at least show the fuel economy decreasing at high speeds, is also suspect because it consists of two straight lines and experimental systems rarely behave in such a simple manner. However, it should be noted that the integration of the UT Fuel Economy model provides a much greater accuracy for various truck configurations not available in data from other studies.

[11] West et al., 1997. Additional resources: www.fhwa-tsis.com

[12] Capps et al., 2008.

[13] UT FEM Model Input: Class 7; Custom; 2004 Sterling MBE 4000; Empty; Congested; Driver Bevo; Tire 295/80/22.5; Weight 30,000lbs; Transmission 12.65,8.38,6.22,4.57,3.4,2.46,1.83,1.34,1;Differential 3.11

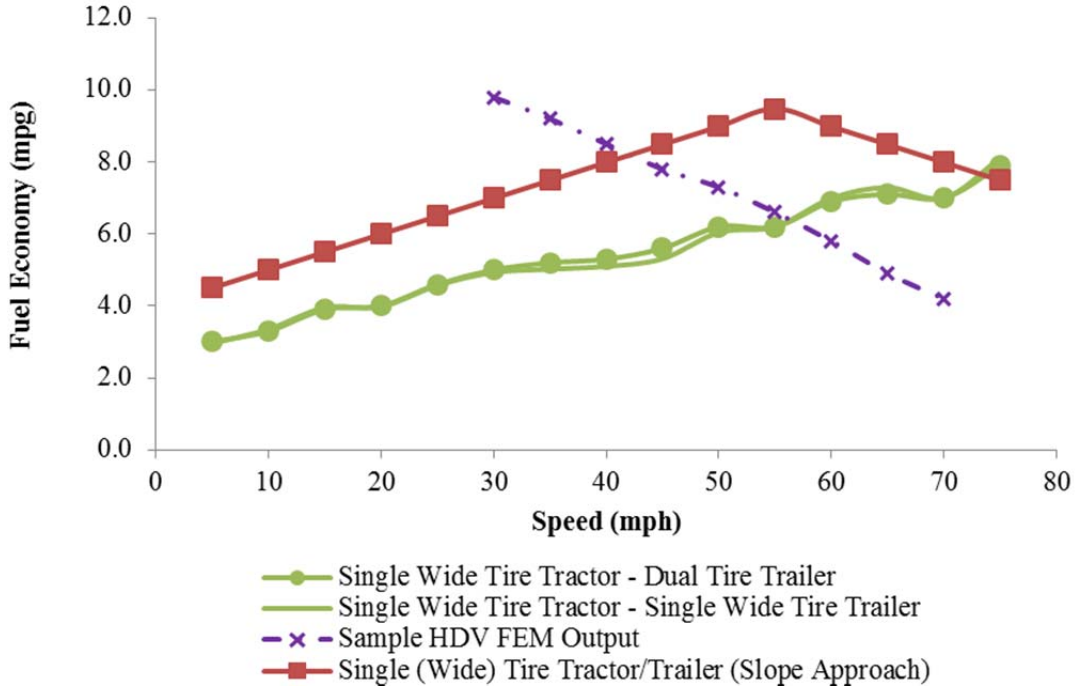

Note: Exact specifications for the experimental trucks were not available for model input, and the experimental trends, at least for the bottom two curves, are highly suspect.

Figure 2.12: Comparison of HDV fuel economy via the UT Fuel Economy Model input to the lookup table approach (HDV FEM) to reported experimental data from other studies.

2.3.5.2. Driver Costs

CT-Vcost provides users with two alternatives for capturing driver cost: Hourly Driver Cost and Per Mile Driver Cost. Hourly driver cost is useful for capturing the cost of delay during congested conditions. This is useful for time-sensitive deliveries such as perishable and high value commodities. An industry average value in 2010 of 40.4 cents a mile is used for the per-mile driver cost (ATRI, 2011).

2.3.6 The Light-Duty Vehicle Drive Cycles Module

This module integrates the Light-Duty Fuel Economy model (developed as part of this study and discussed in Chapter 3) into CT-Vcost. It is mainly an interface between the two programs. This module enables users to choose a drive cycle of interest, select a desired vehicle, and simulate that vehicle over the drive cycle to determine its fuel economy when driven in that manner. In addition, users are able to compare multiple vehicles and drive cycle configurations simultaneously and examine the vehicle's fuel economy over a selected section or range of the entire drive cycle.

Similar to the Single Analysis module, users select a vehicle from the list of available vehicle models and advanced vehicle data from these models are transferred to the *Specify Vehicle and Drive Cycle Parameters* text boxes, as illustrated in Figure 2.13. Data transferred include vehicle weight (in pounds) and the coastdown (target) coefficients A, B, and C retrieved from the EPA database.

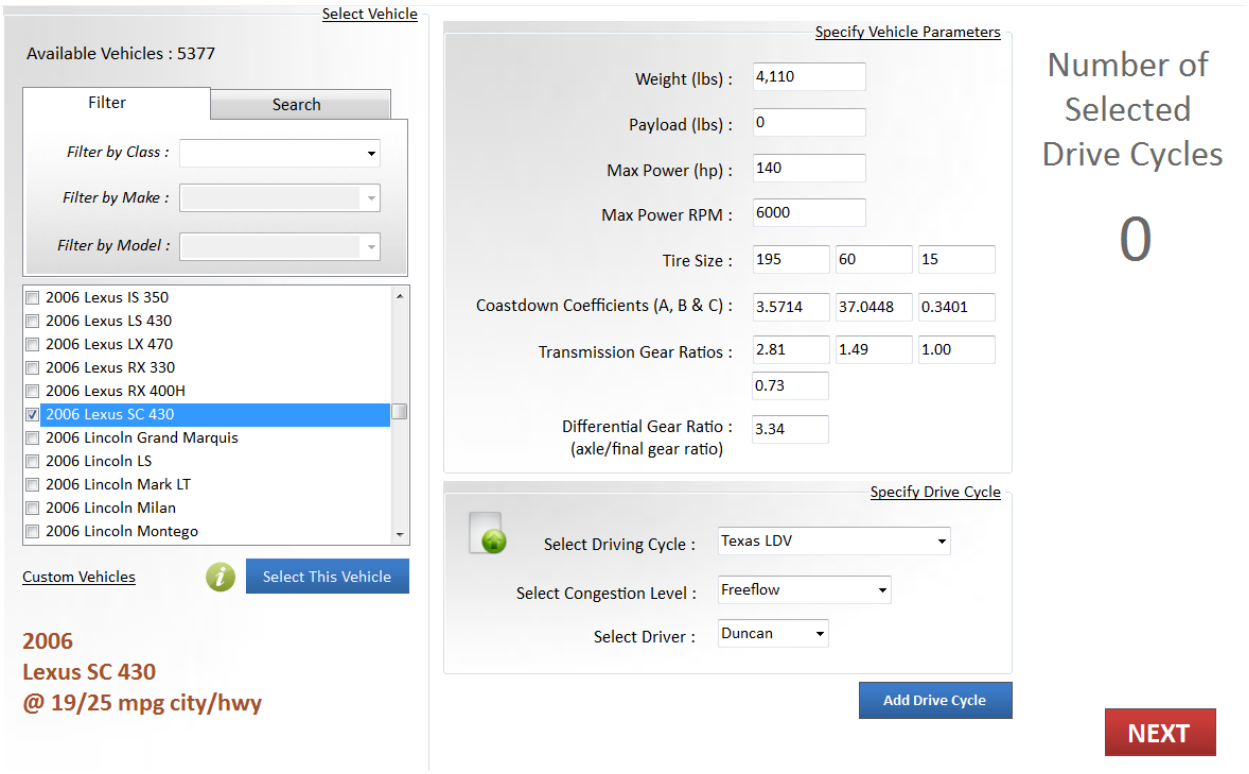

Figure 2.13: Screenshot from CT-Vcost for a light-duty vehicle drive cycle analysis.

Default values in the *Specify Vehicle and Drive Cycle Parameters* text boxes include engine Max Power (the rated power output of the engine in horsepower [hp], which should be available in the owner's manual), Max Power RPM (the engine speed at which the rated power output was measured, which is always listed along with the rated power), Tire Specifications (uses the Section Width/Sidewall Aspect Ratio/Tire and Wheel Diameter convention), Transmission Gear Ratios, and Differential Gear Ratio. Users can change these values but need to ensure that inputs represent a realistic vehicle.

Users must then select a drive cycle from the **Select Drive Cycle** drop-down list located in the *Specify Drive Cycle* group box (see Figure 2.13). If the Texas LDV drive cycle is selected, users have the additional options of selecting a Congestion Level (Congested, Moderate, and Freeflow) and a Driver Characteristic (Conservative, Moderate Male, Moderate Female). Custom drive cycles can also be loaded by users by clicking on the *Upload Custom Drive Cycle* button and uploading a desired drive cycle.

After multiple vehicle specifications and drive cycles have been selected, the Fuel Economy Model must be run for each selection. The multiple drive cycle selections can then be compared by Gear #, Desired Speed [mph], Engine Speed [rpm], Engine Torque [N-m], Fuel Flow Rate [g/s], Instantaneous mpg, Instantaneous Max Torque [N-m], Speed Error [mph], Throttle Position, Vehicle Drag [N], Vehicle Speed [mph], and Vehicle Travel [m].

The fuel economy of a selected vehicle operating over a selected drive cycle can also be examined over a selected section or range of time intervals during the selected drive cycle. Fuel economy versus vehicle speed curves can also be developed and saved by the user to be used in the Route Analysis module.

2.3.7 The Heavy-Duty Vehicle Drive Cycles Module

Similar to its light-duty counterpart, the HDV Drive Cycles module integrates the Heavy-Duty Fuel Economy model (also developed as part of this study) into Vcost. This module comes with 54 default drive cycles from the combination of 3 engine types, 3 traffic congestion conditions, 3 vehicle weights, and 2 drivers. In addition, users can build custom HDV drive cycles by varying the vehicle weights. Multiple drive cycles can be compared simultaneously and a vehicle's fuel economy for a selected drive cycle can also be examined for a section or range of the entire drive cycle.

The HDV Drive Cycles module is much simpler than its LDV counterpart in that the only variables are Vehicle Type, Weight, Congestion Level, and Driver Type. Following are the default values for each characteristic:

- **Vehicle Type:** 2004 Sterling, 2001 Freightliner, 1995 International (see Table 2.3)
- **Weight:** Empty (45,000 lb), Cubed Out (65,000 lb), and Weighed Out (80,000 lb), or the user can input an arbitrary weight, as long as it is reasonable (does not exceed the capabilities of the engine)
- **Congestion Level:** Congested, Freeflow, Moderate
- **Driver:** (Bevo, Longhorn [Aggressive])

Once these characteristics are specified, the user clicks on the *Select Drive Cycle* button to select from the list of drive cycles to be analyzed (see Figure 2.14).

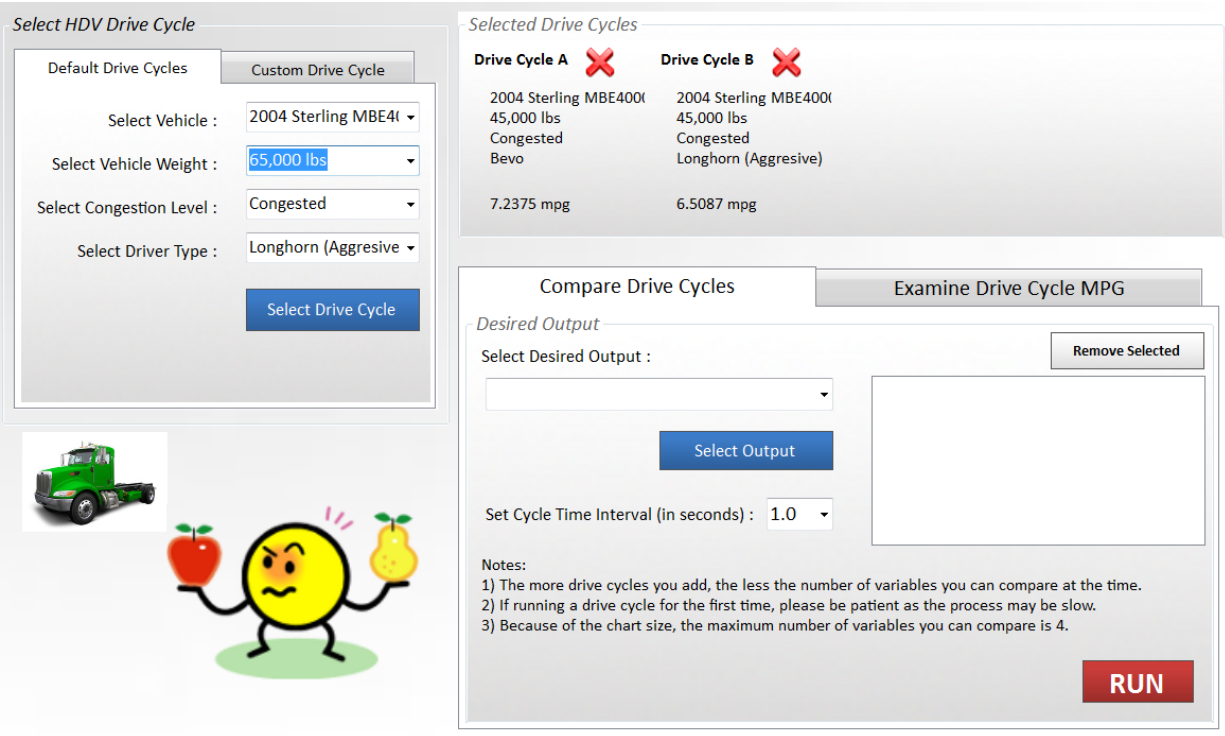

Figure 2.14: HDV drive cycle analysis screenshot.

Similar to its LDV counterpart, drive cycles can be compared and fuel economy over the drive cycle can be examined; fuel economy versus speed curves can also be generated and saved for the Route Cost analysis. Table 2.3 shows some of the specifications of the vehicle types, which are all Class 8 trucks.

Table 2.3: HDV Vehicle Types Specifications.

	1995 International	2004 Sterling (MB)	2001 Freightliner
Engine Model	Cummins M11	MBE4000	Caterpillar C12
Engine Displacement (L)	11	12.8	11.8
Engine Year	1995	2004	2001
# of Cylinders	6	6	6
Rated Power	330 HP @ 1800 rpm	370 HP @ 2000 rpm	410 HP @ 2100
Torque (lbf-ft)	1250 @ 1200 rpm	1450 @ 1100 rpm	1450
Transmission Model	Fuller RT14609A	Eaton Fuller RTLO-14913A	Eaton Fuller FRO-14210B
# of Gears	9	13	10
Differential (Axle) Model	Eaton DS402	Meritor (Rockwell) Hypoid Single Reduction RT-40-145 Tandem Drive Axle	Meritor (Rockwell) Hypoid Single Reduction RT-40-145 Tandem Drive Axle

2.4 Calculations

Calculations are performed for each individual vehicle and not by vehicle class. Default values may be based on the vehicle's class (e.g., SUV, midsize car, standard pickup, etc.) but the calculations are done specifically for each selected vehicle (either Single, Multi-Vehicle, or Fleet analysis).

2.4.1 Fuel Consumption (Single, Multi-Vehicle, and Fleet Analysis)

Fuel consumption, cost, and fuel taxes are calculated differently for Single, Multi-Vehicle, and Fleet Analyses as compared to Route Analysis. For LDVs, data from the EPA city and highway fuel economy measurements are used. For each vehicle in an analysis, a combined fuel economy is calculated in Equation 2.5 as:

$$FE_{comb} = \frac{1}{\frac{City_{ratio}}{FE_{\text{city}}} + \frac{Highway_{ratio}}{FE_{\text{hwy}}}} \tag{2.5}$$

where FE_{comb} is the combined fuel economy (the average fuel economy during the analysis period, not to be confused with EPA's composite fuel economy used for CAFE regulations); $City_{ratio}$ is the percentage of miles driven under city conditions (specified by Common Scenario -> Percent City Mileage), FE_{city} is the EPA reported city fuel economy, $Highway_{ratio}$ is the percentage of miles driven under highway conditions, and FE_{hwy} is the EPA reported highway fuel economy.

Fuel consumption is then calculated annually using the loop:

```
for (int i = 0; i < AnalysisPeriod; i++)
{
        fuelConsumed = AnnualMiles[i] / mpg;
        //Add annual cost to list
        FuelConsumedList.Add(fuelConsumed);
}
```

Fuel cost is calculated via:

```
for (int i = 0; i < AnalysisPeriod; i++)
{
        fuelcost = (fuelPrices[i]/mpg) * AnnualMiles[i];
        //Add annual cost to list
        FuelCostList.Add(fuelcost);
}
```

Fuel tax is calculated via:

```
for (int i = 0; i < AnalysisPeriod; i++)
{
        fueltax = fuelTaxes[i]/mpg * AnnualMiles[i];
        //Add annual cost to list
        FuelTaxList.Add(fueltax);
}
```

2.4.2 Depreciation

Vehicle depreciation is calculated in two stages: 1) first year depreciation, and 2) subsequent year depreciation. The Declining-Balance method (Reducing Balance method) is used. First year depreciation is calculated in Equation 2.6 as

$$\text{Depreciation}_{\text{Year 1}} = \text{New Vehicle Price} \times \text{Deperciation Rate}_{\text{first year}} \tag{2.6}$$

Subsequent year depreciation is calculated annually (i) in Equation 2.7 as

$$\text{Depreciation}_{Year\ i} = \text{Residual Value}_{Year\ i-1} \times \text{Depreciation Rate}_{\text{subsequent years}} \tag{2.7}$$

The following vehicle parameters are used: New Vehicle Price (MSRP), First Year Depreciation, and Subsequent Years Depreciation.

2.4.3 Finance

Vehicle finance is calculated in Equation 2.8 using the amortization formula:

$$A = P\frac{r(1+r)^n}{(1+r)^n - 1} \tag{2.8}$$

where A is the payment amount per period (monthly), P is the initial principal (MSRP minus down payment), r is the interest rate per period (monthly), and n is the total number of payment periods (finance term in months). The following vehicle parameters are used in the code: *New Vehicle Price* (MSRP)*, Down Payment, Interest Rate (APR*), and *Finance Term.*

2.4.4 Insurance and Other Fixed Annual Costs (Registration and Permit Fees)

Insurance and other fixed annual costs (e.g., registration and permit fees) are calculated annually for each year in the analysis period, and included in the vehicle's annual operating cost. The following vehicle parameters are used: *Insurance* and *Other Fixed Annual Cost.*

2.4.5 Maintenance and Repair Calculations

The average annual maintenance cost is calculated as explained in Subsection 2.2.3, Vehicle Maintenance Module. The two types of annual maintenance cost calculations are 1) the *Exact Mileage* calculation and 2) the *Range Interval* calculation. For the *Exact Mileage* calculation, the repair cost is included in the cost calculation at the exact time the vehicle reaches the specified mileage. However, with the *Range Interval*, repair cost is distributed between the start and end mileage range. When a repair item is recurrent, the cost is applied every time the item reaches its mileage interval. Further explanations of both methods are provided in the following code.

2.4.5.1 Exact Mileage Calculation

```
float totalmiles = 0;
for (int year = 0; year < analysisPeriod; year++)
{
       float frequency = annualMiles[year] / float.Parse(servicemiles);
       // if service is Fixed but happens multiple times in a year
       if (recurrent == "1" && frequency >= 1 && float.Parse(servicemiles) < annualMiles[year]
&& frequency != double.PositiveInfinity)
       {
              AnnualCostMM.Add(year.ToString(), (frequency * cost)); // store annual cost
       }
       else
  {// if service is Fixed but happens in say year 3
              totalmiles += annualMiles[year];
    float maintenanceoccurs = totalmiles / float.Parse(servicemiles);
    if (maintenanceoccurs >= 1 && maintenanceoccurs != double.PositiveInfinity)
    {
              AnnualCostMM.Add(year.ToString(), cost); // store annual cost
      totalmiles = 0; //reset to 0 and start accumulating for next occurrence
    }
  }
}
```

2.4.5.2 Range Interval Calculation

```
float totalmiles = 0;
List<int> rangeyears = new List<int>();
string[] milesplitter = servicemiles.Split('-');
float start = float.Parse(milesplitter[0]);
float end = float.Parse(milesplitter[1]);
MultiMap<int> WithinRange = new MultiMap<int>();
for (int year = 0; year < analysisPeriod; year++)
{
 totalmiles += annualMiles[year];
 if (Between(totalmiles, start, end) == true)
 {
  WithinRange.Add((start + end).ToString(), year);
  rangeyears.Add(year);
 }
 if (totalmiles > end && recurrent == "1") //reset to 0 and start accumulating for next
occurrance
 {
  float storestart = start;
  start = end + start;
  end = start + (end - storestart);
 }
}

Dictionary<int, float> YearCostDict = new Dictionary<int, float>();
foreach(string samerange in WithinRange.Keys)
{
 int occurences = WithinRange[samerange].ToList().Count;
 float distributecost = cost / occurences;
 foreach (int year in WithinRange[samerange].ToList())
  YearCostDict.Add(year, distributecost);
}

for (int year = 0; year < analysisPeriod; year++)
{
```

```
 foreach (int yr in rangeyears)
 {
  if(year == yr)
   AnnualCostMM.Add(year.ToString(), YearCostDict[year]); // store annual cost
  else
   AnnualCostMM.Add(year.ToString(), 0); // store annual cost
 }
}
```

2.4.6 Fleet Analysis Calculations

The following algorithm is used by the Fleet Analysis module:

1. Determine annual cost of each vehicle in the fleet independently.
2. Multiply annual cost by the vehicle's composition (vehicle model count in fleet).
3. Sum up the total cost of all the vehicles in the fleet for that year.

The total annual vehicle operating cost is thus the sum of the operating cost of each vehicle model (multiplied by the number of models or vehicle count) in the fleet, as represented in Equation 2.9:

$$\text{Total Annual Vcost} = \sum_{i=\text{model}}^{\text{Number of Models}} \left(\text{Annual Vcost}_{\text{model}} \times \text{Vehicle Count}_{\text{model}}\right) \tag{2.9}$$

2.4.7 Growth Rate and Market Penetration Calculations

The Growth Rate and Market Penetration module varies the vehicle composition for each year in the analysis. Annual vehicle counts are determined using the percentages specified by the user. In addition, the user can specify the number of years that that percentage change occurs. The following subsections further describe the logic behind the Growth Rate and Market Penetration calculation.

2.4.7.1 Growth Rate

The total number of vehicles is multiplied by the user-specified growth rate value (in percentages) and the number of years that the growth rate occurs. For example, if the user specifies a growth rate of 5% over 10 years, the total number of vehicles will grow by compounded increments of 5% over the 10 years. If the growth is set at 5% for 4 years, and 0% for 6 years, the total number of vehicles will grow by 5% for the first 4 years, and the growth rate will remain stagnant for the next 6 years. Table 2.4 provides examples.

Table 2.4: Examples of How Growth Rate Is Calculated

	Yr. 1	Yr. 2	Yr. 3	Yr. 4	Yr. 5	Yr. 6	Yr. 7	Yr. 8	Yr. 9	Yr. 10
5% for 10 years	100	105	110	116	122	128	134	141	148	155
15% for 4 years, 0% for 6 years	100	105	110	116	122	122	122	122	122	122

2.4.7.2 Market Penetration

When a vehicle model's market penetration (MP) is specified by the user in percentages, the change in market penetration is multiplied by the fleet size for that year (the fleet size is determined by the growth rate). Table 2.5 provides an example of how market penetration is calculated when the fleet size is unchanged for 10 years, and the 2008 Volvo XC70 is replaced by the 2011 Nissan Leaf at a rate of 5% annually.

Table 2.5: Example Showing How Market Penetration Is Calculated

Year	Yr. 1	Yr. 2	Yr. 3	Yr. 4	Yr. 5	Yr. 6	Yr. 7	Yr. 8	Yr. 9	Yr. 10
2008 Volvo XC70 with MP of -5% over 10 years	100	95	90	85	80	75	70	65	60	55
2011 Nissan Leaf with MP of +5% over 10 years	0	5	10	15	20	25	30	35	40	45
Total Fleet Size	100	100	100	100	100	100	100	100	100	100

2.4.8 Route Cost Calculation

CT-Vcost calculates the route cost in two segments: 1) time-based route cost, and 2) route-conditions-based cost. The total per mile cost is the sum of the time-based route cost and the route-conditions-based cost. The following subsections further explain these two cost types.

2.4.8.1 Time-Based Route Cost

Time-based route costs are costs that do not vary despite the type of route used. These are annual costs paid by the driver, and are determined by the number of miles driven annually, and not necessarily the condition of the routes. This category includes depreciation, finance, insurance, maintenance, and other costs (registration and permit fees). The per-mile cost of these are calculated by dividing the total cost of each item over the life of the vehicle by the total distance driven over the life of the vehicle. This results in a per-mile cost estimate over the life of the vehicle.

2.4.8.1 Route-Conditions-Based Cost

Route-conditions-based costs are determined by factors such as traffic congestion, traffic speeds, route distance, toll charges, pavement condition, and hourly and per-mile drive costs. Each cost item is independently determined for each section in the route for each vehicle, and the per mile cost of the route is the weighted average of all the sections in that route (see Equation 2.10).

$$\text{Route Cost}_{\text{per mile}} = \frac{\sum_{i=\text{section}}^{\text{Number of Sections}} \left(\text{Item Cost}_{\text{section cost per mile}_{\text{model}}} \times \text{Vehicle Count}_{\text{model}} \right)}{\text{Number of Sections}} \tag{2.10}$$

As discussed earlier in the Route Analysis module section of this report (Subsection 2.3.5), traffic congestion and traffic speeds determine fuel consumption (in MPG). Per-mile fuel cost and fuel tax are determined by dividing the fuel price (or tax) by the calculated fuel economy at that travel speed for each section (see Equations 2.11 and 2.12).

$$\text{Fuel Cost}_{\text{section cost per mile}} = \frac{\text{Fuel Price}}{FE_{\text{section}}} \tag{2.11}$$

$$\text{Fuel Tax}_{\text{section cost per mile}} = \frac{\text{Fuel Tax}}{FE_{\text{section}}} \tag{2.12}$$

Carbon footprint (CO_2 emissions) is calculated by multiplying fuel consumption by 19.4 lb (or 22.2 lb), the amount of CO_2 in every gallon of gasoline (or diesel).

Hourly driver cost is determined by traffic speeds and travel time. A user-specified hourly driver cost is multiplied by the travel time and divided by the distance travelled to determine the per-mile for each section (Equation 2.13).

$$\text{Hourly Driver Cost}_{\text{section cost per mile}} = \frac{\text{Hourly Driver Cost} \times \text{Travel Time}_{\text{section}}}{\text{Distance}_{\text{section}}} \tag{2.13}$$

The per-mile driver drive cost is the same as the user-specified per-mile driver cost. Toll charges are applied on a per-mile basis by dividing the user-specified section toll by the length of the section (Equation 2.14).

$$\text{Toll Cost}_{\text{section cost per mile}} = \frac{\text{Toll}_{\text{section}}}{\text{Distance}_{\text{section}}} \tag{2.14}$$

The total route cost is finally determined by summing the product of the per-mile route cost by the total route distance of each cost item (Equation 2.15).

$$\text{Total Route Cost} = \sum_{i=item}^{\text{Number of Items}} (\text{Route Cost}_{\text{per mile}} \times \text{Total Route Distance}) \tag{2.15}$$

2.5 Data Output

Depending on the analysis type selected by the user, CT-Vcost generates outputs into various formats. The three main types of output in CT-Vcost are the 1) Bar Chart, 2) Line Chart, and 3) Cumulative Line Chart. Other available chart types are the Pie Chart, which shows an annual percent distribution of the cost categories via the size of each slice of pie, and the Route Cost chart, which is a representation of route names and their respective costs. Output data can also be exported as a comma-separated value file (CSV), which can be utilized for other analysis types using spreadsheet software like Microsoft Excel. The following sections detail each of the analysis types described with sample output screens.

2.5.1 Bar Chart

The bar chart shows a breakdown of the total annual cost of the selected vehicle for the specified analysis period. This cost is broken into the following categories: Fuel Cost, Maintenance, Insurance, Finance, Depreciation, and Other Fixed Costs. An example screenshot is provided as Figure 2.15. When a bar is clicked, the annual data is represented as a pie chart, as illustrated in Figure 2.16. This shows a percentage distribution of all the cost categories. The

Multi-Vehicle outputs are similar to the Single Vehicle outputs, illustrated in Figures 2.15 and 2.16, except that more than one vehicle is analyzed and multiple vehicle outputs can be compared simultaneously. Also, bar chart values are not broken down by item (e.g., depreciation, fuel, etc.) but rather summed up as the total for each year in the analysis period. Navigation is based mostly on the icons described in the Quick Reference Guide.

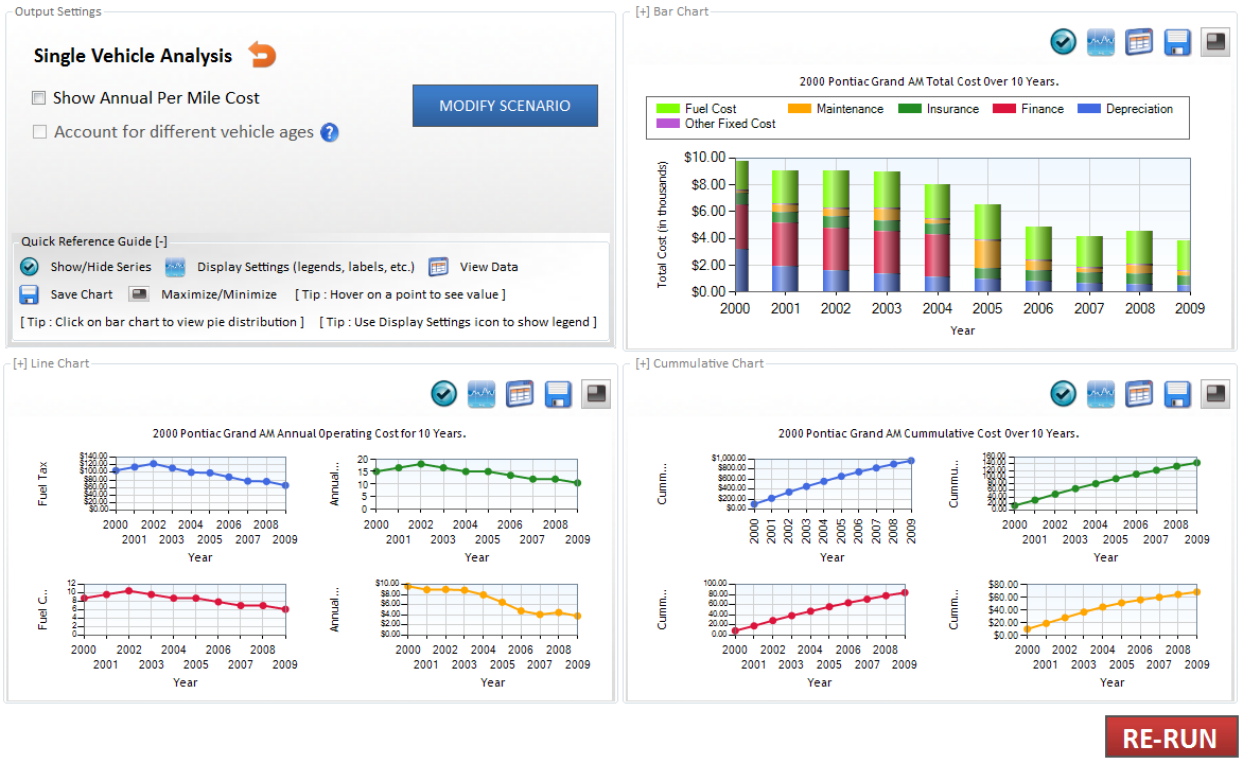

Figure 2.15: Typical Single Vehicle Analysis output screen.

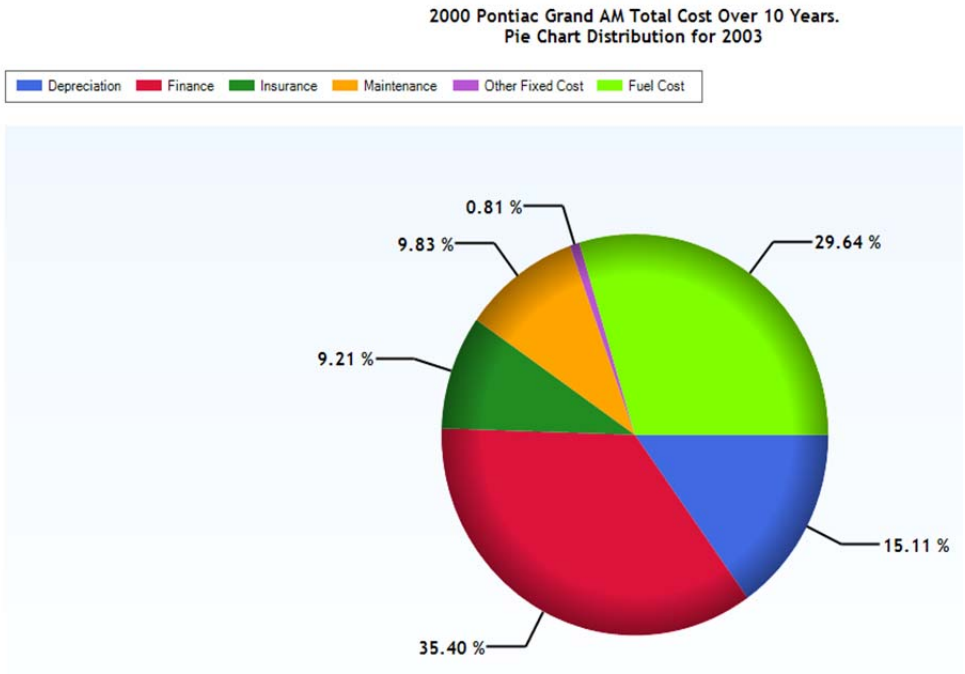

Figure 2.16: Pie chart showing percent distribution of cost categories.

2.5.2 Line Chart

Line charts separate operating costs into annual Fuel Tax, Annual Miles, Fuel Consumed, and Annual Operating Costs, as illustrated in Figure 2.17.

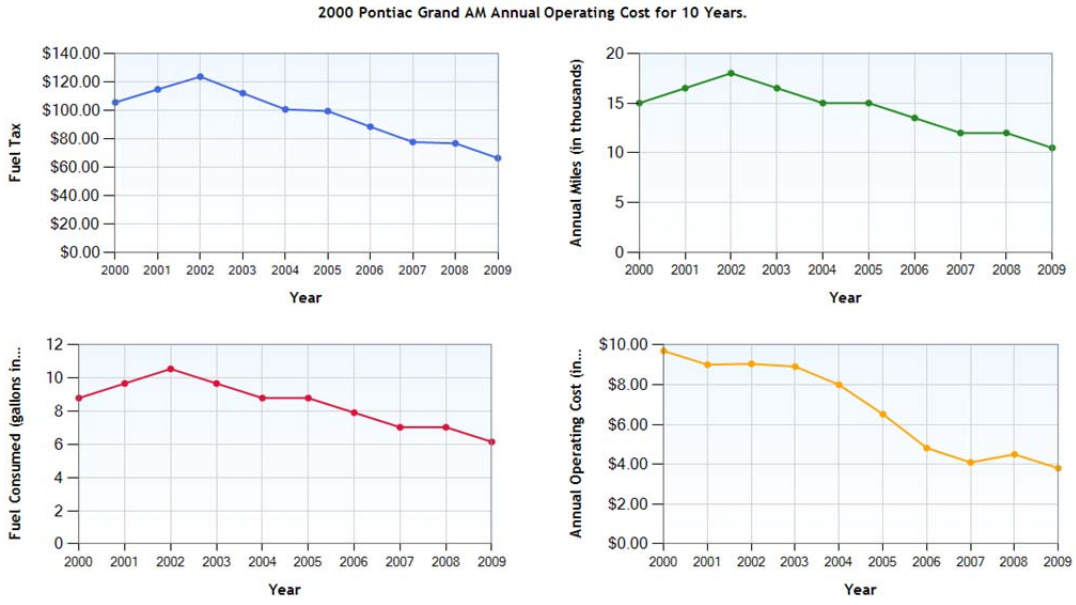

Figure 2.17: Line charts showing Fuel Tax, Annual Miles Driven, Fuel Consumed, and Annual Operating Cost (with their respective units).

2.5.3 Cumulative Line Charts

When this option is selected by the user, the cumulative charts show Cumulative Fuel Tax, Cumulative Annual Miles Driven, Cumulative Fuel Consumed, and Cumulative Operating Cost, as illustrated in Figure 2.18.

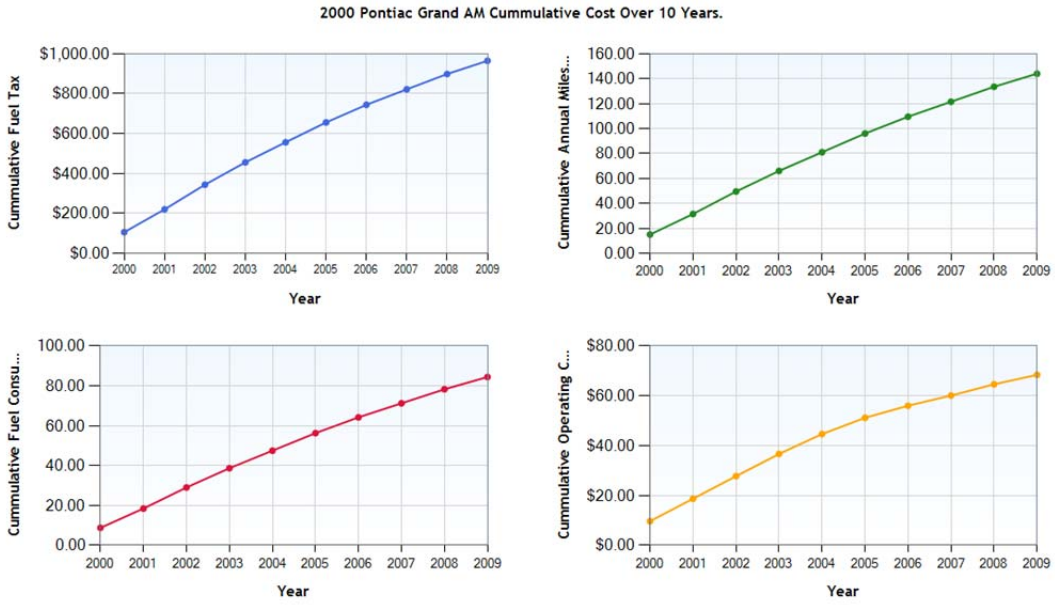

Figure 2.18: Cumulative Chart showing Cumulative Fuel Tax, Cumulative Annual Miles Driven, Cumulative Fuel Consumed, and Cumulative Operating Cost.

Chapter 3. The Fuel Economy Model

Developing models for the fuel economy of current vehicles is extremely important because 1) the prior fuel economy models are a quarter of a century out of date, 2) emissions regulations passed during the last 25 years, together with proposed emissions regulations, especially for heavy-duty vehicles, impacts fuel efficiency, and 3) the increasing price of fuel, together with new Corporate Average Fuel Economy (CAFE) standards and consumer demands, has had an impact on fuel efficiency, especially with respect to the introduction of hybrid cars and trucks. Therefore, the fuel economy models discussed in this chapter differ significantly from those available previously.

For the purposes of emissions and fuel economy regulations, the EPA and the U.S. Department of Transportation divide on-road vehicles into two categories: light-duty vehicles (LDVs) and heavy-duty vehicles (HDVs). To predict the vehicle performance in both the LDV and HDV classes, application of some fundamental principles of physics is required. Following is the final form of the equation for the fuel economy of a vehicle:

$$FE_{no\ wind} = \frac{(\eta_{ti}\eta_c\eta_m)\eta_T\eta_D[\rho_f LHV_P]}{m_e\frac{dV}{dt} + A + B\cdot V + C\cdot V^2 \pm W_{tot}\sin\theta}$$

where $FE_{no\ wind}$ is the fuel economy of the vehicle when the effects of the wind are negligible, the terms within the parentheses are the three fundamental efficiencies of the engine (the "indicated thermal" efficiency or efficiency of the thermodynamic cycle, η_{ti}, times the combustion efficiency; the efficiency the combustion process in converting the chemical energy of the fuel into thermal energy, η_c, times the mechanical efficiency; the efficiency of overcoming frictional and parasitic losses, η_m), η_T is the efficiency of the transmission, η_D is the efficiency of the differential, the terms in square brackets are two properties of the fuel (the physical density, ρ_f, times the chemical energy density or "constant pressure Lower Heating Value" LHV_P), V is the vehicle speed, m_e is the effective mass of the vehicle, and A, B, and C are the coastdown coefficients that represent the combined effects of aerodynamic drag and rolling resistance of the tires. The final term in the denominator accounts for the effect of the grade on the fuel economy, where θ is the angle of the grade and W_{tot} is the loaded weight of the vehicle.

The fuel economy model is discussed in general terms in Section 3.1. Details with respect to LDVs are presented in Section 3.2. Section 3.3 covers HDVs.

3.1 Introduction to the Fuel Economy Model

The physical basis for the fuel economy model is the subject of Subsection 3.1.1. The program logic is the subject of Subsection 3.1.2.

3.1.1 Physical Basis for the Fuel Economy Model

Figure 3.1 is an illustration of the forces resisting the movement of a vehicle driving on a road at a steady speed.

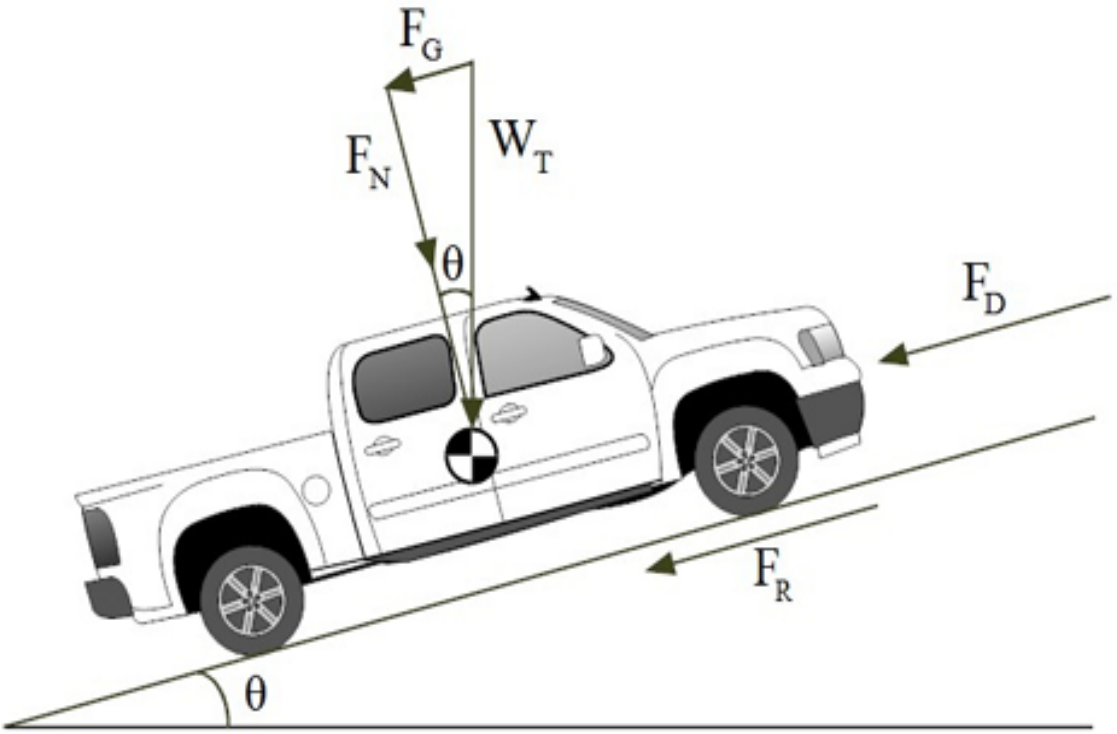

Figure 3.1: Forces acting on a vehicle driving at steady speed.

Newton's Second Law of Motion can be applied to this vehicle (Equation 3.1):

$$F_{net}=F_{mot}-F_{res}=m_e a=m_e \frac{dV}{dt} \tag{3.1}$$

In Equation 3.1, F_{mot} is the motive force at the tire-road interface, F_{res} is the total force resisting the forward motion of the vehicle, m_e is the effective mass of the vehicle (the inertia of the rotating masses must also be overcome when the vehicle accelerates), a is the acceleration of the vehicle in the direction of motion, and V is the vehicle speed. The motive force is the result of the engine torque, as multiplied (inefficiently) in both the transmission and the differential. For a vehicle that is traveling at constant speed, the total resistive force is the result of various individual forces that are additive. These forces are the aerodynamic drag force, F_D, the rolling resistance (friction between the tires and road surface), F_R, and the force imposed by a grade, F_G (Equation 3.2):

$$F_{res}\big|_{V=constant}=F_D+F_R+F_G \tag{3.2}$$

At one time, the EPA required the vehicle manufacturers to determine the drag force via wind tunnel tests and to determine the rolling resistance using tire test machines. However, due to approximations and/or uncertainties in these tests, it was determined that the combined effects of aerodynamic drag and rolling resistance are best determined using "coastdown tests." SAE International's Recommended Practice J1263 describes how on-road coastdown tests can be used

to determine the "road load coefficients." In practice, the coastdown data generally yields a second order fit that includes a term that is linear in vehicle speed (Equation 3.3):

$$F_{res}\big|_{coastdown} = m_e \frac{dV}{dt} + f_0 + f_1 V + f_2 V^2 \tag{3.3}$$

where f_0, f_1, and f_2 are the "target" (i.e., actual on-road, as opposed to on a chassis dyno) coastdown coefficients and the first term on the right hand side is the inertial force. In theory, f_1 should be zero but in practice it is more often non-zero due to the characteristics of the tires. In fact, the tires have a strong effect on the coastdown results. Thus, Equation 3.2 can be restated as Equation 3.4:

$$F_{res}\big|_{V=constant} = f_0 + f_1 V + f_2 V^2 \pm W_{tot} \sin\theta \tag{3.4}$$

where the last term is the grade resistance, the product of the total weight of the vehicle times the sign of the angle of inclination of the grade. Equation 3.4, like Equation 3.2, is valid for a vehicle that is traveling at constant speed. In the more general case when the vehicle is either accelerating or decelerating, the total resistive force is shown in Equation 3.5:

$$F_{res} = m_e \frac{dV}{dt} + f_0 + f_1 V + f_2 V^2 + W_{tot} \sin\theta \tag{3.5}$$

It can be shown that the fuel economy of a vehicle, whether light-duty or heavy-duty, under "road load" conditions (level road with no wind), FE_{RL}, can be calculated from Equation 3.6a:

$$FE_{RL} = \frac{(\eta_{ti}\eta_c\eta_m)\eta_T\eta_D[\rho_f LHV_P]}{m_e \frac{dV}{dt} + f_0 + f_1 V + f_2 V^2} \tag{3.6a}$$

In Equation 3.6a, the terms within the parentheses are the three fundamental efficiencies of the engine (the "indicated thermal" efficiency or efficiency of the thermodynamic cycle, η_{ti}, times the combustion efficiency; the efficiency the combustion process in converting the chemical energy of the fuel into thermal energy, η_c, times the mechanical efficiency; the efficiency of overcoming frictional and parasitic losses, η_m), η_T is the efficiency of the transmission, η_D is the efficiency of the differential, the terms in square brackets are two properties of the fuel (the physical density, ρ_f, times the chemical energy density or "constant pressure Lower Heating Value" LHV_P), V is the vehicle speed, m_e is the effective mass of the vehicle, and f_0, f_1, and f_2 are the coastdown coefficients that represent the combined effects of aerodynamic drag and rolling resistance of the tires.

In Equation 3.6b, the grade resistance term can be incorporated in the denominator of Equation 3.6a if the driving schedule includes a grade (grade as a function of time or distance traveled):

$$FE_{no\ wind} = \frac{(\eta_{ti}\eta_c\eta_m)\eta_T\eta_D[\rho_f LHV_P]}{m_e \frac{dV}{dt} + \{A+BV+CV^2\} \pm W_{tot}\sin\theta} \quad (3.6b)$$

In Equation 3.6b, for convenience the "target" (from actual on-road tests) coastdown coefficients have been given the symbols A, B, and C rather than f_0, f_1, and f_2.

This approach for calculating fuel economy is applicable to both LDVs and HDVs. The EPA publishes coastdown coefficients for all LDVs sold in the U.S. because they are subjected to fuel economy and tailpipe emissions standards (http://www.epa.gov/otaq/crttst.htm). However, because HDVs are not yet subjected to fuel efficiency standards, coastdown coefficients are not readily available for HDVs. In contrast, coastdown coefficients are available for European HDVs (Petrushov, 1997; Petrushov, 1998).

The application of Equation 3.6 to LDVs is discussed in Section 3.2. Section 3.3 provides a discussion of the fuel economy models generated for HDVs.

3.1.2 Fuel Economy Model Program Logic

One of the inputs to the fuel economy model is the driving schedule (or driving cycle), which is typically a prescription of vehicle speed each second and which normally both begins and ends with the vehicle stationary. Furthermore, except for the driving cycles developed for TxDOT Project 0-5974, the grade is zero for all other driving cycles. The coastdown coefficients for the vehicle of interest are also inputs, as is the weight of the vehicle (many of the model inputs are implicit within the model, such that the user does not need to input them directly). As discussed in Subsection 3.1.1, these model inputs are sufficient to completely specify the resistive force each second during the driving cycle, as long as there is no grade resistance. If the vehicle acceleration/deceleration is small, as is the case for most driving cycles, Newton's Second Law of Motion dictates that the motive force must equal the resistive force.

The motive force times the rolling radius of the drive tires is the torque applied to the tire/road interface. This torque is produced by the engine after inefficient multiplication in both the transmission and differential (for front-wheel drive cars, the transmission and differential are contained within the same housing: the transaxle).

This suggests two different methods for determining the fuel consumption each second during the driving cycle: the "backward approach" and the "forward approach." In the backward approach, the motive torque applied via the drive axles and the drive axle rpm (known from the vehicle speed and tire rolling radius) are known. One would then call the differential submodel to calculate the differential input (driveshaft) torque and rpm. Next, the backward approach model would call the transmission submodel to calculate the transmission input torque and rpm, which are necessarily the engine output torque and engine rpm. Finally, the model would call the engine submodel to extract the fuel consumption during that second of the driving cycle. This logic would be repeated for every second of the driving cycle until the driving cycle ended. However, the program logic for the transmission and differential submodels is convoluted because the programmer must work his or her way "upstream" through each of these devices.

In the forward approach, the program logic must include a "driver submodel." The driver submodel controls the accelerator pedal position (the "torque demand") in an attempt to produce the correct vehicle acceleration for each second of the driving cycle. The accelerator pedal position is controlled by the driver submodel based on the difference between the calculated vehicle speed and the desired vehicle speed during that second of the driving cycle (the fact that

these do not perfectly match is the source of the main drawback of this approach). The algorithm monitors the difference between the desired vehicle speed and the calculated vehicle speed (both the value of the error and the rate of change of the error). If the error is large or is becoming large, the throttle position is adjusted up or down accordingly. During deceleration portions of the driving cycle, the algorithm first determines whether or not the rate of change of vehicle speed can be accomplished solely via the combination of engine compression braking (for spark ignition engines and also diesel engines with "Jake brakes"), aerodynamic drag, rolling resistance, and—if applicable for this driving cycle—grade resistance. If this combination is insufficient to produce the required deceleration, the driver submodel applies the brakes. The brakes are controlled in a similar way to the accelerator pedal position. There is an upper limit to the value of the brake force based on the locked wheel braking limit. The friction coefficient between the tires and the pavement is assumed to be 0.90. The accelerator pedal position from the driver submodel is also used as an input to the transmission shift algorithm as well as the engine submodel.

The torque demand output from the driver submodel is an input to the engine submodel. Given the required engine torque, the brake mean effective pressure (BMEP) is calculated. The BMEP is used by engine engineers as a normalized measure of torque, rather than using the torque directly, because the BMEP allows various engines to be directly compared.

When a manual transmission is simulated, except during a shift, the required engine rpm for that second of the driving cycle is calculated from the corresponding vehicle speed plus the tire rolling radius, the differential gear ratio, and the transmission gear ratio.

Given the BMEP and engine rpm, the brake specific fuel consumption map for that category of engine (e.g., light-duty spark ignition) is "read" by the engine submodel, which returns the brake specific fuel consumption (BSFC) that corresponds to that BMEP (load) and engine speed (rpm). The BSFC is the ratio of the fuel consumption rate to the brake power output from the engine at that same combination of BMEP and rpm. The brake power is simply calculated by the engine submodel ($bp=2\pi\tau N$, where N is the engine rpm, τ is the torque, and bp is the brake power). In turn, the fuel consumption rate (typically in g/hr) is calculated from the BSFC and bp. Vehicle speed (e.g., miles/hour) divided by fuel mass flow (e.g., in grams/hour) yields the instantaneous fuel efficiency in miles/gram. Accounting for the density of the fuel yields the fuel economy in miles/gallon. While this might at first seem sufficient, it must be recalled that the driver model has chosen a torque demand, the accuracy of which is still uncertain at this point in the calculations. The engine output torque (which equals the torque demand from the driver submodel) is multiplied inefficiently in both the transmission and differential, yielding the torque applied at the drive wheels. This torque must produce the desired acceleration/deceleration and vehicle speed, or the original torque demand by the driver model was inaccurate.

When the vehicle is stationary, the engine is idling. For heavy-duty diesels, the fuel consumption rate at idle was developed from a study performed by Lim (2003). The relationship for the idle fuel consumption of heavy-duty diesel engines is shown in Equation 3.7a:

$$\dot{V}_{f,idle,HDD}=0.0382D \tag{3.7a}$$

where D is the displacement of the engine in liters. Equation 3.7a provides the mass consumption rate of diesel fuel in gallons/hour. For light-duty gasoline engines, the idle fuel consumption rate

was developed (Equation 3.7b) by combining some equations presented by Nam and Giannelli (2005):

$$\text{"Fuel mep"=Fmep}=\frac{(\dot{m}_f \text{LHV}_p)x}{D \cdot \text{N}} = 2.47 \cdot \text{bmep} + 4.24 \tag{3.7b}$$

where N is the is the engine speed [rpm], Fmep is the fuel mean effective pressure [bar], x is 2 for an engine that operates on the 4-stroke cycle [revolutions/intake-stroke], and BMEP is the BMEP [bar], an engine engineer's method of specifying the normalized engine output. Because the engine does not produce any useful work at idle (other than what is required to overcome frictional and parasitic losses), Equation 3.7b can be modified and rearranged to yield Equation 3.7c:

$$\dot{m}_{f,\text{idle}} = 4.24 \frac{\text{D}}{\text{LHV}_p} \frac{\text{N}_{\text{idle}}}{\text{x}} \tag{3.7c}$$

The transmission submodel is called next. The algorithm first selects from the various types of transmissions: 1) light-duty manual, 2) light-duty automatic, 3) heavy-duty manual, and 4) heavy-duty automatic. Given the transmission input torque and speed (the engine output torque and rpm) and the transmission gear ratio, the transmission submodel calculates the transmission output torque (driveshaft torque for a rear-wheel drive vehicle), the transmission output speed (driveshaft rpm for a rear-wheel drive vehicle), and transmission efficiency. However, one of the required inputs is the gear ratio, which of course depends upon which gear is engaged.

Thus, a "shift strategy submodel" is also required. This shift strategy submodel can be perceived as part of the driver submodel for manual transmissions but must be part of the transmission submodel for automatic transmissions. The transmission shift pattern depends on the transmission input speed and load, but there are many arbitrary elements, similar to a typical stick-shift driver. This is true even for an automatic transmission because the shift pattern for an automatic transmission is controlled, in modern vehicles, by a microprocessor and the logic built into this microprocessor must be mimicked by the shift strategy submodel. The basic logic behind the shift pattern, however, is that the higher the throttle position, the longer the lower gear remains engaged. At full throttle, the lower gear is maintained all the way to the upper speed limit of the engine, assuming that maximum acceleration is required. As the throttle position is relaxed, the speed at which a higher gear ratio is selected is reduced. The selection of speed versus up-shift, however, is arbitrary. Many modern vehicles have a shift indicator on the dash giving the driver with a manual transmission a recommendation to up-shift or not, but of course there is no guarantee that the driver actually follows that recommendation. The shift strategy submodel incorporates two types of down-shifting. The first type is when the vehicle speed slows down due to the requirements of the driving cycle and the engine speed gets too close to its idle speed. When that happens, a down-shift is ordered by the shift strategy submodel. The second type of down-shift is demanded by the shift strategy submodel whenever the relative accelerator pedal position exceeds 90% and the engine speed is below a threshold. Both of these numbers are rather arbitrary, and a different down-shift threshold might produce better vehicle speed tracking (see driver model).

Also, if the vehicle accelerates in low gear from either a complete stop or very low speed, the clutch of a manual transmission is allowed to slip by the shift strategy submodel. Therefore, if the engine speed is less than the "clutch speed," it is assumed that the driver slips the clutch. That allows the engine speed to operate at a more favorable rpm to accelerate the vehicle. There is an inherent energy loss by this, taken into account by the calculations. This simple logic is replaced by a torque converter algorithm for the automatic transmission. The torque converter is more complicated because the torque converter also multiplies the engine output torque before it becomes the transmission input torque, and the converter will slip for certain operating conditions in all gears, not just first gear.

The shift strategy submodel also includes a shift delay. The shift delay (set at 0.3 seconds) eliminates any engine motive force during the shift delay period, after a shift has been ordered. This may be a more important factor for HDVs that take longer to shift and have many more gear ratios that they have to go through.

Given the transmission output torque and speed (the differential input torque and rpm) and the differential gear ratio, the differential submodel calculates the differential output torque (drive axle torque), the differential output speed (drive wheel rpm), and differential efficiency.

Thus, the engine torque is translated into a motive force at the wheel axles by multiplying by the engaged transmission gear ratio, transmission efficiency under these conditions, differential gear ratio and efficiency, and dividing by the rolling radius of the tires. The total resistive force of the vehicle is subtracted, and the forward acceleration calculated, and integrated over the time period (again, generally 1.0 s for most driving cycles) to calculate the change of speed over the time step. This calculated speed is checked against the required speed at that point in the driving cycle. A tolerance of $\pm$2 mph is allowed because this tolerance is also typical when a car is driven on a chassis dyno over a driving cycle during emissions and fuel economy testing. The speed is then integrated again to calculate distance traveled during that time increment. This distance is used to calculate average fuel economy over that time increment and also used as input for a lookup table of distance traveled versus road elevation to calculate grade resistance for those rare driving cycles that have a non-zero grade (such as those developed as part of TxDOT Project 0-5974).

Thus, the required inputs to the fuel economy model are 1) the driving cycle (driving schedule) selected by the user (additional driving cycles can also be input by the user), 2) the vehicle weight, 3) the coastdown coefficients (these are implicit inputs, the user is not required to know them or input them directly), 4) drive tire rolling radius (the user must enter the tire size, obtainable from the sidewall of the tires), 5) engine specifications (displacement, rated power, and peak engine rpm), 6) transmission type (automatic or manual) and gear ratios, and 7) differential (axle) gear ratio and type (e.g., four-wheel drive and all-wheel drive vehicles have two differentials and a transfer case, and this is an implicit input).

3.2 Light-Duty Vehicles

Because manufacturers of LDVs must comply with CAFE standards, the fuel economy model developed for TxDOT Project 0-5974 provides the user with two options:

1) the EPA/NHTSA urban (city) and highway fuel economy, and
2) the ability to perform fuel economy calculations for other driving cycles

For the first option, our research team downloaded data for ~5,000 light-duty 2000–2012 model year vehicles from fueleconomy.gov. This website provides the official urban and highway fuel economy for all LDVs sold in America. The urban and highway fuel economy figures are the result of experiments performed following the protocols established by the EPA (in charge of emissions standards and measurement techniques) and the National Highway Traffic Safety Administration (NHTSA), the arm of the U.S. Department of Energy responsible for fuel economy standards and measurement techniques. These two agencies combine with respect to fuel economy measurements because the same driving cycles are used for both emissions and fuel economy measurements. The user of our model can choose from among these ~5,000 vehicles and the program automatically returns the official urban and highway fuel economy for that vehicle and model year.

The standardized driving cycles currently used for determining compliance with emissions standards and/or are used for measuring the fuel economy of LDVs are the following:

1) the light-duty Federal Test Procedure (FTP), as amended in 1975; often called the 75 FTP;
2) the highway fuel economy test procedure, HFET,
3) a high-speed, hard-acceleration driving cycle, the US06;
4) a driving cycle during which the air conditioning system is always on, the SC03; and
5) the "cold FTP" (for the 75 FTP, the vehicle is stored for 12–36 hours at 68–86 ^{o}F [20–30 ^{o}C] for the cold FTP, the vehicle is stored at 20 ^{o}F before the FTP driving cycle is performed).

Until 2008, the urban fuel economy for each vehicle was determined solely via the 75 FTP test and the highway fuel economy was determined solely via the HFET test. However, due to complaints by consumers that their vehicles never achieved the official fuel economy, the NHTSA developed a formula for calculating the urban fuel economy using fuel economy data from all five cycles. They also developed a different formula for calculating the highway fuel economy using fuel economy data from all five cycles. It was later determined (Federal Register, Vol. 71, No. 248, pp. 77886–77888, Dec. 27, 2006) that the improved fuel economy values could be obtained more simply using just the 75 FTP and HFET fuel economy results via Equations 3.8 and 3.9:

$$FE_{urban} = FE_{city} = \frac{1}{\left(0.003259 + \frac{1.1805}{FE_{FTP}}\right)} \tag{3.8}$$

$$FE_{highway} = \frac{1}{\left(0.001376 + \frac{1.3466}{FE_{HFET}}\right)} \tag{3.9}$$

Coastdown coefficients for LDVs are discussed in Subsection 3.2.1. Driving cycles for LDVs are discussed in Subsection 3.2.2. The various submodels that were developed for predicting the fuel economy of conventional LDVs are discussed in Subsection 3.2.3. The protocol for running the model for predicting the fuel economy of conventional (non-hybrid)

LDVs is discussed in Subsection 3.2.4. The model for light-duty hybrids is the subject of Subsection 3.2.5.

3.2.1 Light-Duty Coastdown Coefficients

All manufacturers of LDVs sold in America must experimentally measure their coastdown coefficients and supply them to the EPA. In turn, the EPA uses them to set the chassis dynamometer resistive load as a function of vehicle speed. Additionally, the EPA posts the coastdown coefficients on their website. Our research team downloaded the coastdown coefficients for approximately 5,000 light-duty 2000–2012 model year vehicles from http://www.epa.gov/otaq/crttst.htm. When the user of either our VCost model or our fuel economy model selects an LDV from the extensive pull-down menu, the corresponding coastdown coefficients are automatically loaded.

3.2.2 Light-Duty Driving Cycles

The fuel economy model developed for TxDOT Project 0-5974 incorporates two standardized driving cycles: 1) the light-duty FTP and 2) a hard-acceleration, high-speed driving cycle, the US06. However, because TxDOT needs a fuel economy model that can be used to estimate TxDOT's revenue from on-road fuel taxes, our research team was asked to develop driving cycles for at least two conditions: congested and freeflow highway driving. Because IH 35 through downtown Austin has been determined to be one of the five most congested highways in Texas, we selected it for development of our driving cycles, shown in Figure 3.2.

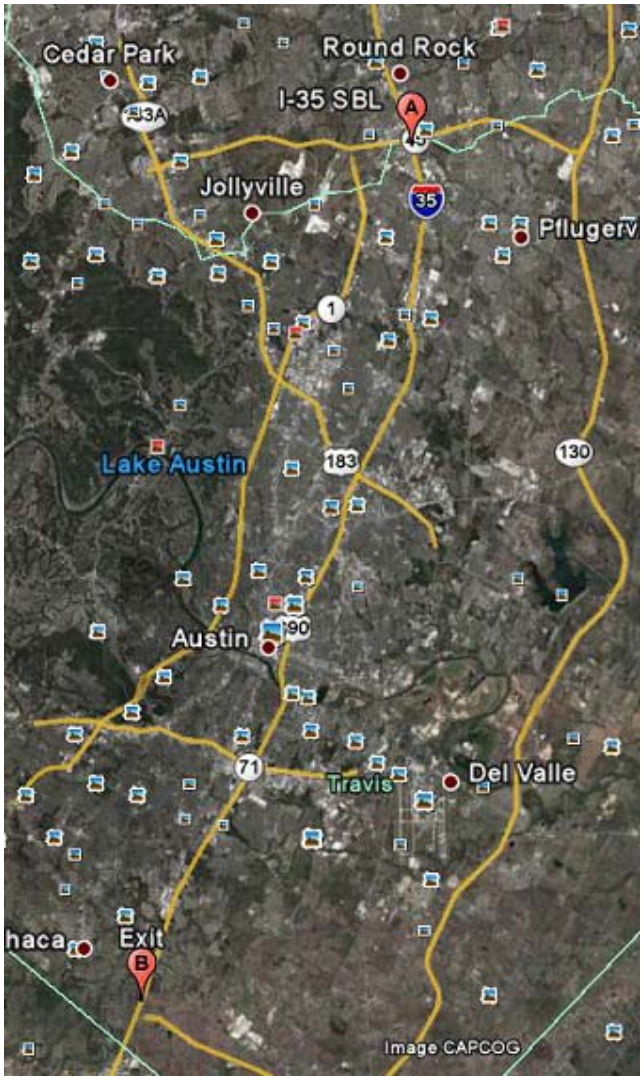

Figure 3.2: Driving cycle data collection route on IH 35 from point A to point B.

Driving cycles for the LDV simulation were recorded on the route shown in Figure 3.2 from point A to point B on IH 35. Data was collected at three different times of the day: 7:30 a.m., 9:30 a.m., and 11:00 a.m. by three different drivers (yielding nine driving cycles for LDVs). These times were recommended by TxDOT drivers. Unfortunately, near the end of the project we learned that afternoon rush hour traffic on IH 35 is significantly worse than morning rush hour traffic, but it was too late to perform both the experiments and the calculations required to analyze the afternoon rush hour traffic.

The distance from point A to point B (Figure 3.2) on IH 35 is 26.9 miles. A 2010 Ford Escape, shown in Figure 3.3, was used to log the driving cycle data.

Figure 3.3: 2010 Ford Escape FlexFuel used in drive cycle data collection.

A GPS data logger, which is capable of logging data onboard the test vehicle, was used to log vehicle speed and elevation every 1 second. A GPS antenna was placed on the roof of the vehicle to improve accuracy while the main unit was located on the dashboard, as shown in Figure 3.4. Scantool.net's ElmScan 5 on-board diagnostics (OBD) reader was used to log engine and vehicle data to a laptop computer using ScanXL software. Driving cycles were generated by using GPS data arrays of vehicle speed and elevation as functions of time. These two arrays combine to form a driving cycle. Here, it should be noted that the vast majority of standardized driving cycles do not account for elevation (grade). However, elevation can have significant effects, especially when simulating the fuel economy of HDVs. Our fuel economy model will calculate the average fuel consumption for that driving cycle. Fuel flow rates were recorded from the engine through the OBD port, and this data was used as a benchmark against our simulations.

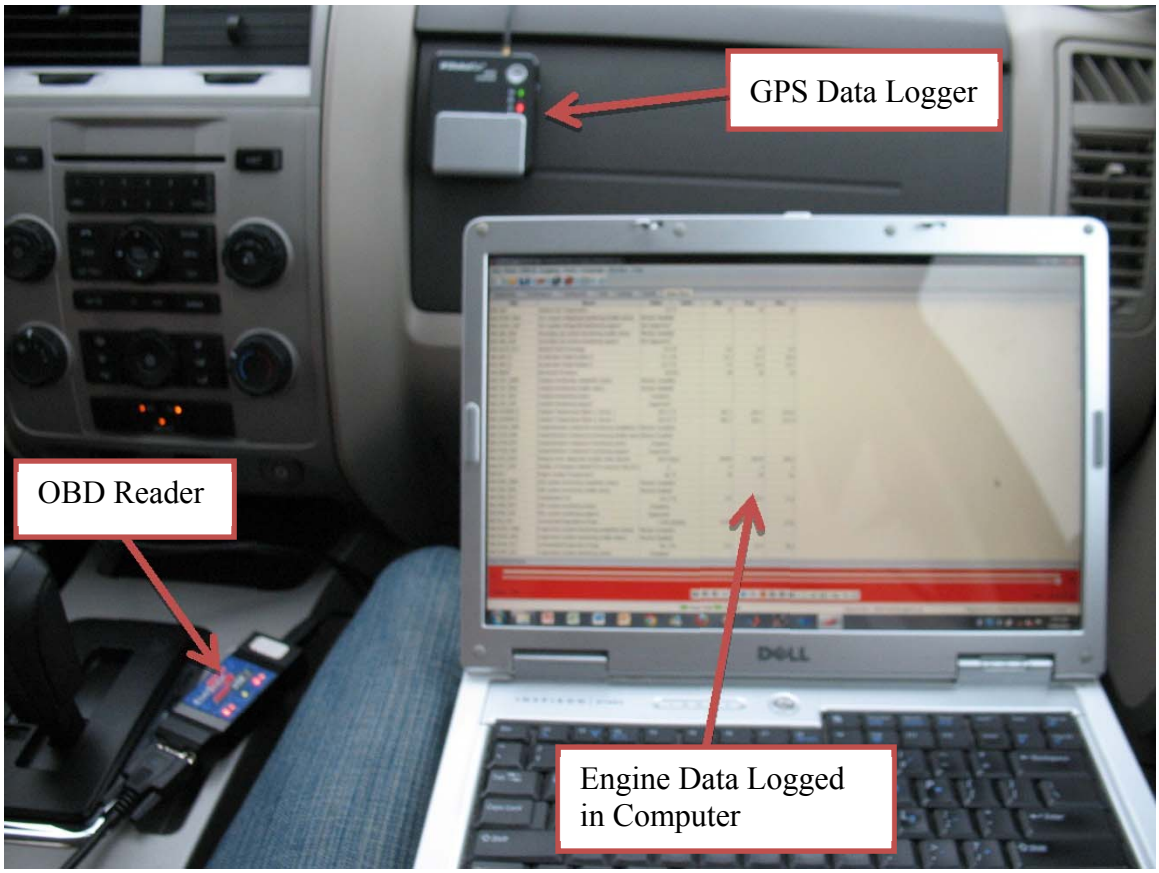

Figure 3.4: Data logging setup for an LDV.

Recorded vehicle speed vs. time data at 7:30 a.m. is shown in Figure 3.5. The average speed for this driving cycle is 42.4 mph and the total driving cycle time is 37 minutes and 51 seconds.

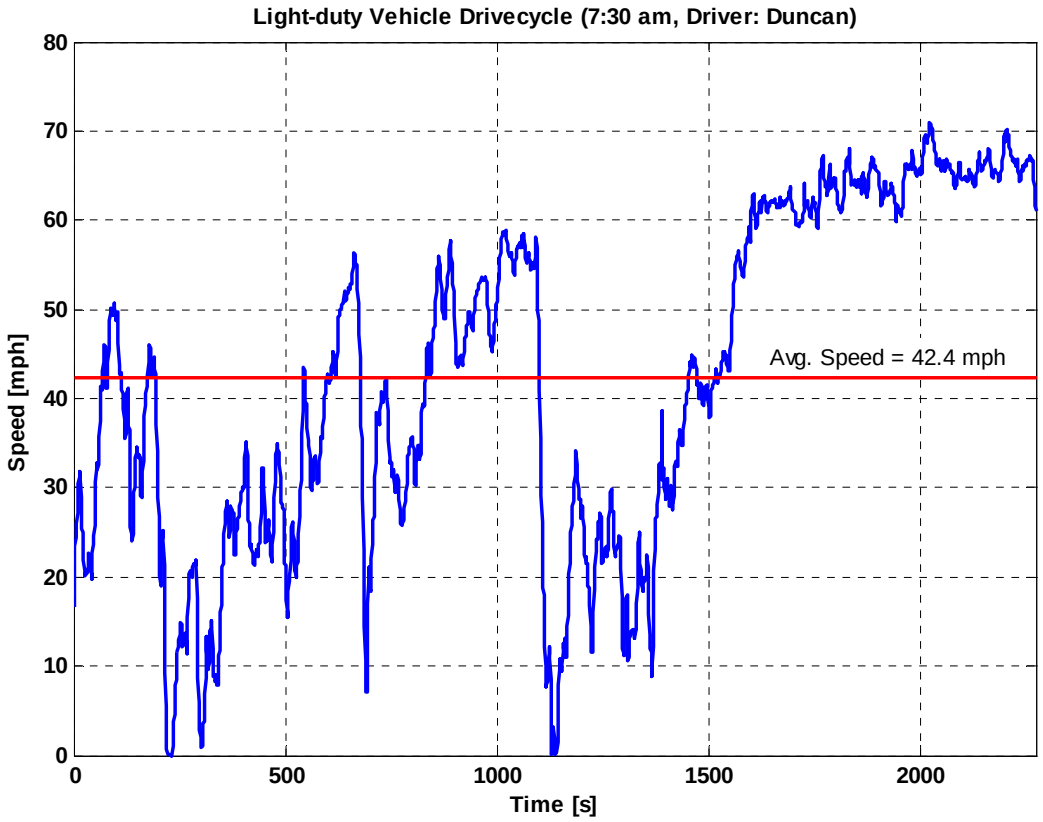

Figure 3.5: An example of an LDV driving cycle.

GPS data naturally has some noise in both the speed and the altitude (elevation) data. We did not smooth the speed data because vehicle speed naturally has some noise due to the vibration of tires and road conditions. However, noise in the altitude data results in big grade differences, which further results in unrealistic road grades. Therefore, it was necessary to smooth the altitude data along with the distance to estimate the road grade correctly.

To this end, the road elevation data was smoothened with a local regression using a weighted linear least squares and a 2nd degree polynomial model. A robust version of this model that assigns lower weight to outliers in the regression was implemented. The method assigns zero weight to data outside six mean absolute deviations. Figure 3.6 shows the whole driving cycle elevation data along with the smoothened data. Some of the details in the GPS elevation data are lost due to unrealistic gradients.

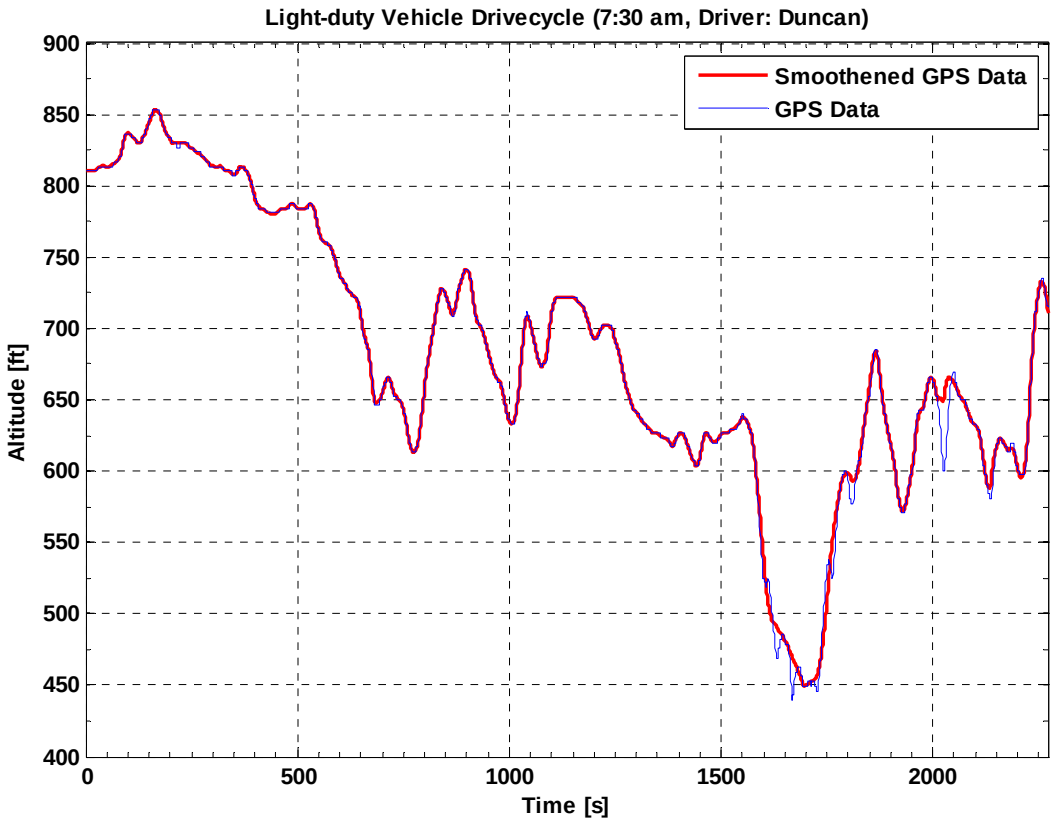

Figure 3.6: Comparison of GPS altitude data and smoothened data.

Figure 3.7 shows a "zoomed in" section of Figure 3.6, illustrating the non-physical (or noisy) nature of the GPS elevation data. Such aspects of the elevation data were removed by smoothening without losing the elevation data.

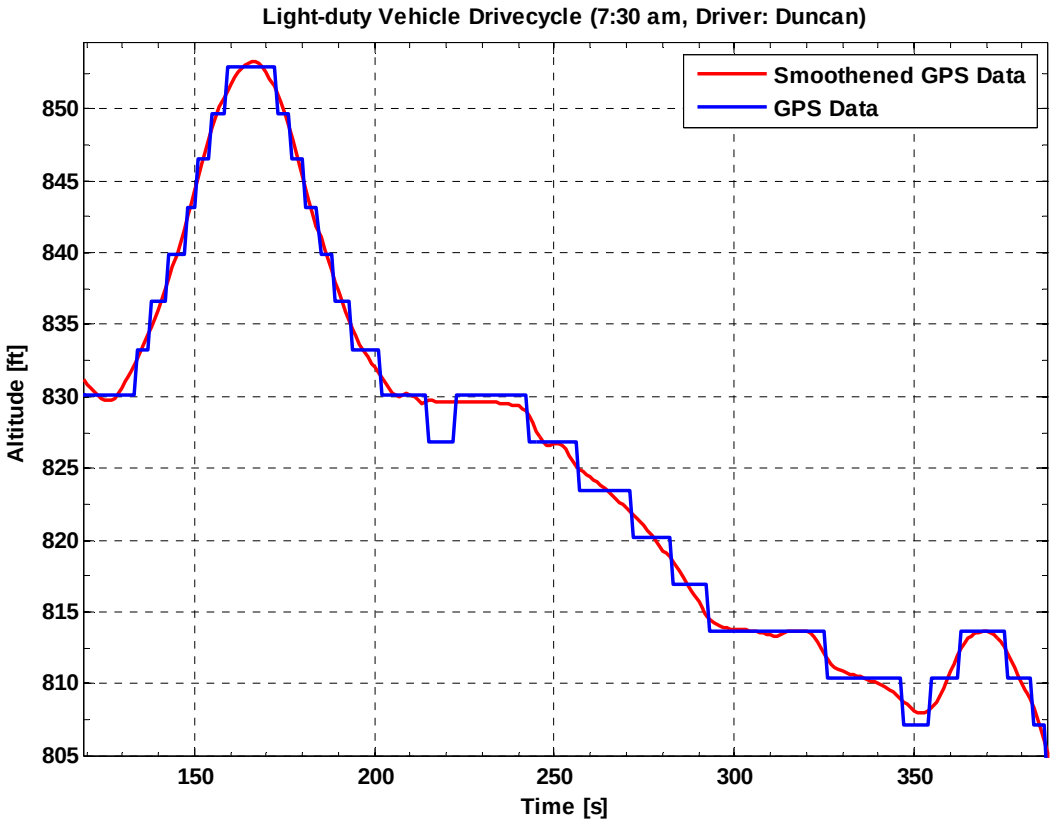

Figure 3.7: Noise in logged GPS data was removed by smoothening the elevation data.

3.2.3 Elements of the Light-Duty Vehicle Fuel Economy Model

As noted previously, the urban and highway fuel economy for ~5,000 LDVs has been downloaded and is available to the user of our VCost and fuel economy models. However, if the user wishes to have the program calculate the fuel economy for the US06, FTP, or Texas LDV driving cycles, our program uses subroutines that perform simulations for the engine, transmission, and differential. Each of these subroutines is briefly discussed below. Details are provided in the appendices. Our model for light-duty hybrids is briefly discussed in Subsection 3.2.4.

3.2.3.1 Light-Duty Engine Submodel

Because our research team has developed an award-winning model for spark ignition engines in the past (the Fractal Engine Simulation, UT FES), it was proposed that we use that model for this aspect of our fuel economy model. However, UT FES was written in the first scientific computing language, Fortran, and a suitable Fortran compiler could not be found. It was also determined that re-writing UT FES into a modern computer language, such as Matlab, required more time than was available for this project. Thus, an alternative method for simulating the engine was required.

The BSFC is an engine engineer's method for quantifying fuel efficiency. It is the ratio of the fuel consumption rate to the power produced at any combination of torque and engine speed (rpm). It is used because it is easily measured, whereas the "indicated thermal efficiency" or the

"brake thermal efficiency" requires sending a sample of the test fuel to a chemical lab for analysis of the constant pressure Lower Heating Value. The BSFC is inversely proportional to fuel efficiency; one wants fuel efficiency to be as high as possible, which also means that one wants the BSFC to be as low as possible.

Maps for the BSFC for three light-duty engines were acquired and used to assess the efficiency of the engine in converting the chemical energy of the fuel to useful rotational mechanical energy at the engine output shaft. One of the engines selected was a "push rod" engine (cam in the block), one was a double overhead cam engine, and the third was the Miller cycle engine used in the Toyota Prius. The BSFC maps for these three engines show "islands" with a periphery of constant BSFC on a graph of BMEP versus percent peak engine speed. The BMEP is used by engine engineers as a measure of the load on the engine (the torque/work or power output). They use the BMEP because it normalizes the power or torque by the displacement and the number of strokes per cycle. This allows easy comparison between two engines, whether they are very similar or very dissimilar. That is, the BMEP allows easy scaling so that the BSFC map for one engine can be scaled for use in simulating any other engine.

The (scalable) BSFC map for the double overhead cam engine was used for all LDVs except light-duty trucks and light-duty hybrid electric vehicles (HEVs). The (scalable) BSFC map for the push rod engine was used for all light-duty trucks. The Miller cycle engine model was used for all light-duty HEVs. Here it should be noted that not all light-duty trucks use push rod engines and not all light-duty cars have double overhead cam engines. Additionally, not all light-duty HEVs use Miller cycle engines. However, the research team believes that the inaccuracies encountered via these assumptions are reasonably small.

3.2.3.2 Light-Duty Transmission Submodel

Most LDVs in the U.S. have automatic transmissions but some have manual transmissions. Thus, models were developed for both, as discussed in detail in Appendix B.

It was decided that a representative light-duty manual transmission and a representative light-duty automatic transmission would be selected and modeled in detail. A method was developed to scale these two models to yield generalized models that are suitable for any light-duty manual transmission and for any light-duty automatic transmission.

Specifics regarding the detailed models for the representative transmissions are provided in Appendix B. The method developed for scaling these two transmissions is also discussed in Appendix B.

3.2.3.3 Light-Duty Differential Submodel

Compared to engines and transmissions, differentials are perhaps less complex. However, just as options exist for engines (with respect to fuel type, thermodynamic cycle, number of cylinders, etc.) and transmissions (automatic or manual, number of gears, etc.), the remaining powertrain configurations can differ in the number of differentials and may also include a transfer case.

For LDVs, four differential models were developed to capture the current vehicle market's powertrain configurations. These models belong to two groups: two wheels driven and four wheels driven. The two-wheels-driven configurations are front-wheel drive (FWD: transaxles) and rear-wheel drive (RWD). A finer distinction exists between the four-wheels-driven configurations: four-wheel drive (4WD) and all-wheel drive (AWD). Though both of the latter configurations can power all four wheels under certain conditions, 4WD vehicles

commonly operate with the transfer case disengaged, causing the engine to power just the rear two wheels (as is the case with RWD). By contrast, AWD powertrains power all four wheels all of the time. Instead of using a transfer case, AWD vehicles may use a center differential, a viscous coupling, or a transfer clutch.

Because the powertrain configuration may differ so widely, modeling a light-duty differential requires a model for each of the four configurations (FWD, RWD, 4WD, and AWD). Hence, the top level of the differential efficiency subroutine must choose between FWD, RWD, 4WD, and AWD. This information needs to be stored for each vehicle just like the coastdown coefficients and other parameters mentioned previously. Once a differential category is chosen, each of the light-duty differential submodels requires as inputs a scaled version of torque coming into the differential, the rotational speed of the shaft transmitting the torque into the differential, and the gear ratio associated with the differential. Once provided with these inputs, the light-duty differential submodel calculates and provides the differential efficiency, a scaled torque coming out of the differential, and the rotational speed of the shafts transmitting the torque out of the differential.

The efficiency output from the differential submodel is useful for creating an efficiency map before the drive cycle simulation begins so that the drive cycle simulator can use a two- or three-dimensional efficiency look-up table. (The extra dimension is the gear ratio, and the other two dimensions are the scaled torque and speed inputs. The gear ratio dimension option is feasible for the light-duty models but not for all of the heavy-duty models.) This option can be used to save computational time: in this case, the code must perform a linear interpolation within the efficiency map rather than computing the efficiency using the differential subroutine at each time step of the drive cycle. Figure 3.8 is a visual representation of a two-dimensional efficiency map. The torque and speed outputs from the differential subroutine are used by the vehicle submodel to calculate the instantaneous vehicle speed and instantaneous vehicle acceleration at each time step during the driving cycle. Running the differential submodel at each time step versus generating 2D or 3-D lookup tables have associated computational storage and processing demands, as illustrated in Table 3.1.

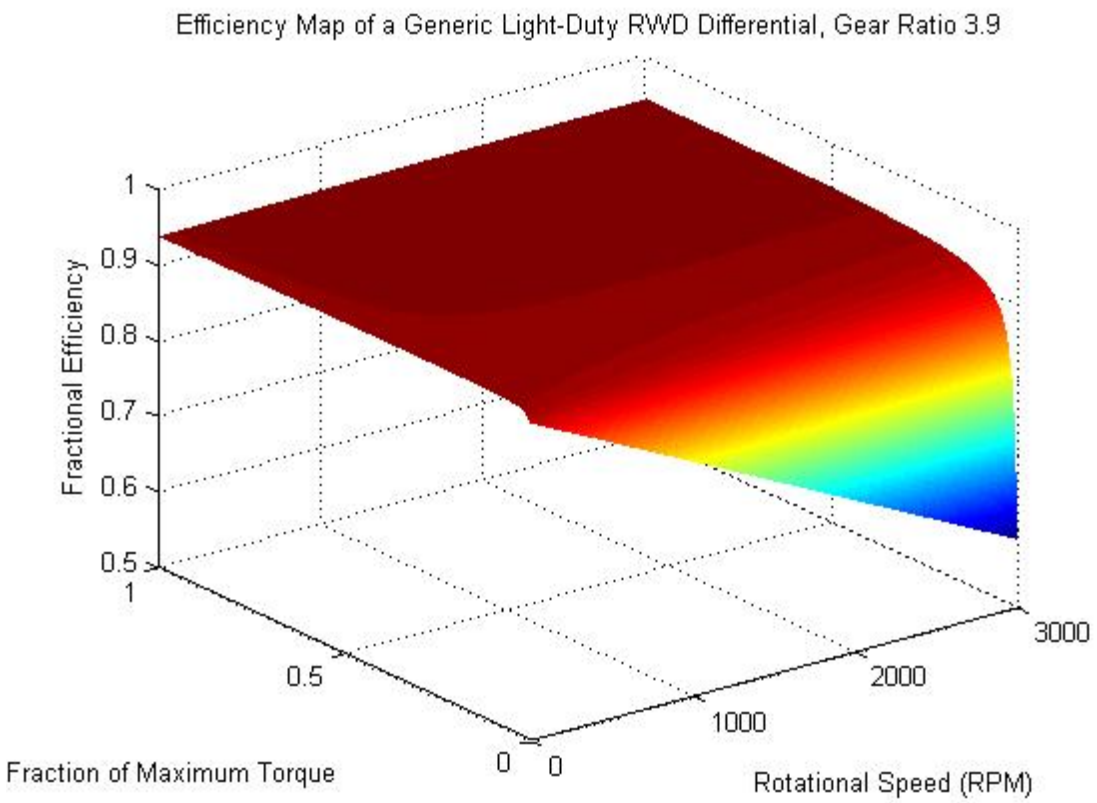

Figure 3.8: Visual representation of a differential's efficiency map in two dimensions.

Table 3.1: Storage and Processing Demands of Various Differential Model Implementations.

Calculation Method	In-Situ Calculation	2-D Interpolation	3-D Interpolation
Storage Efficiency	Best	Better	Good
Processing Speed	Good	Better	Best

Proof-of-concept tests have been run for the FWD and RWD configurations, upon which the other light-duty and the heavy-duty differential submodels are based. The FWD proof-of-concept test compared data taken from a 1980s era Volkswagen Rabbit's 4-speed manual transaxle with the 5-speed manual transmission and FWD differential models. The results for first gear are presented in Figure 3.9, which shows that the models match the data fairly well. The comparisons are similar for the other gears.

First Gear Efficiency Prediction

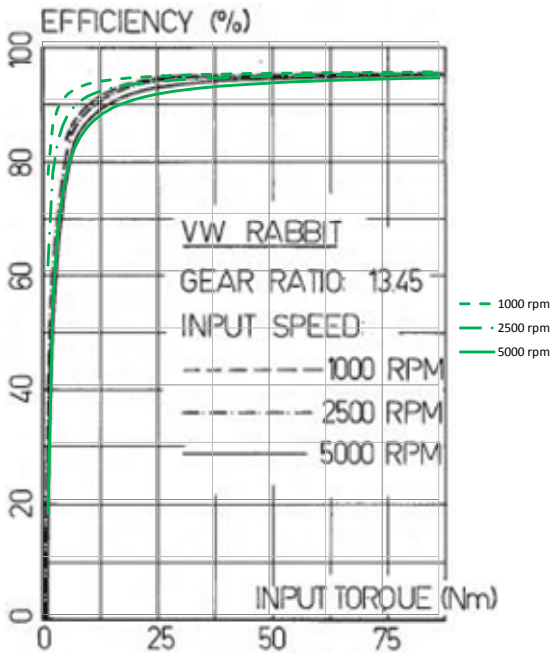

Figure 3.9: Application of the differential submodel to available transaxle data (van Dongen, 1982).

The RWD proof-of-concept test compared a curve-fit from experimental data to the efficiency of a differential operating in a vehicle at constant speed and under road load with the RWD differential model applied to vehicles for which the EPA provided coastdown coefficients and tire specifications, operating under similar conditions. The results are presented in Figure 3.10. Though the fit between the model and the data is visually poor, the model represents an improvement over differential models that assume constant-efficiency. Furthermore, the operating conditions have the differential operating only under low torques, where a slight miscalculation in torque is amplified in the efficiency. In addition, the source of the experimental data and the methods used to obtain the curve-fit or the data upon which it is based have eluded the research team. Finally, the tire size model used in this test has since been modified and will improve the accuracy of the model both at low speed and high speeds.

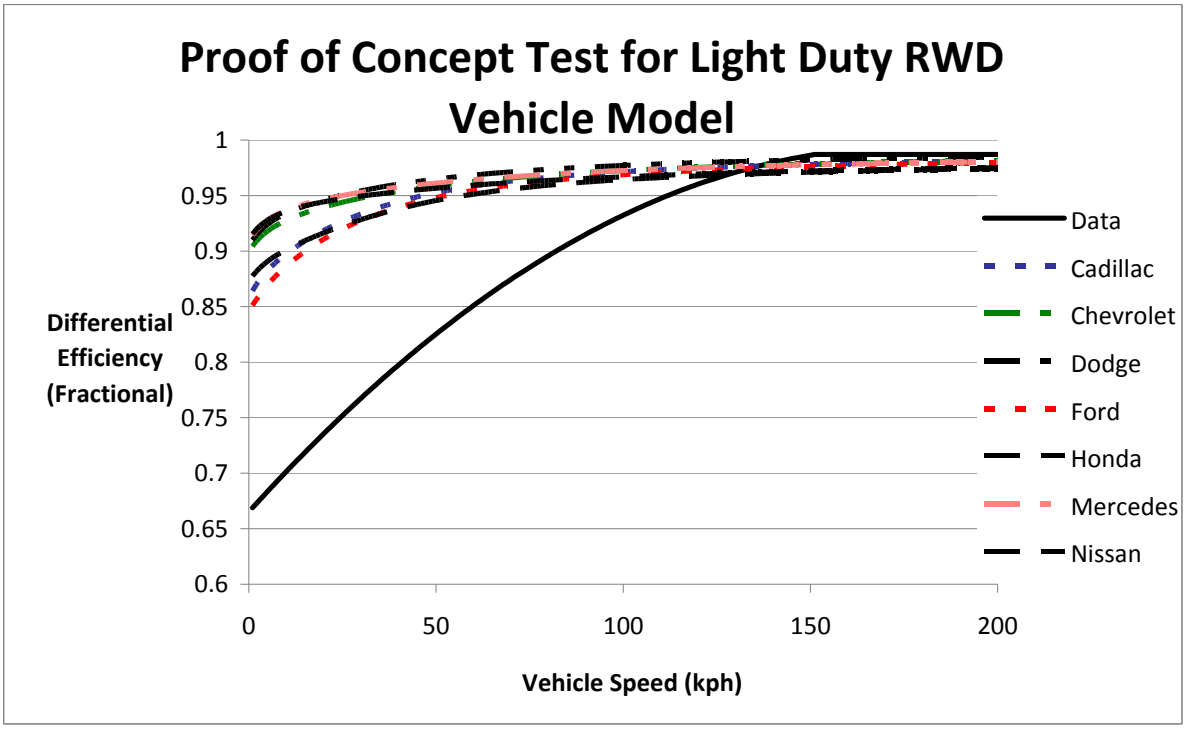

Figure 3.10: Simulated differential efficiency for several RWD vehicles compared to experimental data for a RWD vehicle for which specifics are not available.

The present differential efficiency model was produced within a finite timeframe and with a finite budget. As a result, several areas of the model could be improved. The differential component efficiencies could all be updated. Specifically, the windage loss models could be done through direct numerical simulation to increase accuracy. In addition, friction coefficient models for the gear pairs and seals could be improved. Also, a finite element analysis of the gear pairs would also improve the accuracy of the model. More proof-of-concept tests would increase confidence in the model and allow for some fine-tuning of some of the model parameters. Consideration of bias in torque distribution and bearing loading would improve the accuracy of the model. Limited slip differentials have their own parasitic losses even when not being operated in a mode that uses the limited slip feature, and improving that segment of the model would enhance the model's accuracy. The model still needs a calculation for unconfined aerodynamic shaft windage losses. The chain drive model for the transfer case in 4WD and AWD powertrains could be improved. Consideration of universal and constant-velocity joints would enhance the model's accuracy. Factoring in the effects of vehicle age and wear would also improve the accuracy of the differential model. A vibration model would provide some insight into critical speeds for some of the components of the differential. It is certain that other considerations exist that would enhance the accuracy of the differential model, but these effects are all secondary in comparison with the effects considered in the present model.

3.2.4 Running the Model for the Fuel Economy of Conventional Light-Duty Vehicles

As noted, the user can also choose to have our model perform fuel economy calculations for other driving cycles:

1) US06
2) FTP (the light-duty FTP)
3) HFET
4) Texas LDV (an LDV driving on IH 35 through Austin with three different levels of congestion and three different drivers, for a total of nine Texas LDV cycles)
5) "Constant speed" drive cycle (30–70 mph every 5 mph)

The FTP and HFET are provided as options so that the user can run these two simulations and then apply Equations 3.8 and 3.9 to compare the results of these simulations with the official city and highway fuel economy values provided on the output page.

A separate Fuel Economy model will be delivered after the final modifications have been completed. Thus, the following describes how the user can run the fuel economy model from CT-Vcost. The user of the CT-Vcost model will first see a screen with a "start" button. After selecting this button, the user is taken to the screen shown in Figure 3.11. This screen allows the user to select the type of analysis to be performed. For obtaining fuel economy results, the user should select either "heavy-duty vehicle drive cycles" or "light-duty vehicle drive cycles."

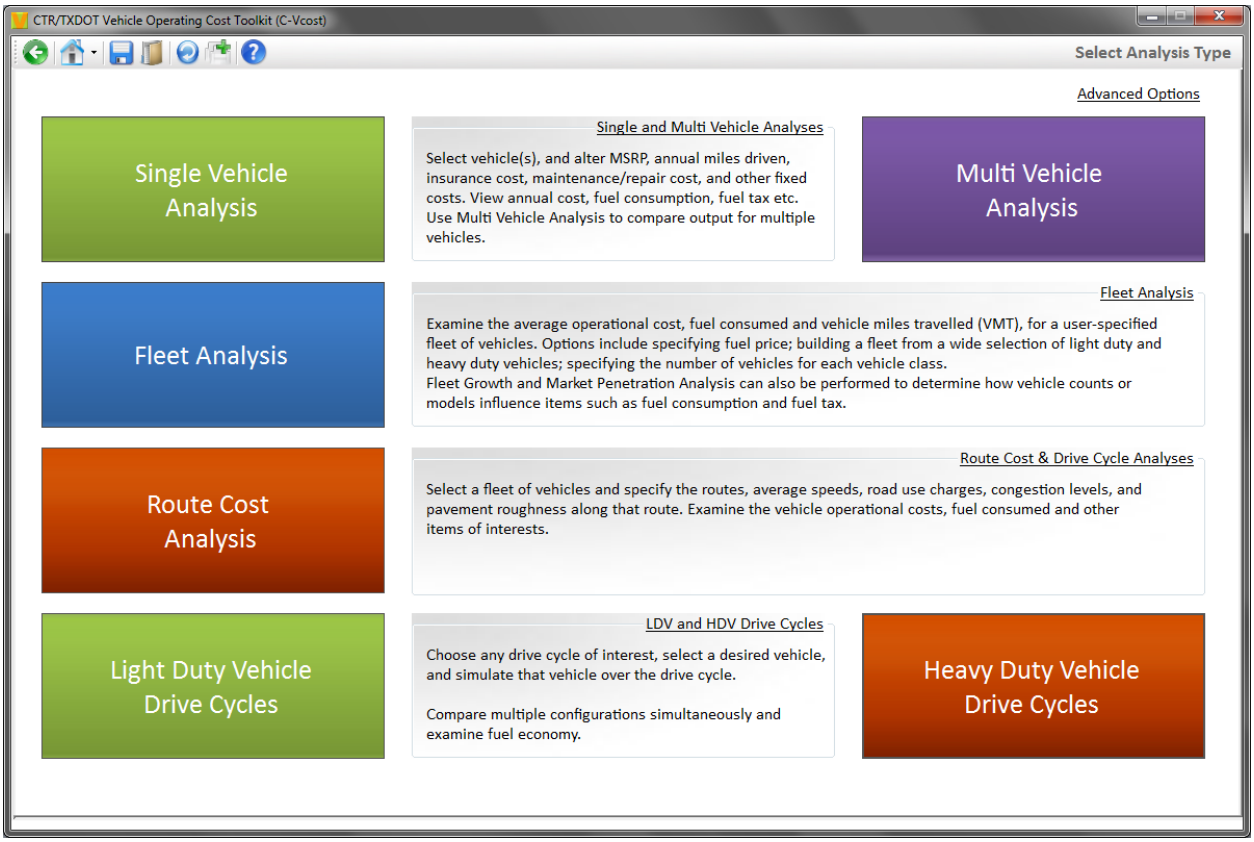

Note: If the user is solely interested in the fuel economy model, he or she should select either "Light Duty Vehicle Drive Cycles" or "Heavy Duty Vehicle Drive Cycles."

Figure 3.11: Screen shot of the CT-Vcost model page that allows the user to select the type of analysis to be performed.

If the user chooses “light-duty vehicle drive cycles,” the CT-Vcost page shown in Figure 3.12 will appear. The user must first select a vehicle from the more than 5,000 LDVs on the pull-down menu or, if the vehicle of interest to the user is not on the pull-down menu, the user can enter the required information for a vehicle of interest. If the user selects a vehicle from the list, the coastdown coefficients and vehicle test weight are automatically entered, as shown in Figure 3.13. If the user chooses not to select a vehicle from the list, the user must enter values for the coastdown coefficients.

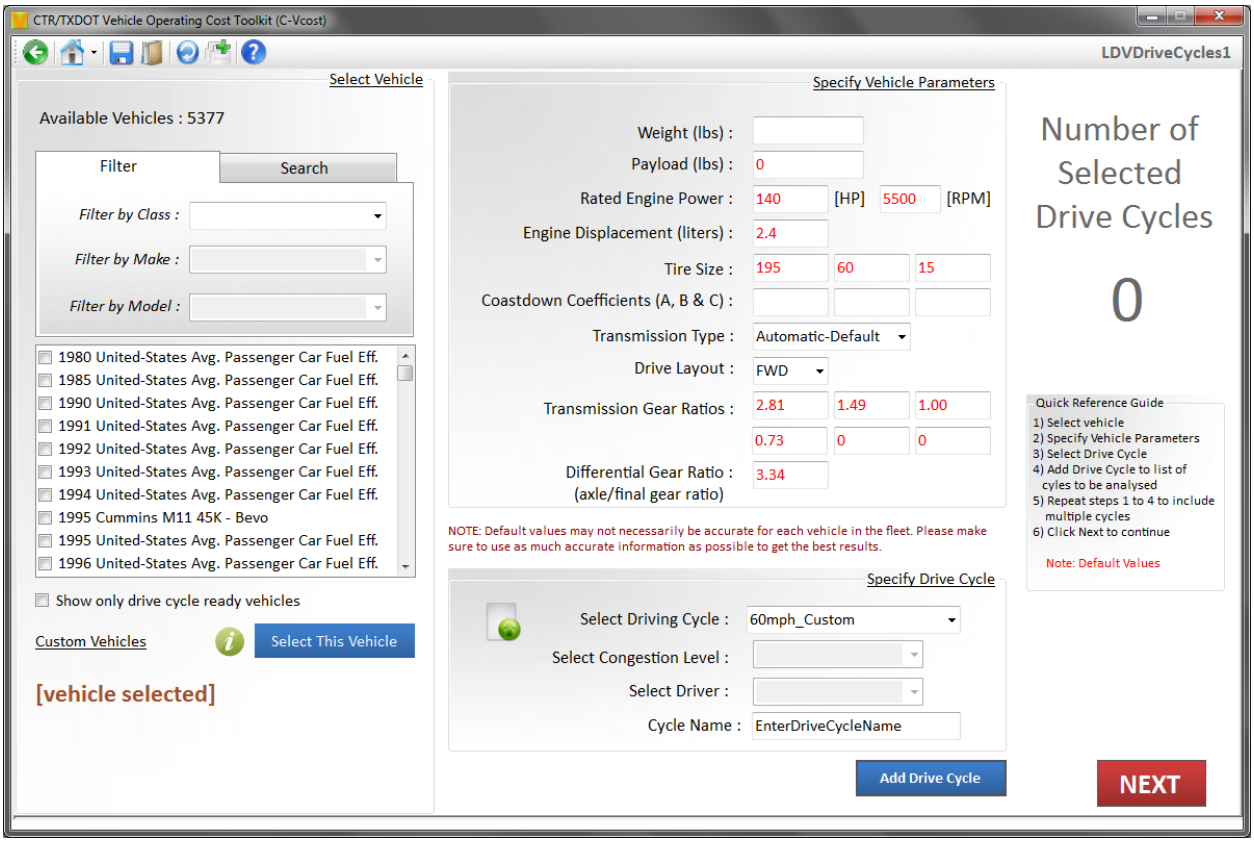

Figure 3.12: Screen shot of the first page of the “Light Duty Vehicle Drive Cycles” analysis.

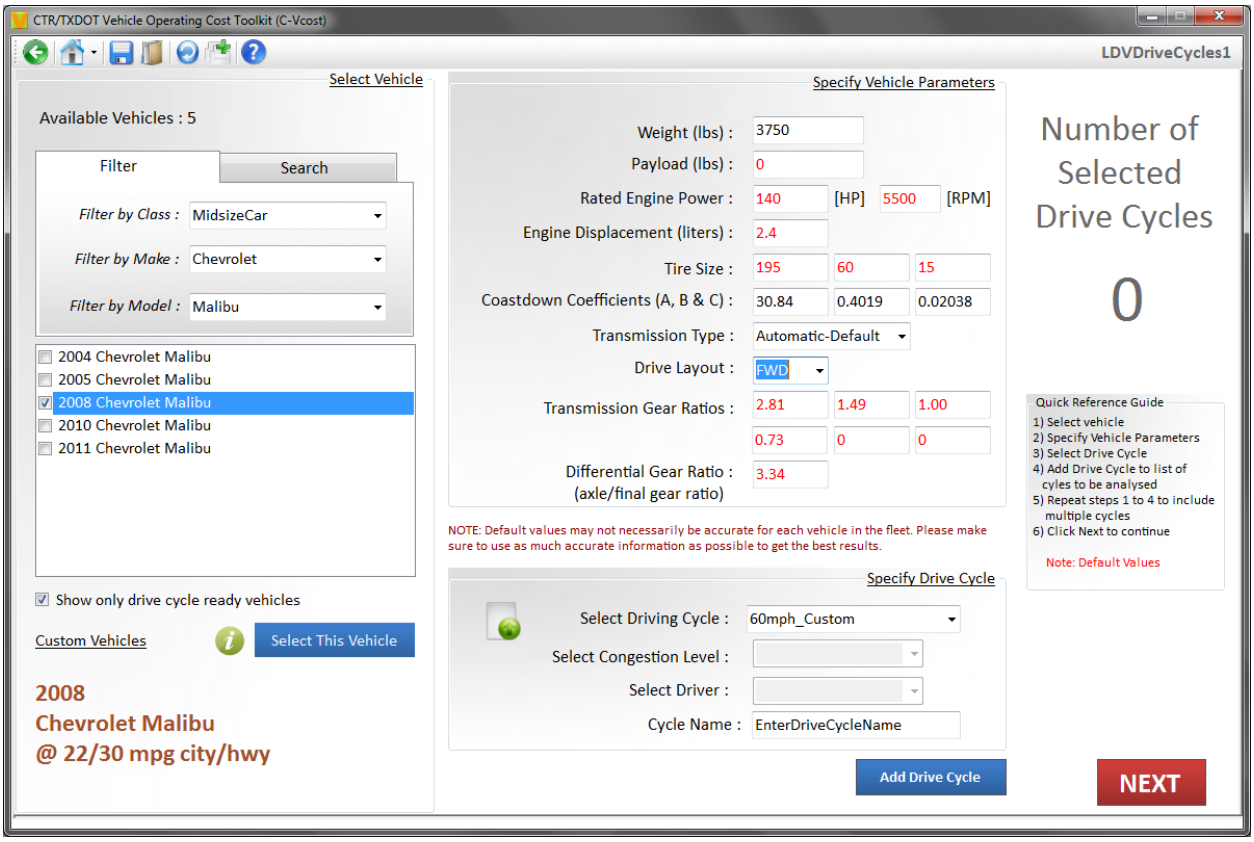

Note that the official EPA/NHTSA city and highway fuel economy values appear automatically as do the coastdown coefficients.

Figure 3.13: Screen shot illustrating selection of an LDV from the pull-down menu.

After the user has selected an LDV for analysis, the vehicle test weight and coastdown coefficients are automatically filled in. All users must enter specifics about the vehicle, replacing the default values that are in red on the screen:

1) payload weight (the official EPA/NHTSA payload for an LDV is 300 lbf but this is included in the test weight that is automatically filled in, so a payload weight of 0 is generally accurate),
2) rated engine power (in hp) at the rated engine speed (in rpm)
3) engine displacement (in liters)
4) tire size
5) transmission type from the pull-down menu illustrated in Figure 3.14
6) drivetrain layout from the pull-down menu illustrated in Figure 3.15: FWD, RWD, 4WD, or AWD
7) gear ratio in each of the transmission gears
8) differential gear ratio

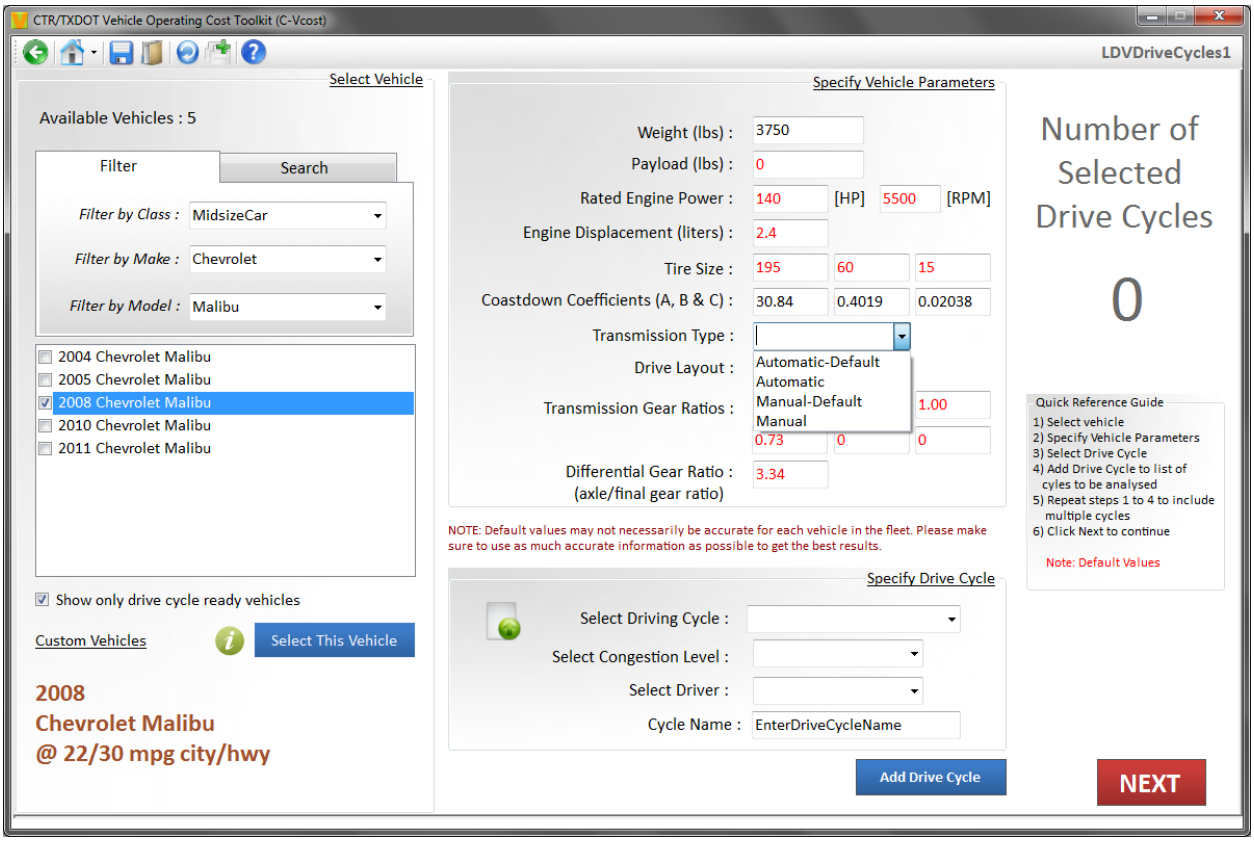

Figure 3.14: The pull-down menu for selection of the type of transmission after the user has selected an LDV for analysis.

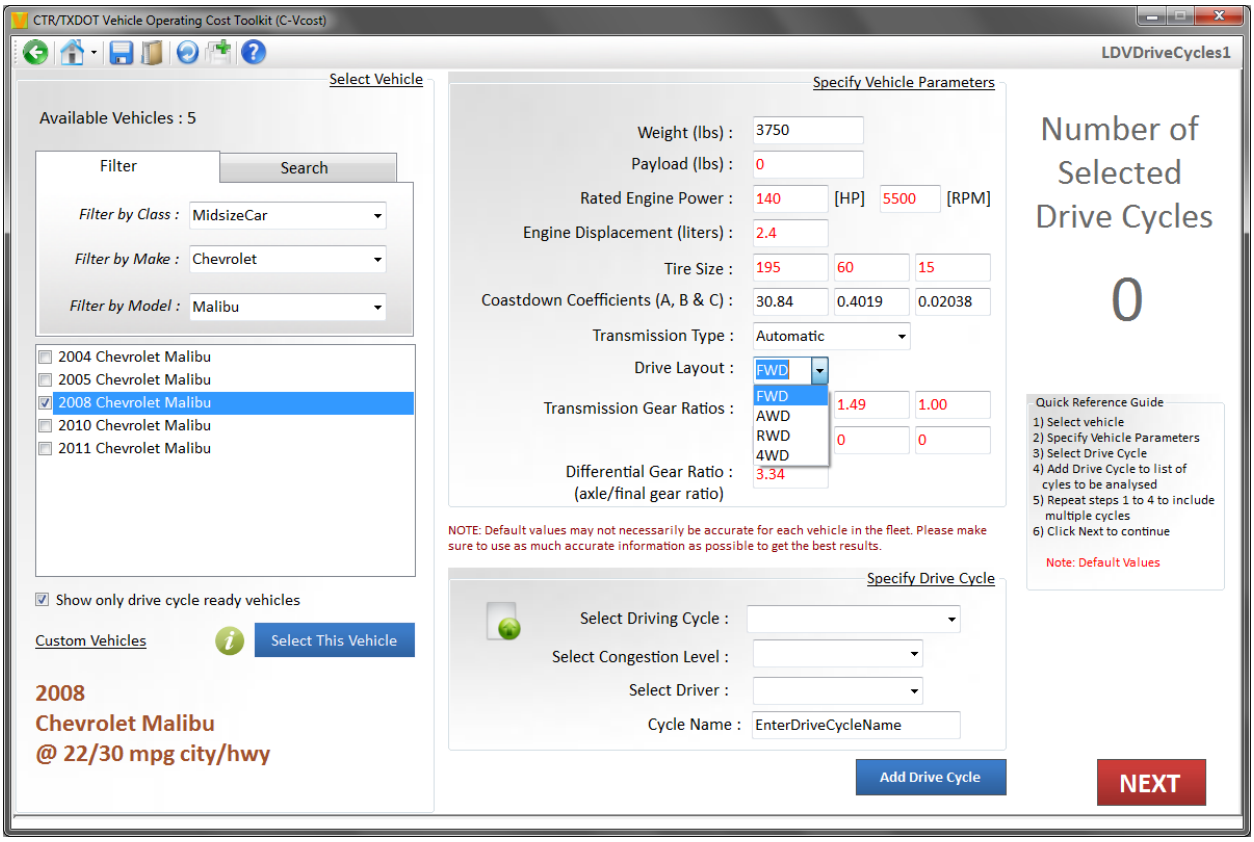

Figure 3.15: The pull-down menu for selection of the drivetrain layout after the user has selected an LDV for analysis.

The user must then select the driving cycle from a pull-down menu. As noted previously, the driving cycle options available from the pull-down menu include the following:

1) US06
2) FTP (the light-duty FTP)
3) HFET
4) Nine Texas LDV drive cycles
5) The "Constant Speed" drive cycle

If the user opts to run the Texas LDV driving cycle, the user must also choose the congestion level (congested, free flow, moderate), the driver (conservative, moderate male, moderate female), and a convenient name for the output.

If the "Constant Speed" drive cycle is selected, the user will get both a table and a graph of fuel economy as a function of speed, with calculations over the vehicle speed range from 30 to 70 mph in 5-mph increments.

Once a driving cycle is chosen, the user hits the "Add Drive Cycle" button and sees the screen shown in Figure 3.16. The user should then hit the "Next" button, and then will be taken to the page shown in Figure 3.17. In this case, the user has selected the US06 driving cycle, hit the "Add Drive Cycle" button and then the "Next" button.

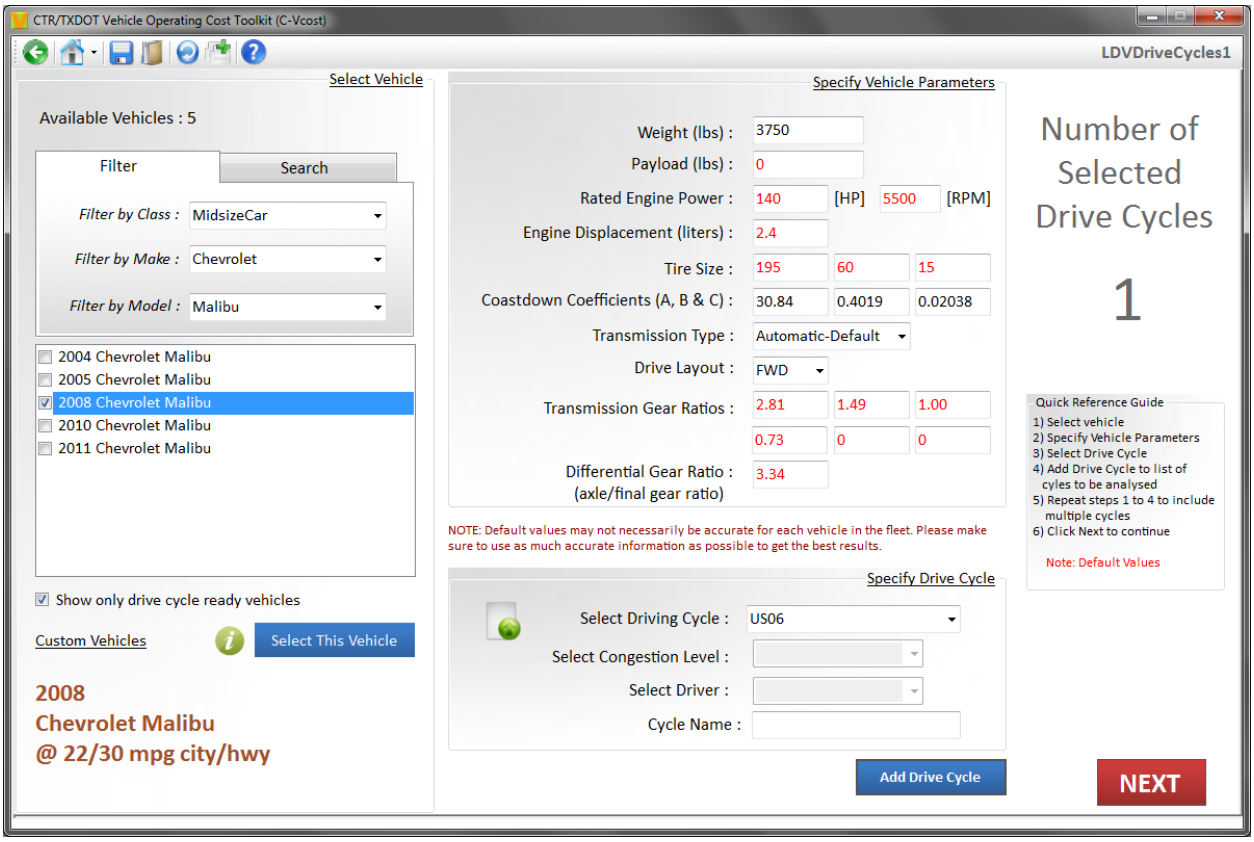

Figure 3.16: Screen shot of the page that appears after the user hits the "Add Drive Cycle" button.

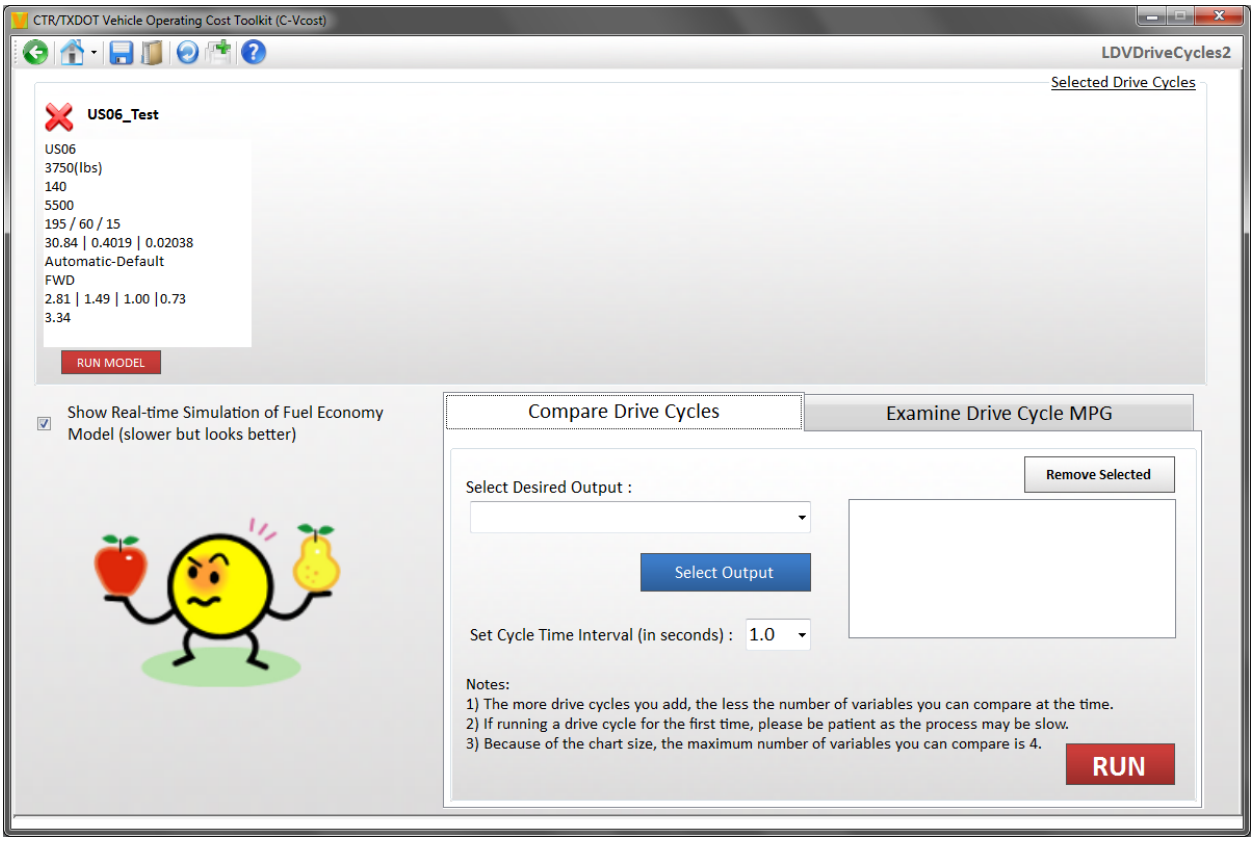

In this case, the user has selected the US06 driving cycle.

Figure 3.17: Page the user is taken to after selecting the "Next" button shown in Figure 3.16.

Once on the page shown in Figure 3.17, the user has several options. The user can simply choose to hit the "Run Model" button appearing below the box in the upper left corner of Figure 3.17. In this case, the user will be taken to the screen shown in Figure 3.18. Note that the fuel economy over the selected driving cycle appears in place of the "Run Model" button.

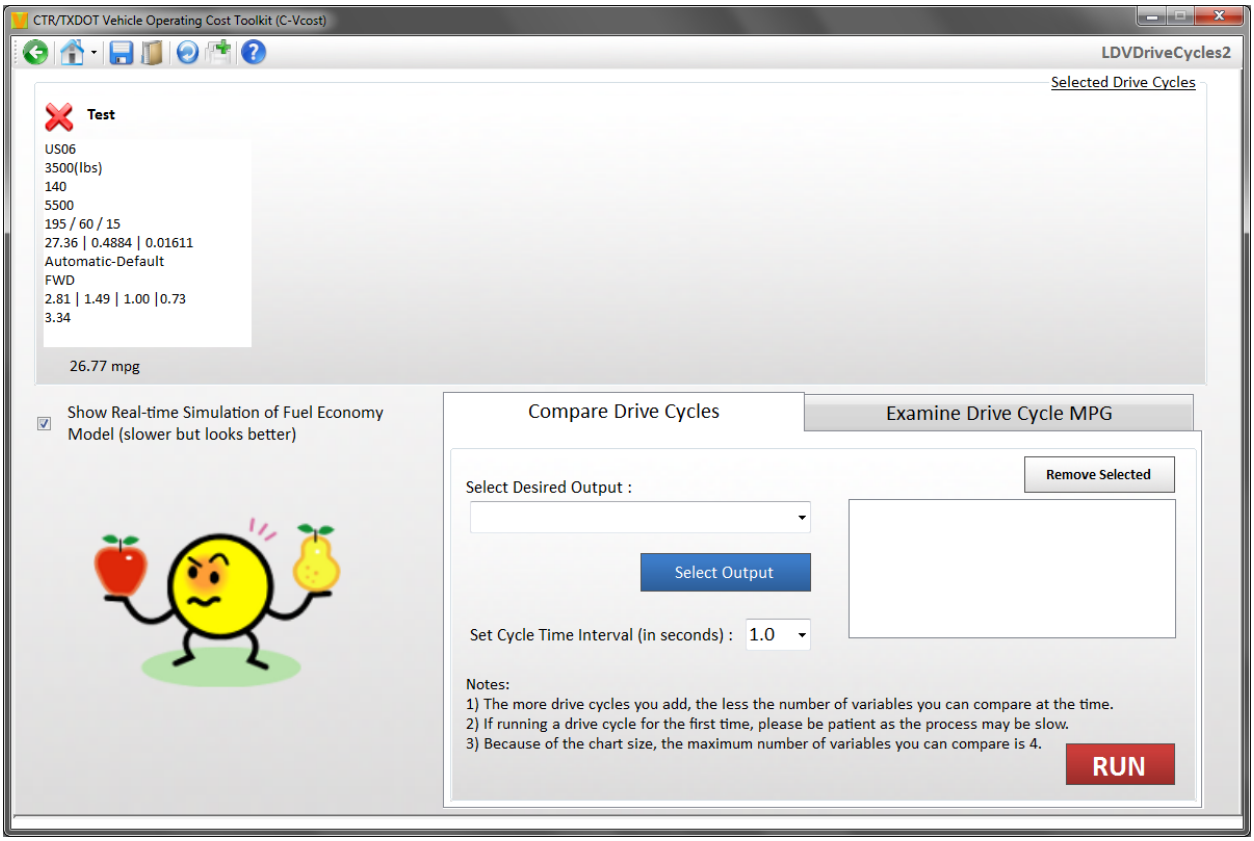

Note that the fuel economy over the selected driving cycle appears in place of the "Run Model" button.

Figure 3.18: Illustration of the screen that will appear if the user selects to hit the "Run Model" button in Figure 3.17.

After the user chooses to select the "Run Model" button in Figure 3.17, the user can select additional driving cycles over which to run the LDV of interest. This is done via the "Compare Drive Cycles" tab near the bottom of the page. Figure 3.19 illustrates selection of the FTP driving cycle for additional analysis of the same vehicle as previously chosen.

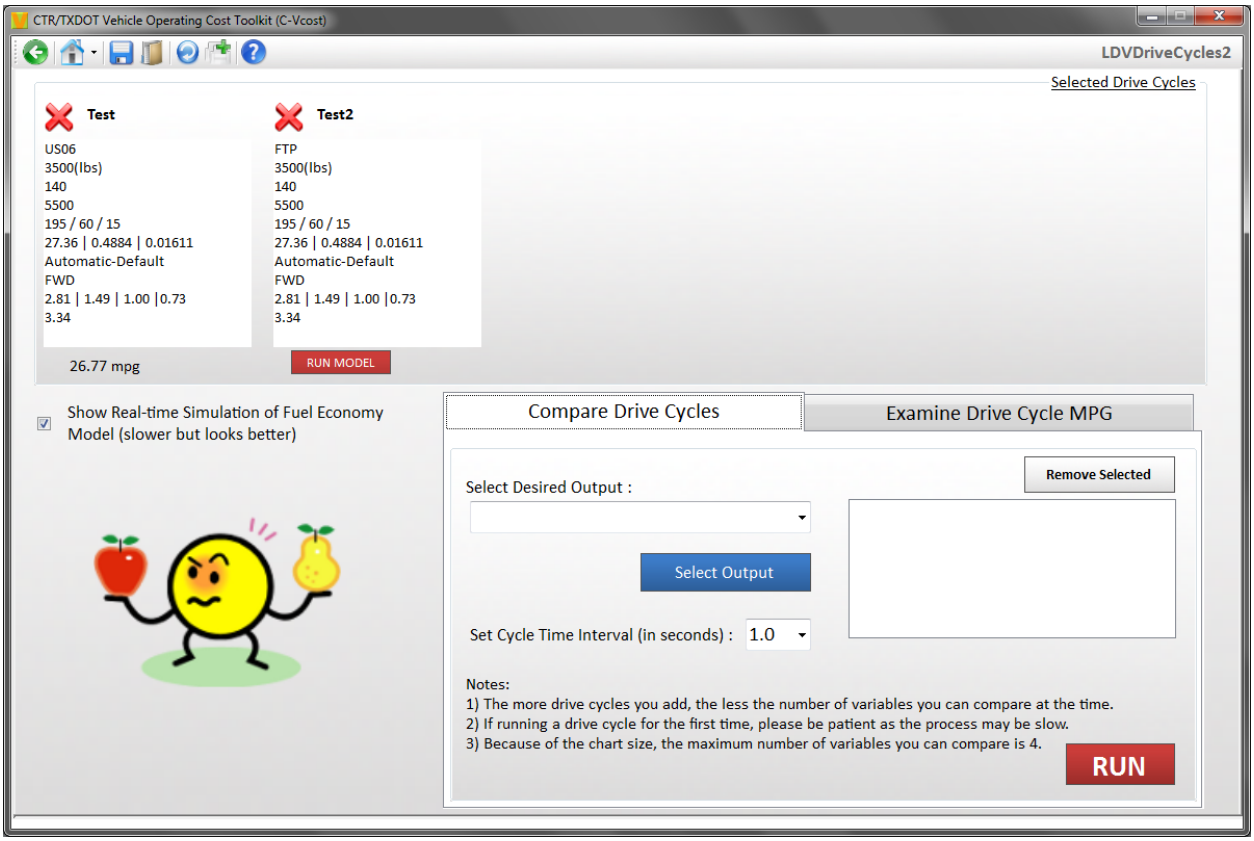

Figure 3.19: Selection of another driving cycle over which to run the same vehicle as previously chosen for analysis.

Selection of a vehicle and a driving cycle will produce several additional screens, as illustrated in Figures 3.20–3.23. Figures 3.20–3.22 show the results of the calculations running in the background. Note that Figure 3.22 shows the results will be written to an Excel file that can be opened by the user to examine details during the driving cycle, such as the instantaneous fuel economy at each point during the driving cycle.

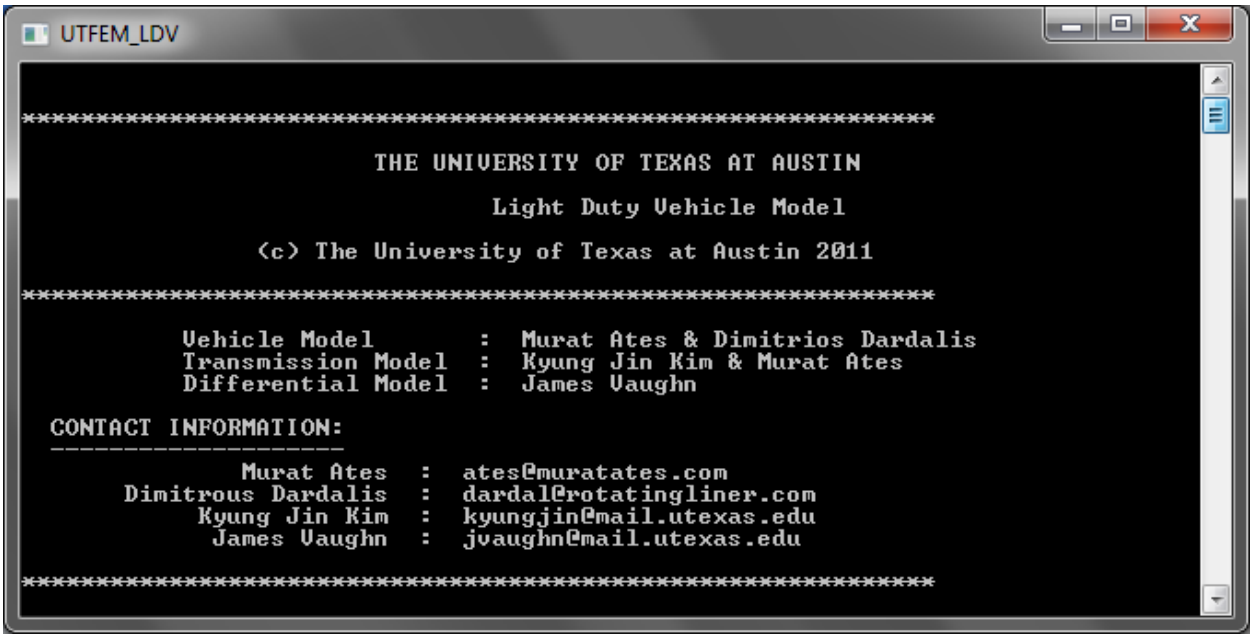

Figure 3.20: Screen shot of a popup window that appears once an LDV and a driving cycle are selected.

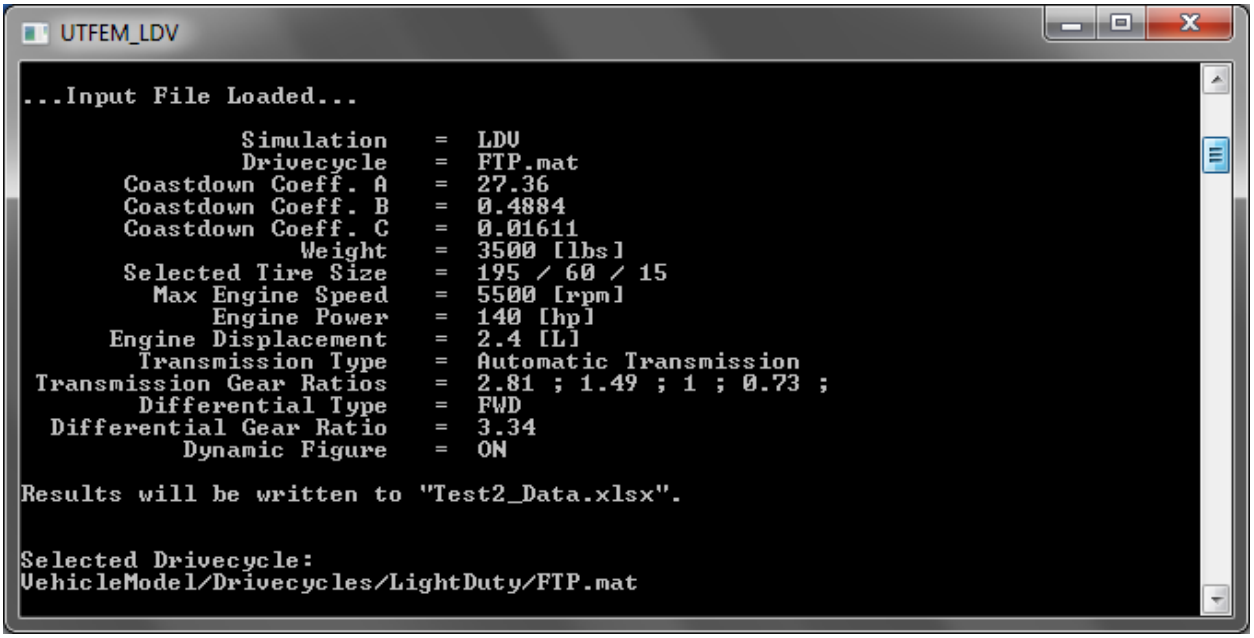

Figure 3.21: More of the popup window illustrated in Figure 3.20.

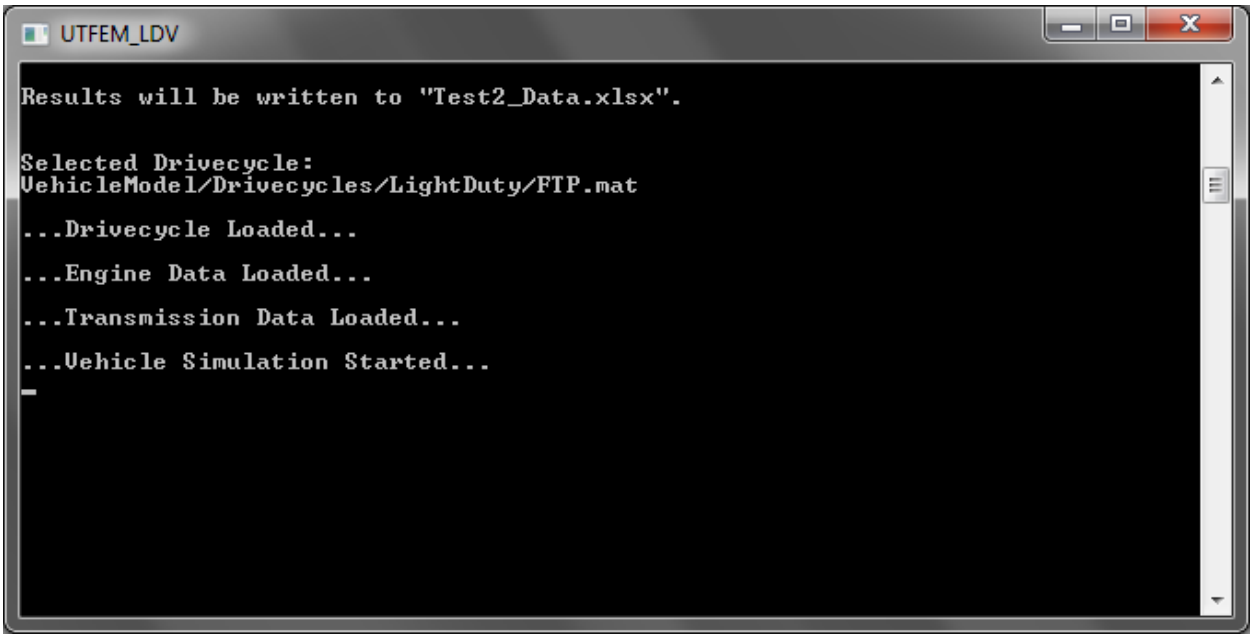

Figure 3.22: More of the popup window illustrated in Figure 3.20.

Figure 3.23 shows some of the graphical output that can be selected for viewing while the computer is running the fuel economy calculations for a selected vehicle and driving cycle. In this case, the user selected to view the desired and calculated vehicle speeds as functions of time during the driving cycle. A second graph, again selected by the user, shows the engine speed and torque converter output speed as functions of time during the driving cycle. There are also two bar graphs, again selected by the user, that illustrate the gear the transmission is in at each instant during the cycle and the percent throttle position at each instant. A graphic illustrates the instantaneous grade, which is zero for all light-duty cycles except for the "Texas LDV" driving cycles generated during this TxDOT project (Project 0-5974). Finally, the text box in the upper right hand corner of Figure 3.23 displays the instantaneous vehicle speed, the instantaneous transmission gear, the instantaneous throttle position, and the gallons of fuel used up to this time during the driving cycle.

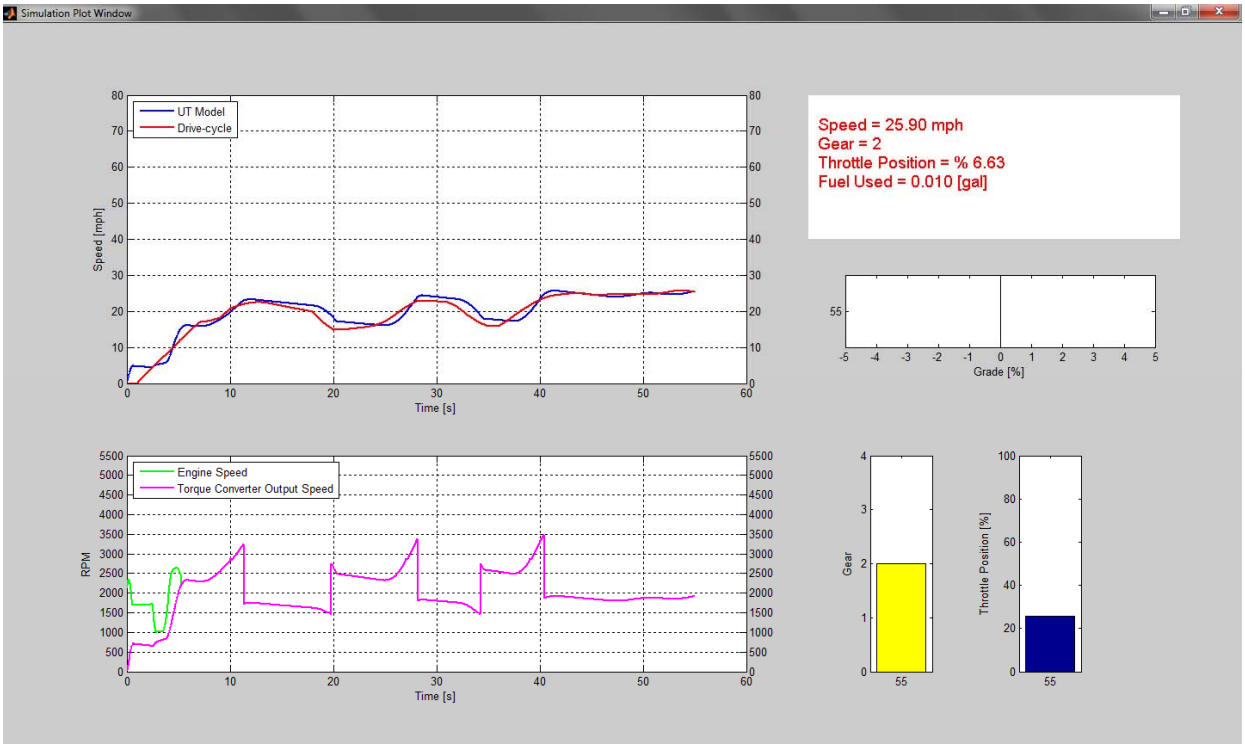

Figure 3.23: Illustration of some of the graphics that can be chosen for viewing while the fuel economy model is running.

Again, the FTP and HFET are provided as driving cycle options for LDVs so that the user can run these two simulations and then apply Equations 3.8 and 3.9 to compare the results of these simulations with the official city and highway fuel economy values provided on the output screen. Example comparisons are provided in Figures 3.24 and 3.25, illustrating the accuracy of the LDV fuel economy model. The vehicles chosen for this analysis include both manual and automatic transmissions and also include two-wheel drive, 4WD, and AWD powertrains. As shown in Figure 3.24, the predictions of the CT-Vcost Fuel Economy Model are quite good (predictions ranging from 6.2 to 13.5% of the official city fuel economy values) for four of the eight vehicles but not as good for the remaining four (with errors ranging from 16.4 to 25.5%). In every case, the city fuel economy prediction is too high relative to the official city

fuel economy. As shown in Figure 3.25, the highway fuel economy predictions are not quite as good with the error in the predictions ranging from 13.1 to 26.6%. In the case of the highway fuel economy, the predictions are consistently too low, rather than too high, as was the case for the city fuel economy. Too little time was available to allow the research team to determine the source of the discrepancies in the predictions.

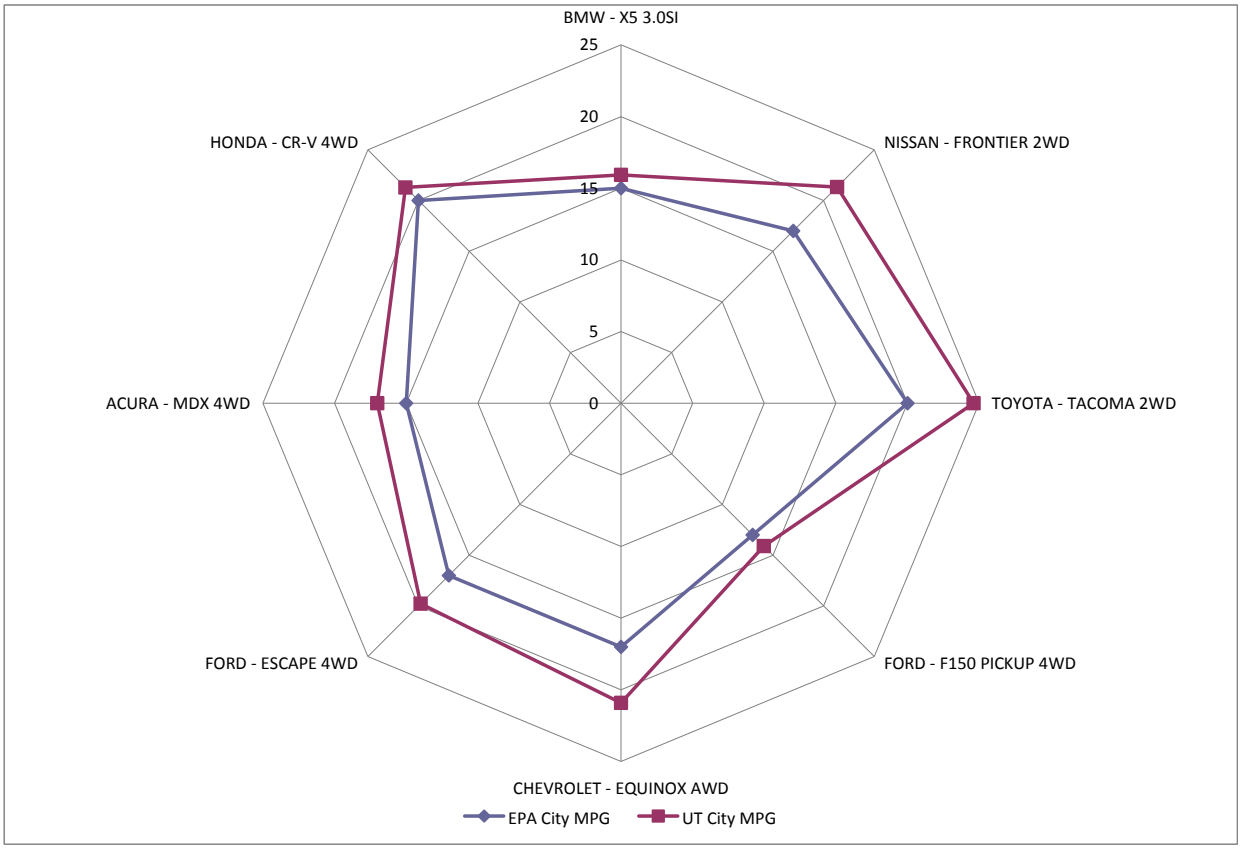

Figure 3.24: Spider graph comparing the official city fuel economy of a variety of LDVs with the city fuel economy predicted by the present model.

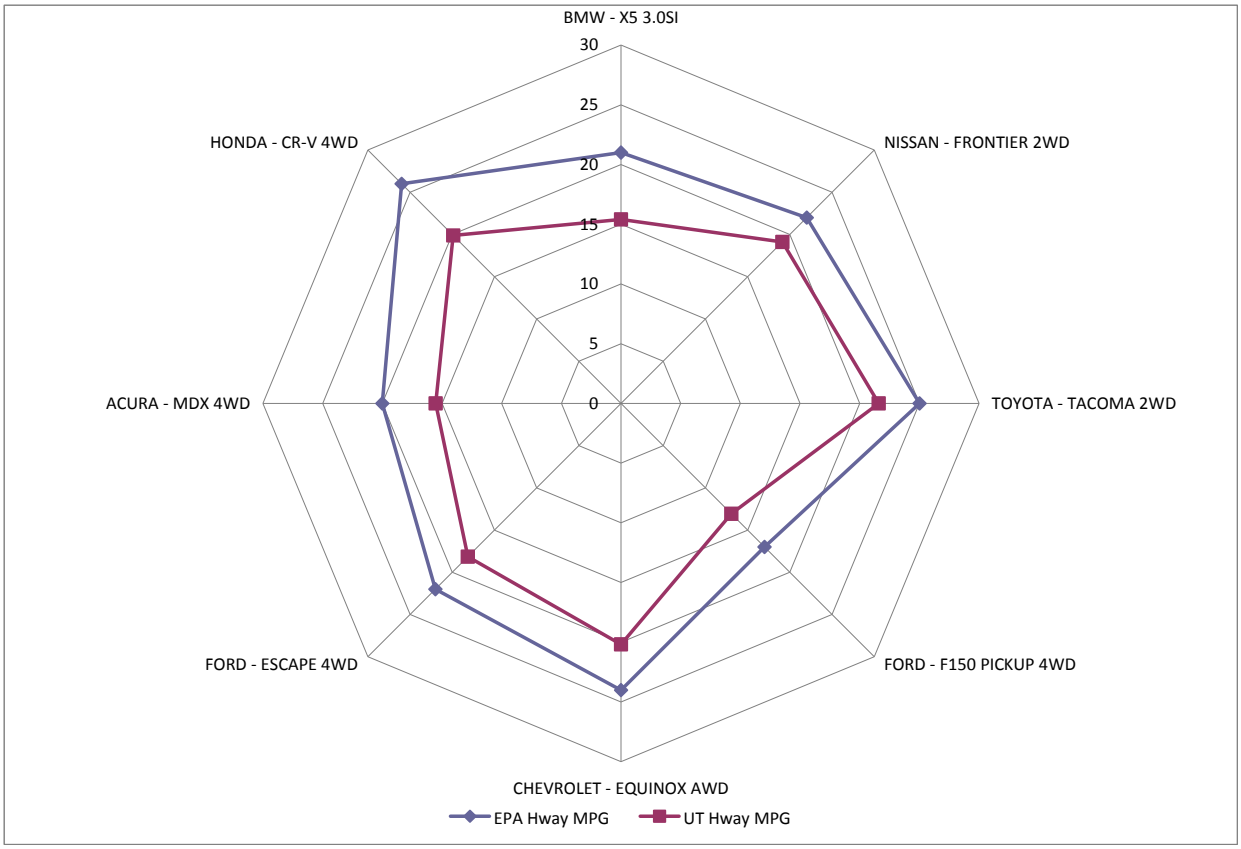

Figure 3.25: Spider graph comparing the official highway fuel economy of a variety of LDVs with the highway fuel economy predicted by the present model.

If the user selects "heavy-duty vehicle drive cycles" rather than "light-duty vehicle drive cycles" from the screen shown in Figure 3.11, the protocol for examining the fuel economy of conventional HDVs is discussed in Subsection 3.3.4.

3.2.5 Light-Duty Hybrids

The light-duty hybrid vehicle fuel economy model focused on Toyota's "synergy drive," because it is used not only in the Prius but also in the Ford Escape hybrid, the Nissan Altima hybrid, Toyota's Camry and Highlander hybrids, the Lexus RX 400h/RX 450h, GS 450h, LS 600h/600hL, and HS 250h. Hybrids produced directly by Toyota make up ~75% of U.S. hybrid sales. Other companies generally give the hybrid synergy drive (HSD) a different name. Toyota's HSD is illustrated in Figure 3.26.

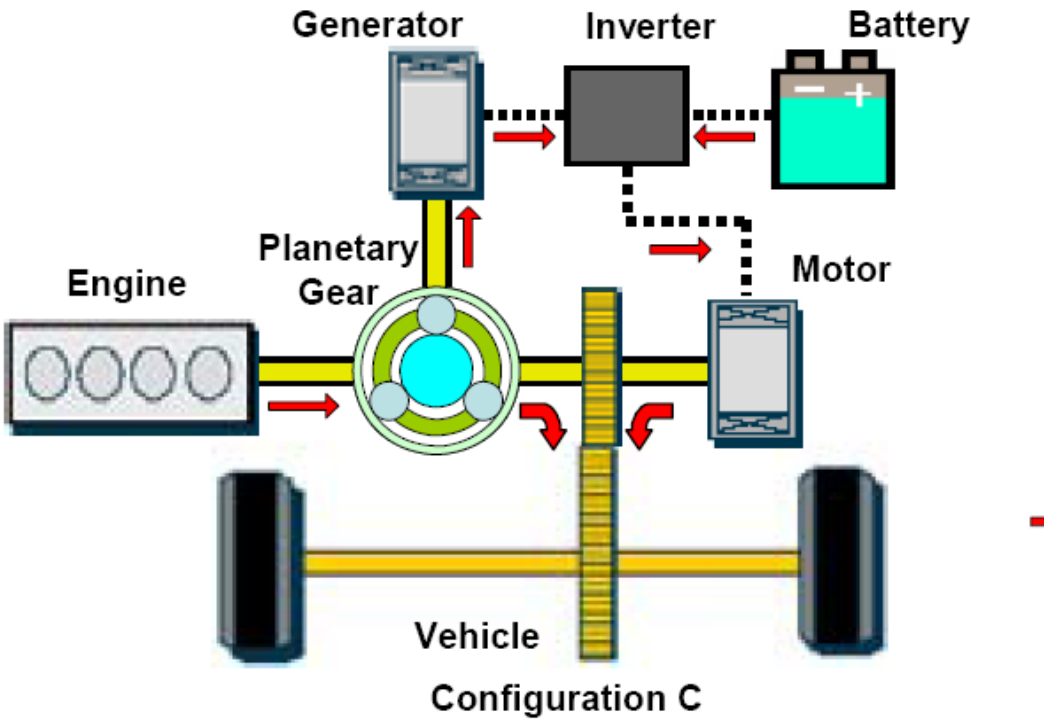

Figure 3.26: Schematic diagram of Toyota's synergy drive.

Toyota's HSD features a planetary gear set with the engine coupled to one of the three planetary gears (planetary gear sets are also used in automatic transmissions, as discussed in Appendix B), one motor-generator (MG1) coupled to the sun gear, and another motor-generator (MG2) attached to the ring gear, which drives the differential. Even though MG1 is labeled as a generator and MG2 is labeled as a motor in Figure 3.26, both can function either as a motor or a generator. For example, MG2 can operate as a motor to supply torque to the differential but it also act as a generator for regenerative braking, converting the kinetic energy of the vehicle to electrical energy to recharge the battery pack. Also, MG1 can help manipulate the engine speed or torque to ensure that the engine operates near the highest efficiency (minimum BSFC) operating condition.

That is, the HSD allows for a "power split" between torque from a motor and torque from the engine. In fact, this torque assist mode is one of five different operating modes for the HSD. The torque assist mode is illustrated in Figure 3.27. Torque is provided both by the engine and MG1 acting as a motor. This depletes the battery state-of-charge (SOC) and it is not possible to keep the engine near its maximum efficiency operating condition.

Figure 3.28 is a schematic of the HSD operating in the mode where all of the motive torque is provided by the MG1 and battery pack. This depletes the battery SOC.

Figure 3.29 is a schematic of the synergy drive operating in a moderate torque demand mode such that the engine provides all of the motive torque and also recharges the battery pack via MG2. Obviously, this increases the battery SOC.

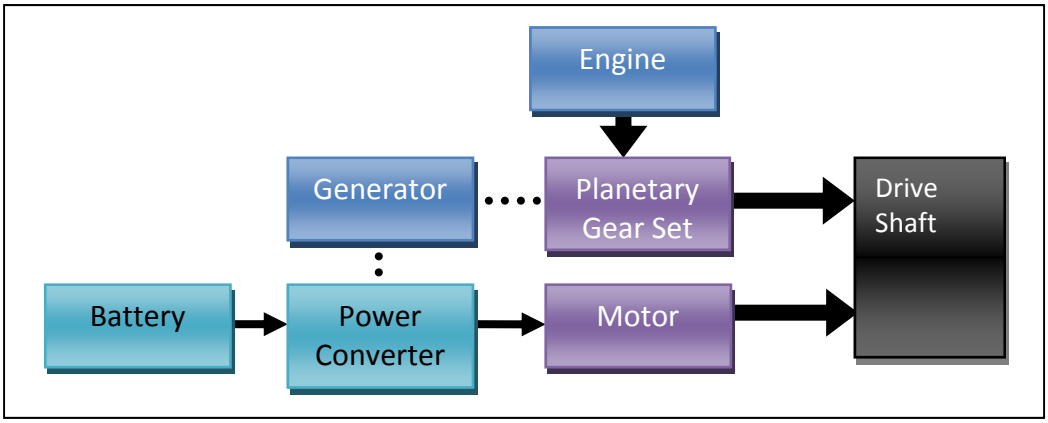

Figure 3.27: Schematic of the HSD operating in torque assist mode ("Mode 1").

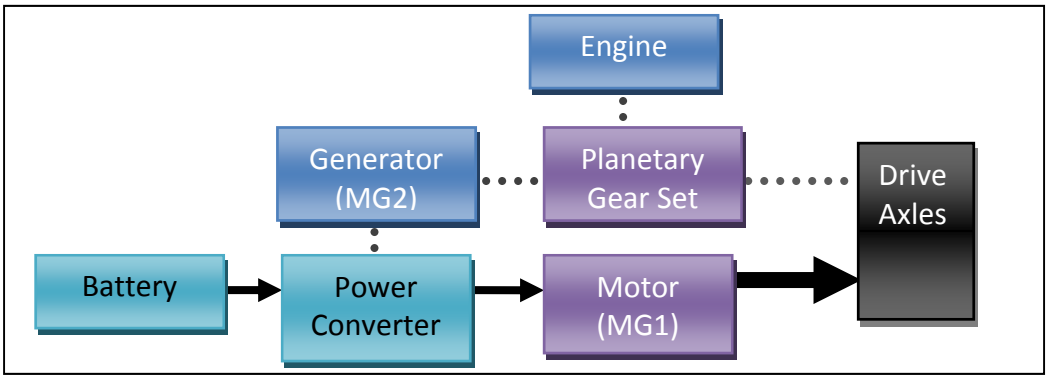

Figure 3.28: Schematic of the HSD operating in electric-only mode ("Mode 2").

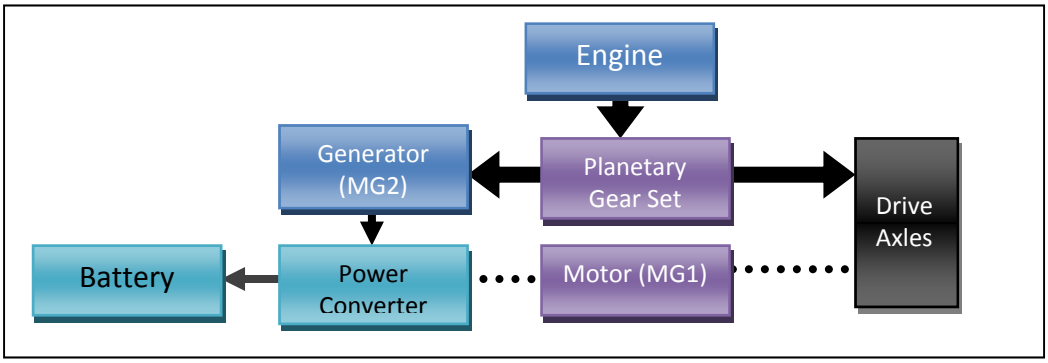

Figure 3.29: Schematic of the HSD operating during moderate torque demand such that the engine provides all of the motive torque and also recharges the battery pack ("Mode 3").

Figure 3.30 is a schematic of the synergy drive operating in "engine-only" mode. There is no effect on the battery SOC.

Figure 3.31 illustrates the HSD operating in regenerative braking mode. In this mode, "motor" MG1 acts as a generator, loading the driveline to generate energy to recharge the batteries. This slows the vehicle down. If it does not slow sufficiently to meet the driver's "demand," as assessed via the brake fluid pressure, the friction brakes are also applied. This mode increases the battery SOC. Because no motive torque is required, the engine is turned off during this mode to improve fuel economy.

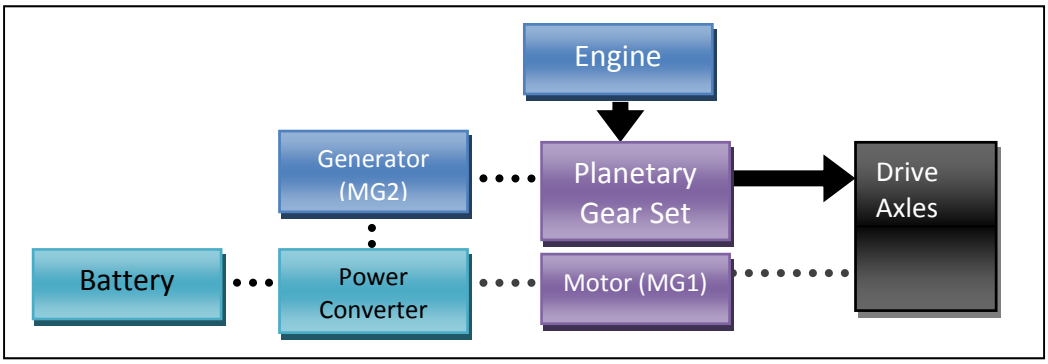

Figure 3.30: Schematic of the HSD operating in engine-only mode ("Mode 4").

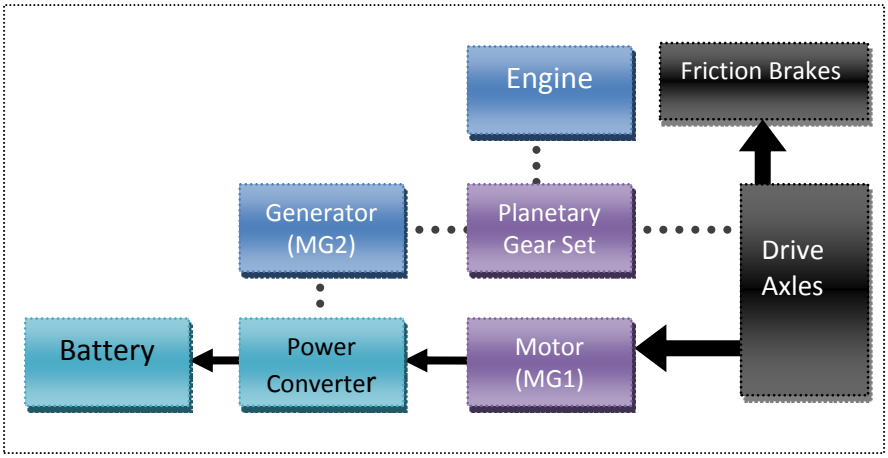

Figure 3.31: Schematic of the HSD operating in regenerative braking mode ("Mode 5").

Simulating the fuel economy of a light-duty hybrid synergy drive is more difficult than modeling the fuel economy of a conventional vehicle because the on-board computer is programmed to protect the battery pack by not letting it get too discharged or overcharged. The on-board computer is also programmed to use MG1 to control the engine to ensure that it runs near the "minimum BSFC island" whenever possible. Thus, the logic of the computer control system must be simulated in the hybrid model, determining when to use each of the five modes of operation, what the torque and speed demands on the engine are for each of the instantaneous modes for the instantaneous vehicle speed and driver's torque demand, etc. The fuel economy model for a light-duty hybrid is discussed in detail in Appendix D.

3.3 Heavy-Duty Vehicles

Coastdown coefficients for HDVs are discussed in Subsection 3.3.1. Subsection 3.3.2 covers driving cycles for HDVs. The elements of the fuel economy model for conventional HDVs are discussed in Subsection 3.3.3. Running the fuel economy model for conventional HDVs is discussed in Subsection 3.3.4. Models for the fuel economy of heavy-duty hybrids are discussed in Subsection 3.3.5.

3.3.1 Heavy-Duty Coastdown Coefficients

As noted earlier, the EPA publishes coastdown coefficients for all LDVs sold in the U.S. because they are required to perform chassis dynamometer tests for emissions compliance and fuel economy measurements (CAFE). However, emissions regulations for HDVs require testing the engine by itself on an engine dynamometer and there are currently no fuel economy regulations for HDVs. That is, coastdown coefficients for HDVs are not readily available.

Some coastdown coefficients are available for European HDVs (Petrushov, 1997; Petrushov, 1998) and there is a formula used by EPA in their Motor Vehicle Emission Simulator (MOVES) model. The coastdown coefficient formula developed by EPA for MOVES was derived from Petrushov (1997) and lacks the term that accounts for the linear speed dependence.

Therefore, our research team had to perform coastdown experiments with heavy-duty trucks in order to have heavy-duty coastdown coefficients for our fuel economy model. These experiments were discussed in detail in our final report for the initial portion of this study (Welter et al., 2009) and, therefore, do not merit additional discussion.

Table 3.2 shows the resultant coastdown coefficients for the heavy-duty trucks tested via TxDOT Project 0-5974. These coastdown coefficients are used to calculate the road load force in the HDV fuel economy simulations. The results shown in Table 3.2 are for the vehicles as weighed immediately before the coastdown tests. The user of the UT Fuel Economy Model (including within the CT-VCost model) can select other vehicle weights. In this case the code uses a least-squares analysis to determine each of the coastdown coefficients as a function of loaded vehicle weight.

Other coastdown coefficients for HDVs are also available. Examples are provided in Table 3.3. Coastdown coefficients were also found for long combination vehicles (LCVs) (Petrushov, 1997). Long combination vehicles are not legal in Texas, but they are of significant interest. Incorporating LCVs into CTR's new CT-Vcost model would allow users to compare the fuel economy of these vehicles, per ton of payload, with conventional Class 8 trucks. Unfortunately, the format of the coastdown coefficients from this source is incompatible with the new fuel economy model and there was insufficient time to develop a technique to put the LCV coastdown coefficients into the accepted format.

Table 3.2: Coastdown Coefficients for Heavy-Duty Vehicles.

	A	B	C	Avg. R^2
F150 – 5890 lb	17.0981	2.4838	0.0133	0.9991
Class 7 – 27785 lb	143.9200	9.8285	0.0310	0.9993
Class 7 – 36300 lb	208.2923	9.5271	0.0593	0.9993
Class 7 – 44700 lb	233.6523	9.9640	0.0676	0.9994
Class 8 – 31910 lb	203.7321	2.9143	0.1811	0.9998
Class 8 – 56470 lb	305.7169	5.4165	0.1221	0.9997
Class 8 – 78785 lb	386.2433	5.4766	0.1579	0.9996
HEB* – 28760 lb	178.2051	2.7707	0.2159	0.9983
HEB* – 55760 lb	363.0530	5.6753	0.1318	0.9987
HEB* – 81010 lb	477.6786	5.6684	0.1721	0.9991

*The Class 8 trucks that HEB allowed us to perform coastdown tests on were equipped with low rolling resistance "wide single" Michelin tires.

Table 3.3: Heavy-Duty Vehicle Coastdown Coefficients Obtained from Other Sources.

Road Load Parameters†			
Vehicle Mass*	**A [lb_f]**	**B [lb_f/mph]**	**C [lb_f/mph^2]**
$m < 7000$ lb_m	$1.0156\times10^{-2}\,m$	0	$0.051+1.064\times10^{-6}\,m$
$7000 \le m < 14000$ lb_m			$0.066+1.064\times10^{-6}\,m$
$14000 \le m \le 33000$ lb_m	$8.9225\times10^{-3}\,m$	0	$0.087+1.202\times10^{-6}\,m$
$m > 33000$ lb_m	$6.7403\times10^{-3}\,m$	0	$0.1298+8.579\times10^{-7}\,m$
Buses	$6.5568\times10^{-3}\,m$	0	$0.1447+1.031\times10^{-6}\,m$

† Developed from Petrushov (1998, 2009) and used in EPA's MOVES model.
*At sea level, mass and weight are equivalent in the American Conventional System of units.

3.3.2 Heavy-Duty Vehicle Driving Cycles

In HDV simulations, the driving cycle is very important primarily due to the weight of HDVs. Specifically, a heavily loaded truck cannot follow the driving schedule developed for a lightly loaded truck. In the literature, all well-known driving cycles for HDVs are simply specifications of vehicle speed as a function of time, generally with the speed specified each second. This, of course, corresponds with driving cycles for LDVs. However, the grade plays a very significant role for HDVs, unlike LDVs. Therefore, we logged speed data along with elevation data to account for the effect of the grade in our heavy-duty driving cycles and simulations. Additionally, we collected driving cycle data with trucks with payloads ranging from empty to full. Gross vehicle weight rating (GVWR) of 45,000, 65,000, and 80,000 pounds were used in this study.

The same section of IH 35, as used for development of the LDV driving cycles and shown in Figure 3.2 was used to generate the driving cycles for HDVs. Similarly, data were collected at three times during the morning: 7:30 a.m., 9:30 a.m., and 11:00 a.m. Also, two truck drivers were used but they were different from the LDV drivers. In addition to time of day,

loaded vehicle weight, and driver parameters, we also recorded vehicle specifications as new parameters to driving cycle data logging for the HDVs (Table 3.4). Because engine power is another variable that affects the ability of a truck under load, three different heavy-duty trucks with different engines were selected. In addition to rated engine power, the type of heavy-duty transmission is another parameter that needs to be considered regarding the performance of the truck. To cover different truck driving behaviors, we selected trucks with 9, 10, and 13 speed manual transmissions. The trucks used in this study are classified via the EPA rating system as Class 8 trucks. However, the driving cycles generated by these trucks are used for Class 7 trucks.

Table 3.4: Specifications of the Heavy-Duty Trucks Used in Driving Cycle Data Collection.

	1995 International	2004 Sterling	2001 Freightliner
Engine Model	Cummins M11	MBE4000	Caterpillar C12
Engine Displacement (L)	11.0	12.8	11.8
Engine Year	1995	2004	2001
# of Cylinders	6	6	6
Rated Power (HP)	330 HP @ 1800 rpm	370 HP @ 2000 rpm	410 HP @ 2100
Peak Torque (lb-ft)	1250 @ 1200 rpm	1450 @ 1100 rpm	1450
Transmission Model	Fuller RT14609A	Eaton Fuller RTLO-14913A	Eaton Fuller FRO-14210B
# of Gears	9	13	10
Differential (Axle) Model	Eaton DS402	Meritor (Rockwell) Hypoid Single Reduction RT-40-145 Tandem Drive Axle	Meritor (Rockwell) Hypoid Single Reduction RT-40-145 Tandem Drive Axle

A driving cycle recorded with a 2001 model Class 8 truck powered by a 410 hp Caterpillar C12 engine and having a 10-speed Eaton Fuller transmission is shown in Figure 3.32. This data was recorded at 7:30 a.m. with a 65,000 pound loaded vehicle weight with the second truck driver. The average speed for this driving cycle is 33.3 mph and the elapsed time is 48 minutes and 11 seconds. Given 3 trucks, 3 drivers, and 3 times of the day, with repeat tests, a total of 54 driving schedules were developed for HDVs.

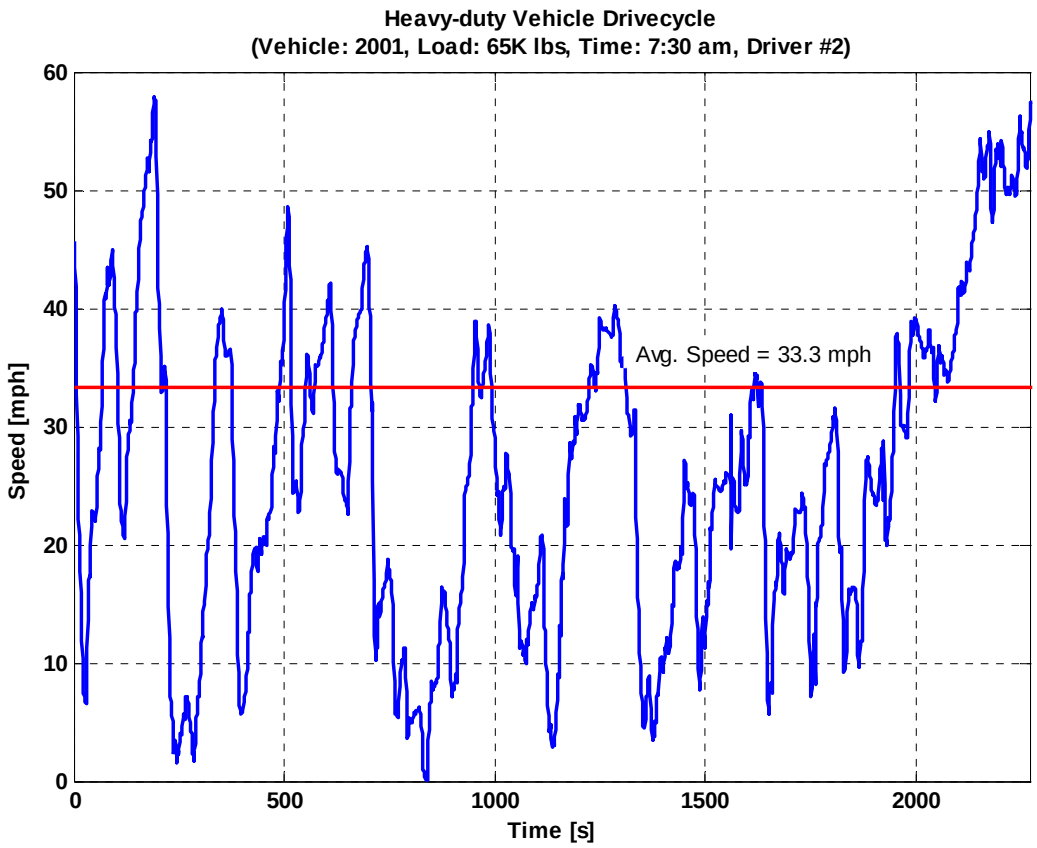

Figure 3.32: An example of a HDV driving cycle developed during TxDOT Project 0-5974.

3.3.3 Elements of the Heavy-Duty Vehicle Fuel Economy Model

Our HDV fuel economy model uses subroutines for the engine, transmission, and differential. Each of these is briefly discussed below. Details are provided in the appendices. Our models for heavy-duty hybrids are discussed in Subsection 3.3.5.

3.3.3.1. Heavy-Duty Engine Model

Our initial plan was to modify the UT FES to make it suitable for diesels as well as spark ignition engines. However, as discussed earlier, a suitable Fortran complier could not be located so an alternative plan was developed. This alternative was similar to that for the light-duty gasoline engines. Specifically, BSFC maps for three heavy-duty engines were used for the HDV simulations (see Appendix A). For EPA Class 8 trucks, BSFC maps for a Cummins M11 engine and for a Caterpillar C12 engine were incorporated in the HDV fuel economy model. The BSFC map for a Detroit Diesel Series 30 engine was used for all EPA Class 7 trucks. Insufficient time was available to allow the research team to develop a technique to normalize these three heavy-duty BSFC maps such that the heavy-duty fuel economy model could simulate heavy-duty diesel engines of other displacements and peak speeds.

3.3.3.2. Heavy-Duty Transmission Model

A detailed model for a 10-speed Eaton Fuller FRO16210C manual transmission was developed. This transmission was chosen because it is very popular, and therefore representative of heavy-duty manual transmissions. Details are provided in Appendix B.

However, HDVs can be equipped with transmissions having a different number of "speeds" or gears other than the 10 speeds of the Eaton Fuller FRO16210C. Because it is a very long process to develop a transmission model for each transmission available in the heavy-duty market, a generic heavy-duty transmission model was developed for use whenever the model user does not specify a 10-speed manual transmission.

Our generic heavy-duty transmission model is based on gear ratio, torque input to the transmission (torque output from the engine), and rotational speed (rpm) input to the transmission (engine rpm).

Figure 3.33 shows efficiency points drawn as red dots for the 10-speed Eaton Fuller FRO16210C model developed for this project. In this figure, the surface is the generic heavy-duty transmission model.

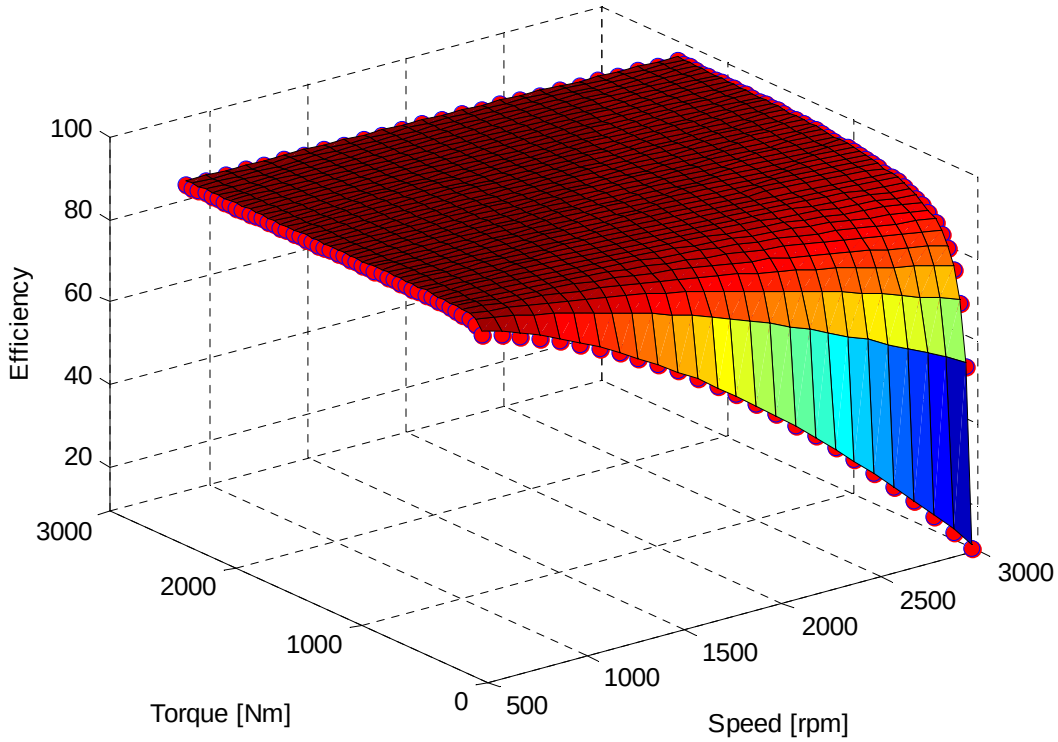

Figure 3.33: Efficiency map generated by our model for 1st gear of the Eaton Fuller FRO16210C transmission.

Equation 3.10 is the generic formula developed for the heavy-duty manual transmissions. Specifically, the transmission efficiency (η_T) can be estimated as a function of gear ratio (R_T), input speed (N_e), and input torque (τ_e):

$$\eta_T = \left(\frac{p_1 R_T^3 + p_2 R_T^2 + p_3 R_T + p_4}{R_T^3 + q_1 R_T^2 + q_2 R_T + q_3} \right) N_e^b \tau_e^c + d \tag{3.10}$$

Estimation of the efficiencies for broad ranges of speed (500–3000 rpm) and torque (50–2400 N-m) for the 10-speed Eaton Fuller FRO16210C is compared with the transmission model specific to the 10-speed Eaton Fuller FRO16210C transmission is shown in Table 3.5. These results show that the generic transmission model is sufficiently accurate to use in the estimation of the transmission efficiencies for other heavy-duty manual transmissions.

Table 3.5: Comparison of Efficiencies Estimated with the Generic Transmission Model to those from the Model Specific to the 10-speed Eaton Fuller FRO16210C Transmission.

Gear	R^2
#1 (12.69:1)	0.9839
#2 (9.29:1)	0.9844
#3 (6.75:1)	0.9820
#4 (4.90:1)	0.9996
#5 (3.62:1)	0.9900
#6 (2.59:1)	0.9945
#7 (1.90:1)	0.9956
#8 (1.38:1)	0.9952
#9 (1.00:1)	0.9892
#10 (0.74:1)	0.9994

3.3.3.3. Heavy-Duty Differential Model

As for LDVs, HDVs utilize differentials in their powertrains. However, heavy-duty differentials can be divided into only two categories, both of which are subsets within the RWD configuration. Some HDVs implement a "dual" differential in their RWD configuration. A dual differential is essentially a two-speed gearbox attached to the front of an RWD differential. This is an alternative to containing a second gear stage within a heavy-duty transmission. This allows HDVs to keep the transmission simple while providing more gear ratio options. Because dual differentials are being implemented today, a model for them is included with the conventional heavy-duty RWD model. Thus, the two heavy-duty differential models are RWD and dual.

The top-level in the heavy-duty differential subroutine chooses between the RWD and dual differential models. This information must be available for each vehicle before it can be modeled. Unlike the RWD and the light-duty models, the dual differential model requires information above and beyond the scaled input torque, input speed, and differential gear ratio. In much the same way that the transmission submodel needs to know all of the gear ratios and which gear has been selected, the dual differential model needs to know what two gear ratios are available (although high gear is assumed to have a ratio of unity) and which of the two gears is selected. The shifting submodel will determine which gear is selected, but the low-gear ratio will need to be specified with the rest of the vehicle information. As mentioned previously, this

makes the two- and three-dimensional efficiency maps more challenging to implement. However, the implementation methods are the same as for the light-duty case.

3.3.4 Running the Model for the Fuel Economy of Conventional Heavy-Duty Vehicles

Again, a separate Fuel Economy model will be delivered after the final modifications have been completed. Thus, the following describes how the user can run the fuel economy model from CT-Vcost. The user of the CT-Vcost model will first see a screen with a "start" button. After selecting this button, the user is taken to the screen shown in Figure 3.11. This screen allows the user to select the type of analysis to be performed. For obtaining fuel economy results, the user should select either "heavy-duty vehicle drive cycles" or "light-duty vehicle drive cycles." If the user selects "heavy-duty vehicle drive cycles," he or she will be taken to the screen illustrated in Figure 3.34. As shown in Figure 3.34, the user can select a cycle name because there are no official driving cycles for HDVs (the engines in HDVs are operated over a standardized cycle rather than the entire vehicle). As also illustrated in Figure 3.34, one can then select to examine either a Class 7 or Class 8 truck, as coastdown coefficients were obtained for these two categories of heavy-duty trucks.

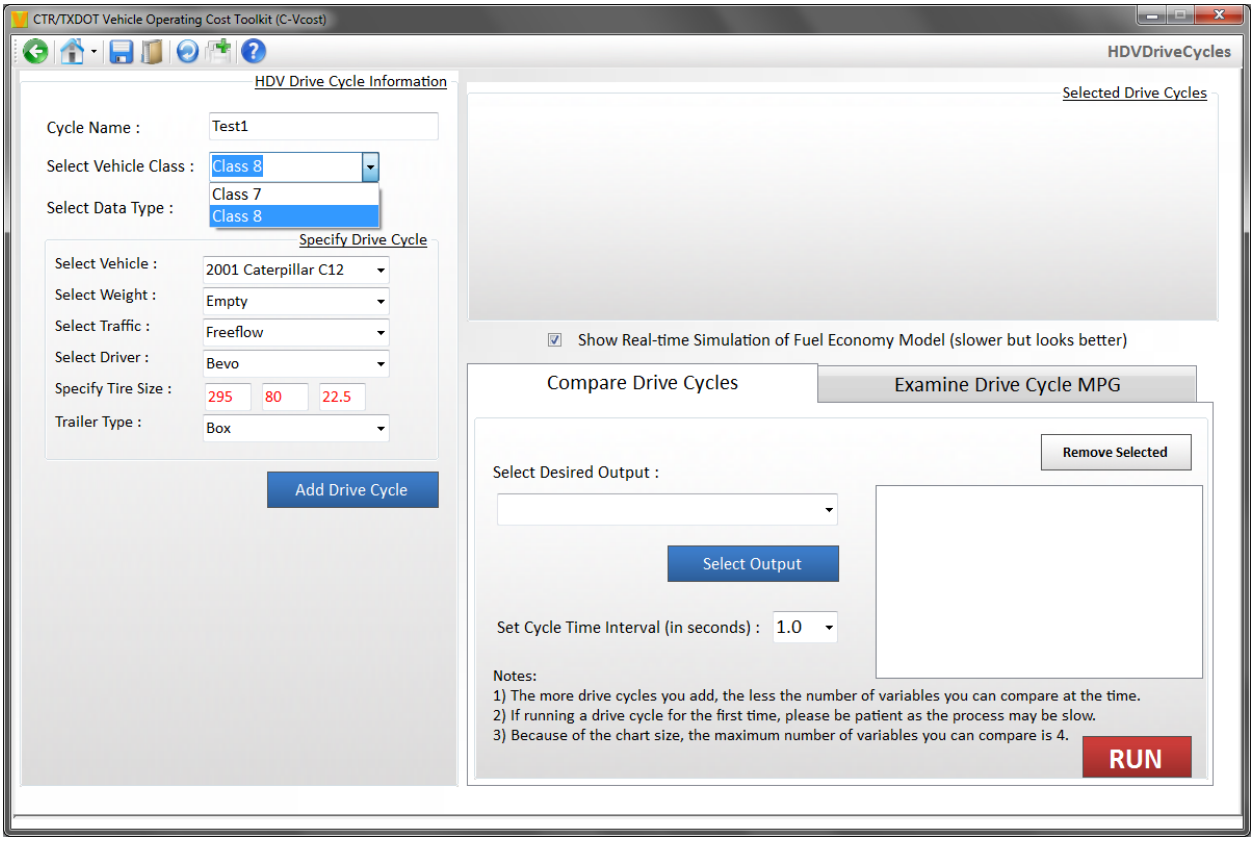

Figure 3.34: Illustration of the screen that is obtained after selecting "heavy-duty vehicle drive cycles" from the screen shown in Figure 3.11.

As shown in Figure 3.35, the user then selects “Data Type” from a pull-down menu. Here, the two options are “Default” and “Custom.”

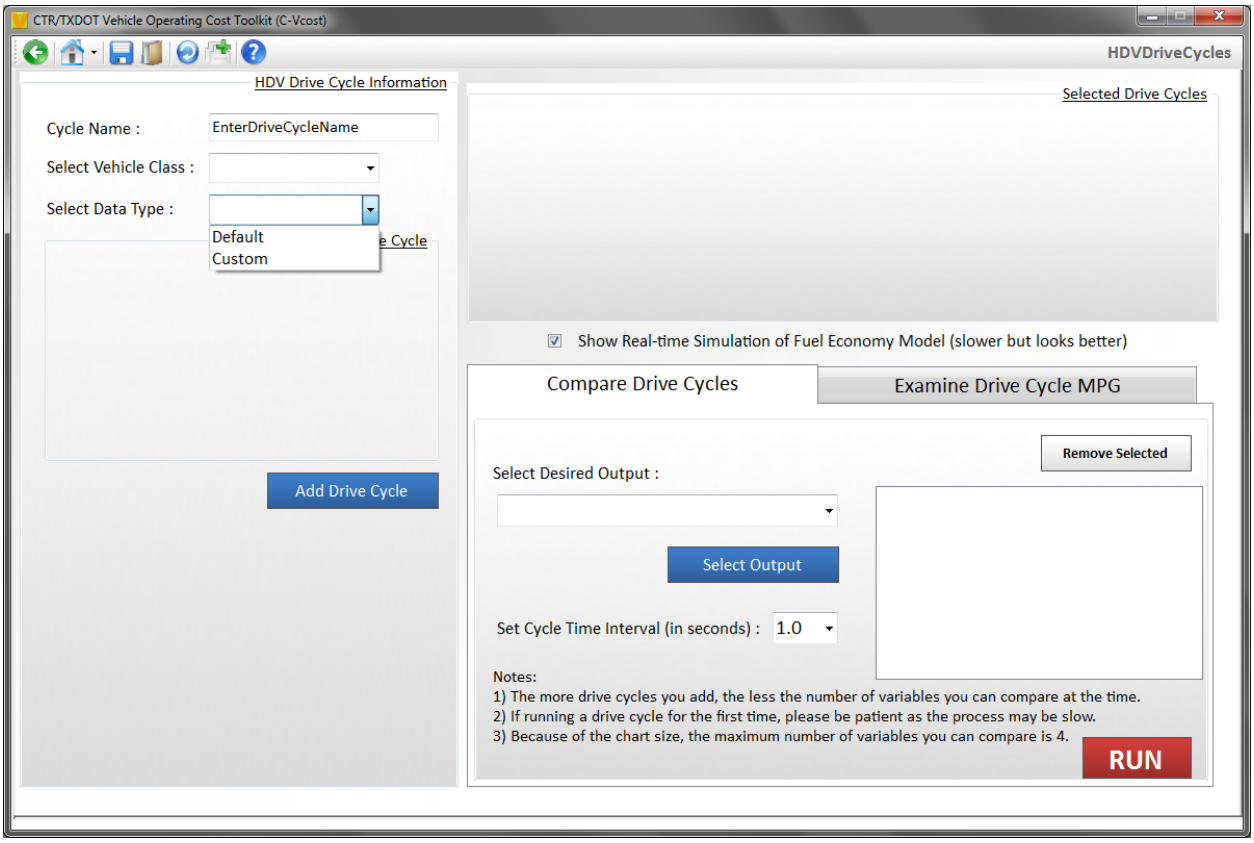

Figure 3.35: Illustration of the pull-down menu for “Select Data Type.”

If the user selects "Default" from the pull-down menu illustrated in Figure 3.35, additional pull-down menus appear, as shown in Figure 3.36.

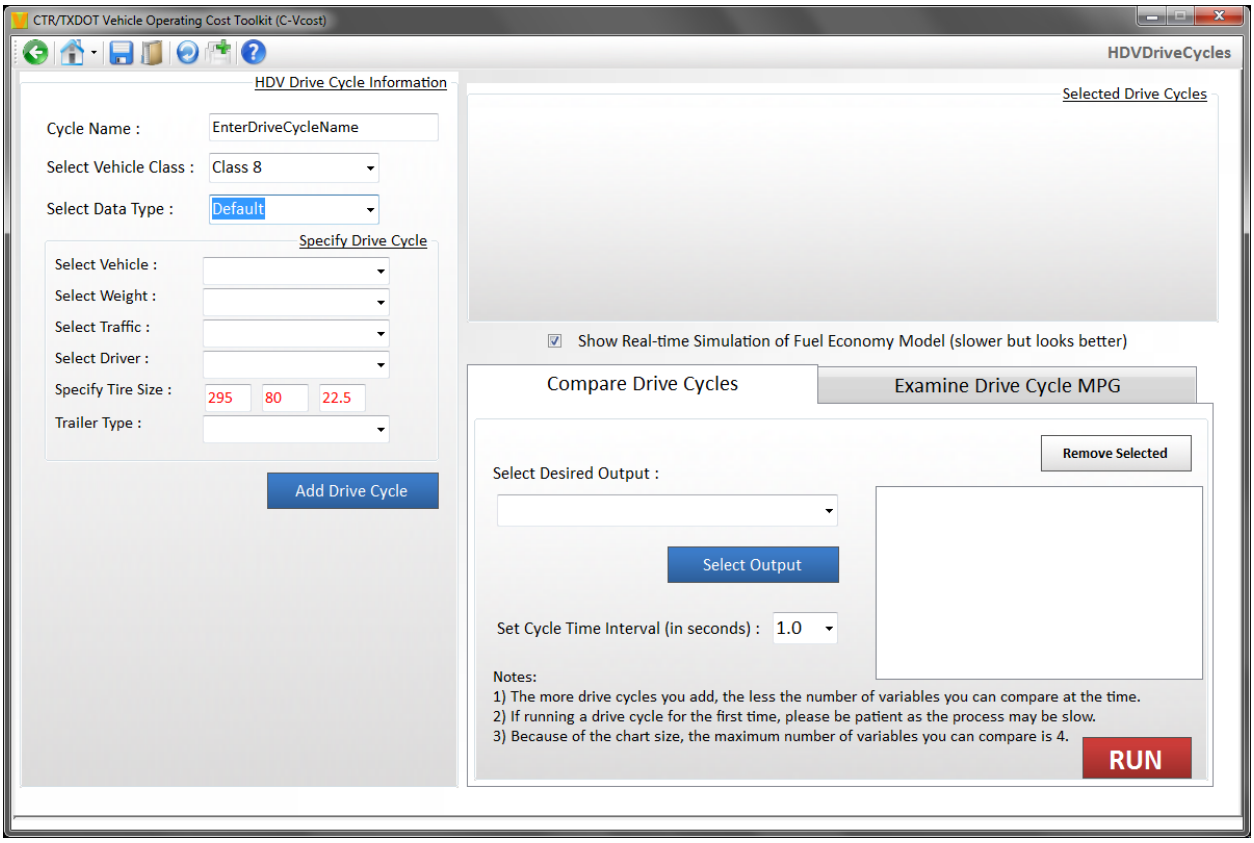

Figure 3.36: Additional pull-down menus that appear if the user selects "Default" as the data type.

For the "Default" data type selection, the user can select between the three heavy-duty trucks that were used to generate heavy-duty drive cycles for the IH 35 traffic through downtown Austin, as shown in Figure 3.37.

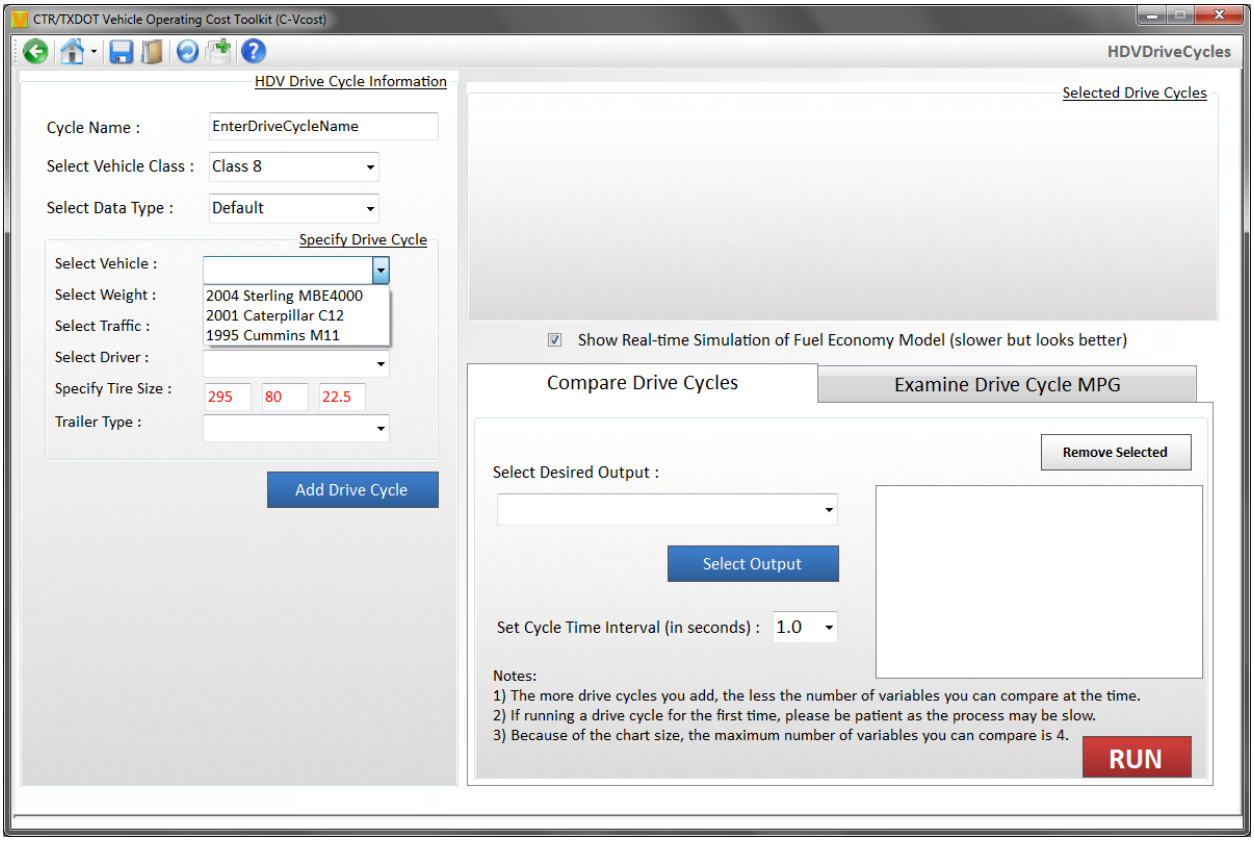

Figure 3.37: The pull-down menu for "Select Vehicle" when the "Default" data type is chosen.

Again for the "Default" data type selection, as shown in Figure 3.38, the user then selects the loaded vehicle weight from three options: "Empty," Cubed Out," and "Weighed Out." *Empty* was the measured weight for the selected vehicle when it had an empty trailer. *Cubed Out* is the typical weight of this vehicle when it was running with a full trailer but with a low density cargo. *Weighed Out* is the typical weight of this vehicle when running with a trailer full of high density cargo.

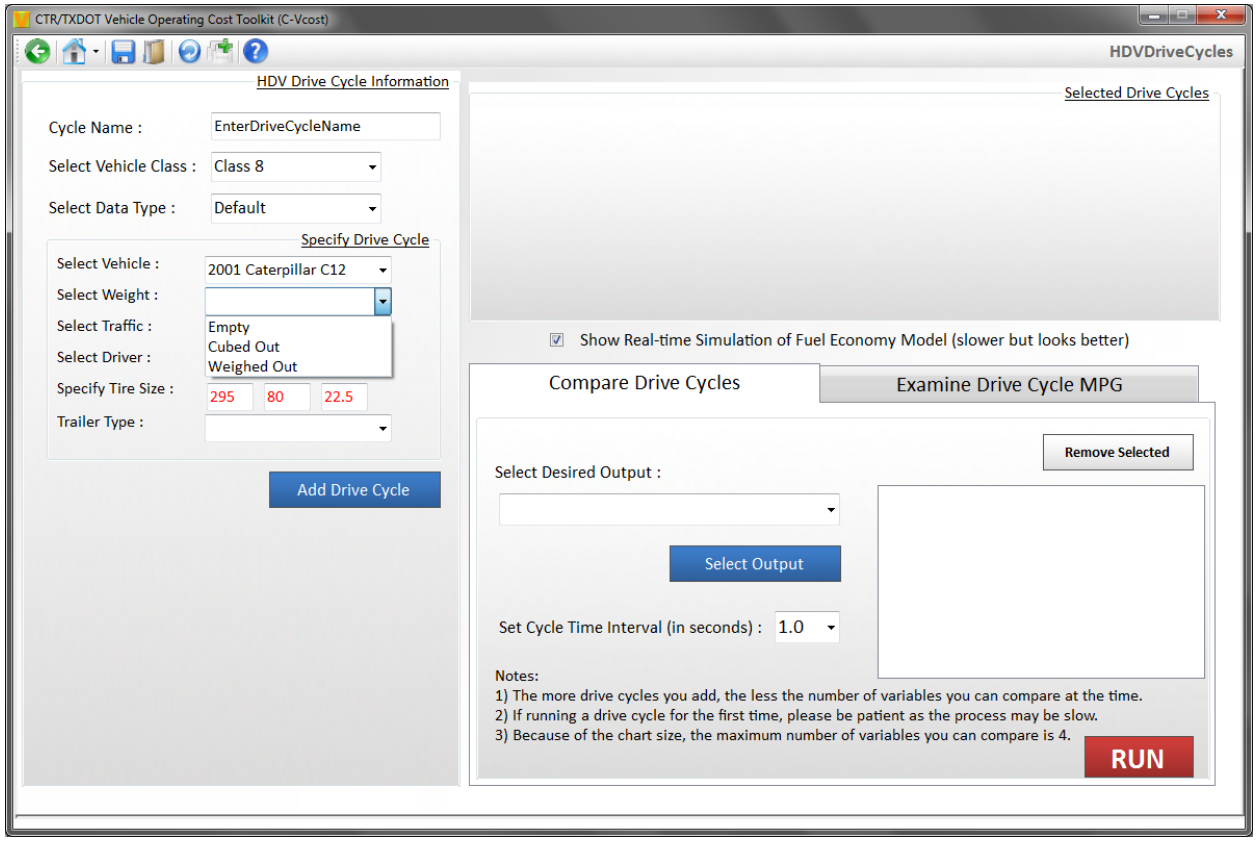

Figure 3.38: The pull-down menu for "Select Weight" when the "Default" data type is chosen.

Again for the "Default" data type selection, the user then selects the level of traffic congestion (free flow, moderate, or congested), as illustrated in Figure 3.39, after which he or she selects the category of driver ("Longhorn" is an aggressive driver, "Bevo" is a typical driver), as illustrated in Figure 3.40.

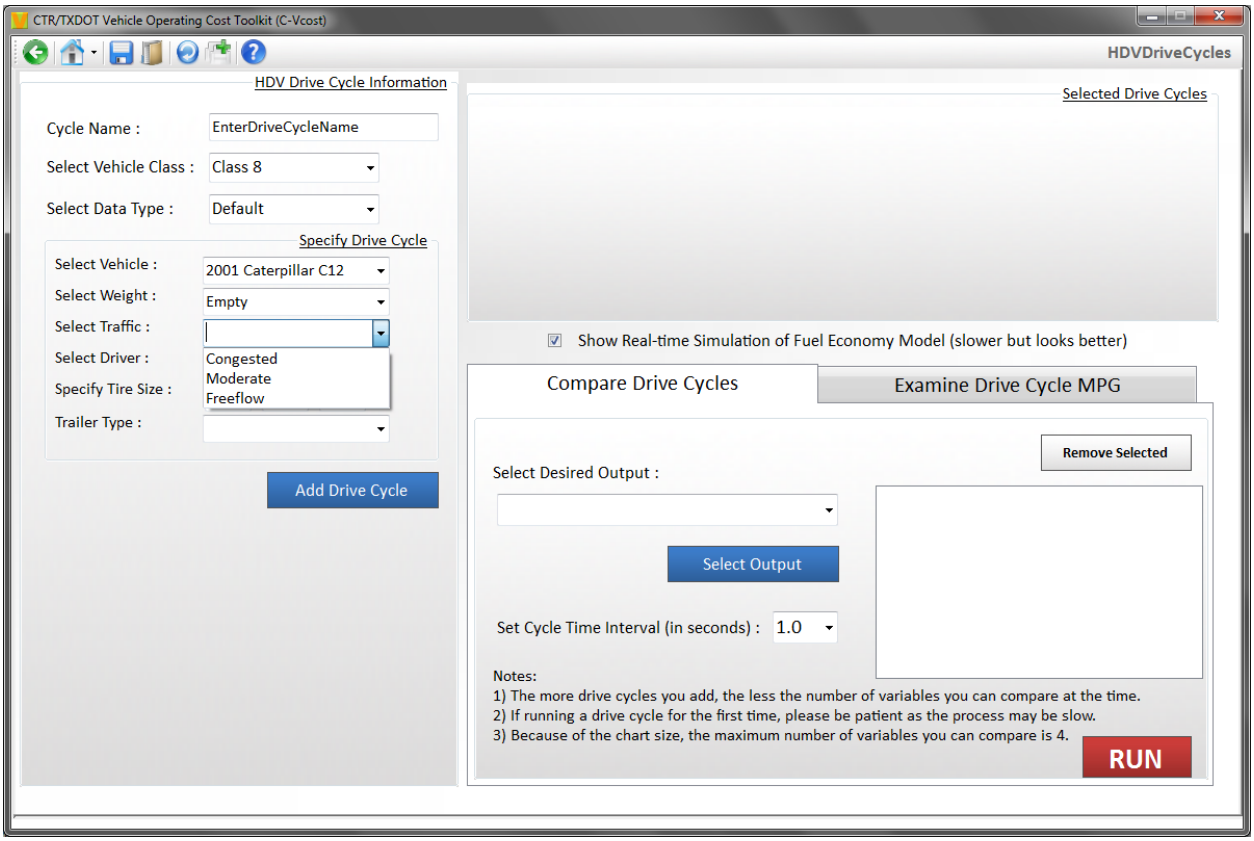

Figure 3.39: The pull-down menu for "Select Traffic" when the "Default" data type is chosen.

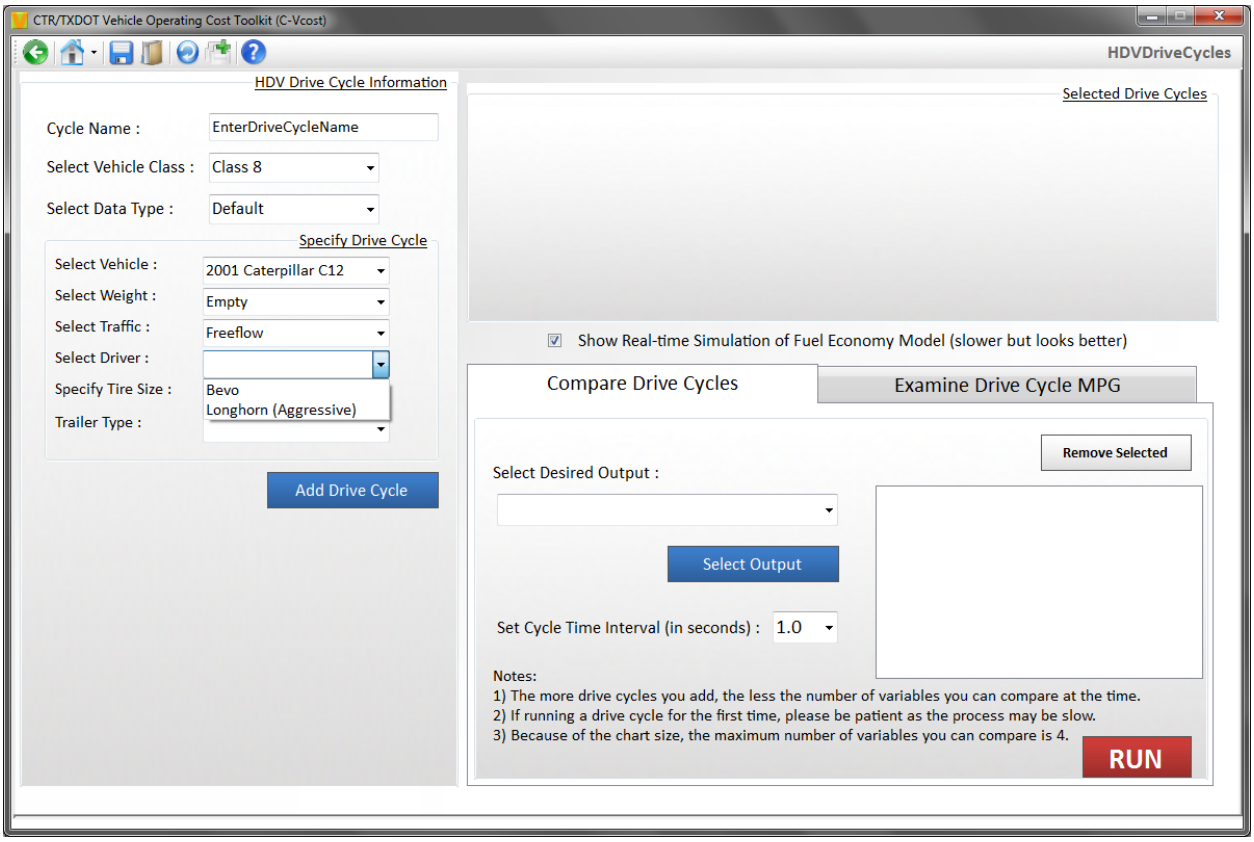

Figure 3.40: The pull-down menu for "Select Driver" when the "Default" data type is chosen.

Again for the "Default" data type selection, the user then inputs the size of the drive tires and, from another pull-down menu, the type of trailer (flat bed or box van), as illustrated in Figure 3.41.

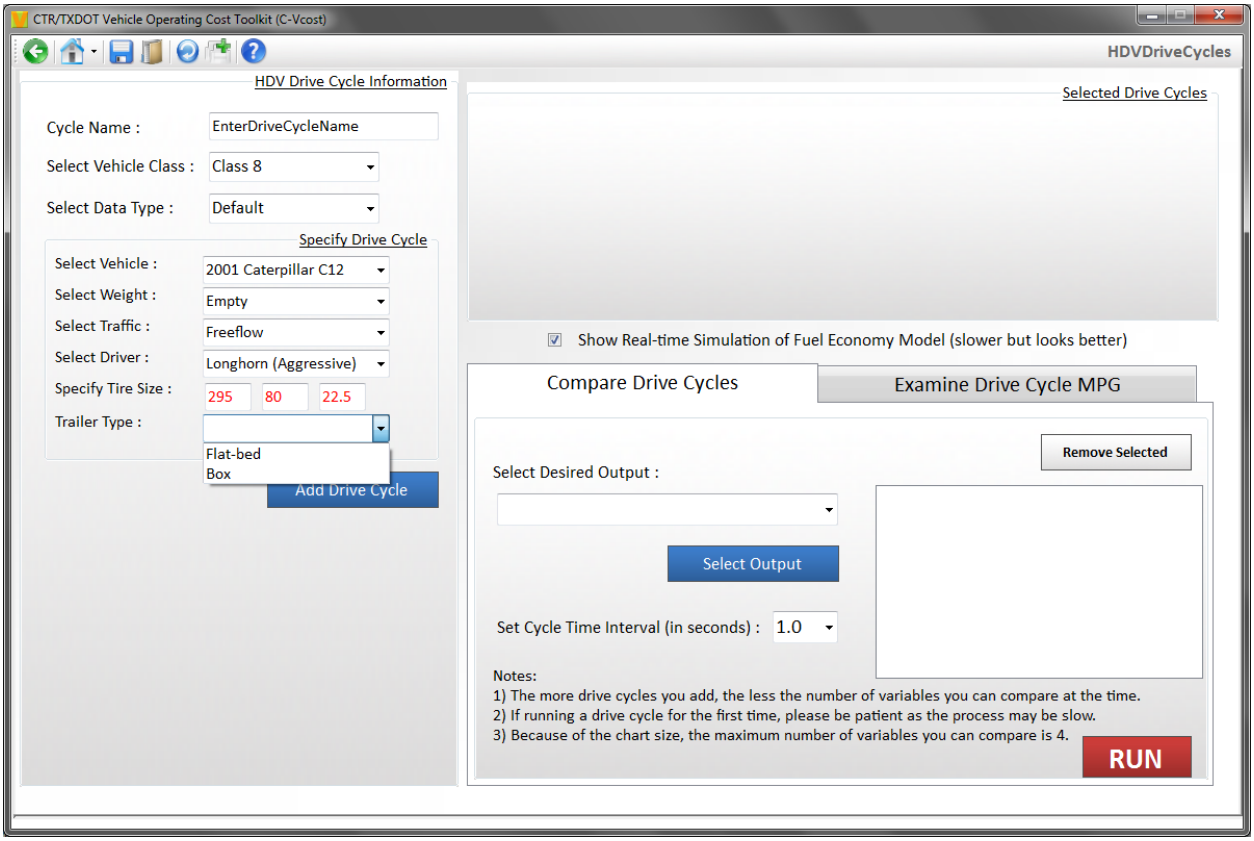

Figure 3.41: The pull-down menu for "Trailer Type" when the "Default" data type is chosen.

If instead of the "Default" option under the "Select Data Type" pull-down menu illustrated in Figure 3.35, the user selects "Custom," additional options appear, as shown in Figure 3.42. In addition to the pull-down menus that also appear for the "Default" data type option (Select Vehicle, Select Weight, Select Traffic, Select Driver, and Select Trailer Type) and the tire size specification, additional information is required from the user.

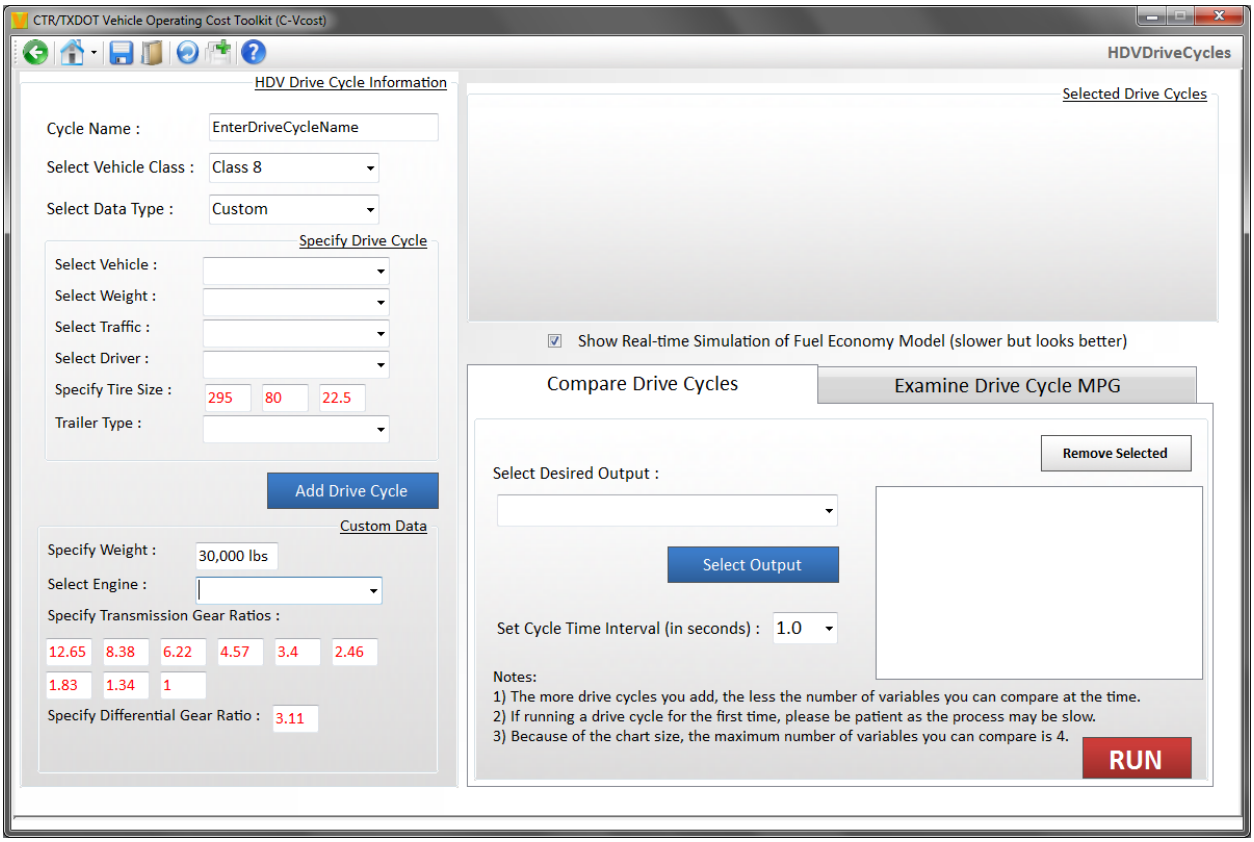

Figure 3.42: Additional pull-down menus that appear if the user selects "Custom" from the "Select Data Type" pull-down menu.

Specifically, the user must input the specific loaded vehicle weight (rather than empty, cubed out, or weighed out), select an engine from the pull-down menu shown in Figure 3.43, and input the transmission gear ratios.

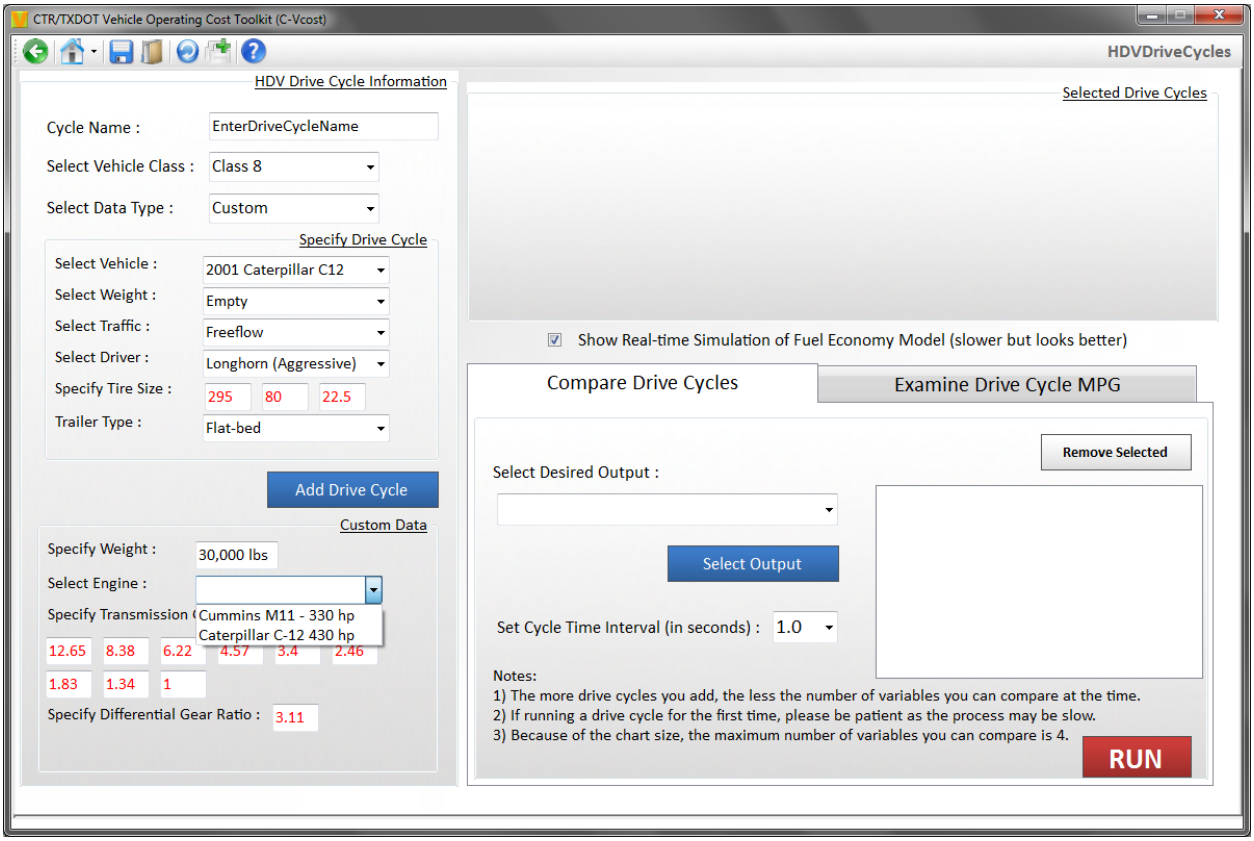

Figure 3.43: Pull-down menu for "Select Engine" that appears if the user selects "Custom" from the "Select Data Type" pull-down menu.

Furthermore, the user must select the type of differential from the pull-down menu illustrated in Figure 3.44 and must input the differential gear ratio.

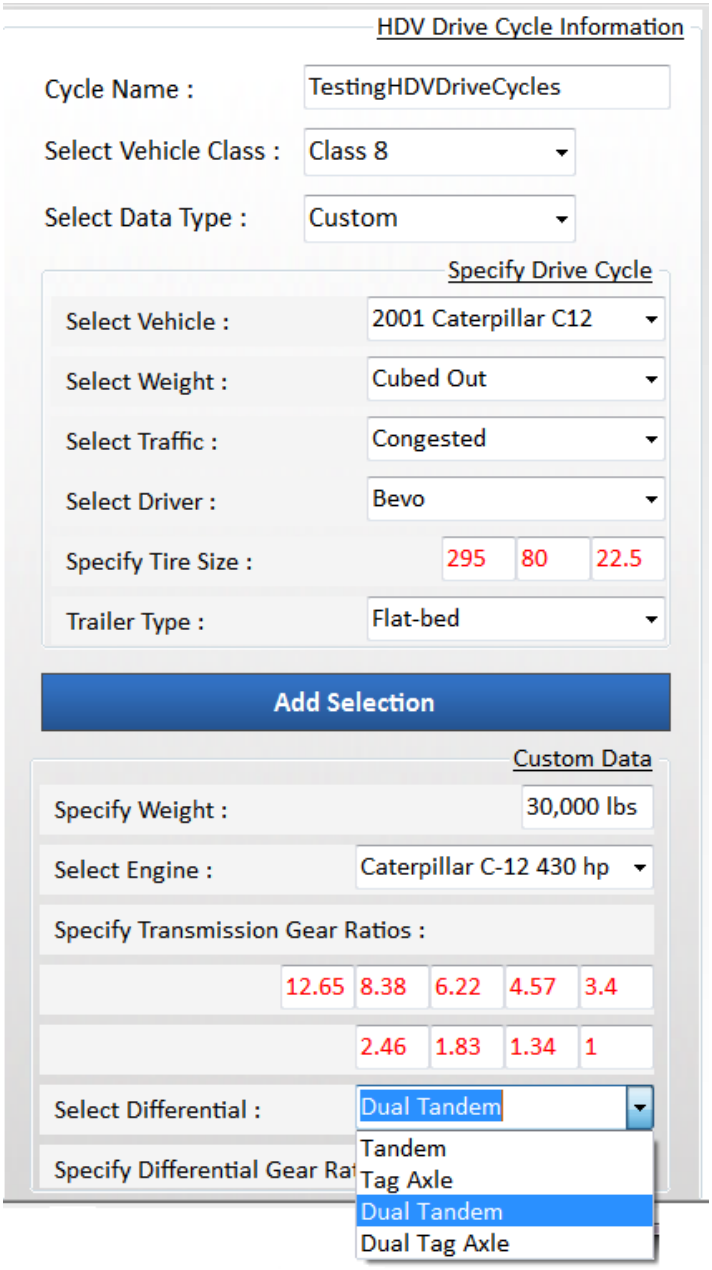

Figure 3.44: Pull-down menu for "Select Differential" that appears if the user selects "Custom" from the "Select Data Type" pull-down menu.

For either the "Default" or "Custom" option from the "Select Data Type" pull-down menu, after completing the required input fields, the user then hits the "Add Drive Cycle" button and a box appears in the upper part of the screen, as illustrated in Figure 3.45.

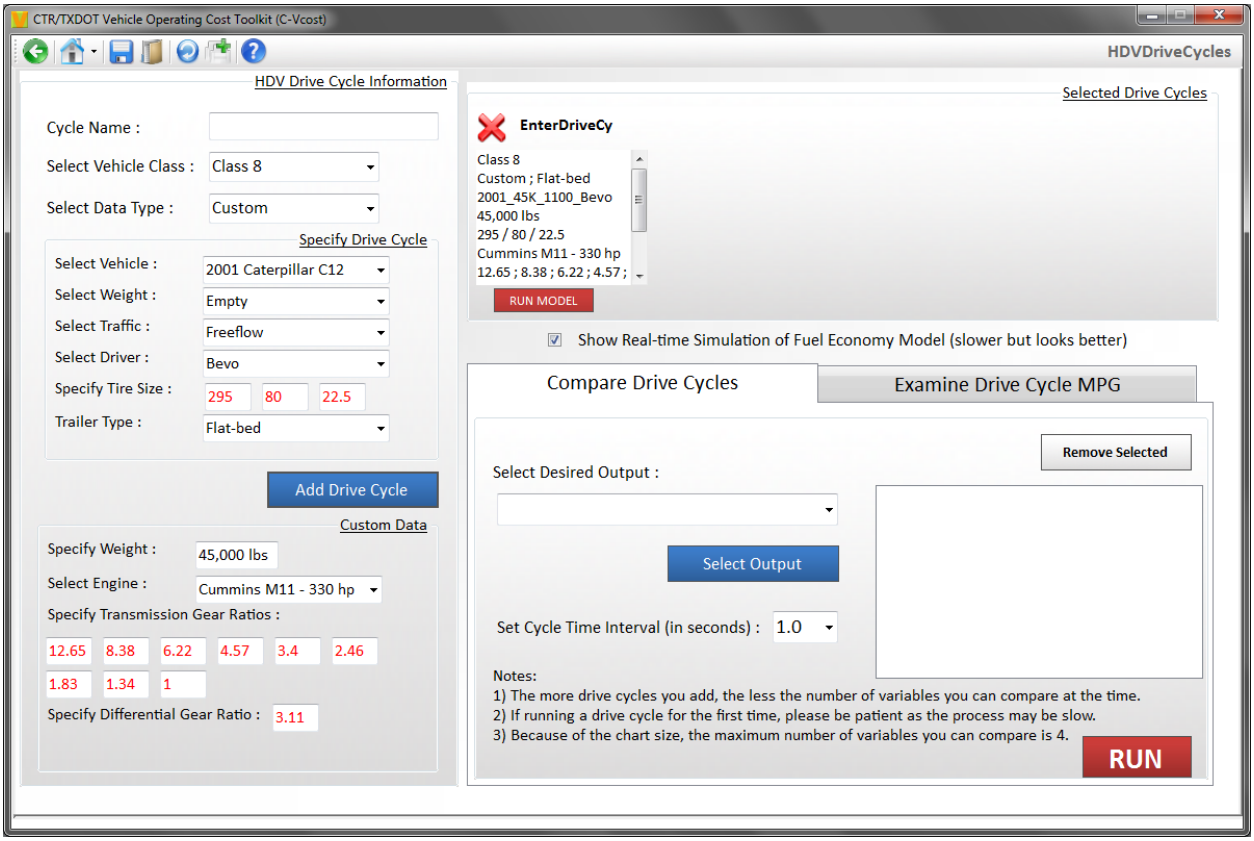

Figure 3.45: Screen that appears after the user hits the "Add Drive Cycle" button from either the "Default" or "Custom" selection from the "Select Data Type" pull-down menu.

The user may then hit the "Run Model" button or first select, from the "Select Output" button, the output to watch while the fuel economy program is running.

Figure 3.46 shows the screen that appears after the program has run and calculated the fuel economy for the HDV over the selected IH 35 driving cycle. Here, it should be noted that this is a screen shot after the fuel economy program has finished running and, thus, shows the fuel economy of the selected HDV after running the IH 35 drive cycle with free flow traffic.

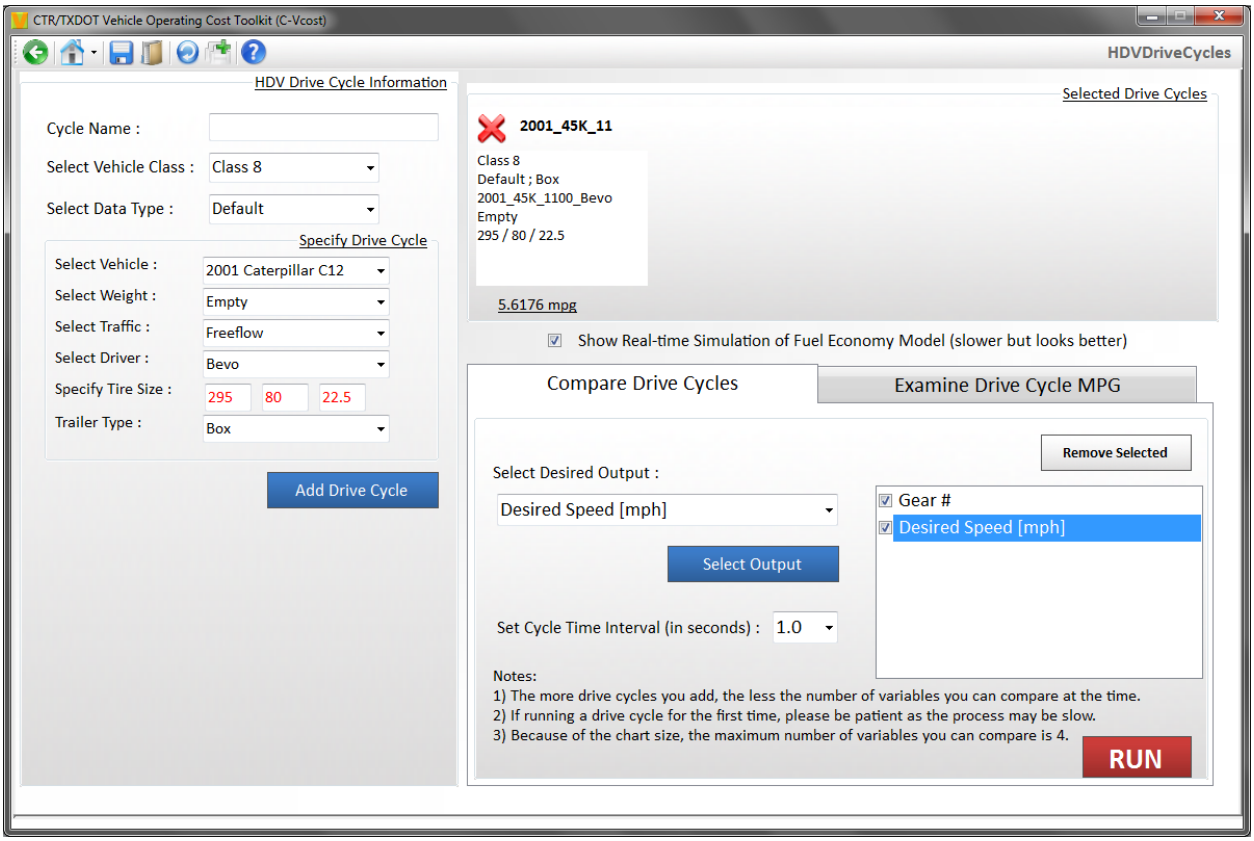

Figure 3.46: Screen that appears after the user has selected the output to display (gear number and desired [and calculated] vehicle speed).

Figure 3.47 shows a screen shot of what the user has chosen to watch while the fuel economy program is running. Specifically, there are graphical displays of the desired and calculated vehicle speeds, the grade, bar charts for the instantaneous engine speed and throttle position, and a table that shows the instantaneous vehicle speed, transmission gear, and throttle position, as well as the TxDOT revenue from the beginning of the driving schedule to the current time during the selected driving schedule. Other options for the displays the user can choose are shown on the pull-down menu in Figure 3.48.

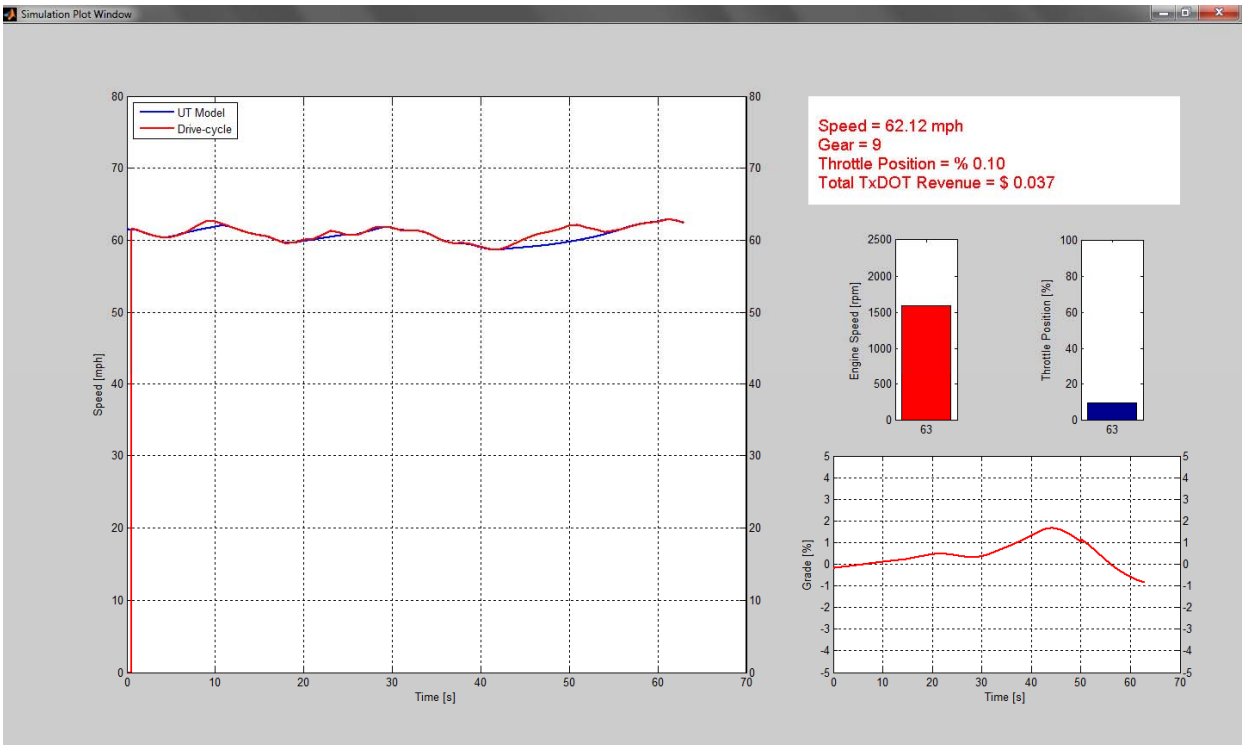

Figure 3.47: Screen shot of what the user has selected to watch while the fuel economy program is running.

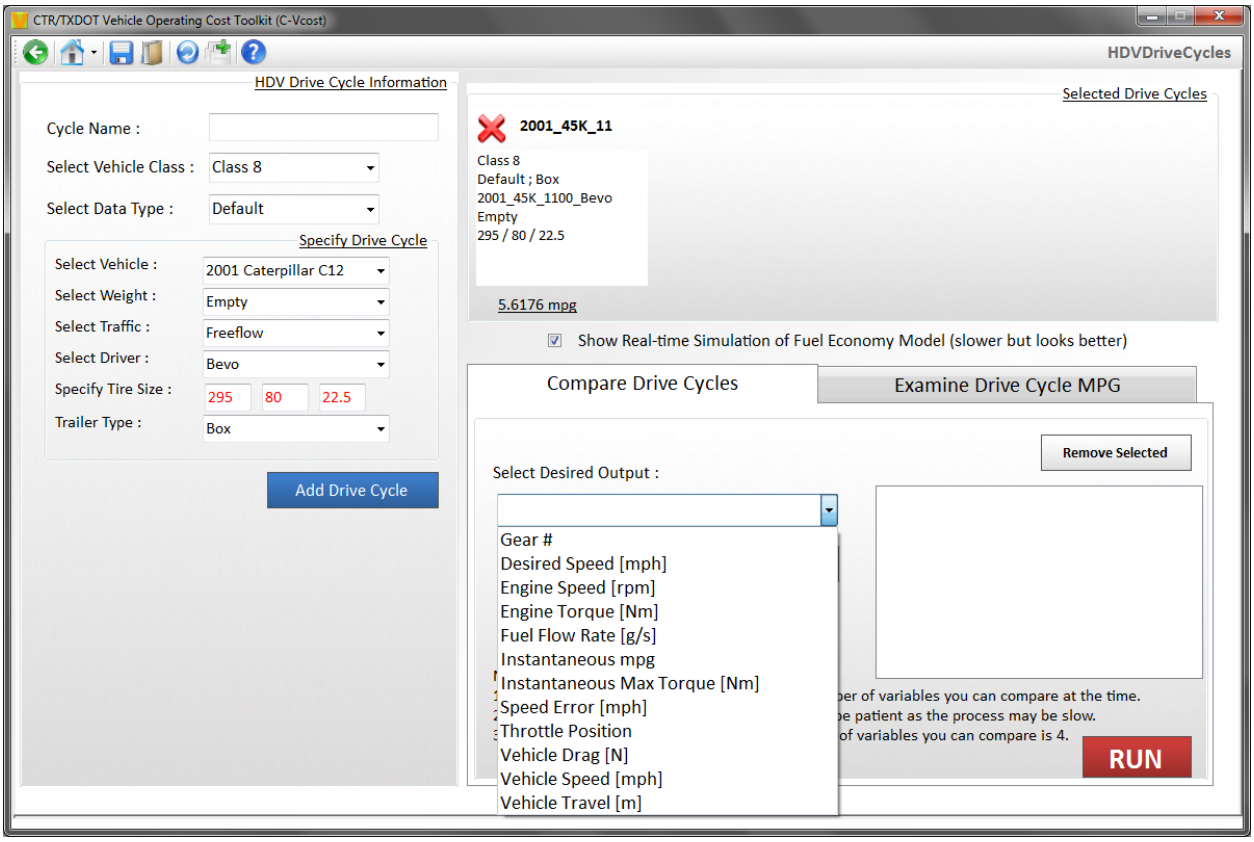

Figure 3.48: Pull-down menu for displays the user can choose to watch while the HDV fuel economy program is running.

The user can also choose to compare the fuel economy of two HDVs, as illustrated in Figure 3.49, or the fuel economy of the same vehicle operating with two different types of traffic congestion, etc.

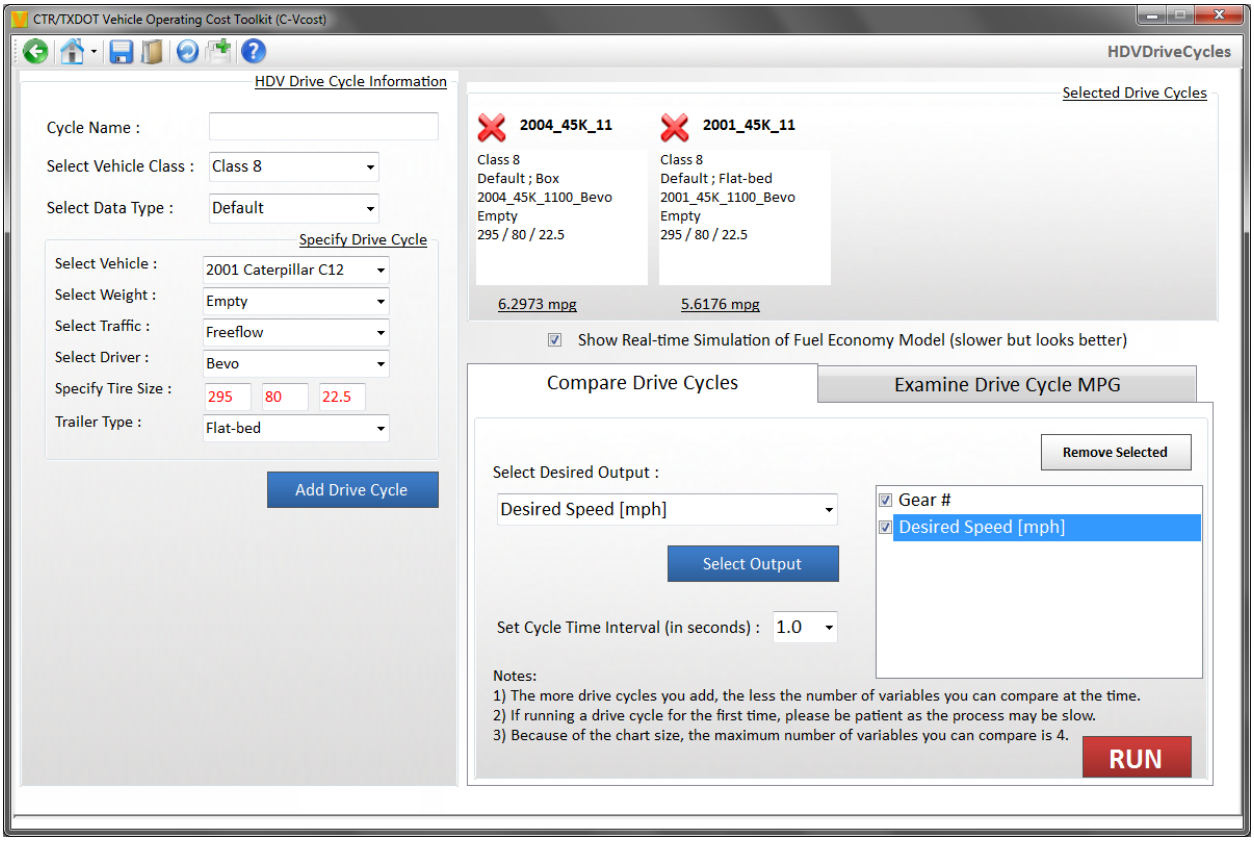

Figure 3.49: Screen shot illustrating comparison of two Class 8 HDVs.

3.3.5 Heavy-Duty Hybrids

Two types of heavy-duty hybrid vehicles were simulated as part of TxDOT Project 0-5974: HEVs and hydraulic hybrids. The heavy-duty HEV models are briefly discussed in Subsection 3.3.5.1. The heavy-duty hydraulic hybrid vehicle models are the subject of Subsection 3.3.5.2.

3.3.5.1 Heavy-Duty Hybrid Electric Vehicles

Hybrid electric vehicles (HEVs) have gained much attention due to their superior fuel economy and low emissions, and they have shown great potential for use in a wide variety of HDVs, especially for urban transit buses, courier trucks, and refuse trucks, which primarily run under stop-and-go conditions and low city traffic speeds.

For TxDOT Project 0-5974, our research team at the UT Center for Transportation Research developed models for both "series" and "parallel" HEVs, including those for both LDVs and HDVs. Submodels included simulations for the hybrid vehicle drivetrain components, a "driver" submodel, a shift strategy submodel, a regenerative braking submodel, and submodels for the control strategies for both series and parallel HEVs.

Each HEV simulation is carried out from the throttle pedal position, through each component of the drivetrain, down to the wheels for a specified driving cycle, which is the desired speed vs. time profile. Thus, one of the inputs to the HEV model is the desired vehicle speed, and one of the outputs is the actual (calculated) vehicle speed. A driver submodel is needed to control the throttle pedal and brake pedal positions based on the error between the actual vehicle speed and the desired speed. A shift control submodel is also important to provide the best match between the power system, the transmission gear ratio, and the vehicle driving condition.

The heavy-duty series HEV simulated as a test case is a standard type-C school bus with a series plug-in HEV configuration. For this series plug-in HEV, the "charge depleting" mode ('thermostat' control concept) was adopted. The engine/generator is operated at its optimum operating point and is used only to maintain the given SOC of the battery pack within a desired window. Compared with the original diesel school bus, the simulated fuel economy was found to improve by 10–15%, and the simulation results were comparable to the experimental results.

The heavy-duty parallel HEVs simulated as model test cases included the P70H and P100H hybrid vans operated by United Parcel Service (UPS). The parallel electric hybrid maintains the vehicle's conventional drivetrain layout and uses patented electric components to blend engine torque with electric motor torque to propel the vehicle. For this project, we chose the torque-based control strategy, and the parallel electric hybrid system model included the following features: electric launch, an engine auto stop/start function, engine-only operation, hybrid traction, battery charge sustaining control, and regenerative braking. The simulation results showed that the fuel economy of the hybrid van is improved by 20–30% compared to the original 70D and 100D diesel vans, and the simulation results agreed closely with the experimental results.

Details of the heavy-duty HEV model are provided in Appendix E.

3.3.5.2 Heavy-Duty Hydraulic Hybrid Vehicles

A hydraulic hybrid powertrain is an alternative type of hybrid that has gained recent interest, especially for HDVs. Hydraulic hybrids have the benefit of having a very high power density and the ability to use many "off the shelf" hydraulic components. The drawback to this technology is that it has much lower energy density when compared to an electric hybrid. Two of the main applications that have seen use of these types of hybrids are refuse trucks and delivery trucks. Both of these applications exhibit duty cycles that involve a great deal of starting and stopping. However, this interest is not limited to HDVs. In January 2011 Chrysler and the EPA announced that a feasibility study would be conducted to evaluate the potential of a hydraulic hybrid system for a large passenger car or LDV.

Specifications for typical hydraulic hybrids were developed. Then models for the pumps, controllers, gear boxes, and accumulators were developed based upon these specifications. Detailed information on these models can be found in Appendix F, which discusses the hydraulic hybrid systems. These submodels were then joined together to predict the fuel economy of the representative vehicles below.

3.4 Parallel Hydraulic Hybrids

The parallel hydraulic hybrid has seen a great deal of interest in refuse truck applications. The typical fuel economy of these vehicles in an urban environment ranges from 1.3 to 2.3 mpg and these refuse trucks travel 8,400 to 9,500 miles/year (Ivanič, 2007; Eaton, 2009). The poor

fuel economy is due to the frequent starts and stops made by the vehicle coupled with its heavy weight. Because of its weight, it also has a very large power requirement during hard accelerations and decelerations. This makes it very well-suited for a hydraulic hybrid system.

The refuse truck that the specifications for the model were drawn from was a Peterbilt 320. This truck can be seen in Figure 3.50 and is commercially available as a hybrid. The layout of the parallel hydraulic hybrid offered by Eaton on the 320 is slightly different than its electric counterpart. Rather than mounting the pump between the engine and transmission, it is mounted between the transmission and differential. While this does provide more room for installation of the additional components, it also requires the addition of a transfer case and limits the pump to recharge only while the vehicle is moving. A depiction of this layout is provided in Figure 3.51.

Figure 3.50: Image of Peterbilt 320 hydraulic hybrid refuse truck (Peterbilt, 2010).

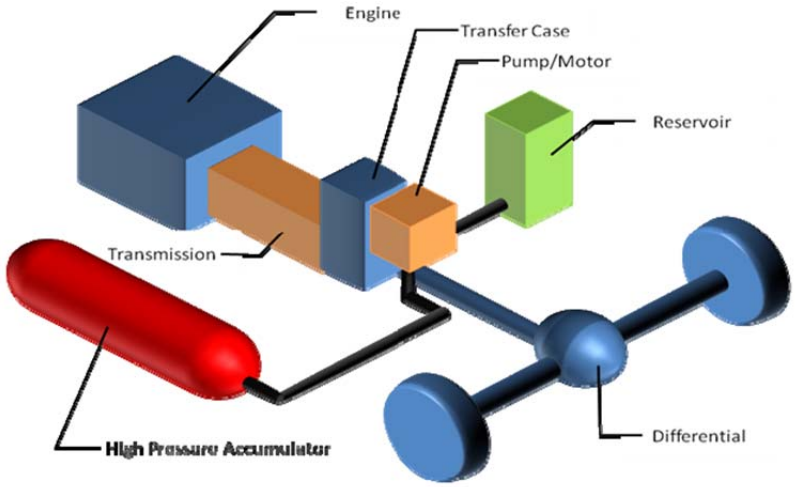

Figure 3.51: Basic representation of typical hydraulic parallel hybrid.

3.5 Series Hydraulic Hybrids

The series hydraulic hybrid has been tested in delivery truck applications with UPS. The EPA, UPS, and International jointly developed this vehicle. The delivery application also has frequent stops and starts like a refuse truck but is much lighter. The series configuration offers the ability to completely decouple the engine from the wheels. This allows the engine to operate independently of vehicle speed and also allows the accumulators to be charged while the vehicle is at rest.

The vehicle used for this model was assumed to be a UPS step van, as shown in Figure 3.52. The specifications for the base vehicle were taken from a study conducted by the National Renewable Energy Laboratory in conjunction with UPS (Lammert, 2009). These specifications are provided in Table 3.6. A basic depiction of the series architecture is show in Figure 3.53.

Figure 3.52: Image of a series hydraulic hybrid being evaluated by UPS (Barry, 2008).

Table 3.6: Basic Parameters for the Step Van Used as a Basis for the Series Hydraulic Hybrid Model (Lammert, 2009).

Parameter	Value
Vehicle Weight	17,500 lb
GVWR	23,500 lb
Engine	VT275
Transmission	Allison automatic

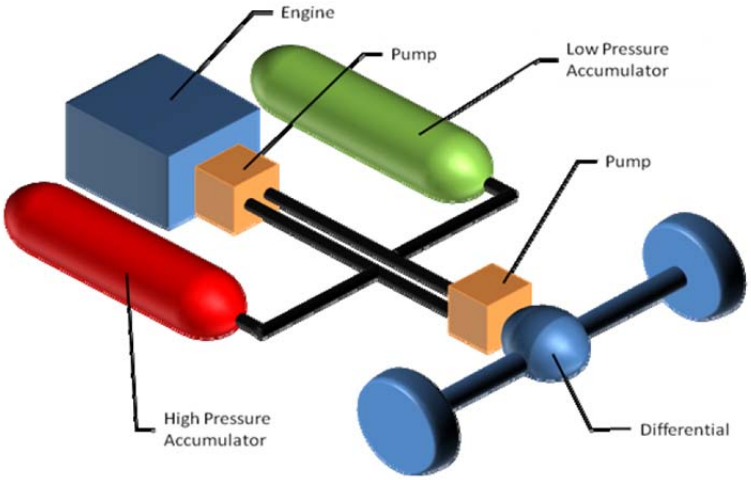

Figure 3.53: Basic representation of a typical hydraulic series hybrid.

3.6 Results

The parallel hydraulic hybrid truck model was evaluated through several standard drive cycles that are representative of a variety of urban drive cycles. The following cycles were used to evaluate the performance of the hydraulic hybrid model.

- New York Truck Cycle
- Central Business District Cycle
- Orange County Bus Cycle
- Heavy Duty Urban Dynamometer Driving Schedule
- West Virginia University (WVU) City Cycle

As would be expected, the hybrid system exhibited a range of performance over the various drive cycles. The results of the simulations can be seen in Table 3.7. The drive cycles that had less idling and more frequent stops yielded the best performance for the hybrid system. A strategy that turned the engine off could help to improve the fuel economy further.

Table 3.7: Predicted Fuel Economy of a Parallel Hydraulic Hybrid.

	New York Truck Cycle	**Heavy Duty Urban Dynamometer Driving Schedule**	**Orange County Bus Cycle**	**West Virginia University City Cycle**	**Central Business District Cycle**
Conventional (mpg)	3.06	6.29	4.53	3.77	4.68
Hybrid (mpg)	3.38	6.71	5.22	4.16	5.91
Percent Improvement	9%	6%	13%	9%	21%

The same drive cycles used for the refuse truck were also used to simulate the delivery trucks. However, a conventional truck was not simulated for comparison because actual data was available for a subset of these cycles for comparison. The NREL complete chassis dyno tests with a conventional and electric parallel hybrid can be seen in Table 3.8.

Table 3.8: Test Results for P100 UPS Delivery Trucks (Lammert, 2009).

	WVU City	**CBD**
Conventional truck	6.87	6.83
Electric hybrid	9.38	9.16

The results from the series hydraulic hybrid model are provided in Table 3.9. There is some variance between the performance of the actual electric hybrid and the simulated hydraulic hybrid. A portion of this can be attributed to the engine on/off operation that was not incorporated in the hydraulic hybrid's operation. This still does not fully account for the performance of the hydraulic hybrid on the WVU City cycle.

It should also be noted that the test weight of the NREL trucks was 17,500 lb while the simulated truck was 23,000 lb. This was done to eliminate any bias that may be present from the heavier hydraulic system.

Table 3.9: Predicted Fuel Economy of a Series Hydraulic Hybrid Delivery Truck.

	New York Truck Cycle	Heavy Duty Urban Dynamometer Driving Schedule	Orange County Bus Cycle	West Virginia University City Cycle	Central Business District Cycle
Hybrid (mpg)	6.06	14.90	9.13	6.73	9.39

3.7 Summary and Conclusions Regarding Modeling Fuel Economy

A new fuel economy model has been developed as a key component of CTR's new CT-Vcost model.

This fuel economy model is "mechanistic;" that is, it is based upon a fundamental treatment of the drivetrain in terms of the relevant physics. The fuel economy model includes a driver submodel that ensures that the vehicle is traveling at the instantaneous speed prescribed by the driving cycle (driving schedule). The driver submodel is in control of the accelerator pedal and the brake pedal. The vehicle submodel uses coastdown coefficients to account for the combined effects of aerodynamic drag and rolling resistance. The powertrain of the vehicle depends upon whether or not it is an LDV or an HDV and also upon whether or not it is a hybrid.

For conventional LDVs, the powertrain consists of an engine submodel, a transmission submodel, and a differential submodel. The light-duty engine submodel relies upon BSFC maps for three types of engines. A BSFC map for a double overhead cam gasoline engine was used for all LDVs except for hybrids and light-duty trucks. This BSFC map is for a vehicle that is approximately 10 years old. Since then, "cam phasers" have been introduced to the market and ~85% of current LDVs have cam phasers. The research team obtained a BSFC map for a cam phaser engine but, due to lack of time, could not incorporate it into CT-Vcost. However, it can be rapidly implemented if either implementation funds for TxDOT Project 0-5974 become available or a follow-on project is funded. A BSFC map for a "push rod" gasoline engine was used for all light-duty trucks and a BSFC map for a Miller cycle engine was used for all light-duty hybrids. Mechanistic models were developed for both light-duty manual transmissions and light-duty automatic transmissions. Mechanistic models were also developed for the differentials in transaxles, for RWD differentials, for AWD differentials, and for the transfer cases in AWD vehicles.

For conventional HDVs, the powertrain consists of a diesel engine submodel, a heavy-duty manual transmission submodel, and a heavy-duty differential submodel. BSFC maps were incorporated for three different heavy-duty diesel engines. Insufficient time was available to allow the research team to develop a technique to normalize these three heavy-duty BSFC maps such that the heavy-duty fuel economy model could simulate any user-specified heavy-duty diesel engine. Heavy-duty differential submodels were developed for tandem differentials, tag axles, and dual differentials.

Mechanistic models for both HEVs and hydraulic hybrid vehicles were also developed for TxDOT Project 0-5974. Both light-duty and heavy-duty HEVs were simulated. The light-

duty HEV model was focused on the Toyota Synergy Drive, which is used not only in the Prius but also in many light-duty hybrids manufactured by other auto companies. Heavy-duty hydraulic hybrids were also simulated, and both series and parallel hydraulic hybrid models were developed. Although executable files were generated for all of these hybrids, there was insufficient time to incorporate them into CT-Vcost. However, these models can be implemented fairly rapidly.

3.8 Resources in the Appendices

The Mechanical Engineering team completed a wide variety of research activities that will enhance future versions of the CT-Vcost model and prove valuable for other researchers examining the impact of future vehicle engineering changes. This research is presented as a series of appendices:

- Appendix A. Engine Models
- Appendix B. Transmission Models (includes light and heavy-duty manual and automatic)
- Appendix C. Differential Models (includes light-duty transaxles, rear wheel and four wheel drive and heavy-duty)
- Appendix D. Light-Duty Hybrid Electric Vehicle Model
- Appendix E. Heavy-Duty Hybrid Electric Vehicle Models
- Appendix F. Heavy-Duty Hydraulic Hybrid Vehicle Model

The next chapter provides a summary of the report and makes recommendations for future work as new vehicle designs are introduced in this decade.

Chapter 4. Summary, Conclusions, and Recommendations

The 0-5974 work was completed in two phases: an initial 2-year study demonstrating "proof of concept" (as Vcost studies are notoriously difficult) and a second of equal length that focused on those issues most important to the sponsor. The first produced a basic Vcost model focusing on gasoline light-duty (auto and pickup) vehicle fuel and other operating costs, together with experiments needed to measure heavy truck fuel consumption. The results are recorded in the study report 0-5974-1. The second phase, as noted in Chapter 1, was a 2-year period focused on three objectives: 1) improving the Vcost model, 2) measuring heavy truck fuel consumption, and 3) developing fundamental models for two hybrid autos and a single heavy truck. The ambitious structure of the fuel element in the work aimed at modeling, measuring, and then synchronizing engine, transmission, and differential forces to more accurately estimate total vehicle operating costs.

Modeling vehicle operating costs, whether by operator surveys or experimental methods, is challenging as noted in the introduction of this report. A single vehicle model (usually an auto) was generally the base for all Vcost estimation until the World Bank HDM III study reported its findings in the mid-1980s. This was a major improvement in cost estimation but one which still lacked transferability over time, even when Vcost estimates used mechanistic techniques, because of the rapidly changing field of mechanical and computer technologies. The last two decades to 2012 witnessed the implementation of an array of design elements, materials, sensors, and computer systems in the new designs of all vehicles. These aimed at to increase efficiency—particularly fuel consumption and drive train longevity, and environmental aspects—in order to meet a series of tighter EPA exhaust emissions standards, particularly for heavy trucks[14].

4.1 Conclusions

The challenge for the team was to design an approach that could be updated as further improvements are introduced by mechanical engineers and vehicle designers. Box 4.1 records various technologies being evaluated or slowly introduced in 2011 and likely to be adopted over the coming decade in the area of fuel efficiency—a critical area for TxDOT funding[15]. The team was split into mechanical engineers who selected representative vehicle engine, transmission, and differential designs reflecting the 2010 Texas motor vehicle fleet and a CTR team that modeled the findings so that TxDOT staff could use updated Vcost estimates. The model containing the results and a user manual were the products of the work.

Box 4.1: Engine Fuel Efficiencies

1. Cam Phasers
2. Direct Injection Spark Ignition (DISI)
3. Mild Hybrids
4. Extended range electric vehicles (EREVs)
5. Dual mode hybrids
6. High speed diesels
7. Dual clutch transmissions
8. Heavy duty automatic transmissions

This report addresses the following:

[14] These started in the late 1990s, with the most stringent being 2001 and 2010.

[15] This is in the United States—high speed diesels and dual clutches are already operating in Europe.

1. Heavy trucks, particularly the ubiquitous 80,000 lb. semi-trailer that accounts for almost 80% of long distance freight in the state,
2. Engine-transmission-differential systems,
3. Hybrid models for autos and heavy trucks, and
4. Report of the findings in an enhanced version of the Vcost model.

The study timetable required that all technical elements be finalized by the end of May for incorporation into the model, as invariably unintended consequences arise when a new element is substituted within a large model. The mechanical engineering research continued until the end of the project and, although it appears in the various appendices, much of the summer 2011 work is not reflected in the Vcost model itself. While this is disappointing, reporting the fundamental work required for any future Vcost model improvement will be a major contribution to its likely success.

The basic Vcost model, as detailed in Chapter 2, was termed CT-Vcost and utilizes an object-oriented programming structure where modules are developed to perform specific tasks. The toolkit's default data are based on verified secondary vehicle cost data and certified vehicle databases, including the EPA's Fuel Economy and Annual Certification Test Results databases. The toolkit also allows users to change parameters so that cost calculations are specific to any particular situation, and can be updated as the economic or technological landscape changes. Cost categories in the CT-Vcost toolkit include the following:

1. Depreciation,
2. Financing,
3. Insurance,
4. Maintenance costs,
5. Fuel cost,
6. Driver costs,
7. Road use fees, and
8. Other fixed costs, such as annual vehicle registration and inspection fees.

Analysis types that can be performed with CT-Vcost include single vehicle analysis, multi-vehicle comparisons, fleet vehicle analysis, growth rate and market penetration simulation, and route cost analysis. CT-Vcost is compatible with the sophisticated fuel economy prediction models also developed in this study and discussed in Chapter 3. The fuel economy models have the ability to predict fuel consumption for default or custom drive cycles specified by the user. Output from the fuel economy models can be used within the toolkit to perform route cost analyses. CT-Vcost is also updatable and can be easily calibrated for other states or regions. In summary, CT-Vcost was designed to be intuitive and flexible enough for simulating different scenarios and situations that users may envision.

4.2 Recommendations

The CTR team responsible for the CTR-Vcost model intends to promote its use within TxDOT during the coming year in a variety of areas. The model was successfully used to examine trucker use of SH 130, and was able to explain both the low utilization and the trucker choice of segments. Where possible, the team will also make changes to the model to capture some of the mechanical engineering results reported but not modeled due to contract deadlines. The team will also calibrate the model based on feedback from Texas truck operators.

The broad range of Vcost—in terms of aggregate cost and its sub-components—will critically impact TxDOT in the coming decade. A major factor is the revenue derived from both diesel and gasoline consumption in the state.

However, in addition to changes in consumer demand, two regulatory factors will drive both the heavy-duty trucking industry and the light-duty vehicle manufacturers to increase fuel economy more significantly than annual increases noted over the last quarter of a century. This suggests that the use of historic time series data may provide poor estimates of actual fuel purchases. Fuel economy standards for light-duty vehicles were stagnant for about 20 years, until slightly more stringent new standards were implemented for a phase-in from 2011 to 2015. However, on July 29, 2011, President Obama announced the implementation of new standards that will require the doubling of corporate average fuel economy, relative to 2010, between 2017 and 2025. Additionally, heavy-duty vehicles have never been subjected to fuel economy standards. On August 9, 2011, President Obama announced heavy-duty vehicle fuel efficiency standards that will be phased in from 2014 to 2018. These standards will require an ~20% improvement in the fuel economy of semi-trucks, an ~15% improvement in the fuel economy of heavy-duty pickup trucks and vans, and an improvement in the fuel economy of "vocational vehicles," such as delivery trucks, buses, and garbage trucks, by approximately 10%.

These new regulations will force the development of new technologies that are not included in the CT-Vcost Fuel Economy Model. However, due to the structure of this model (the fact that it is based on fundamental physical models of vehicle subsystems), the CT-Vcost Fuel Economy Model can be modified to include these new technologies as they emerge. The trucking sector has, however, already begun to implement a wide variety of policies and equipment changes to address what they believe will be the inevitable rise in fuel costs over the coming decade. Figure 4.1 shows that latest Volvo 2011 tractor being introduced as the key vehicle in the HEB grocery distribution system.[16] A wide range of technical changes including engine, transmission, aerodynamics, and low rolling resistance extra-wide tires have enabled this specification to exceed the 2011 Obama 2017 fuel consumption targets.

The rapidly changing world of vehicle engineering, design, and Vcost estimation will further impact TxDOT in these aspects:

1. Fleet replacement, as the latest engines are more expensive and drivers are increasingly demanding automatic gearboxes.
2. Economic models needed for bonus and penalty calculations and a variety of cost-benefit calculations.
3. Higher costs may alter vehicle miles of travel (VMT) estimates used in a range of planning models.

[16] HEB has over 500 tractors and 2,200 trailers, both 53' and 57' ft. (the latter is permitted in Texas with no increase in weight).

4. Improving trucker use of toll road systems. The current traffic and revenue studies cannot provide accurate cost benefits for truck use and the evidence strongly suggests that toll rates are currently set too high if they are intended to stimulate truck utilization.

Figure 4.1: Volvo 2011 tractor

The key objective of 0-5974 in 2007 was to provide TxDOT staff with a model that reflected the new Texas fleet rather than that of the 1980s when the last study was conducted. CT-Vcost is a milestone in providing TxDOT with current auto and trucking cost estimates. It is being used in a new study—0-6692, Truck-Rail Intermodal Flows: A Corridor Toolkit—which will be designed to identify the cost point where rail intermodal can compete with trucks on a range of Texas corridors. The model is designed to be updated relatively easily as new technologies are adopted by the industry and users and the work reported in the appendices should assist in keeping the model up to date and relevant to TxDOT needs.

Appendix A. Engine Models

Engine models were required for both spark ignition (SI) engines and diesel engines. It was originally intended that the award-winning UT Fractal Engine Simulation (UT FES) could be used directly for the SI engine model and modified for use as the diesel engine model. However, UT FES was written in Fortran and a compatible complier could not be found. Thus, as was explained in Subsection 3.2.3.1, maps of the brake specific fuel consumption (BSFC) as a function of normalized load (brake mean effective pressure, or BMEP) and engine speed (rpm or percent peak rpm) were used for the engine modeling task.

The BSFC maps for SI engines are discussed in Section A.1 and the BSFC maps for diesels are discussed in Section A.2.

A.1. SI Engines

As discussed in Section 3.2.3.1, a (scalable) BSFC map for a double overhead cam engine was used for all LDVs except light-duty trucks and light-duty hybrid electric vehicles (HEVs). A (scalable) BSFC map for a push rod engine was used for all light-duty trucks. A BSFC map for the Miller cycle engine in the Prius was used for all light-duty HEVs. Here it should be noted that not all light-duty trucks use push rod engines and not all light-duty cars have double overhead cam engines. Additionally, not all light-duty HEVs use Miller cycle engines. However, the research team believes that the inaccuracies encountered via these assumptions are reasonably small.

The BSFC map for the double overhead cam engine is shown in Figure A.1. The BSFC map for the push rod engine is shown in Figure A.2. The BSFC map for the Miller cycle engine is shown in Figure A.3.

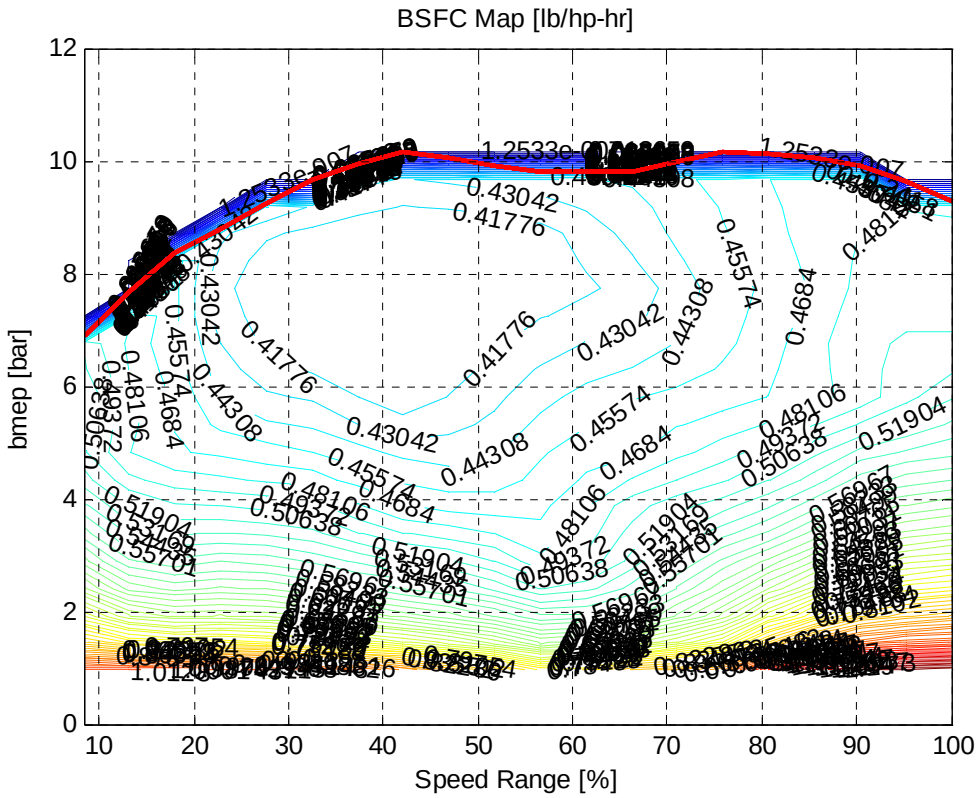

Figure A.1. This BSFC map was scaled for use to simulate all light-duty SI engines except for light-duty trucks and light-duty HEVs (Wipke et al., 1999, version 2002).

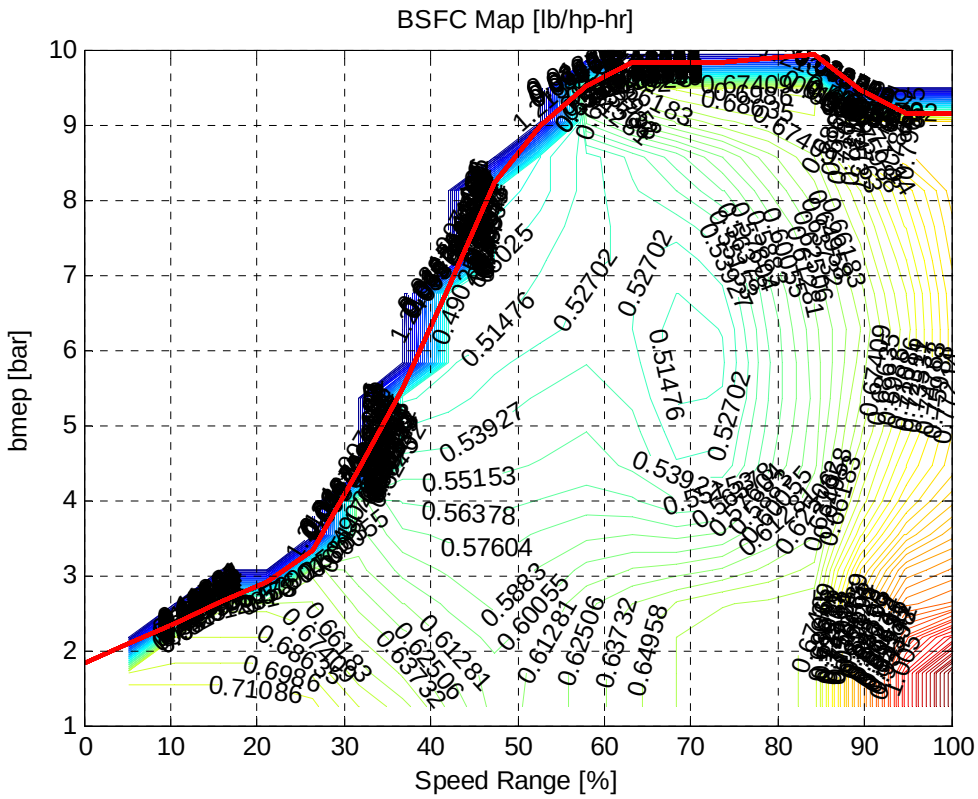

Figure A.2. This BSFC map was scaled for use to simulate all light-duty trucks (Wipke et al., 1999, version 2002).

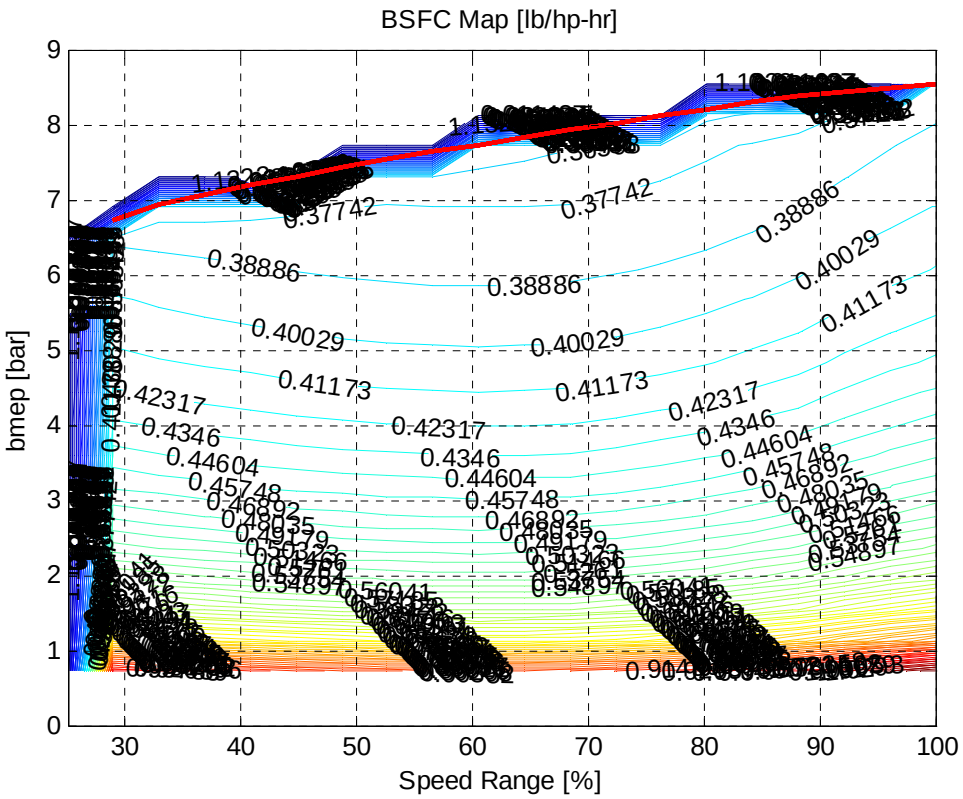

Figure A.3. This BSFC map was scaled for use to simulate all light-duty HEVs (Wipke et al., 1999, version 2002).

A.2. Heavy-Duty Diesel Engines

Figure A.4 shows the BSFC map for a Detroit Diesel Engine Company Series 30 7.3 L, 171 kW diesel engine that was used to simulate the engine in all EPA Class 7 trucks.

BSFC maps for two heavy-duty diesel engines were used for EPA Class 8 trucks. Figure A.5 is the BSFC map for a 10.8 L, 246 kW Cummins M11-330 heavy-duty diesel engine. This map was scaled for application to all diesel engines. Figure A.6 is the BSFC map for an 11.8 L, 306 kW Caterpillar C12 heavy-duty diesel engine.

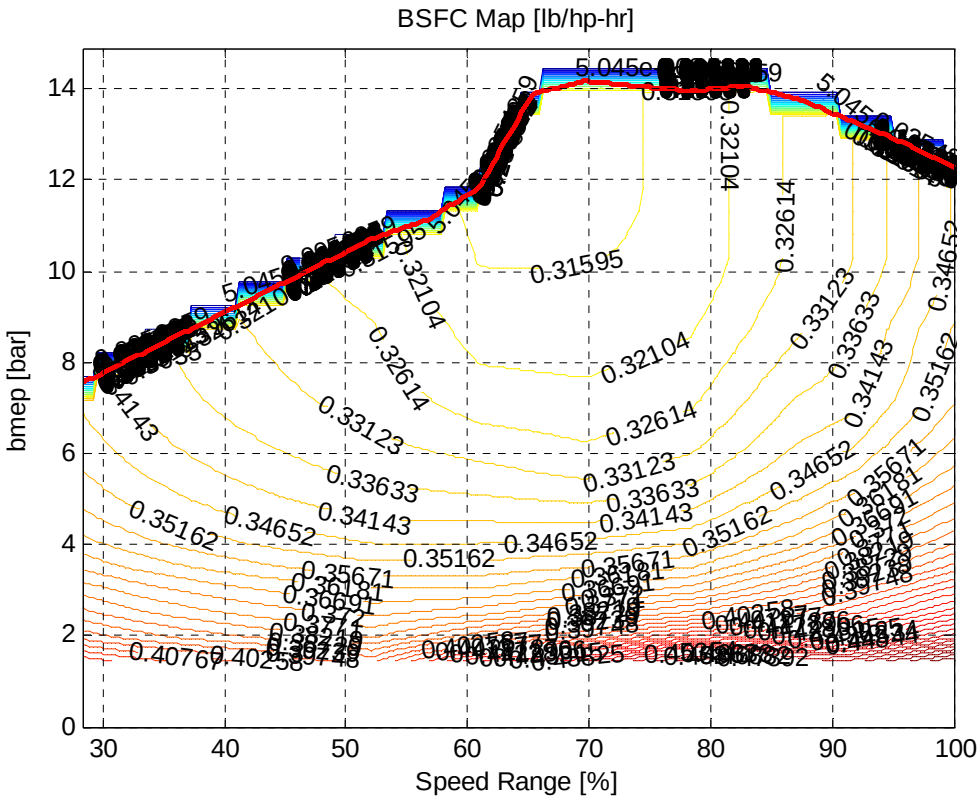

Figure A.4. The BSFC map for a 7.3 L, 171 kW Detroit Diesel Series 30 heavy-duty diesel engine (Wipke et al., 1999, version 2002).

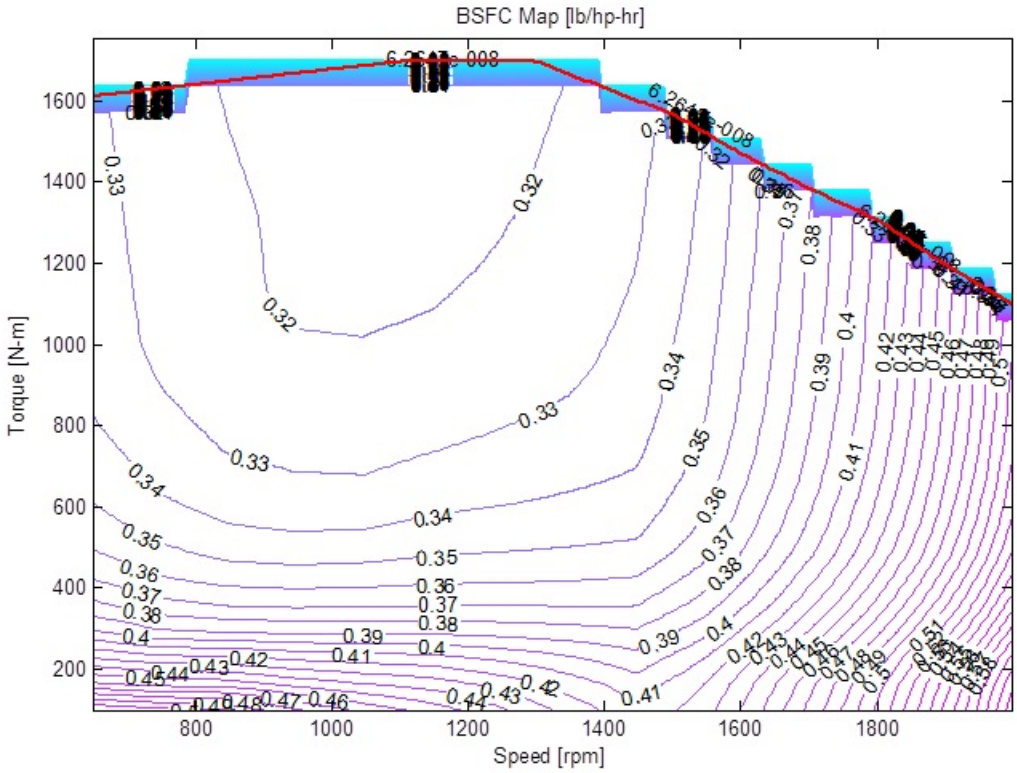

Figure A.5. The BSFC map for a 10.8 L, 246 kW Cummins M11-330 heavy-duty diesel engine (Wipke et al., 1999, version 2002).

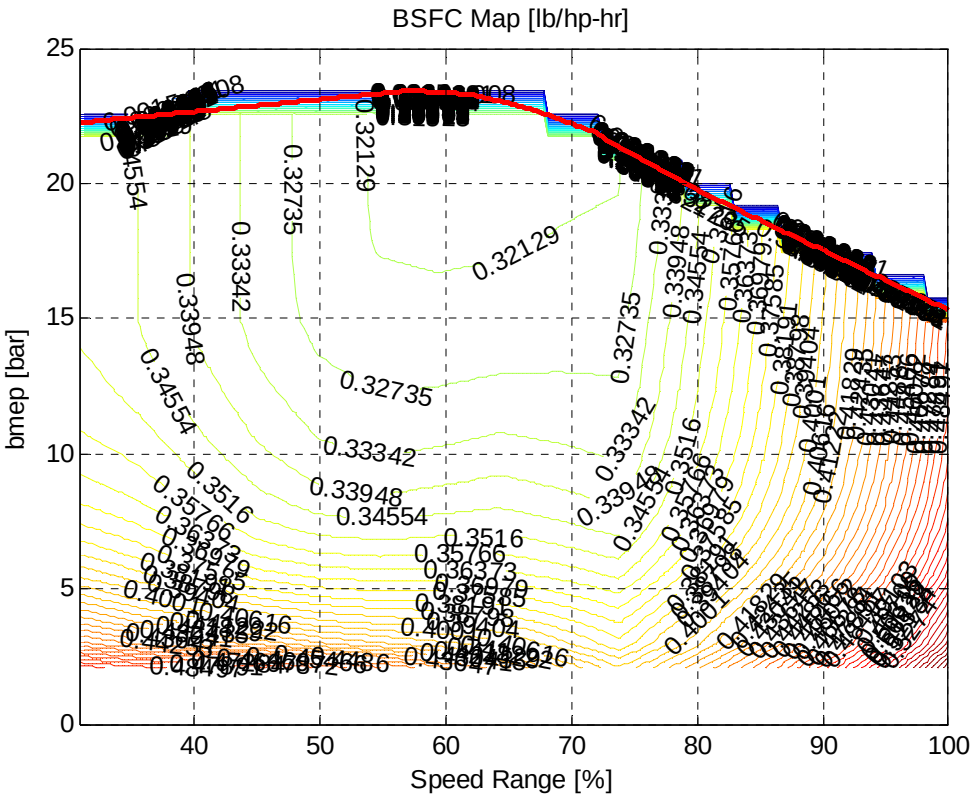

Figure A.6. The BSFC map for an 11.8 L, 306 kW Caterpillar C12 heavy-duty diesel engine (Wipke et al., 1999, version 2002).

Appendix B. Transmission Models

Transmissions are used to provide both a torque multiplication and a rotational speed reduction between the engine output and the differential input. However, the torque multiplication is inefficient due to gear pair losses, "windage" losses, bearing losses, seal losses, etc. Models for the various categories of transmissions are required in order to account for these losses.

Physically based models were developed for both manual transmissions (as discussed in Section B.1) and automatic transmissions (discussed in Section B.2). These models are the subjects of the following sections of this appendix.

B.1. Manual Transmissions

The efficiency of a manual transmission is a result of frictional losses in the gear pairs and other losses (bearings, the input shaft seal, the output shaft seal, and aerodynamic and hydrodynamic drag on the rotating elements). This section of Appendix B provides the fundamentals of the manual transmission models developed for the TxDOT Project 0-5974.

The base transmissions chosen for three different vehicle classes are discussed in Subsection B.1.1. The various torque loss factors included in the model development for a manual transmission (or transaxles) are discussed in Subsection B.1.2. The models' results and verification are discussed in Subsection B.1.3.

B.1.1. Base Transmissions for Each Class

As numerous manual transmissions have different designs, gear ratios, torque capacities, and components (e.g., gears and bearings), beginning the transmission modeling task by developing a generic transmission model would be extremely difficult and would yield an inaccurate model. Therefore, it was decided to select one of the most popular manual transmissions in each vehicle class—light-, medium-, and heavy-duty vehicles—and then develop a detailed model for each of these representative transmissions.

The three transmissions chosen were the Tremec T5 for LDVs, the Eaton Fuller FS6306A for medium-duty trucks, and the Eaton Fuller FRO16210C for HDVs.

Each of the three selected manual transmissions were disassembled either by the PhD student who developed the transmission models (Kyung Jin Kim) or by a professional mechanic. After disassembly, all necessary specifications were measured and recorded to aid development of computational models that predict the transmission efficiency.

B.1.1.1. Tremec T5 Light-Duty Manual Transmission Model

The Tremec T5 is a 5-speed manual transmission initially manufactured by Borg-Warner in 1980. The current manufacturer, the Transmission Technologies Corporation (TTC), bought the rights to manufacture this transmission design in 1998 and sells it under the brand name "Tremec." The T5 transmission has been in production longer than any other manual transmission. This manual transmission has been used in more than 20 different vehicles manufactured by both domestic and overseas car companies. Vehicles that have used the T5 transmission include the Ford Mustang, Ford Fairmont, Thunderbird, Mercury Cougar, Chevrolet Camaro, Pontiac Firebird, Chevrolet Blazer, and Chevrolet S-10.

Due to this popularity and long history, the T5 transmission was chosen to represent light-duty manual transmissions for this project. The Tremec T5 has had more than 40 different models (design variations) since its first production. Among those 40 different models, the version used for the base model for this project was the Tremec T5 "World Class." The specific version of the Tremec T5 World Class used for this project is discussed below.

Naunheimer and coauthors (2010) categorize gearboxes using the term "stage." The stage refers to the torque flow from one shaft to another. For example, if the input torque (the engine output torque) is transmitted to the output shaft via an intermediate shaft (the "layshaft"), then the transmission is categorized as a two-stage gearbox (input shaft to layshaft and layshaft to output shaft). In some designs, the layshaft is the output shaft. In this case, the transmission is categorized as a single-stage gearbox. Normally, the term "stage" is sufficient for the discussion of how a manual transmission works, but for improved understanding the term "gear step" can be used as an alternative. The gear step implies torque conversion via one gear pair, which consists of a "drive" gear and a "driven" gear. A basic schematic and specifications for the Tremec T5 two-stage transmission are provided in Figure B.1 and Table B.1.

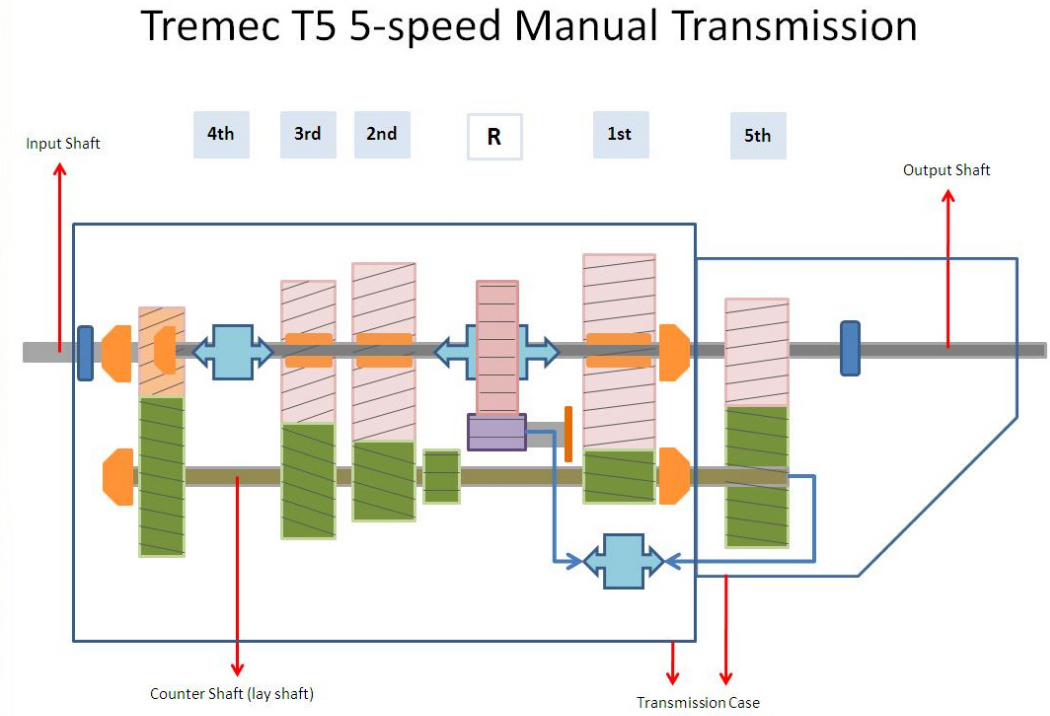

Figure B.1. Schematic of a Tremec T5 WC transmission.

Among 33 variations of the T5 WC design, the base light-duty manual transmission model was based on T5 transmission part number 1352-000-208. This 5-speed base transmission has some interesting design features such as two separate cases (a separate case for the overdrive gear pair), and the fact that high gear (4th) is "direct drive" (in 4th gear, the input shaft is directly coupled to the output shaft with no torque conversion through gear pairs [zero gear steps]). Except for the direct drive/driven 4th gear, all gear speeds function via torque transmission from the input shaft to the layshaft, and then from the layshaft to the output shaft through two gear steps.

In Figure B.1, the orange colored blocks are bearings, the blue colored blocks are rubber seals, and the light blue colored blocks with arrows pointing two directions represent the synchronizers.

One of the lubricants recommended by the manufacturer, Royal Purple Synchromax synthetic transmission fluid, was used as the transmission fluid in the present model for the T5 transmission.

Table B.1. Tremec T5 WC Transmission Specifications

(from http://www.ttcautomotive.com/English/products/T-5.asp).

Tremec T5 (Part #: 1352-000-208)	
Torque capacity	**175–230 lb-ft**
Weight	75 lb
1st gear ratio	3.35
2nd gear ratio	1.99
3rd gear ratio	1.33
4th gear ratio	1.00
5th gear ratio	0.68
Reverse gear ratio	3.15

B.1.1.2. The Eaton Fuller FS6306A Medium-Duty Manual Transmission Model

Generally, 6-speed and 8-speed manual transmissions are the two most popular types of manual transmissions used for medium-duty vehicles although some medium-duty vehicles are equipped with 5-speed manual transmissions. According to unofficial sales data provided by Peterbilt Motors Company, 55% of the Class 5 trucks they produce are equipped with 6-speed manual transmissions and the remaining 45% use 8-speed manual transmissions. The Eaton Fuller FS6406A and FSO6406A 6-speed manual transmissions are the bestselling transmissions for Class 5 trucks. The FSO6406A is the overdrive version of the FS6406A transmission with a different 6th gear ratio. Therefore, those two transmissions can be considered as essentially the same.

The Eaton Fuller FS6306A transmission was chosen for the current project as the base manual transmission model for medium duty vehicles. The Eaton Fuller FS6306A is the previous version of the current FS6406A transmission. Simply, the FS6406A is the upgraded version of the FS6306A but both have the same torque capacity and gear ratios. This two stage transmission provides 6 gear ratios with no overdrive gear, and a direct drive connection (locking the input shaft to the output shaft) supplying the torque for the 6th speed. When not in 6th gear, the torque is increased via two gear steps just as for light-duty manual transmissions.

A basic schematic and specifications of the FS6306A are provided in Figure B.2 and Table B.2 (from www.roadranger.com and "Eaton Fuller Heavy Duty Transmissions Service Manual: TRSM0110"). The orange, blue, and turquoise colored blocks in Figure B.2 indicate the bearings, rubber seals, and synchronizers, respectively. The power take off function that is available on some variations of this transmission was not included in the model because it is irrelevant to the purpose for the model. The properties for one lubricant that meets the

manufacturer's specifications for this transmission, Chevron Delo Synthetic Transmission Fluid SAE50, were used in the present model.

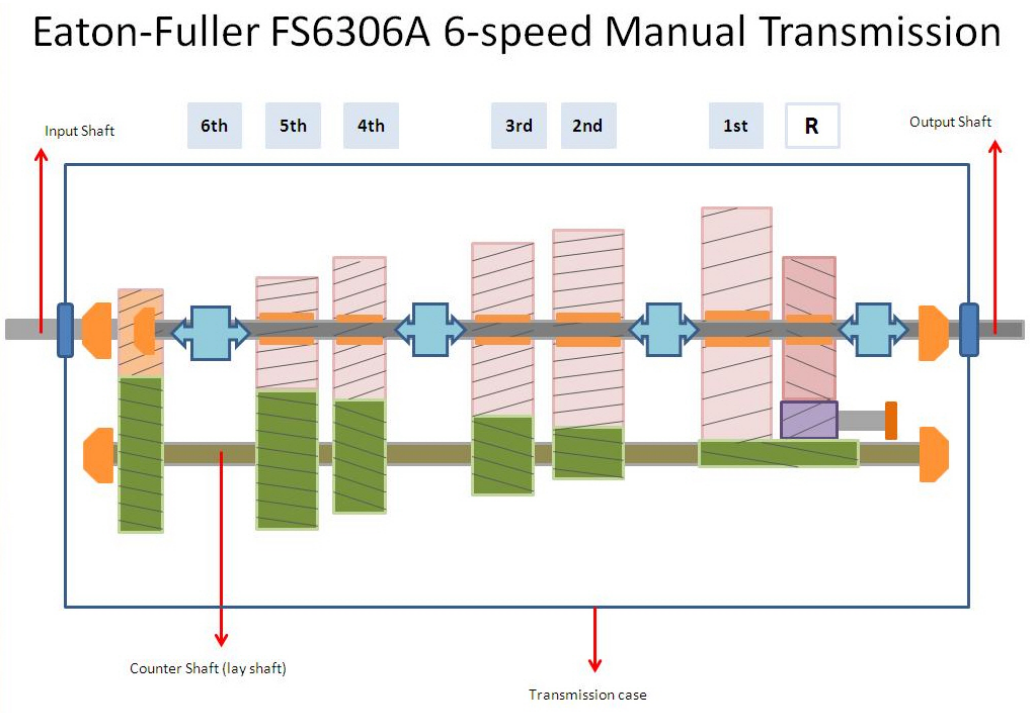

Figure B.2. Schematic of the Eaton Fuller FS6306A 6-speed medium-duty manual transmission.

Table B.2. Medium-Duty Manual Transmission Specifications
(from "Specifications Guide 2007–2008," Eaton Corporation)

Eaton Fuller FS6306A	
Torque capacity	660 lb-ft
Weight	359 lb
1st gear ratio	9.01
2nd gear ratio	5.27
3rd gear ratio	3.22
4th gear ratio	2.04
5th gear ratio	1.36
6th gear ratio	1
Reverse gear ratio	8.63

B.1.1.3. The Eaton Fuller FRO16210C Heavy-Duty Manual Transmission Model

According to unofficial 2009 sales data provided by the Peterbilt Motors Company, 10-, 13-, 15-, and 18-speed manual transmissions were used in their Class 8 trucks. Approximately 50% of the Class 8 trucks were equipped with 10-speed manual transmissions, and 18-speed manual transmissions were installed in ~39% of the Class 8 trucks, with 13- and 15-speed manual transmission accounting for the remaining 11%. Due to their market share, 10-speed

manual transmissions were selected as the base case for heavy-duty trucks. The most popular model among the 10-speed manual transmissions for heavy-duty trucks was the Eaton Fuller FRO16210C transmission.

Technical data regarding the Eaton Fuller FRO16210C transmission was obtained from the website of Road Ranger Products from the Eaton Corporation (http://www.roadranger.com) and from "Service Manual of Fuller Heavy-Duty Transmissions, TRSM2400, 01/201." This transmission provides 10-gear ratios with overdrive in 10th gear. This transmission is composed of front and auxiliary sections. The basic schematic and specifications are provided in Figure B.3 and Table B.3. The front section controls 5-speeds along with a 2-speed auxiliary gear box. Therefore, this transmission is two manual transmissions connected in series. One key difference between this heavy-duty transmission in comparison to light- and medium-duty transmissions is that there are twin counter shafts (layshafts) instead of a single counter shaft, as shown in Figure B.3. A second unique feature is that sliding clutches are used for shifting instead of synchronizers, as shown in Figure B.3. The gear ratio of 9th speed is 1.00, meaning that both the front and auxiliary sections are in direct drive, which is a zero "gear step" process. From 1st to 5th speeds, the torque is increased via 4-gear steps (2 gear pairs on each of the two counter shafts). From 6th to 10th speed except for 9th speed, the torque is transmitted through 1-gear step as direct drive in the auxiliary section is engaged for all five of the top gears. Spur gear pairs are used in the front section gear box and helical gear pairs are used in the auxiliary unit. The lubricant properties used for this model are identical to those for the transmission fluid incorporated in the model for medium-duty transmissions.

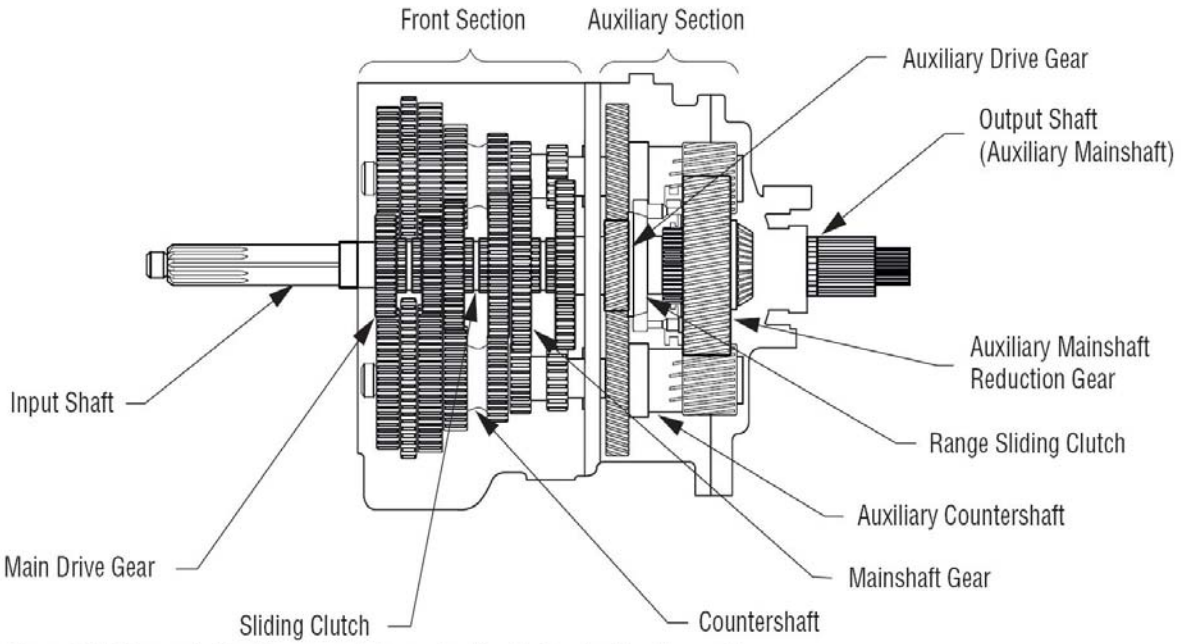

Figure 2-3. Transmission Components Important for Understanding Power Flow

(from "Fuller Heavy-Duty Transmissions Service Manual, TRSM2400, 01/2010")

Figure B.3. Schematic of the Eaton Fuller FS6306A heavy-duty manual transmission

Table B.3. Eaton Fuller FRO16210C Specifications

(from Eaton Corporation "Specifications Guide 2007–2008")

Eaton Fuller FRO16210C	
Torque capacity	1650 lb-ft
Weight	592 lb
1st gear ratio	12.69
2nd gear ratio	9.29
3rd gear ratio	6.75
4th gear ratio	4.90
5th gear ratio	3.62
6th gear ratio	2.59
7th gear ratio	1.90
8th gear ratio	1.38
9th gear ratio	1.00
10th gear ratio	0.74
Reverse gear ratio (low)	13.75
Reverse gear ratio (high)	2.80

B.1.2. Torque Loss Modules and Mechanisms

Several factors cause torque losses in a manual transmission. Each torque loss factor is analyzed in this section of Appendix B. The following sections provide the fundamentals of each torque loss factor: gear pair losses in Subsection B.1.2.1, bearing losses in Subsection B.1.2.2, windage losses in Subsection B.1.2.3, and seal losses and oil pump losses (if applicable) in Subsection B.1.2.4. Subsection B.1.2.5 covers the general power flow through the transmission, explaining when and where each of these torque loss factors must be accounted for.

B.1.2.1. Gear Pair Losses

Because the torque is multiplied and transmitted through gears, manual transmissions are complicated gearboxes composed of gear pairs on two or three shafts. When torque is delivered through a gear pair, a torque loss occurs due to sliding friction between the gears. For example, when the input torque is transmitted from the drive gear to the driven gear of one gear pair, the output torque will be the input torque multiplied by the gear ratio and also by the gear pair efficiency:

$$\tau_{driven} = \tau_{drive} r_{gear} \eta_{gear\ pair} \tag{B.1}$$

Therefore, the gear pair torque loss can be calculated via.

$$\tau_{gear\ pair\ loss} = \tau_{drive} r_{gear} \left(1 - \eta_{gear\ pair}\right) \tag{B.2}$$

There are several formulas that can be used to calculate gear pair efficiency, such as Buckingham's equation (Buckingham, 1949), Merritt's equation (Merritt, 1946), and Niemann's equation (Niemann and Winter, 1983). A detailed explanation of each of these equations and the

differences between them are beyond the scope of this introduction to the subject of gear pair losses. For the present project, the Buckingham equation was used for the determination of the gear pair efficiency as the difference between the calculated gear pair efficiency with all three equations was less than 0.05%. Buckingham's equation was chosen because it is applicable to both spur gears and helical gears, the two categories of gears that predominate in manual transmissions. The gear pair efficiencies are also considered when the torque loss caused by gear or other components needs to be included in the drive torque, such as consideration of total torque losses caused by reverse idle gear. Relevant references in the area of gear pair losses include Yada (1997) and Hohn et al. (2007).

B.1.2.2. Bearing Losses

As mentioned above, the Tremec T5 and Eaton Fuller FS6306A are two-stage transmissions and the torque changes by two gear steps except when in direct drive. Therefore, there are three shafts: the input, counter, and output shafts. Normally, two bearings are used to support each shaft, with the bearings located on each end of each shaft. For all transmissions analyzed for this project, there are two bearings on each of the counter and output shafts, but only one bearing on the input shaft. Generally, tapered roller bearings are used for gear trains with helical gears due to the axial forces generated, and cylindrical roller bearings are used for gear boxes with spur gears. However, ball bearings designed to support an axial load can be used for both spur and helical gears but the use of ball bearings in manual transmissions is relatively rare. Helical gears are used in all light-duty transmissions and many, if not most, medium- and heavy-duty transmissions.

The bearing loss modules were generated for the computational transmission model by the following process. First, after the transmission disassembly task, the types and dimensions of every bearing were measured. Moreover, the distances from the middle of each bearing to the centerplane of every gear on that shaft were measured. Then, with the measured distances, the force-moment equations were created for the axial and separation forces applicable to each bearing. If the gear train consists of only spur gears, then the force-moment equation for only the separation force is created. Technically, the radius of the bearing should be included in the force moment equation for accuracy of the applying force, however, the bearing radius is smaller than a gear radius which means that the contributing portion of the bearing is much smaller than any other parameters, so that the bearing radius is not considered and the term that includes the bearing diameter is assumed to be zero. As a final step, the Timken bearing loss equations for support bearings were implemented in the module. In addition, normally there are radial or thrust needle bearings inside the freewheeling gears located on the output shaft. In addition to the shaft support bearings, these bearings were also considered. The equations used in the transmission efficiency submodel were taken from the on-line Timken Bearing Company websites ("Timken Product Catalog, Section A: Engineering" <http://www.timken.com/en-us/products/Documents/Engineering Section.pdf> and "Timken Product Catalog, Section B: Roller Bearings" <http://www.timken.com/en-us/products/Documents/Ball Bearings.pdf>).

B.1.2.3. Windage Losses

Windage losses refer to the combination of aerodynamic drag and hydrodynamic drag losses caused by the rotation of gears and bearings. The windage loss is sometimes referred to as the "oil churning loss" because hydrodynamic drag normally dominates aerodynamic drag. This third torque loss factor is caused by gears that are totally or partially submerged in the

transmission fluid, although the oil mist also plays a role. It should be possible to approximate the windage losses via:

$$\tau_{loss,\ windage} = X\tau_{oil} + (1 - X)\tau_{air} \tag{B.3}$$

where X is the fraction of the surface area of the gear that is submerged in the transmission fluid (oil). To apply Equation B.3, the fraction of the surface that is exposed to oil, X, is needed. For a manual transmission in a car or truck, this can be determined via inspection of how much of each gear is below the oil fill level. Usually, only the gears on the counter shaft are partially submerged in the transmission fluid. The "X" term in Equation B.3 is determined by measuring the vertical distance to the oil fill hole from the bottom of the transmission case, the vertical distance from the transmission case to the center of each of the gears, the outer diameters of each gear, and the face width of each of the gears. For the gears not submerged in the transmission fluid, those gears are that gears are lubricated by the oil mist. In this case, it is reasonable to assume the same 3% (X=0.03) that Anderson and Loewenthal (1980) used. The τ_{oil} torque loss terms are functions of the density and kinematic viscosity of the oil, the outer diameter and facewidth of the gears, the gear speed (rpm), and a gear enclosure constant. The density and kinematic viscosity of air are used for calculation of τ_{air}. Because the viscosity and density of oil are functions of temperature, Walther's equations were used for determination of the viscosity of oil versus temperature and experimental data for density versus temperature for transmission oil which was provided by the lubricant's manufacturer. For the air properties, it was assumed that air is an ideal gas and ideal gas relationships were used. Relevant references for gear windage losses include Dawson (1984), Dawson (1988), and ASTM Standard D341-09.

B.1.2.4. Seal Losses and Oil Pump Losses

Other factors causing toque loss are seals and oil pumps (in those cases that the manual transmission incorporates an oil pump). Among the three selected representative manual transmissions, an oil pump is installed only on the Eaton Fuller FRO16210C to provide sufficient fluid circulation and to maintain the oil pressure. However, it was discovered that the oil pump in heavy-duty manual transmissions are driven by a separate source, not by the transmission itself. Because the oil pump is not involved in the transmission operation, the efficiency is not affected by the oil pump so that the oil pump loss was omitted.

Normally two seals, one each on the input and output shafts, are used for manual transmissions. However, the magnitude of the torque loss caused by the seal is very small compared to the other losses. Although there are several existing equations that have been published by many scientist, calculating the exact seal loss is not an easy task unless a lot of information about the seal and its environment are available. Therefore, a relatively simple equation was used for calculation of the seal loss (Meuller and Nau, 1998):

$$\tau_{loss,\ seal} = 2\pi R_{shaft}^{2} F'_{tan} \tag{B.4}$$

where R_{shaft} is the radius of the shaft and F'_{tan} is the tangential friction per unit shaft circumference. The tangential friction per unit circumference value is a function of the seal material and oil pressure applied at each seal. Nitrile is a very popular material for automotive transmission and engine seals due to its good performance, durability, and low manufacturing

cost, so it was assumed that all seals are made of nitrile. The tangential friction per unit circumference value was acquired from the seal manufacturing company's sales brochure (e.g., "ERIKS Shaft Seals: Sealing Elements" on-line product brochure; http://ebookbrowse.com/eriks-vr-shaft-seals-en-pdf-d38544397).

B.1.2.5. Power Flow

In this section, the "power flow" (the terminology generally used, although "torque flow" would be more accurate) of transmissions is discussed, including an explanation about the process of torque calculation with torque losses previously discussed. As mentioned above, the base light-duty and medium-duty transmissions have three shafts: the input, counter and output shafts. In contrast, the baseline heavy-duty manual transmission, the Eaton Fuller FRO16210C, has five shafts, because it is essentially two gearboxes in series and because the first stage/section/gearbox has two countershafts in order to accommodate the high torque throughput. The heavy-duty FRO16210C is simply two manual transmissions connected in series; therefore, further explanation is given based on the medium-duty Eaton Fuller FS6306A 6-speed manual transmission.

The transmission models developed for this project are intended to provide outputs of transmission output speed (rpm), transmission output torque, and overall transmission efficiency. The transmission models were designed to operate independently as well as dependently by slightly modifying the code. The transmission output speed can be easily and accurately (assuming no slip in the clutch or torque converter) predicted by dividing the engine output speed by the transmission gear ratio. However, predicting the output torque, which is the core of these models, and the transmission efficiency requires complicated calculations. The control volume is taken to be each of the shafts. This means that the input torque (to the shaft under consideration) and all torque losses related to the shaft and output gear under consideration are calculated before the delivered (output) torque is calculated. Therefore, the transmission model calculates the "driving torque" delivered to the output gear on the shaft under consideration with considerations of all torque losses associated with that control volume—either the input, counter, or output shaft. A power flow chart is shown in Figure B.4. As shown in Figure B.4, the program contains the same number of modules as the number of available gear ratios ("speeds").

Several inputs need to be provided by the user or passed through from the main section of the fuel economy program: the ambient air temperature, the gear ratios, the engine speed (rpm), and the engine output torque. The ambient air temperature is used for calculating the air and oil temperatures, and the corresponding properties, in the transmission, as needed for calculating the bearing and windage losses. The assigned number of forward transmission gears is used to determine the required number of gear modules for the counter and output shaft torque calculations. Regardless of the number and magnitude of the gear ratios, even for a direct drive case, all torque passes through the input shaft so the input shaft modules are located on top of each gear module and shared.

When all of the required inputs are assigned by the user or passed through from the main fuel economy program, the program calculates the torque input to the initial drive gear on the input shaft. It is assumed that there is no torque loss due to clutch slip when the clutch is engaged. The torque delivered from the engine to the initial drive gear on the input shaft can be expressed via Equation B.5, with deductions for the seal, bearing, and windage losses from the input shaft.

$$\tau_{\text{drive, input shaft}} = \tau_{\text{engine}} - \left(\tau_{\text{loss, input shaft seal}} + \tau_{\text{loss, input shaft bearing}} + \tau_{\text{loss, input shaft windage}} \right) \quad \text{(B.5)}$$

The driving torque from this initial drive gear ($\tau_{\text{drive,input shaft}}$) is then delivered to the initial driven gear on the counter shaft ($\tau_{\text{driven,counter shaft}}$) through a gear pair with an increase of torque due to the gear ratio ($r_{\text{gear,input to counter}}$) and associated torque loss due to gear pair efficiency ($\eta_{\text{gear pair, input to counter}}$).

$$\tau_{\text{driven, counter shaft}} = r_{\text{gear,input to counter}} \tau_{\text{drive, input shaft}} \eta_{\text{gear pair,input to counter}} \quad \text{(B.6)}$$

Here, it must be noted that the user of the fuel economy or Vcost program will not know this gear ratio ($r_{\text{gear,input to counter}}$). Instead, the user should know the overall gear ratio for each gear ($r_{\text{gear i,overall}}$):

$$r_{\text{gear i}}^{\text{overall}} = r_{\text{gear,input to counter}} \cdot r_{\text{drive gear i,counter to output}} \quad \text{(B.7)}$$

In the transmission submodel, it is assumed that the initial gear ratio is what was measured for the Tremec T5 to be $r_{\text{gear,input to counter}} = 1.478$. This assumption allows Equation B.6 to be used to calculate the torque delivered to the driven gear on the counter shaft and Equation B.7 to be used to calculate the counter shaft to output shaft gear ratios for each of the forward gears.

At this point, because all torque losses from the input shaft have been accounted for, the control volume for the torque analysis shifts to the counter shaft, and the program moves to the assigned gear module for determination of other torque losses. To determine the bearing losses for the bearings supporting the counter shaft, the torque delivered to all of the drive gears on the counter shaft must be calculated, even if most of these drive gears are only driving freewheeling gears on the output shaft because the bearing losses for the bearings within the freewheeling gears and the windage losses of the freewheeling gears require some torque input to overcome these losses. At this point in the program, an estimate is made for the torque delivered to the selected drive gear on the countershaft:

$$\tau_{\text{drive gear i,counter to output}}^{\text{estimate}} = \tau_{\text{driven gear,counter shaft}} - \sum \tau_{\text{loss,counter shaft windage}} \quad \text{(B.8)}$$

This estimate is used to calculate the loads on the bearings that support the countershaft. Then the counter shaft bearing torque losses can be determined. It is necessary to note that equation B.8 is only used for calculating the bearing losses. Once the bearing losses on the counter shaft have been calculated, the torque actually delivered to the selected drive gear on the counter shaft can be accurately calculated. (Note that the counter shaft does not have any seals, and thus seal losses do not apply to the counter shaft.) One important component in this step is the reverse idler gear torque loss. Even when reverse is not engaged, as is the case for all standardized driving cycles, there are windage and bearing (if applicable) torque losses associated with the reverse idler gear. These torque losses are identical to the torque required by the counter shaft drive gear that rotates the reverse idler gear. Therefore, given the gear ratio and gear pair efficiency this torque loss is accounted for through the reverse drive gear on the counter shaft via Equation B.9.

$$\tau_{\text{loss,rev. idler drive,counter shaft}} = \tau_{\text{loss,rev. idler drive, windage}} + \frac{\tau_{\text{loss,rev. idler driven, windage}} + \tau_{\text{loss,rev. idler shaft bearings}}}{r_{\text{counter shaft to rev. idler}}\eta_{\text{gear pair,counter to rev idler}}} \quad \text{(B.9)}$$

Here, this gear ratio ($r_{\text{counter shaft to rev. idler}}$) is also not known by the program user, so the measured value for the Tremec T5 was used (2.133). With this new reverse drive gear torque loss, now the real actual torque of the drive gear on counter shaft can be determined via:

$$\tau^{\text{actual}}_{\text{drive gear i,counter to output}} = \tau_{\text{driven gear,counter shaft}} - \sum \tau_{\text{loss,counter shaft windage}}$$

$$- \sum \tau_{\text{loss,counter shaft bearings}} - \tau_{\text{loss, rev.idler drive,counter shaft}} \quad \text{(B.10)}$$

Because the actual torque output from the drive gears on the counter shaft has been determined, the control volume for the analysis now shifts to the output shaft. The torque delivered to the driven gear on the output shaft is calculated via the same process as used for the initial drive/driven gear pair:

$$\tau_{\text{driven, output shaft}} = r_{\text{gear i,counter to output}}\tau^{\text{actual}}_{\text{drive gear i,counter to output shaft}}\eta_{\text{gear pair,counter to output}} \quad \text{(B.11)}$$

After considering all the torque losses on the output shaft, the final torque coming out of the transmission and the overall transmission efficiency can be determined:

$$\tau_{\text{gear i,transmission output}} = \tau_{\text{driven, output shaft}} - [\sum \tau_{\text{loss,windage, output shaft}} + \sum \tau_{\text{loss,bearings, output shaft}}]$$

$$- \tau_{\text{loss, output shaft seal}} \quad \text{(B.12)}$$

$$\eta_{\text{transmission, gear i}} = \frac{\tau_{\text{gear i, transmission output}}}{\tau_{\text{engine}} r^{\text{overall}}_{\text{gear i}}} \quad \text{(B.13)}$$

Note that gear ratio in Equation B.13 is the overall gear ratio that the program user should know and be able to input to the program.

So far, the power flow and calculation process for a manual transmission has been explained, with the exception of those transmissions with "direct drive." Direct drive is a relatively modern feature for improving the efficiency of the transmission when in "high gear"—the gear for which the overall gear ratio is 1.00. In this case, one wants the output shaft speed to equal the input shaft speed. In older manual transmissions, this was accomplished by, for example, a gear ratio of 1.35:1 from the input shaft to the counter shaft, followed by a gear ratio of 1/1.35= 0.741:1. However, this requires two gear pair losses. These gear pair losses are eliminated when in high gear in modern manual transmissions via a design feature that directly couples the output shaft to the input shaft when the driver selects high gear. However, this does not mean that the transmission is 100% efficient when in direct drive because the input shaft is still rotating the counter shaft, invoking windage and bearing losses (although the bearing losses are minimized due to the very small amount of torque transmitted to the counter shaft), and there are still windage, bearing, and seal losses on the output shaft (and the input shaft). Therefore, for the direct drive case, the output torque of the transmission is calculated via:

$$\tau_{\text{direct drive,transmission output}} = \tau_{engine} - \left[\sum \tau_{\text{losses, input shaft}} + \sum \tau_{\text{losses, counter shaft}} + \sum \tau_{\text{losses, output shaft}} \right] \quad \text{(B.14)}$$

Because of the absence of torque losses from two gear pairs, and the greatly decreased bearing torque losses on the counter shaft, direct drive results in a higher transmission efficiency, as discussed in the following section. Now all three output parameters are predicted. The output torque and output RPM from the transmission are directly fed to the differential submodel and the calculated final transmission efficiency is passed to the vehicle submodel for use in developing a "target" for the engine submodel.

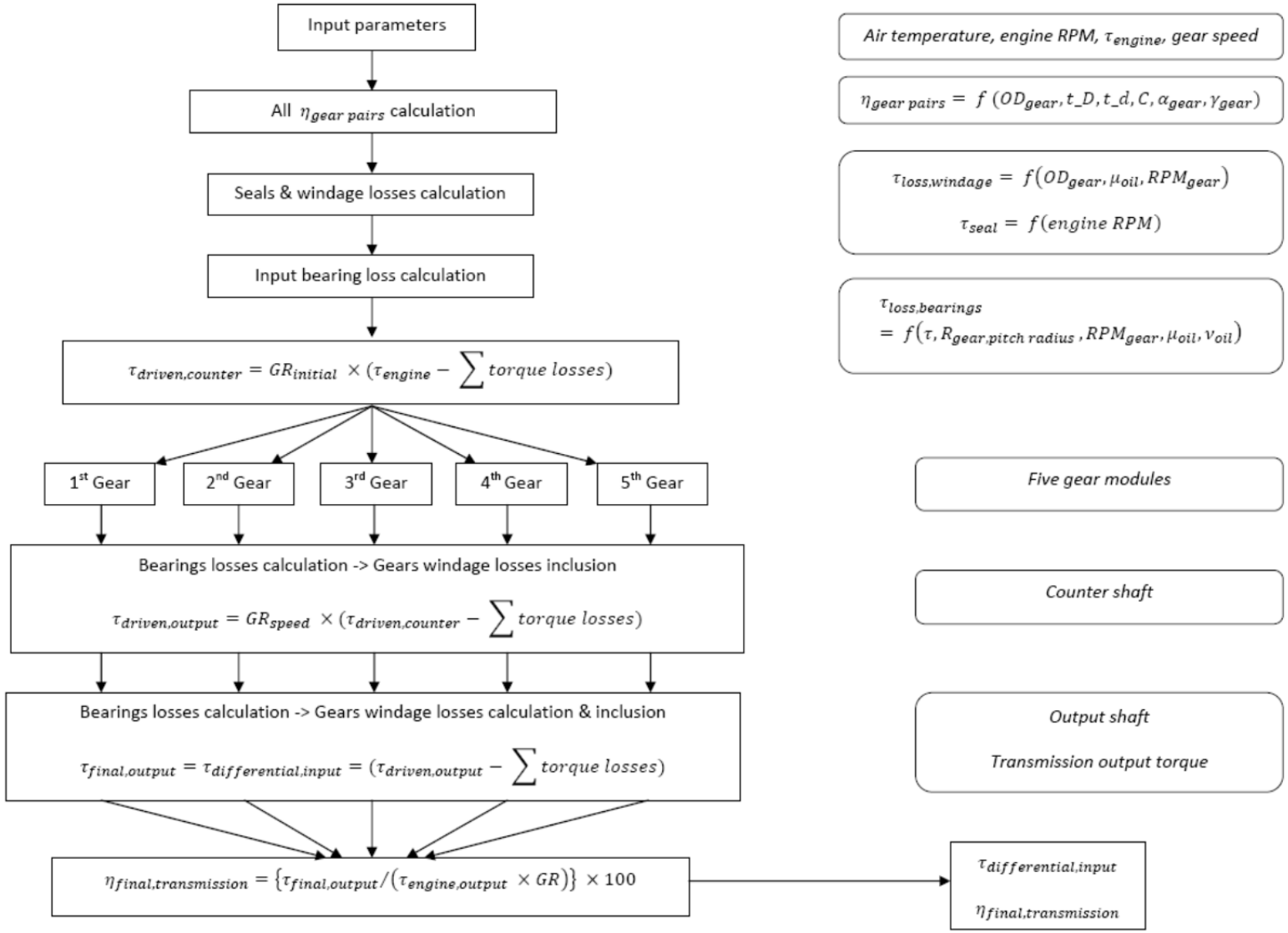

Figure B.4. Manual transmission model flow chart (specifically for the Tremec T5 WC 5-speed transmission).

B.1.3. Results from the Manual Transmission Models

In this subsection, the results of the manual transmission models are presented. The best method for validating these models would be by a direct comparison of the predicted and real test values. This would require performing experiments on all three types of transmissions. However, due to several difficulties, this direct comparison was not attempted. Therefore, for an indirect comparison, efficiencies of the developed manual transmissions under different conditions are compared with several available experimental or computation results for verification. The predicted transmission efficiency map depends on initial values input by the user, including the ambient temperature. For the comparisons discussed below, 60 ^{o}F was used as the ambient temperature.

B.1.3.1. Example Results from the Light-Duty Manual Transmission Model

The transmission map of the Tremec T5 was generated by running the model numerous times, and the graphs indicating the overall transmission efficiency versus engine speed a range of engine torque were generated. The goal of this was to determine whether not only the values of transmission efficiency but also the general curve trends of efficiency matched with the experimental or computation data.

Figures B.5 and B.6 indicate the final efficiencies of a light-duty manual transmission in 1st and 4th gear over a range of input torques and speeds. In both figures, the *x*-axis is engine torque and the *y*-axis is transmission efficiency. The nine different RPM cases are included to show the general trend of the curves. There are interesting features shown on the figures. First, the efficiency in 4th gear is clearly higher than for 1st gear due to the absence of gear pair losses in 4th gear, as expected because 4th gear is direct drive. In addition, with the same input torque, the higher RPM results in higher windage losses so that the transmission efficiency decreases with increasing input speed. Also, when the input torque increases, the bearing and seal torque losses become smaller relative to the input torque, so that the transmission efficiency increases with increasing input torque for all input speeds. In fact, the effects of increased input torque dominate the effects of increasing input speed, so that the curves for the various speeds tend to converge.

For a verification of these results, several test cases were used. First, to compare with the predicted efficiency, around 30 data points for unrealistic conditions, such as 300 N-m of torque at engine idle speed, were removed from the light-duty manual transmission map, and the remaining efficiency map was then compared with data by Greenbaum and coworkers (1994).

Greenbaum and coworkers analyzed three light-duty manual transmissions for compact pickup trucks. Although the authors failed to clearly label their results with the transmission model numbers, indirectly the results for each transmission can be analyzed. According to Figure 7 in their paper, the transmission from the Chevrolet S-10 was analyzed. The transmission used in the Chevrolet S-10 at the time when the paper was published was the Tremec T5 transmission, the selected base transmission modeled for light-duty manual transmissions for the present study. Due to the wide variation of the Tremec T5 transmission line up, it is hard to discover the specific model among the Tremec T5 transmissions, however, the design and structure of all Tremec T5 transmissions are quite similar. Thus, it was concluded that “Trans A” in the Greenbaum et al. paper was a Tremec T5.

The results for “Trans A” from Greenbaum and coworkers (1994) match very well with the results of the present T5 transmission model, as shown in Figure B.7. The differences of predicted value of T5 transmission and the values generated from other computational model are

all within ± 1.2%, and these differences are reduced to ± 0.5% if 10 more data points are removed from the predictions of the current model. The data points removed from the data set were for unrealistic operating conditions. In addition, the predicted efficiencies of the model under normal conditions agree well with the efficiencies of the "Transmission B" case in Kluger et al. (1995).

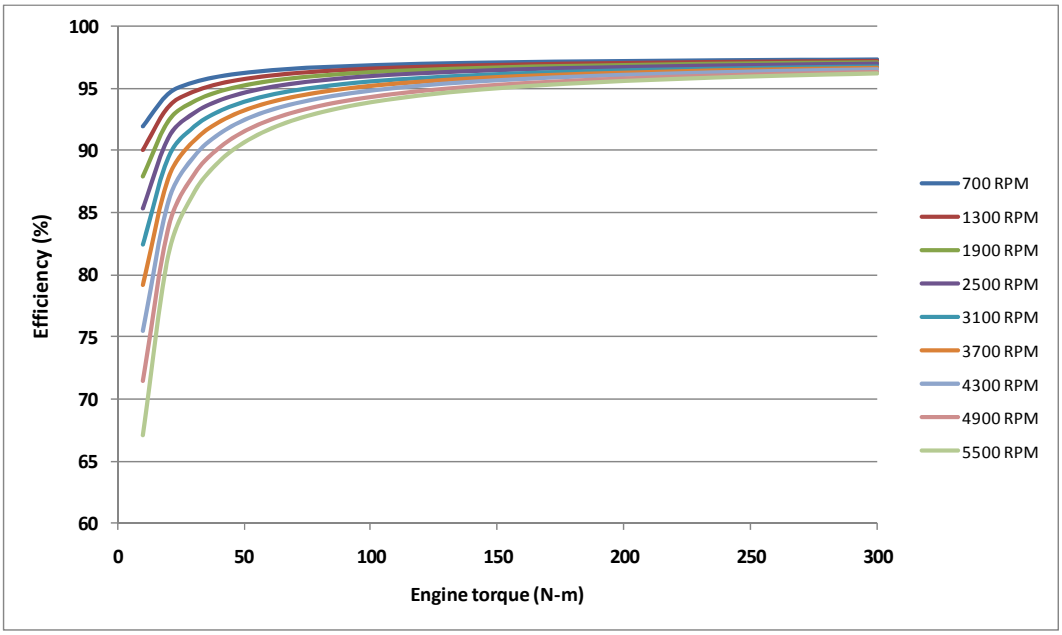

Figure B.5. Efficiency of a light-duty manual transmission in 1st gear.

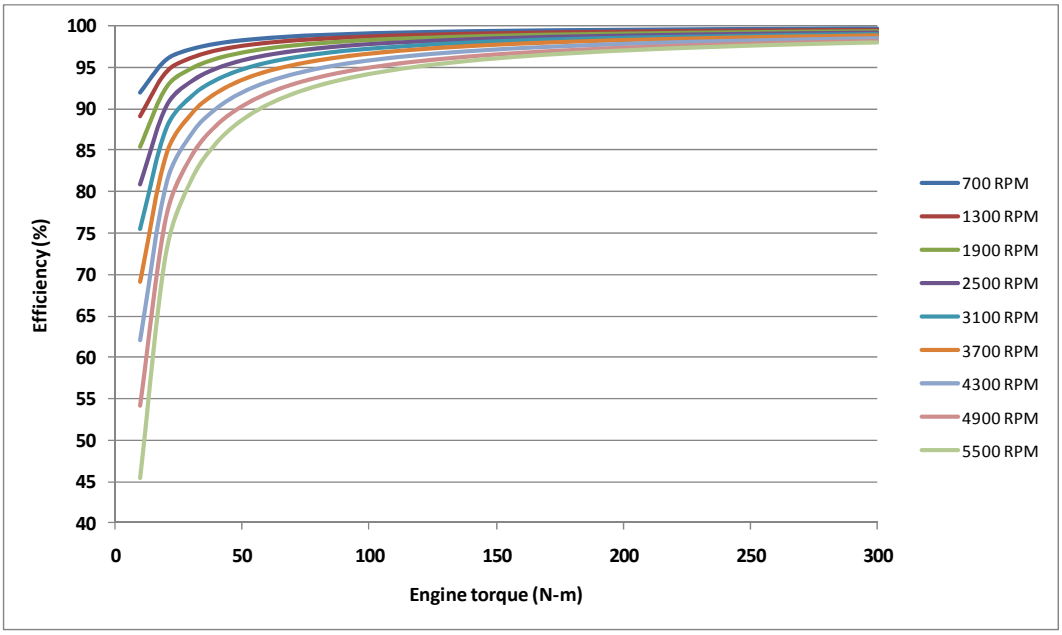

Figure B.6. Efficiency of a light-duty manual transmission in 4th gear.

Note: The bars span the range of efficiencies observed over the torque and speed ranges studied.

Figure B.7. Comparison of transmission efficiencies predicted by the light-duty manual transmission model, labeled Tremec T5, and data from Greenbaum et al. (1994), labeled Trans A.

As a third test of the accuracy of the present model for the efficiency of a light-duty manual transmission, the experimental results for a Volkswagen Rabbit 4-speed manual transaxle were used for comparison (van Dongen, 1982). This comparison required combining the model for a light-duty manual transmission with the model for the differential in a transaxle (as also developed for this project) and also generalizing the Tremec T5 model so that user-defined gear ratios (rather than only the gear ratios for the Tremec T5) can be simulated. The results are provided in Figures B.8 and B.9. As shown in these figures, the model predictions are quite good and show the correct trends as the input speed, input torque, and gear ratio are varied.

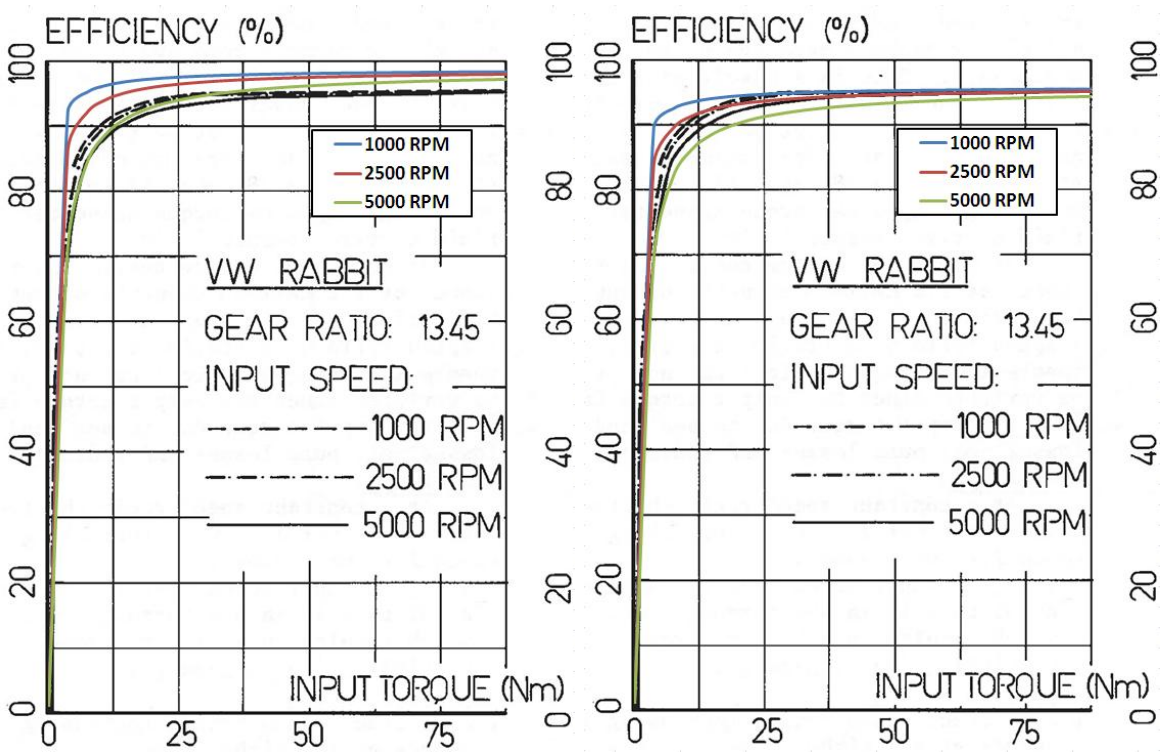

Note: The legend (color coding) for the model predictions is provided within the box in the figure. The figure on the left compares the predicted transmission efficiency only without the differential model, and the figure on the right shows the combined efficiency from the transmission and transaxle differential models.

Figure B.8. Comparison of the efficiency of a Volkswagen Rabbit manual transaxle in 1st gear (van Dongen, 1982) and the model predictions.

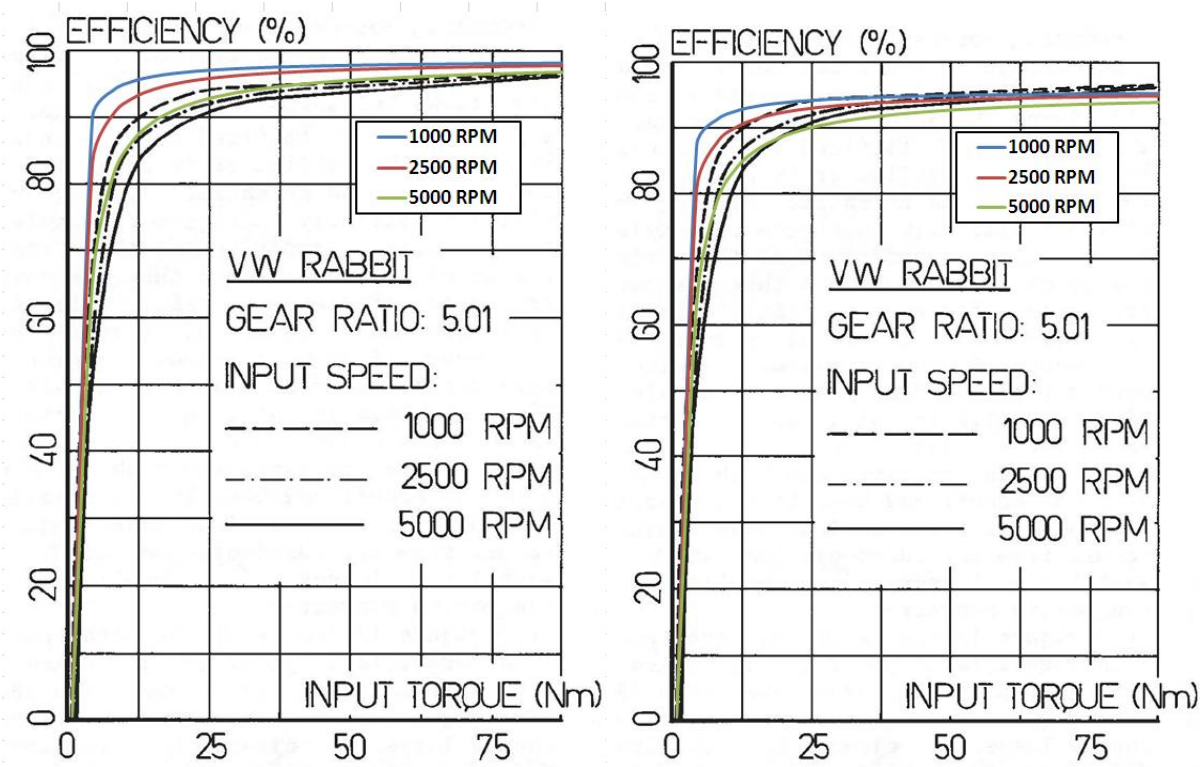

Note: The legend (color coding) for the model predictions is provided within the box in the figure. The figure on the left compares the predicted transmission efficiency only without the differential model, and the figure on the right shows the combined efficiency from the transmission and transaxle differential models.

Figure B.9. Comparison of the efficiency of a Volkswagen Rabbit transaxle in 3rd gear (van Dongen, 1982) and the model predictions. B.1.3.2. Example Results from the Medium-Duty Manual Transmission Model

Unfortunately, no published experimental or computational results were found the efficiency of a manual transmission for medium-duty vehicles. However, the basic design of the light- and medium-duty transmission models is quite similar. One difference is that a two stage gear box is used for many medium-duty manual transmissions, but there are a similar number of bearings and seals and helical gears are mainly used in both transmission gear boxes. Therefore it can be easily anticipated that the efficiency curves for a medium-duty manual transmission will produce similar trends relative to the light-duty manual transmission.

As shown in Figures B.10, B.11, and B.12, the general efficiency trends of a medium-duty manual transmission are very similar to the light-duty trends. However, the torque losses of the medium-duty transmissions are larger than those of a light-duty manual transmission due to bigger size gears and bearings, and to higher input torque causing higher gear pair torque losses and bearing losses. Thus it is concluded that the present model for a medium-duty manual transmission is proper to use in the vehicle operating cost code.

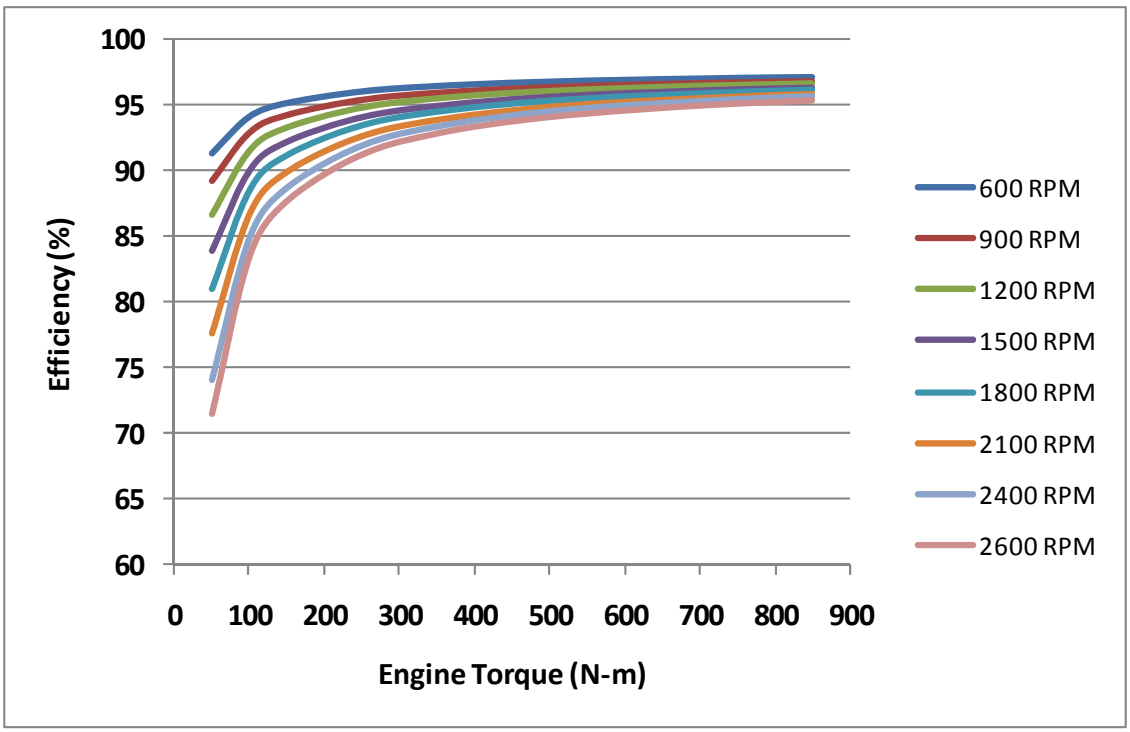

Figure B.10. Predicted efficiency of a medium-duty manual transmission in 2nd gear.

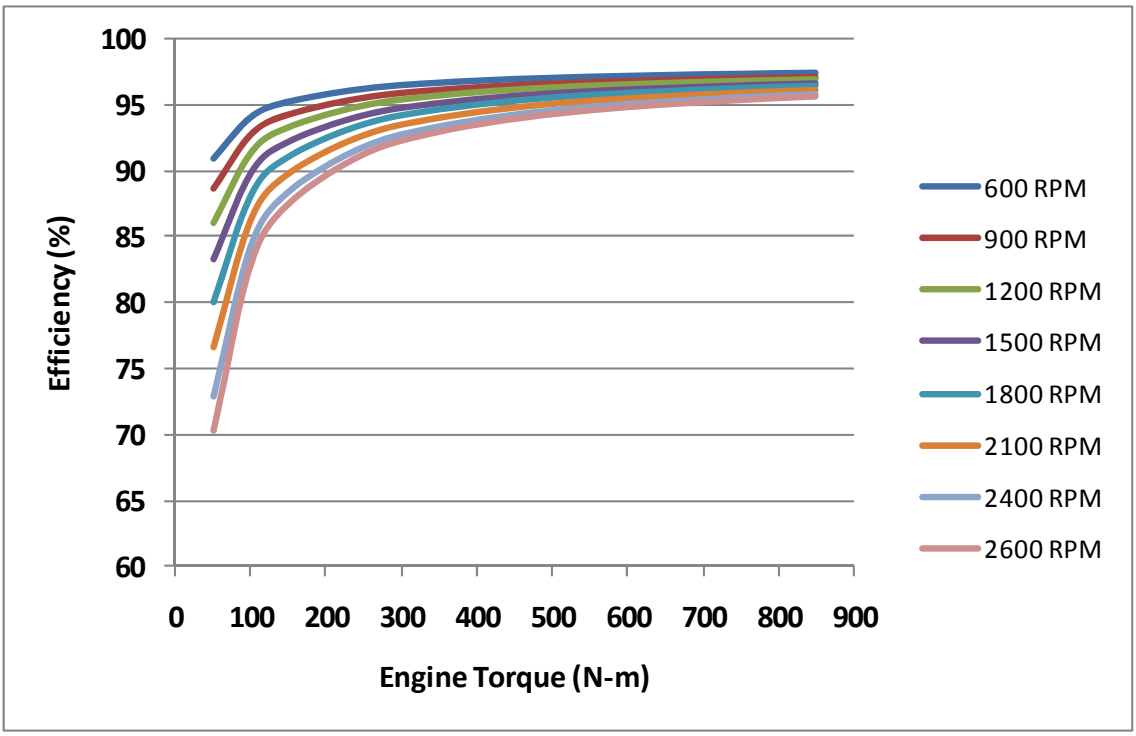

Figure B.11. Predicted efficiency of a medium-duty manual transmission in 4th gear.

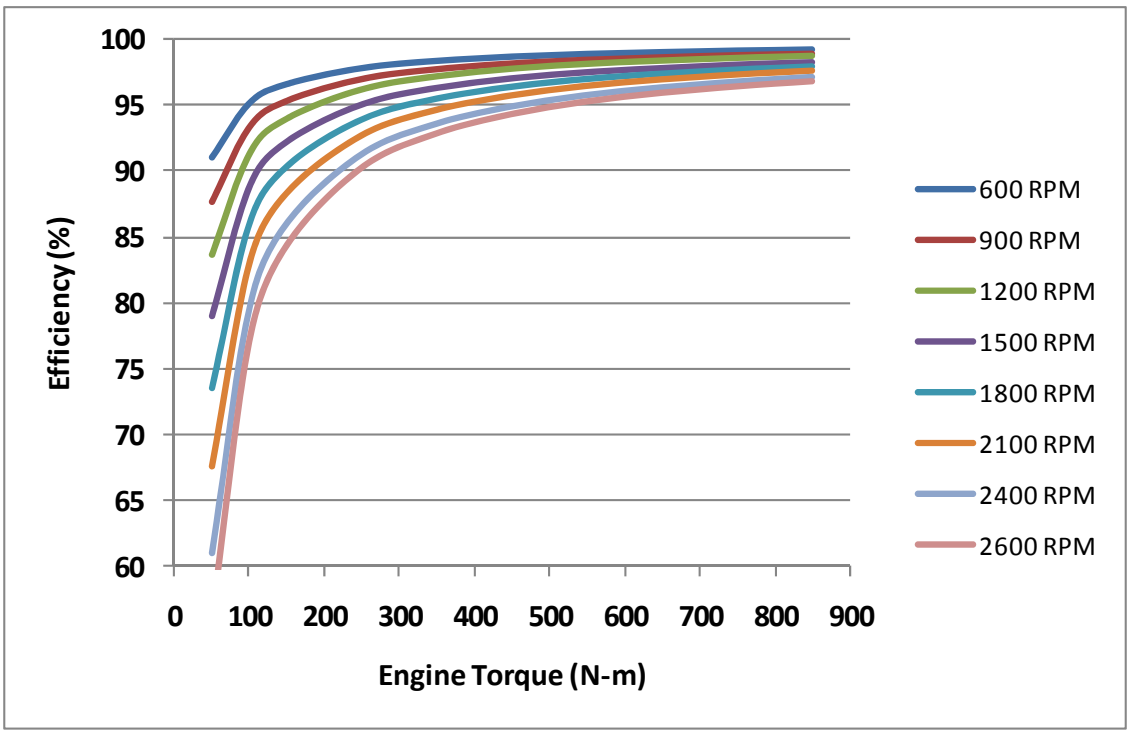

Figure B.12. Predicted efficiency of a medium-duty manual transmission in 6th gear.

B.1.3.3. Example Results from the Heavy-Duty Manual Transmission Model

Just as was the case for medium-duty manual transmissions, neither published experimental nor computation data for the transmission efficiencies for heavy-duty manual transmissions could be found. Therefore, we were again forced to compare the results of the heavy-duty model with those from the light-duty model with the same procedure that was used for medium-duty manual transmissions. Unlike the medium- and light-duty transmissions, heavy-duty manual transmissions are composed of two separate gearboxes with twin counter shafts to accommodate the higher torque. Although the magnitudes of the individual torque losses are not so big compared with the input torque, the magnitudes of the overall torque losses caused by gear pairs, windage, and bearings are almost double that of a single counter shaft. Therefore, the heavy-duty transmission efficiency for each gear is expected to be somewhat lower than for a medium- or light-duty transmission, although the trends of efficiency curves are similar.

The heavy-duty transmission efficiencies for 1st, 2nd, 4th, 9th, and 10th gear are shown in Figures B.13 to B.17. Comparisons with prior figures for light- and medium-duty manual transmissions reveal the expected result that the heavy-duty manual transmission is less efficient. Also, 1st gear has the lowest efficiency due to the high gear pair losses associated with the high gear ratio. In comparison, the results for 2nd gear are approximately 1% higher. In the case of 4th gear, the torque is transmitted through a direct drive system in the first stage of the two stage transmission so the efficiency is higher than for 1st and 2nd gears. Direct drive in both the main and auxiliary stages of the transmission is accomplished in 9th gear. Due to the direct drive, not only the efficiency reaches very closely to 100% but also the gradient of the efficiency curve increases because of higher windage torque losses. The efficiency gradient becomes bigger for the 10th speed, which is the overdrive gear, due to bigger windage torque loss.

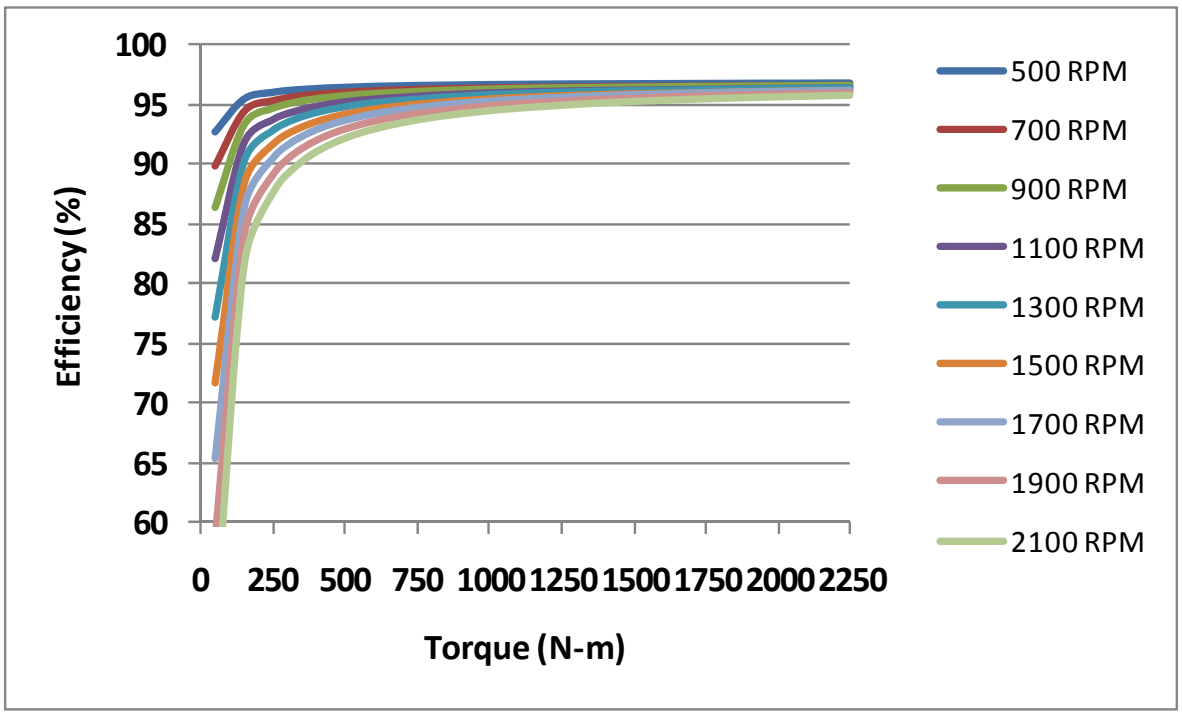

Figure B.13. Efficiency curves for a heavy-duty manual transmission in 1st gear.

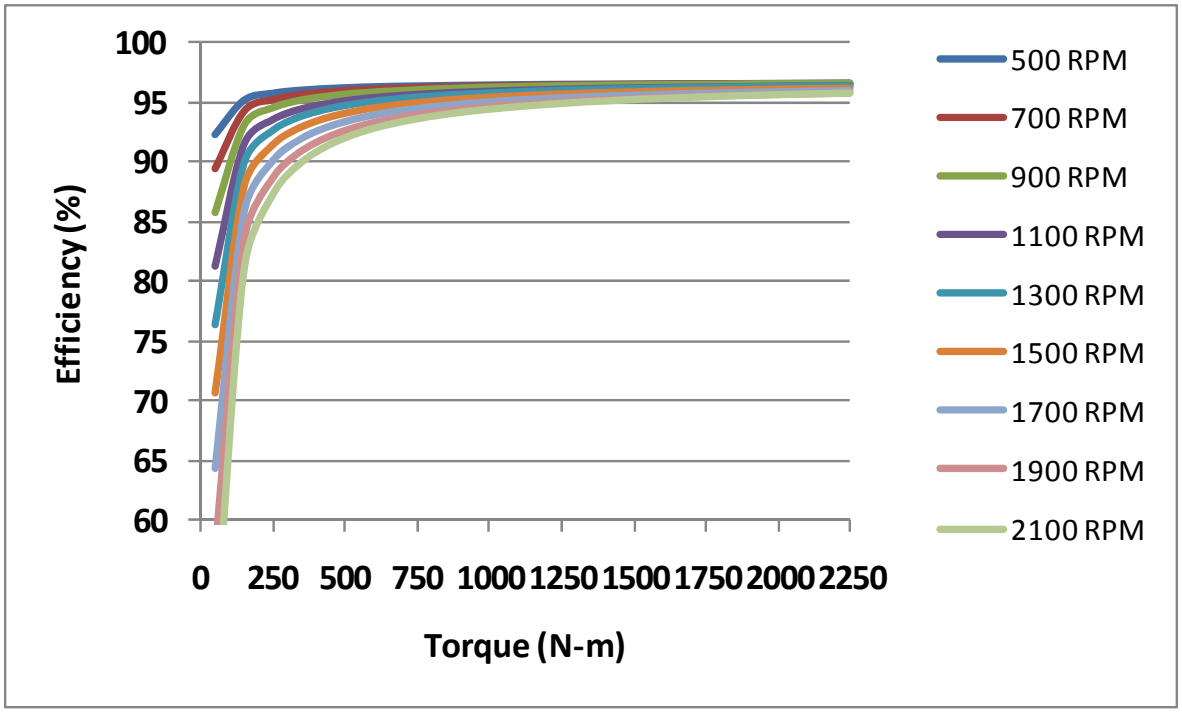

Figure B.14. Efficiency curves for a heavy-duty manual transmission in 2nd gear.

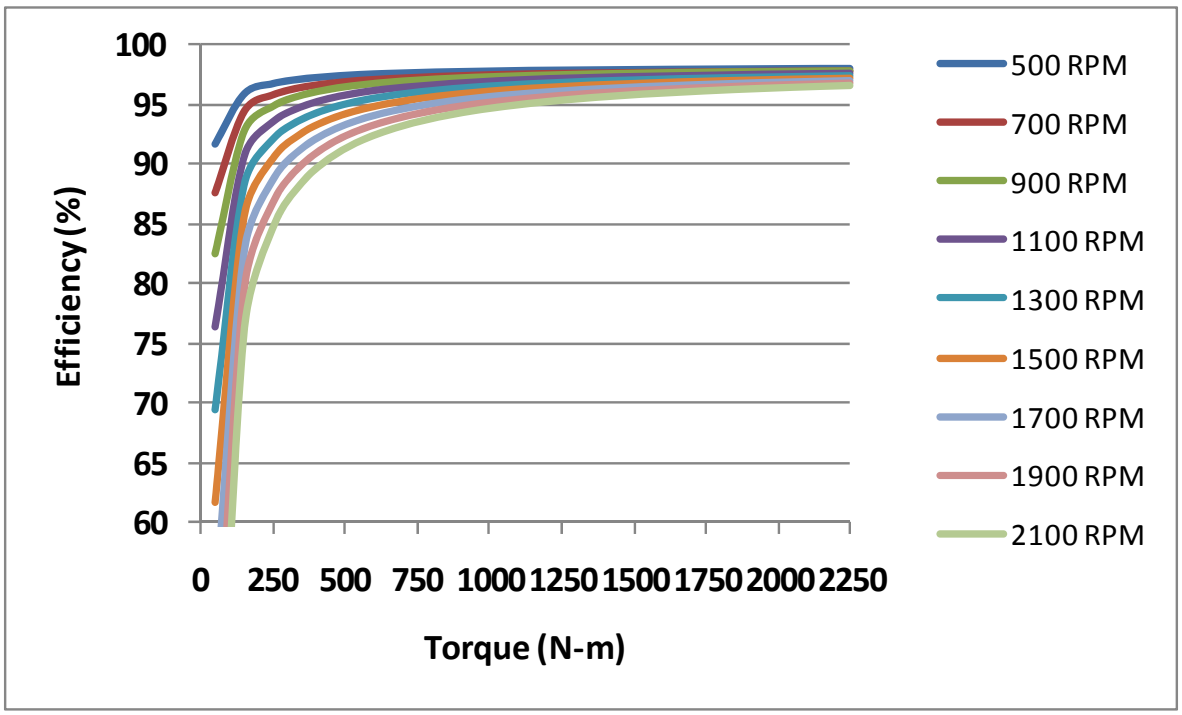

Figure B.15. Efficiency curves for a heavy-duty manual transmission in 4th gear.

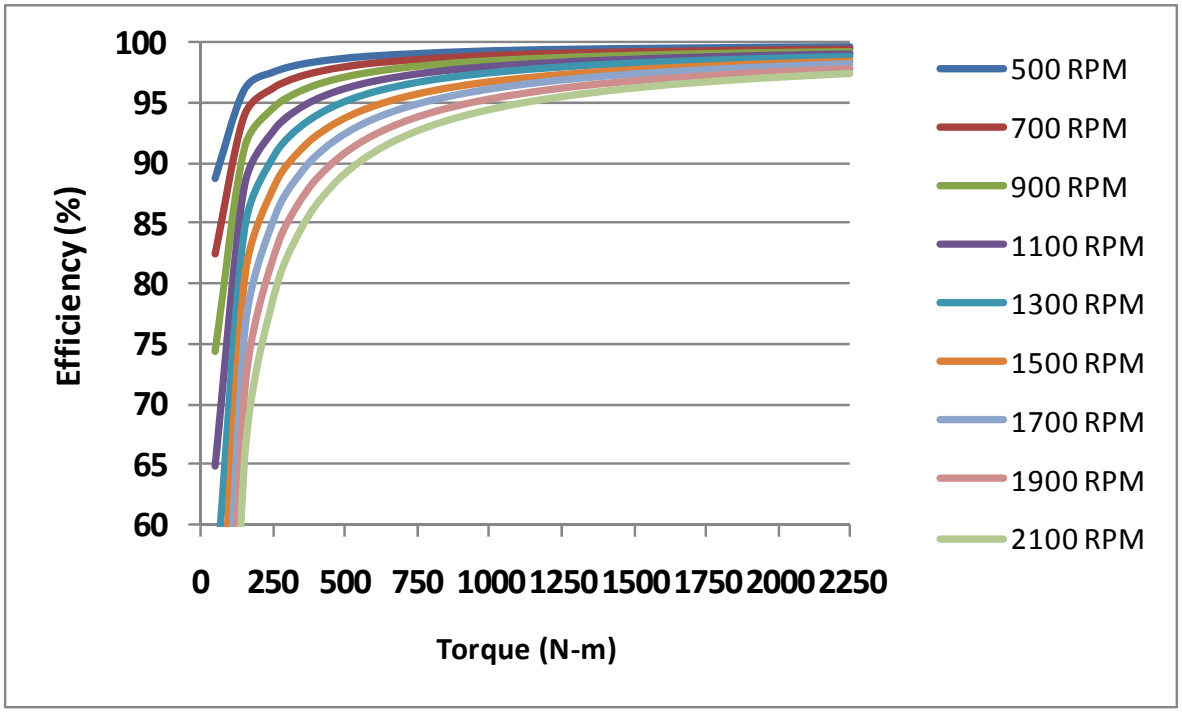

Figure B.16. Efficiency curves for a heavy-duty manual transmission in 9th gear.

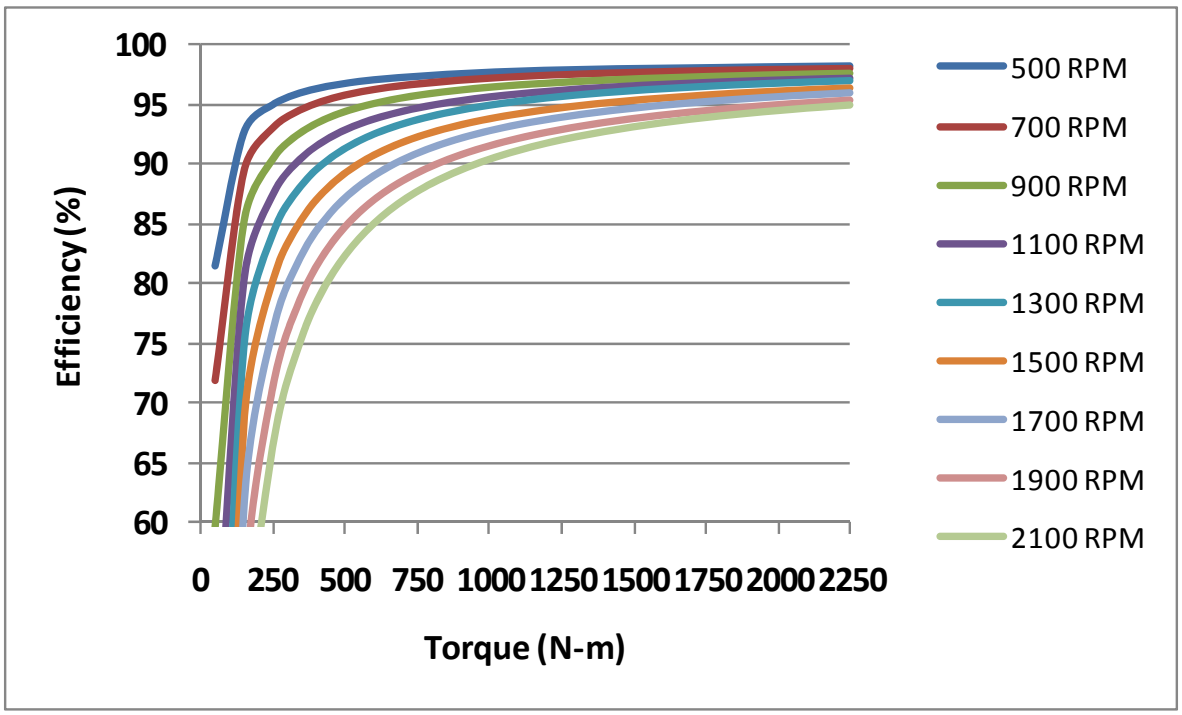

Figure B.17. Efficiency curves for a heavy-duty manual transmission in 10th gear.

B.2. Automatic Transmissions

Automatic transmissions (including transaxles) differ from manual transmissions in three fundamental ways. First, although a transmission fluid pump is used on some heavy-duty manual transmissions but not on medium- or light-duty manual transmissions, a transmission fluid pump is required for all automatic transmissions. Second, a torque converter in an automatic transmission performs the function of the clutch in a manual transmission. Finally, although both incorporate gears to provide torque multiplication and rotational speed reduction, the gearboxes are quite different. Manual transmissions use gear pairs on two parallel shafts, but automatic transmissions use a planetary (or epicyclic) gearbox. A sun gear, pinion gears (planets) anchored to a carrier, and a ring gear are incorporated in a planetary gear system. Any of these three can be the input and any other can be the output, with the third of the three gear sets held stationary. An assortment of wet clutches and band brakes are used to determine which of the three gear sets performs each of the three functions, thereby determining the gear ratio. That is, different gear ratios are obtained in an automatic transmission via control of the planetary gear box.

The fundamentals of the automatic transmission model developed for TxDOT Project 0-5974 are the focus of this section of the Final Report. The base transmissions chosen for detailed modeling in the light-, medium-, and heavy-duty categories are discussed in Subsection B.2.1. All torque loss factors affecting the final efficiency and transmission output torque are discussed in Subsection B.2.2. Example results from the models and comparisons with published data are discussed on Subsection B.2.3.

B.2.1. Base Automatic Transmissions for Each Vehicle Class

The same strategy was applied for the automatic transmission models as was used for manual transmissions: two automatic transmissions were selected for detailed analysis and code

development, one for LDVs and the other for both medium- and heavy-duty vehicles. These are the subjects of the following two subsections.

B.2.1.1. The Aisin A245E as the Basis for the Light-Duty Automatic Transmission Model

The Aisin A245E is a 4-speed fully automatic transmission manufactured by the Aisin Company. The Aisin A240E, the initial version of the A245E, was first manufactured in the early 1980s. Since its first production, Aisin made six modifications and upgrades during the last 20 years and, currently, the A246E is still in the market. Aisin A245E transaxles were installed in the Toyota Corolla, Matrix, and Celica from the mid-1990s to the late 2000s. Because relatively few design modifications were made to this transmission (mostly gear ratio adjustments and some minor parts upgrades such as bearing and seals), it can be stated that the A245E transmissions (or transaxles) were on the market for about 30 years. Although many LDVs currently sold are equipped with 5- or 6-speed automatic transmissions (or transaxles) due to advanced power train technology, still vehicles with 4-speed automatic transmission have a significant market share. Therefore, the Aisin A245E was chosen as the basis for the light-duty automatic transmission model.

A used A245E transmission was disassembled for collection of all necessary specifications. Dimensions of the components were measured for this analysis. Also, the power flow through the transmission was determined via technical papers, repair manuals, etc. Additionally, a 2004 Toyota Corolla with an Aisin A245E transaxle was tested using a portable OBD2 scanner for a several purposes. The differential part of the Aisin A245E transaxle was not considered. Basic specifications and a diagram of the A245E are provided in Table B.4 and Figure B.18. The relevant properties of Royal Purple Max ATF (automatic transmission fluid) were used in the model.

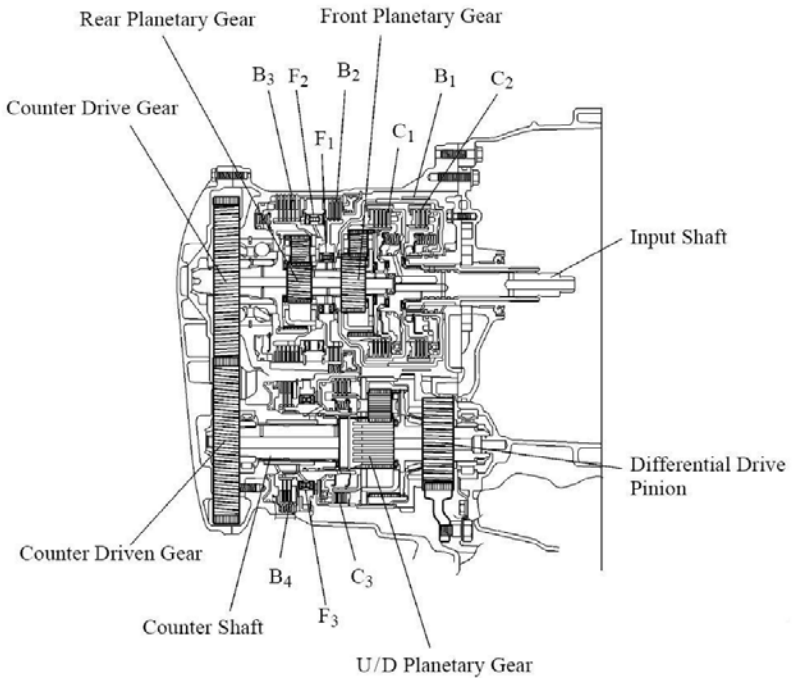

(from "Repair Manual: A245E, A246E Automatic Transaxle," No. RM941U, Toyota Motor Company, January 2002).

Figure B.18. Schematic of the Aisin A245E transaxle

Table B.4. Aisin A245E Transaxle Specifications

Aisin A245E	
Torque capacity	240 lb-ft (A240E)
Weight	162 lb
1st gear ratio	3.643
2nd gear ratio	2.008
3rd gear ratio	1.296
4th gear ratio	0.892
Differential gear ratio	2.655
Reverse gear ratio	2.977

Source: "Repair Manual: A245E, A246E Automatic Transaxle," No. RM941U, Toyota Motor Company, January 2002, and http://www.carolinadsm.com/alan/matrix/2003_Toyota_Matrix_Reference%20a/New%20Features%20Manual/ch/a246etra.pdf

B.2.1.2. The Allison 4000 HS as the Basis for the Medium- and Heavy-Duty Automatic Transmission Model

Automatic transmissions for medium- and heavy-duty vehicles are a relatively new product that was introduced to the market within the last decade so that there are few product varieties in this category. In addition, the majority of HDVs are still equipped with a manual transmission. Allison Transmission Company has ~100% of the U.S. market but has only two automatic transmissions suitable for HDVs and only six for medium-duty vehicles. Because all

of these transmissions are believed to have the same or very similar designs, one transmission was chosen to cover both the medium-duty and heavy-duty categories. The base automatic transmission selected for both categories was the Allison 4000HS 6-speed automatic transmission. Because this product is so new, finding one for disassembly was not possible. As an alternative, a TxDOT vehicle was sought that has an Allison 4000HS automatic transmission, but none are yet in the TxDOT fleet. Allison was contacted in an attempt to acquire the design details required for the development of the model, but they did not wish to share any relevant information about their 4000HS transmission. Therefore, TxDOT agreed that the development of this submodel could be omitted from the task list for TxDOT Project 0-5974.

B.2.2. Torque Loss Mechanisms and Modules

Some of the torque loss modules that were developed for the manual transmission models were implemented without any change as part of the automatic transmission model. However, because an automatic transmission has many differences relative to a manual transmission, additional torque loss modules had to be created. A brief explanation about each torque loss module is provided in the following subsection. An overview of the power flow through an automatic transmission is provided in Subsection B.2.2.9.

B.2.2.1. Torque Converter Loss

To fulfill the function of the clutch in a manual transmission, automatic transmissions have a "torque converter." A detailed description of the mechanism of a torque converter is beyond the scope of this section. In brief, the housing of the torque converter is bolted to the flywheel of the engine, so it turns at engine speed. There are four components inside the very housing of the torque converter: a pump, a turbine, a stator, and automatic transmission fluid (ATF). The ATF pump is directly connected to the torque converter housing, so it also turns at engine speed. The turbine shaft is the input shaft to the gear box of the automatic transmission. The turbine rotates due to fluid drag caused by rotation of the vanes in the pump. Shear of the ATF between the pump and the turbine heats the ATF (so a transmission fluid cooler is generally required) and is one of the primary sources of inefficiency of the automatic transmission (Numazawa et al., 1983; Park et al., 1996; Johanson and Duffy, 2005; Nunney, 2010).

Due to slippage between the pump speed (engine speed) and the turbine speed (gear box input speed), a key parameter in the model for an automatic transmission is the speed ratio (SR):

$$SR = \frac{N_{turbine}}{N_{pump}} \tag{B.15}$$

where N is rotational speed (in rpm). Given the vehicle speed, tire rolling radius, differential gear ratio, and instantaneous transmission gear ratio, the transmission input shaft speed can be calculated, and this is equal to the turbine speed in Equation B.15. Given the engine speed as another input to the transmission model, the pump speed is known because the pump rotates at engine speed. Thus, the instantaneous speed ratio can be determined via Equation B.15.

Unlike the clutch in a manual transmission, the torque converter also provides a torque multiplication. Thus, another important modeling parameter is the torque ratio (TR):

$$TR = \frac{\tau_{turbine}}{\tau_{pump}} \tag{B.16}$$

A torque ratio and efficiency versus speed ratio diagram for the Aisin A240E (Type 1), which is the initial version of the A245E, is provided as Figure B.19. Given the calculated speed ratio, the data Figure B.19 can be used to determine the torque output from the torque converter, which is the torque input to the gear box of the automatic transmission:

$$\tau_{turbine} = \tau_{pump} \cdot TR = \tau_{engine} \cdot TR \tag{B.17}$$

If a different automatic transmission is under investigation, the torque converter efficiency and torque ratio versus speed ratio curves will be different than those in Figure B.19 due to different torque converter designs. Thus, our code relies on scaling of the model for the Aisin A245E to simulate other automatic transmissions.

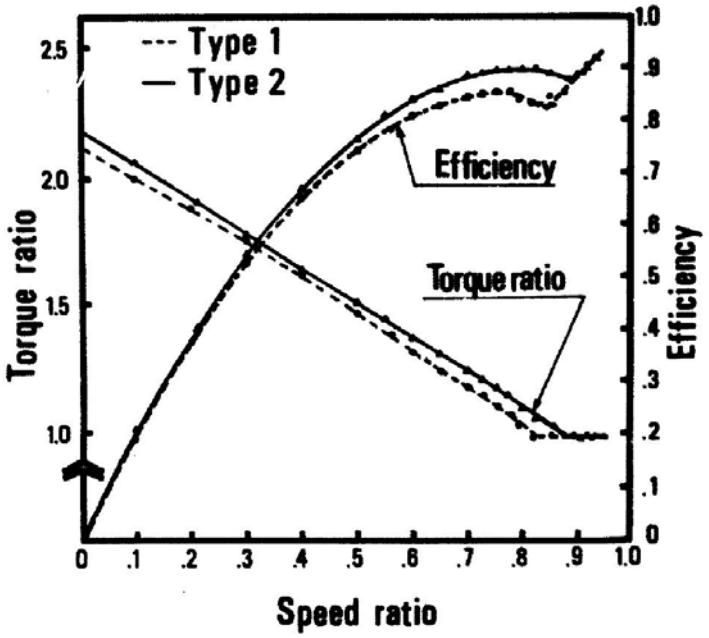

Figure B.19. Torque ratio and efficiency versus speed ratio of the Aisin A240E torque converter (Numazawa et al., 1983).

Actually, there are two types of torque converters: lock-up torque converters and conventional (non lock-up) torque converters. Because much of the inefficiency of an automatic transmission relative to a manual transmission is due to fluid shear (slip between the pump speed and the torque converter speed), mechanically locking the pump and turbine shafts together when the speed s are similar will improve the transmission efficiency. Modern automatic transmissions mostly incorporate lock-up torque converters but older automatic transmissions did not. When the torque converter exceeds a certain speed ratio, then a lock up clutch connects the pump shaft to the turbine shaft. In this case, the torque ratio is 1.0, and the torque converter efficiency

becomes linear function of the speed ratio. The normal lock-up speed ratio point is 0.88, as shown in Figure B.19.

B.2.2.2. ATF Pump Torque Loss

The pump was discussed as a component of the torque converter above. Because automatic transmission uses ATF as a working fluid, it must be maintained with relatively high pressure. The pump is designed to maintain the ATF pressure and circulate the ATF. The ATF pump torque loss equation is a function of many parameters, such as the pressure, flow rate, drag coefficient, ATF properties, etc. (Kluger et al., 1996). With several unknown parameters, for accuracy of the results of the model, it was decided to derive a polynomial equation that is a function of engine speed based on ATF pump test results for the Aisin A240E that have been published by the manufacturer (Kuromachi et al., 1984). Figure B.20 shows the test results for the ATF pump loss of the A240E transaxle.

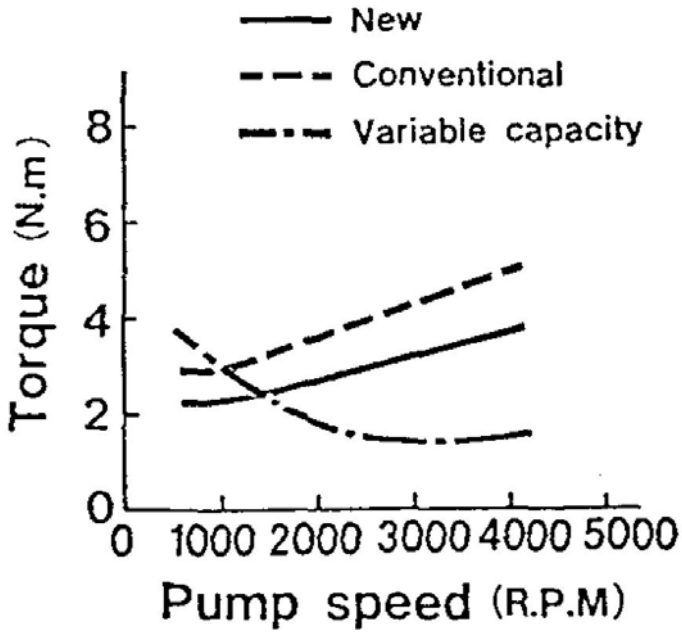

Figure B.20. ATF pump torque loss versus torque converter pump speed of Aisin A240E transaxle (Kuromachi et al., 1984).

B.2.2.3. Planetary Gear Set Loss

There are several common planetary gear sets that are used for modern automatic transmissions, including Simpson, Ravigneaux, and Lepelletier gear sets. Manufacturers sometimes modify these gear sets or add some parts to fulfill their objectives. In addition, by applying different shift control mechanisms, the transmission can have higher gear speeds with the same gear set type or an equal number of planetary gear systems. However, normally the Simpson gear set is used for automatic transmissions that have up to 4 forward speeds and the Ravigneaux gear set can accomplish up to 5-gear speeds. The Lepelletier gear set can provide 6 or more forward speeds if additional planetary gears are added. There are some efficiency equations that have been proposed for some planetary gear sets. However, a different approach

was implemented for the present model development because of other torque loss factors. The basic torque loss process and equations are well described by Krstich. (1987).

First, the number of teeth of each gear are determined or calculated. The carrier is not a gear but the imaginary gear teeth number is calculated for use in the efficiency equation because if the carrier is an output component transmitting torque, then the gear teeth number is definitely necessary. Then the equation is derived by applying a torque balance equation with constant external and internal gear mesh efficiencies. The derived efficiency equation is a function of gear teeth numbers so that the efficiency is determined by the input and output components (gears) of the planetary system. When the entire gear component is held by fixing band brakes or one-way clutches, then direct drive is accomplished and the planetary gear set efficiency becomes 1.0 (Park et al., 1996; Krstich., 1987).

B.2.2.4. Gear Pair Losses

Automatic transmissions are normally single stage transmissions because of the absence of conventional gear pairs that produce a torque loss. However, for an automatic transaxle, one gear pair is always used to switch the direction of the delivered torque, from the main shaft to a countershaft. This is required in order to minimize the length of the transaxle so that combined length of the engine and transaxle can fit transversely in the engine compartment. The gear pair efficiency for this extra gear pair for a transaxle relative to a rear-wheel drive transmission is calculated with the exact same equation as used for manual transmissions: the Buckingham equation.

B.2.2.5. Windage Losses

It is somewhat hard to calculate the windage losses for the automatic transmission because, generally, the gear size is smaller than for manual transmissions, and the gears are in a planetary gear set. As a result, the windage losses for the sun gear, pinion gear, ring gear, and carrier are calculated and combined as a total windage loss in the automatic transmission model. (Although the windage losses of the pinion gears are relatively small, they are calculated along with the carrier windage loss.) If the carrier is in rotation, the total windage loss of the carrier is the sum of the pinion windage loss and the carrier windage loss. The same principle is applied for the case of carrier free rotation. If the carrier is fixed, then only the windage loss caused by the pinion gears was considered. When the carrier and pinion gears are locked up, such as in direct drive mode, only the surface area of the carrier is used for calculation of the windage loss without consideration of the pinion gear windage loss. The equation used for calculation of the windage losses for the manual transmission is then used for calculation of the windage losses of an automatic transmission.

B.2.2.6. Bearing Losses

There are not many support bearings in automatic transmissions because the transmission design is entirely different than for the manual transmission. Instead of the support bearings, many needle bearings are installed in each planetary gear system. With the measured helix angle of the sun gear, the forces applying in each direction are calculated and used for the bearing loss calculation. For shaft support bearings, the same procedure that was used for the manual transmissions is used.

B.2.2.7. Seal Losses

There are normally two or more oil seals in an automatic transmission, just like in manual transmissions. Therefore, the same equation is used for calculation of the seal losses for both types of transmissions.

B.2.2.8. Other Losses

There are several other torque loss factors that occur when the automatic transmission is in operation. Those are clutch torque losses, torque losses in one-way clutches, and band brake torque losses. Clutches are necessary components in automatic transmissions but one-way clutches and band brakes are not if the transmission uses a different shifting mechanism or gear holding units. These torque loss factors are functions of many parameters that are not easy to acquire, and the equations predicting the magnitude of these torque losses are complicated (Park et al., 1996). Therefore, available test results for those factors for similar sized automatic transmissions manufactured by various companies were used to derive simple equations that are functions of only engine speed. Because these torque losses are relatively small compared to the other losses in an automatic transmission, the values calculated via this approximation method are deemed to be sufficiently accurate for the purposes of this model.

B.2.2.9. Power Flow

In this subsection, the transmission power flow and torque calculation procedure are discussed. Both automatic transaxles and transmissions can be explained quite similarly because the only difference is the counter shaft. Further explanation is given based on the Aisin A245E transaxle. The power flow chart of this automatic transmission is shown in Figure B.21.

Unlike the manual transmission model, due to slip in the torque converter the output speed of an automatic transmission is an unknown value that cannot be simply calculated knowing the engine speed and the gear ratio. However, because the transmission output speed is equal to the differential input speed, the transmission output speed can be calculated given the vehicle speed, drive tire rolling radius, and differential gear ratio. Therefore the desired vehicle speed must be passed to the automatic transmission subroutine from the main program. Along with vehicle speed, four additional inputs are the ambient air temperature, the number of transmission gears (e.g., a 4-speed transmission has 4 forward gears), engine output speed, and engine torque. The basic role of each parameter has already been explained. The speed ratio of the torque converter is thus easily calculated as the ratio of engine speed to gearbox input speed. The gearbox input speed is the transmission output speed times the gear ratio. In the same manner of a manual transmission, the automatic transmission models have the number of forward gear ratios that setup a corresponding number of gear modules. The control volume for torque analysis of the automatic transmission gearbox is the planetary gear system. Therefore, after calculating the torque converter torque ratio using the torque converter speed ratio and accounting for the oil pump loss, the gearbox input torque is passed to the gear modules for calculation of the remaining torque loss factors for each planetary gear system.

When all of the required input parameters are provided by the program, the automatic transmission submodel calculates the turbine shaft torque of the torque converter which is the input torque to the front planetary gear system via.

$$\tau_{\text{input, gearbox}} = \left(\tau_{\text{engine}} - \tau_{\text{loss, front seal}} - \tau_{\text{loss, ATF pump}} \right) \cdot \text{TR}_{\text{torque converter}} \tag{B.18}$$

Equation B.18 yields the torque delivered to the input of the gearbox. The total torque losses within the gearbox, including bearings, windage, and other losses (e.g., clutch losses, band brake losses), are then calculated and subtracted from the gearbox input torque. This yields the torque delivered to the output component within the gear box. That is, the output torque from the front planetary gear system is calculated including the front planetary gear set efficiency and gear ratio. The front planetary gear system efficiency and gear ratio are different when other gear speeds are under calculation because different components are in use as the input and output gears of the planetary gear system.

$$\tau_{\text{output,front planetary gear set}} = r_{\text{gear,front planetary gear set}} \eta_{\text{front planetary gear set}}$$

$$\times \left(\tau_{\text{input, gearbox}} - \left[\sum \tau_{\text{loss, bearings}} + \sum \tau_{\text{loss, windage}} + \sum \tau_{\text{loss, "other"}} \right]_{\text{front planetary}} \right) \quad \text{(B.19)}$$

The output from the front planetary gear system is the input to the rear or second planetary gear system. Thus, calculations may now be performed for the second planetary gear system. The same principle is applied and the output torque from the rear planetary gear system can be calculated via Equation B.20:

$$\tau_{\text{output,rear planetary gear set}} = r_{\text{gear,rear planetary gear set}} \eta_{\text{rear planetary gear set}}$$

$$\times \left(\tau_{\text{input, rear planetary gear set}} - \left[\sum \tau_{\text{loss, bearings}} + \sum \tau_{\text{loss, windage}} + \sum \tau_{\text{loss, "other"}} \right]_{\text{rear planetary}} \right) \quad \text{(B.20)}$$

The manual transmission has a separate gear set for reverse (typically, a drive gear on the counter shaft, an idler gear, and a driven gear on the output shaft), but automatic transmissions can achieve reverse by controlling the planetary gear set holding devices (e.g., band brakes) without any additional parts. For a transaxle, now the output torque from the rear (second) planetary gear system is transmitted to the drive gear on the main shaft and then to the driven gear on the countershaft. However, for a transmission, no such gear pair exists, so in this case the calculation proceeds directly to the next (final, underdrive) planetary gear set. The torque losses related to this drive gear, if applicable (i.e., only for transaxles), are only windage and bearing losses.

$$\tau_{\text{output, drive gear, main shaft}} = \tau_{\text{output, rear planetary gear set}} - \left(\sum \tau_{\text{loss, bearings}} + \sum \tau_{\text{loss, windage}} \right)_{\text{drive gear}} \quad \text{(B.21)}$$

where it must again be noted that this refers to a gear pair that is only present in transaxles.

The torque losses on the counter shaft that decrease the torque delivered to the driven gear on the counter shaft are now considered, along with the inefficient torque multiplication by this gear pair:

$$\tau_{\text{output, driven gear, counter shaft}} = \tau_{\text{output, drive gear, main shaft}} \cdot r_{\text{gear pair,transaxles}} \cdot \eta_{\text{gear pair,transaxles}}$$

$$- \left(\tau_{\text{loss,bearings}} + \tau_{\text{loss,windage}} \right)_{\text{driven gear}} \quad \text{(B.22)}$$

where, again, it must be noted that this refers to a gear pair that is only present in transaxles.

The output torque from the driven gear on the counter shaft is used to drive the third planetary gear system, which is also called the under drive planetary system. The total torque loss occurring in the under drive planetary unit can be calculated via.

$$\tau_{\text{output, transmission}} = r_{\text{gear, 3rd planetary}} \cdot \eta_{\text{gear, 3rd planetary}}$$

$$-\left(\tau_{\text{input, 3rd planetary}} - \left[\sum \tau_{\text{loss, bearings}} + \sum \tau_{\text{loss, windage}} + \sum \tau_{\text{loss, other}}\right]_{\text{output shaft}} - \tau_{\text{loss, output shaft seal}}\right) \quad \text{(B.23)}$$

Equation B.23 provides the final torque that the automatic transmission is providing to the differential. The overall transmission efficiency can be calculated via.

$$\eta_{\text{auto transmission}} = \frac{\tau_{\text{output, transmission}}}{\tau_{\text{engine}} r_{\text{gear,overall}} TR_{\text{torque converter}}} \quad \text{(B.24)}$$

In Equation B.24, it is noted once again that the torque was already multiplied by the torque converter before entering the gearbox of the automatic transmission/transaxle.

The overall gear ratio term in Equation B.24 is the gear ratio that the user should be able to easily find from the owner's manual. It includes the ratio of each planetary gear set as well as the gear ratio between the drive and driven gear pair located between the rear and underdrive planetary gear units.

$$r_{\text{gear,overall}} = r_{\text{gear,front planetary}} \cdot r_{\text{gear,rear planetary}} \cdot r_{\text{gear pair,input-to-countershaft}} \cdot r_{\text{gear,3rd (UD) planetary}} \quad \text{(B.25)}$$

When direct drive is accomplished in the automatic transmission, the underdrive gear ratio and planetary gear efficiency both become 1.0, but other torque loss factors contribute to inefficiency. The transmission efficiency and transmission output torque calculated by the automatic transmission submodel are now passed to the differential submodel.

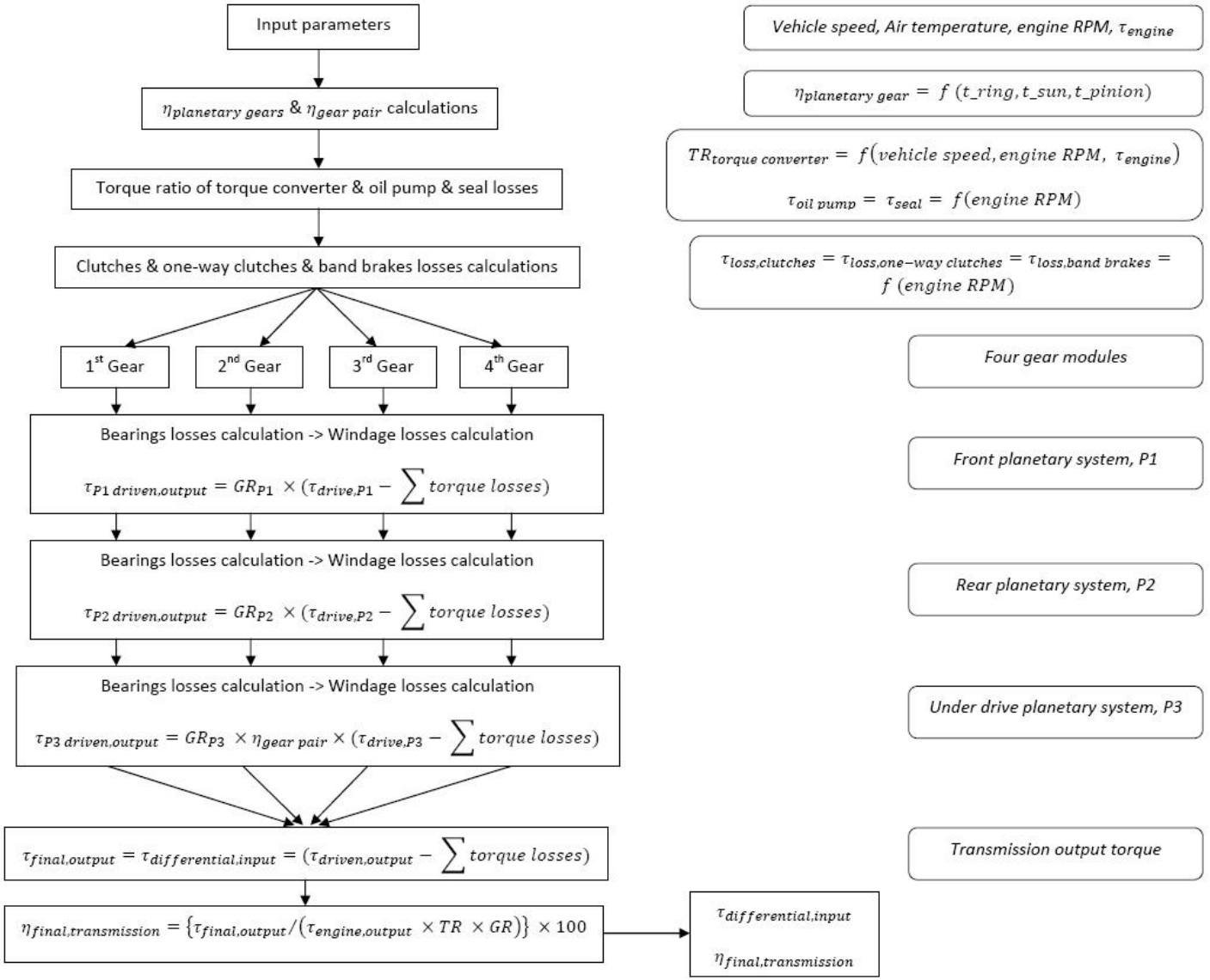

Figure B.21. Automatic transmission model flowchart (Aisin A245E transaxle).

B.2.3. Example Results from the Automatic Transmission Model

In this subsection, some example results from the automatic transmission (or transaxle) models are presented. For validation of the models, the predictions of the model are compared to published data with the same input parameter values. Unlike the manual transmission models, a transmission map (lookup table) cannot be generated due to additional input parameters, such as the vehicle speed, and uncertainty regarding the shift strategy employed.

B.2.3.1. Example Results from the Light-Duty Automatic Transaxle Model

Validation of the model for an automatic transmission is much more difficult than for a manual transmission due to the speed ratio term that describes the slip in the torque converter. The instantaneous speed ratio for each second during the driving schedule can be calculated given the instantaneous vehicle speed, the differential gear ratio, and the instantaneous overall transmission gear ratio. Therefore, an equation predicting the vehicle speed at a given engine speed (rpm) for each overall gear ratio was derived based upon experimental data collected through a test drive with a 2003 Toyota Corolla with the Aisin A245E transaxle.

In this subsection, three published technical papers' results are compared with the results from the model. First, the model is compared to the results published by Park and coworkers (1996) for a Hyundai A4BF1 transaxle. Like the Aisin A425E, this is also a 4-speed automatic transaxle with Ravigneaux type planetary gear sets. However, the gear ratios are not similar: 2.846 for the Hyundai in 1st vs. 3.643 for the Aisin, 1.581 in 2nd vs. 2.008; 1.0 in 3rd vs. 1.296, and 0.685 in 4th vs. 0.892 for the Aisin A245E. Here it must be noted that the similarities in results for these two transmissions (discussed below) in spite of the differences in gear ratios demonstrates that the efficiency of automatic transmissions is not dominated by gear pair efficiencies.

Park and coworkers did not specify whether or not they made their measurements at the transmission output or at the transaxle output. Thus, two cases were run using the automatic transmission model: one for a transaxle and the other for a RWD automatic transmission.

Using the same values of the input parameters: 88 N-m of engine torque, 2500 and 4500 rpm engine speeds, and status of the lock-up torque converter (either “locked” or not), the present light-duty automatic transmission model provided very similar results as shown in Figures B.22, B.23, and B.24. Although the 4500 rpm cases for 3rd and 4th gear are also included in the technical paper, the vehicle speeds under these conditions are unlikely to happen. Therefore, these two cases were not analyzed for the comparison.

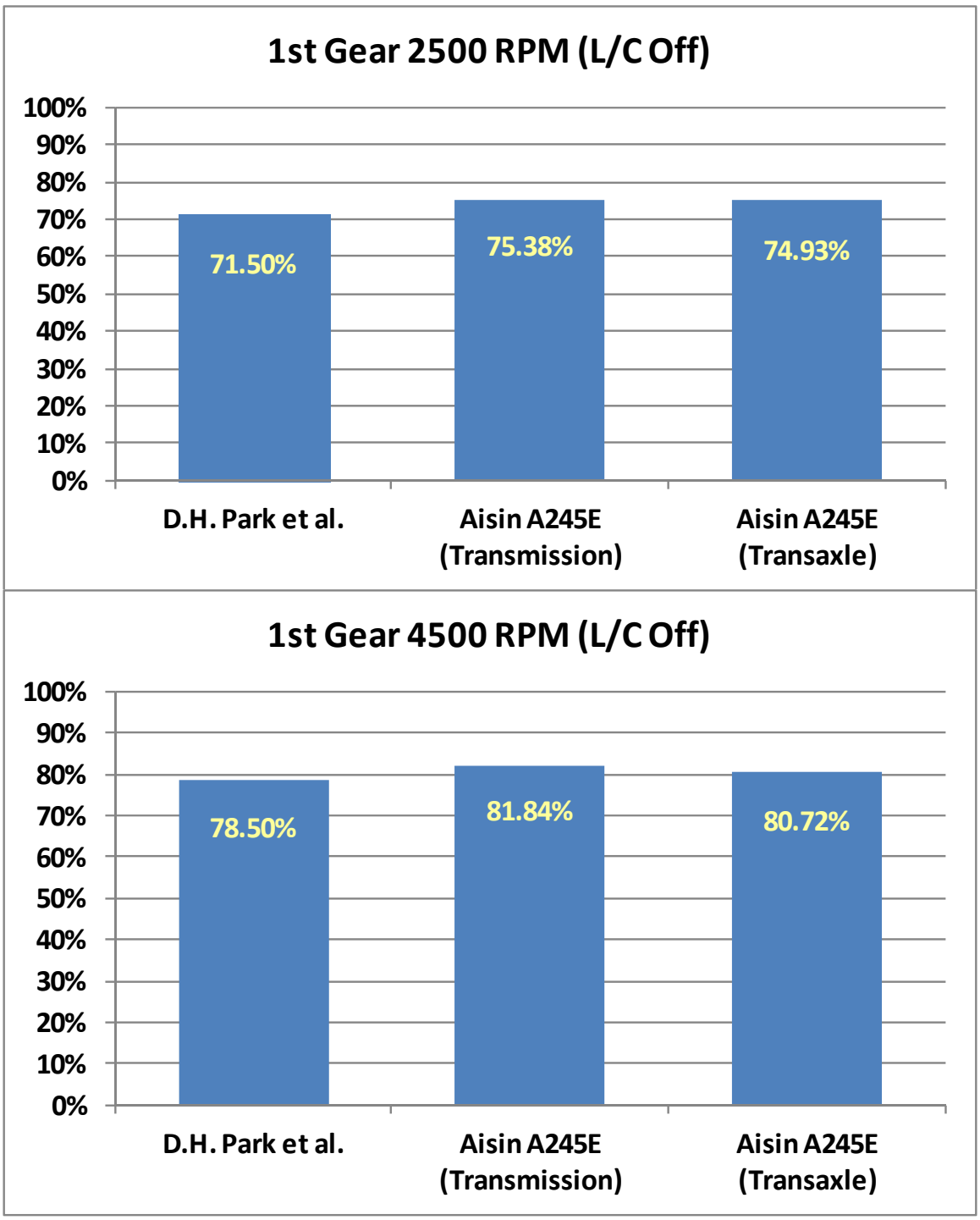

The Hyundai transaxle results are from Park et al. (1996).

Figure B.22. Comparison of the present light-duty automatic transaxle and transmission models predictions with results for a Hyundai A4BF1 transaxle in 1st gear and 88 N-m of engine torque.

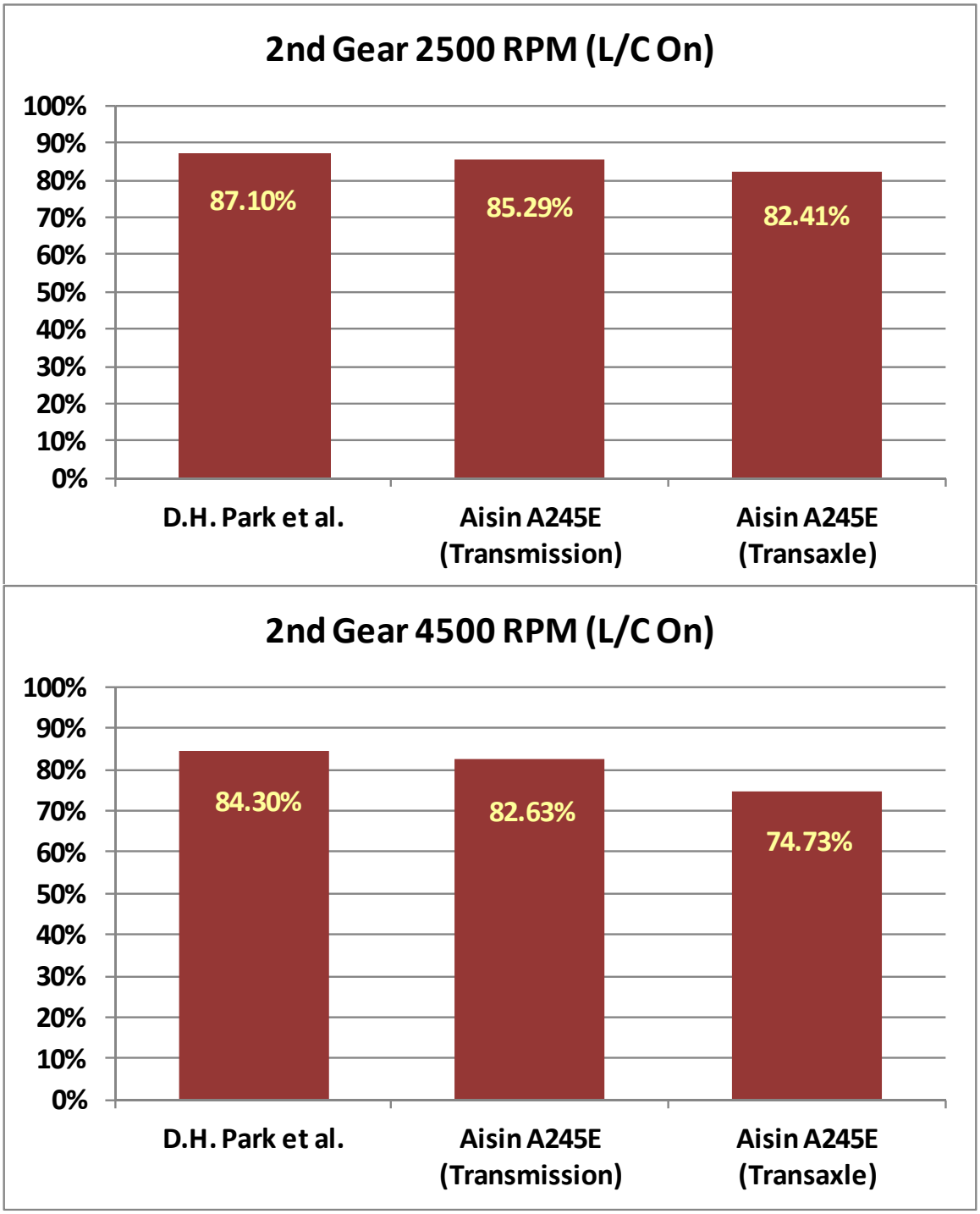

The Hyundai transaxle results are from Park et al. (1996).

Figure B.23. Comparison of results from the present models for the efficiency of a light-duty automatic transaxle and transmission with results for a Hyundai A4BF1 transaxle in 2nd gear with 88 N-m of input torque from the engine.

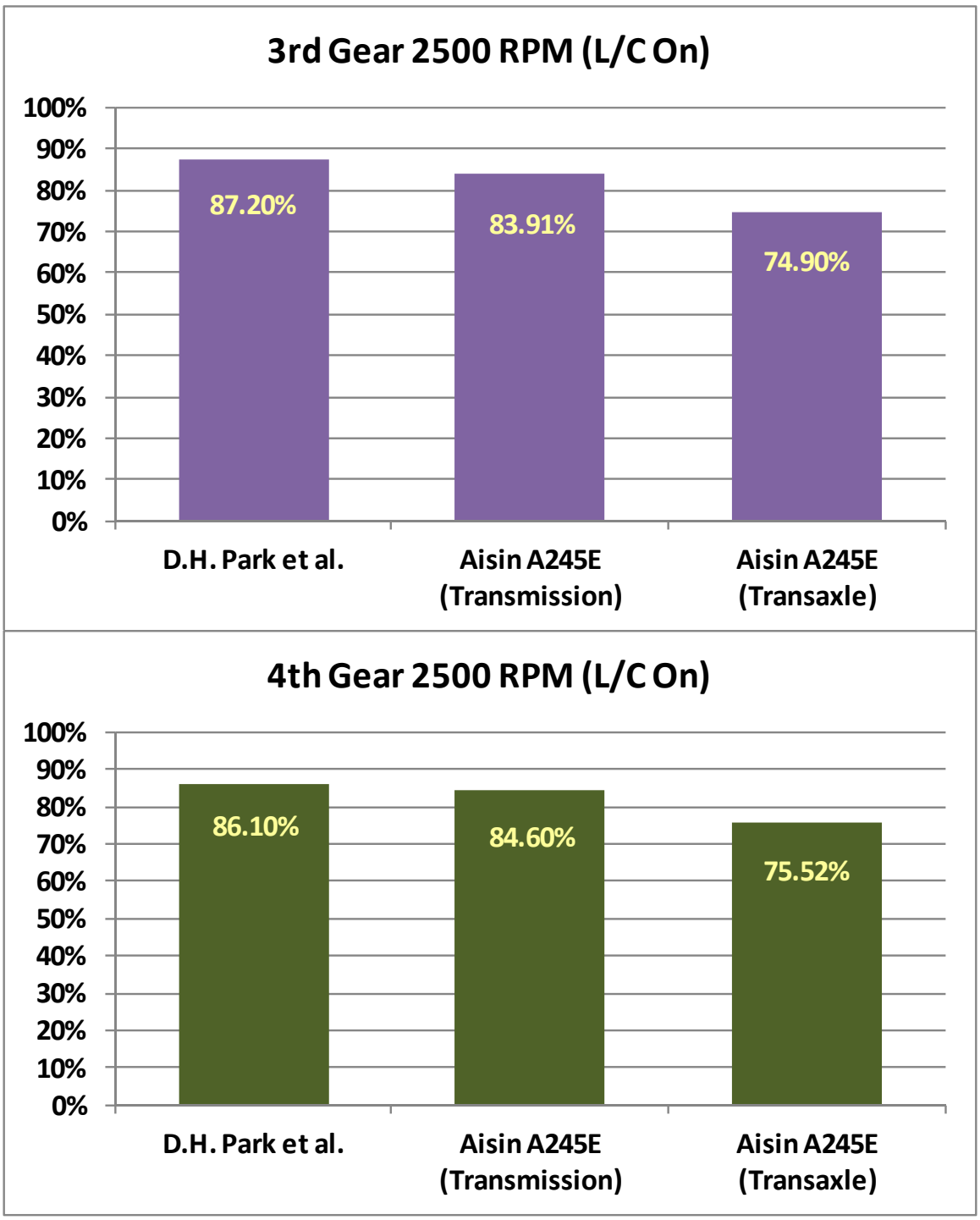

The Hyundai transaxle results are from Park et al. (1996).

Figure B.24. Comparison of results from the present models for a light-duty automatic transaxle and transmission with those for a Hyundai A4BF1 transaxle in 3rd and 4th gears with the engine operating at 2500 rpm and producing 88 N-m of torque.

As a second test of the automatic transmission model, results from Kluger and Greenbaum (1993) were compared with the present model's predictions, as Figure B.25 shows.

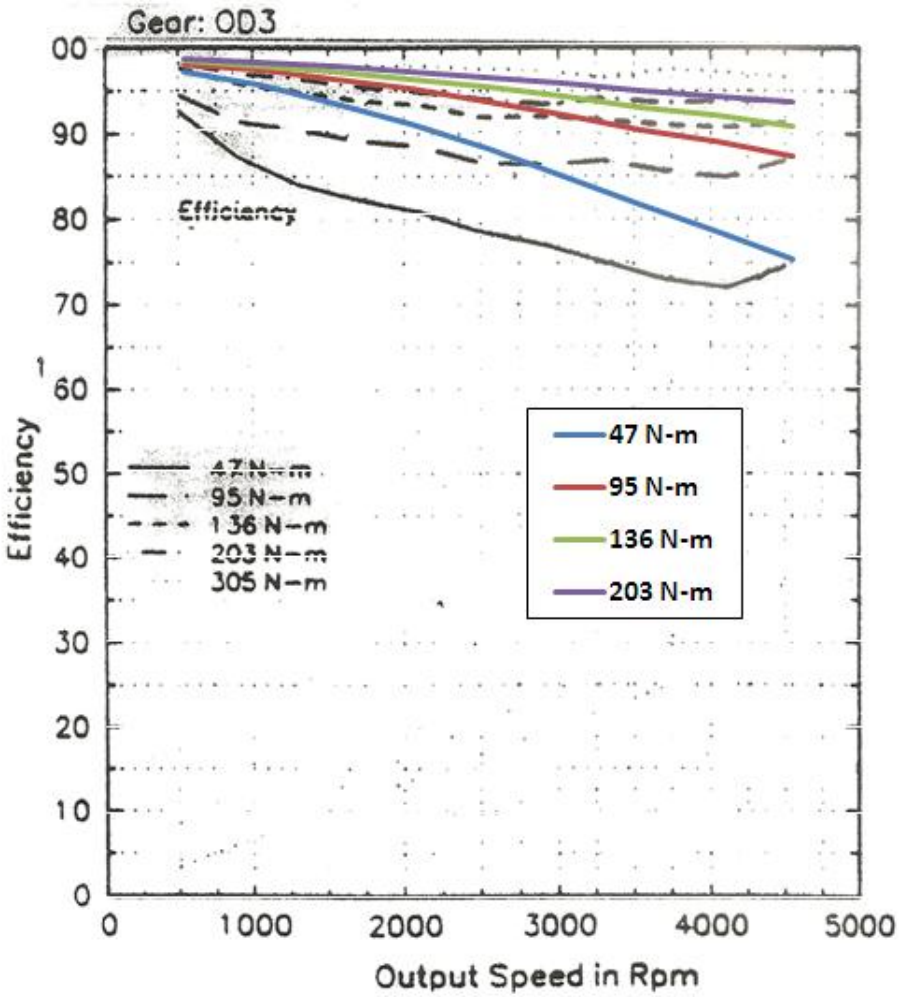

The truck transmission results are from Kluger and Greenbaum (1999).

Figure B.25. Comparison of the present light-duty automatic transmission model predictions with results for 3.0–5.8 L truck transmissions with locked torque converters in 3rd gear and several different engine torque inputs.

These investigators analyzed 13 automatic transmissions for 3.0~5.8 L trucks, and when the size of the transmission get bigger, a larger size torque converter is installed and the efficiency of the torque converter is clearly higher than for a smaller torque converter. These investigators developed a data regression methodology for prediction of the performance of an automatic transmission. Although the efficiency values predicted by the present light-duty automatic transmission model shows bigger differences compared to the results from Kluger and Greenbaum relative to the comparison for the Hyundai A4BF1 transaxle, the trends of the efficiency curves are reasonably similar. The efficiency curves from the Aisin A245E transmission model shows similar trends under the same transmission input conditions as Kluger and Greenbaum's regression for 13 different sized transmissions for trucks. With unknown specifications of Kluger and Greenbaum's generic transmission, such as torque capacity, type of planetary gear set, and gear ratio, direct comparison between Kluger and Greenbaum regression

results and the Aisin A245E transmission model via scaling is restricted. However, the similar general trends imply that the torque analysis task was successful.

The last published data the present model predictions were compared against for model validation is data for a Volkswagen Rabbit 3-speed automatic transaxle (van Dongen, 1982). However, the torque converter lock-up point is 10% different: SR = 0.8 for the Volkswagen Rabbit versus 0.88 for the Aisin A245E, and the torque input flowing to the transmission is not only small but also hard to calculate because van Dongen failed to provide the input torque clearly. Therefore, only a few cases were analyzed for 1st, 2nd, and 3rd gear. However, van Dongen did provide details regarding the effects of input speed on the relationship between the torque ratio and the speed ratio of the torque converter, as illustrated in Figure B.26.

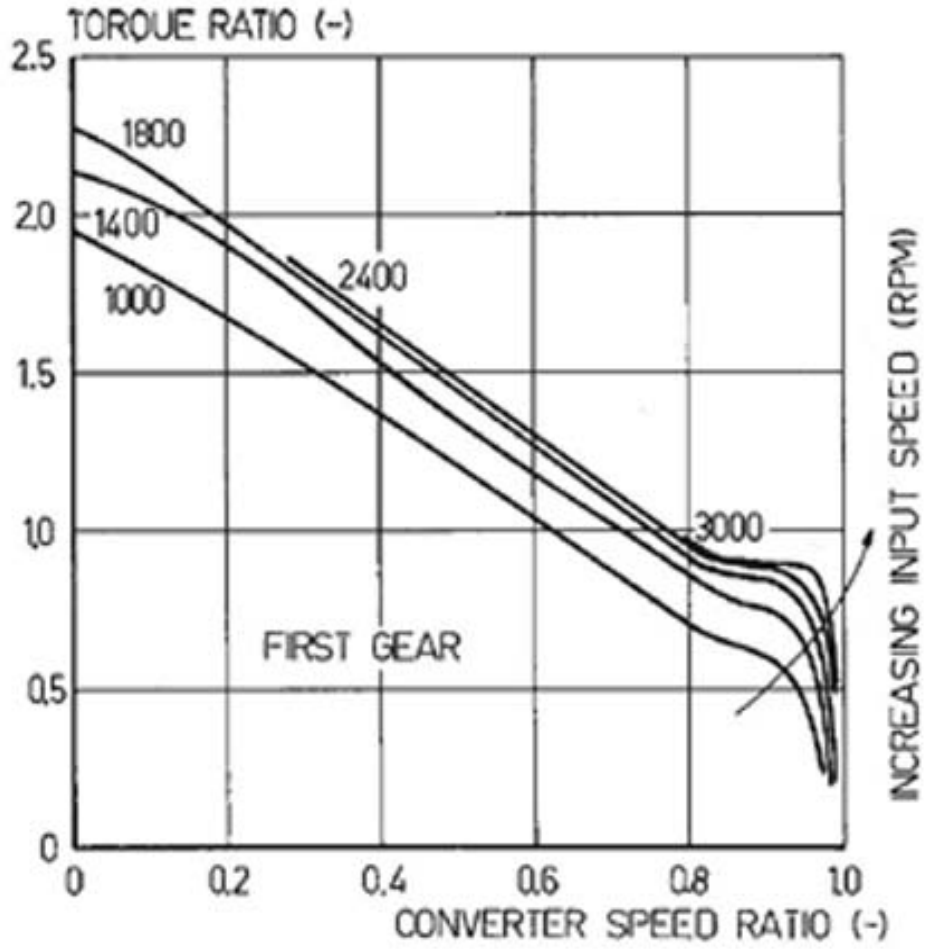

Figure B.26. The effect of engine speed on the relationship between the torque ratio and the speed ratio for the torque converter of a Volkswagen Rabbit 3-speed automatic transaxle (van Dongen, 1982).

Because the torque ratio is dependent upon the engine rpm, which is the input speed to the automatic transaxle model, for a better comparison result, the Volkswagen Rabbit torque converter efficiency values were combined with the remaining parts of the Aisin A245E automatic transaxle model including the differential submodel.

Although only selected cases' results were compared, the trends of the efficiency curves for this automatic transmission were very close, as shown in Figures B.27, B.28, and B.29. The 3rd gear of the Volkswagen Rabbit transaxle was direct drive mode; therefore, 4th gear for the Aisin A245E automatic transaxle was compared to 3rd gear of the Volkswagen Rabbit automatic transaxle. As shown in Figures B.27, B.28, and B.29, the values for the present model's efficiency are somewhat lower compared to the experimental data, but the slope is very close. The reason for these differences is believed to be that the Volkswagen Rabbit transaxle has fewer planetary gearsets and a smaller torque capacity. The smaller torque capacity implies that smaller size gears were used, and thus the windage torque losses were smaller than for the larger Aisin A245E.

After all of these validation tasks, it is concluded that the present automatic transmission model predicts highly reasonable efficiency values and gives efficiency predictions that are sufficiently good to use for the remaining program.

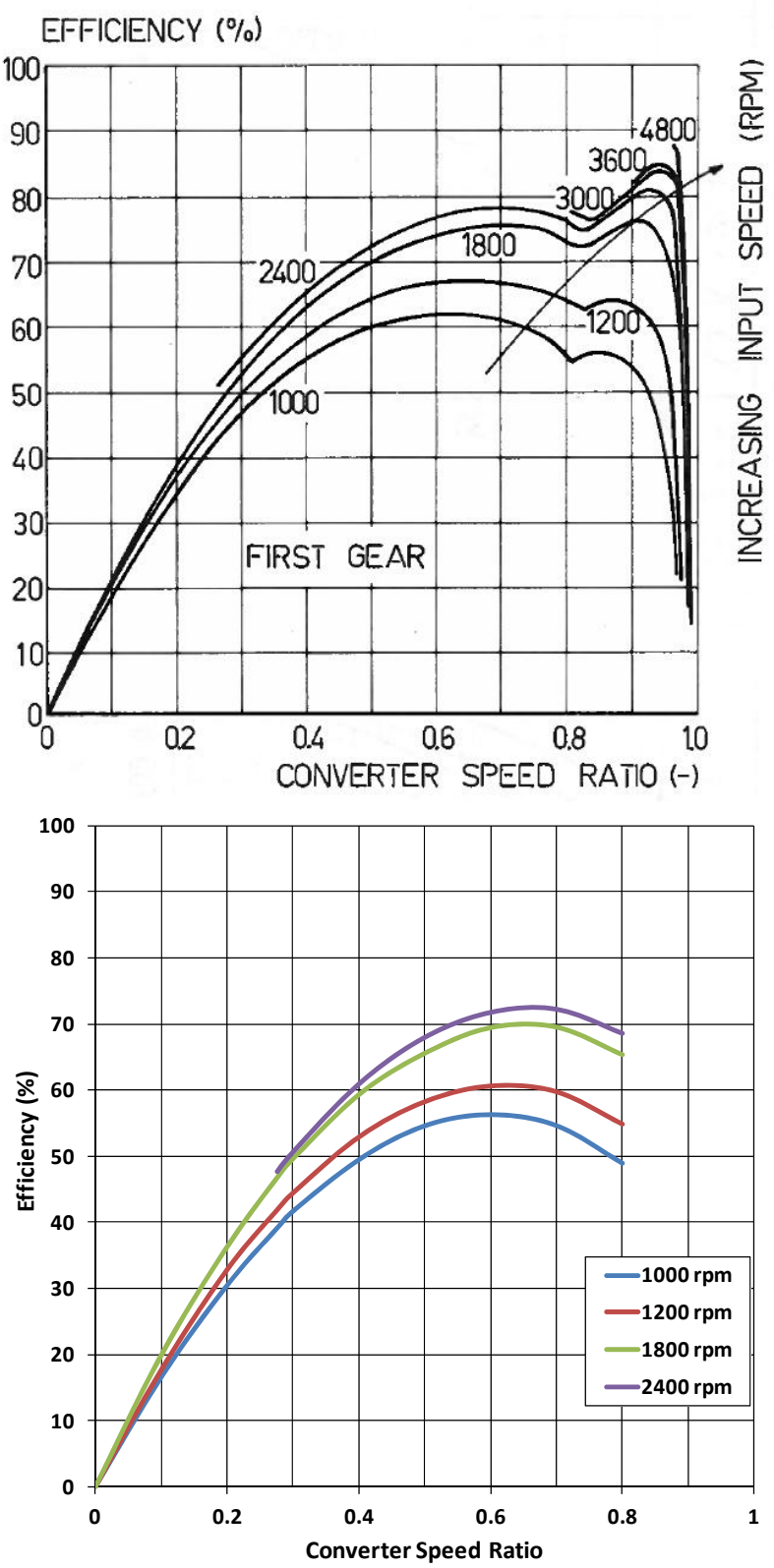

Figure B.27. The 1st gear efficiencies for a Volkswagen Rabbit transaxle (van Dongen, 1982) and from the present light-duty automatic transmission model (based on the Aisin A245E).

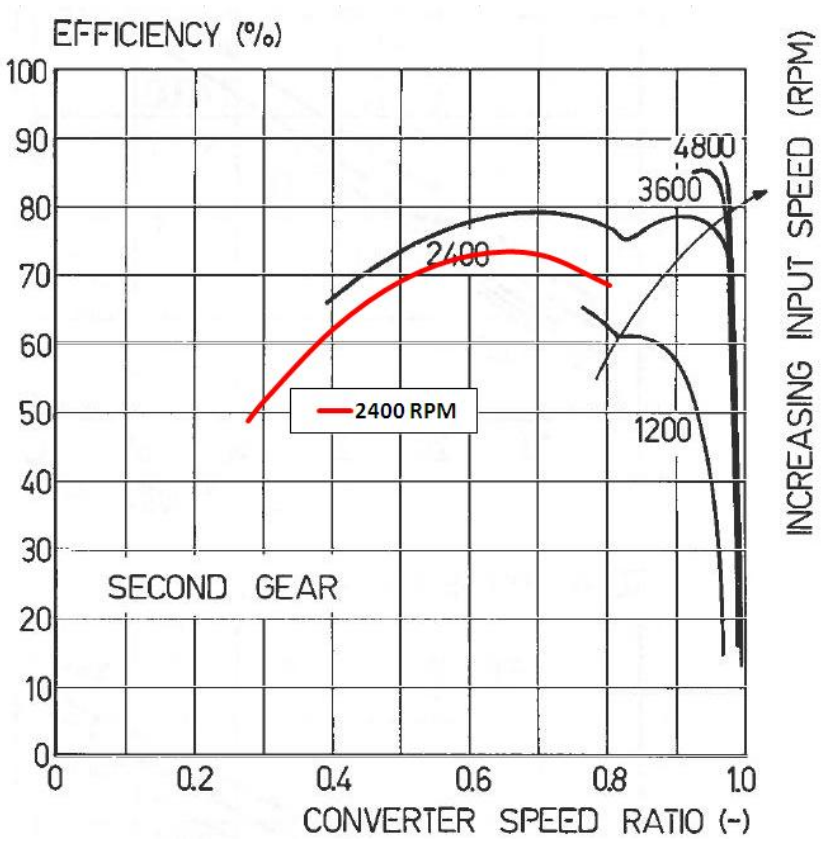

The model results are only shown for 2400 rpm case.

Figure B.28. The 2nd gear efficiencies for a Volkswagen Rabbit transaxle (van Dongen, 1982) and the present light-duty automatic transmission model (based on the Aisin A245E).

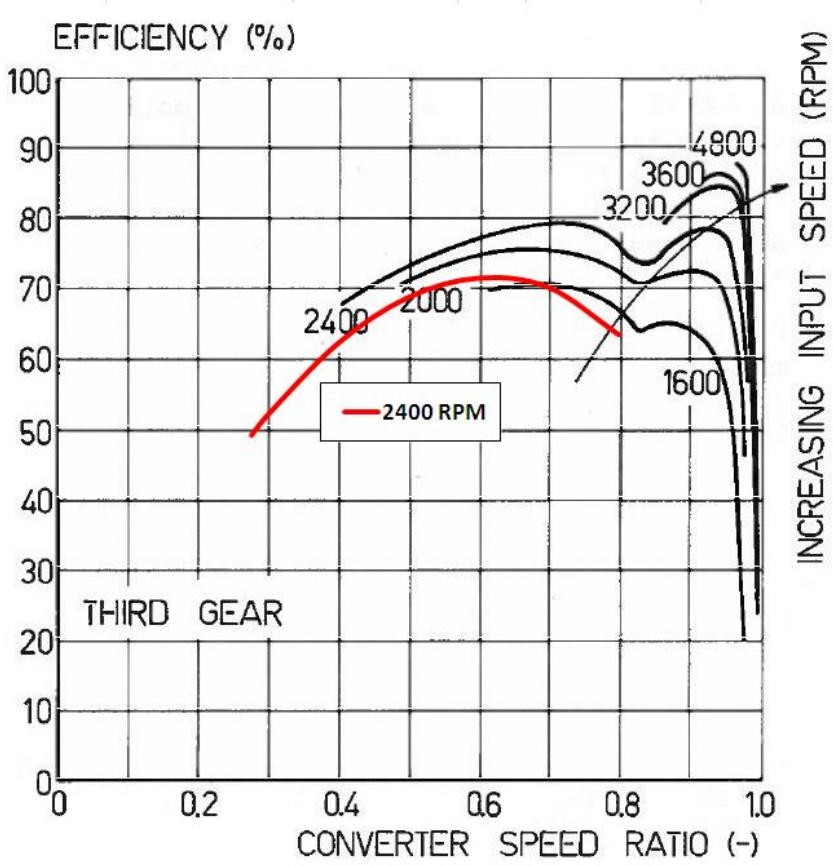

Only the model predictions for the 2400 rpm case are shown.

Figure B.29. The 3rd gear efficiencies for a Volkswagen Rabbit transaxle (van Dongen, 1982) and the present automatic transmission model (based on the Aisin A245E).

Appendix C. Differential Models

C.1. Introduction

Automobile manufacturers have used automotive differentials since before World War II. Over the decades since their inception, automotive differentials have seen several improvements and specializations. Because automotive differentials exist between the engine and the tires of all currently available four-wheeled vehicles, differentials have an effect on the fuel economy of such vehicles.

The engine does not extract all of the energy stored in and liberated from the fuel. The combustion efficiency tracks how close to equilibrium the series of chemical reactions came and, therefore, what ratio of the chemical energy that could have been liberated from the fuel was, in fact, liberated from the fuel and converted to thermal energy. The indicated thermal efficiency tracks how much of the released thermal energy was converted to useful work at the top of the piston throughout the cycle before the exhaust left the cylinder. The indicated thermal efficiency is always much less than one, as the Second Law of Thermodynamics requires that heat losses occur in a heat engine when the cold reservoir is above absolute zero. The volumetric "efficiency" keeps track of how close the engine got to filling the combustion chamber completely with air. The last efficiency is in quotations because it is not a true efficiency: though some loss of pressure occurs when the air travels from the intake, through the filter, around the intake valve, and into the cylinder, these pressure losses can be offset (and actually overcome) by tuning the intake acoustics. It is possible to have a volumetric efficiency that is greater than 100%. None of the other mechanical components has any efficiency associated with it besides the mechanical efficiency, which is the efficiency of converting the useful work at the top of the piston(s) to useful rotational mechanical energy at the engine's output shaft. Hence, the engine efficiency can be proven to be the product of the four aforementioned fundamental engine efficiencies.

Similarly, the efficiency of the powertrain can be proven to be the product of all of the efficiencies of its components. In turn, these efficiencies are related to the fuel economy that the vehicle produces. Imagine a powertrain that is 50% efficient. In order to get a given torque delivered to the tire(s) traveling at a given speed, twice the power that is delivered to the tire(s) must be consumed in the engine. Utilizing twice the fuel causes the fuel economy to be cut in half, so it is easy to see that efficiency will be proportional to fuel economy at any given instant. It is very important to accurately quantify the efficiencies of the components of the powertrain. Differentials are part of the powertrain, so their efficiency is of interest.

Two easier methods for approximating the efficiency of a differential exist, but neither is a fundamental model. First, data can be collected for the efficiency of a "typical" differential of a vehicle operating at an average speed over average terrain. The efficiency of a differential can then be assumed to be the average efficiency of the data collected. This method will fail to capture four of the five factors that affect the efficiency of the differential: torque, speed, gear ratio, and duty classification. However, an intelligent model utilizing this efficiency value could conceivably still account for powertrain configuration. It is suggested that the reader refer to the section on powertrain configurations (Subsection C.4.2) for a deeper understanding of this.

Another method for approximating the efficiency of a differential is to take data for every conceivable value of any or all of the effects mentioned in the introduction (and more). The

quantity of data required to develop a five-dimensional efficiency map with an appreciable amount of resolution is reasonable for the average computer memory storage device. The product of powertrain configurations and duty classifications will produce the number of vehicles for which data would be collected. Effects of speed and torque would require a resolution of 10 speed values by 100 torque values easily. Finally, the effects of gear ratio would likely require a resolution of at least 10 distinct gear ratios. Assuming that 1000 models of vehicle are currently in operation, this method would require the collection (on a chassis dynamometer, using sophisticated strain gauges, and having completed coastdown tests) of efficiency values numbering at least ten million (10^7). The resolution for the efficiency should allow the ability to discern between 1000 values. This can be accomplished by using 10 binary terms per value, or roughly one byte of data per value. This would necessitate the ability to store 10 MB. A computer's operating system today is usually 100 times that size, and computer users are typically allowed 10–100 times as much storage as the operating system. Computers have been capable of storing such an efficiency map for the last decade or two, according to the rule that storage density has doubled every year.

The problem with completing a data set lies mainly in the cost of testing. First, the chassis dynamometer and strain gauges need to be purchased, as does the test bed in which they are to be installed. Second, coastdown tests need to be completed in order for the chassis dynamometer to simulate road load conditions. Third, the equipment must be attended, most feasibly by humans, while the data collection process occurs. Finally, the time required to logistically use vehicles and then store them or return them to their owners would present a challenge.

A third option is to model the efficiency of the differential. This is the least expensive option and offers the interested engineer the greatest flexibility.

The computer model developed for the efficiency of a differential for TxDOT Project 0-5974 is based on fundamental principles that would be able to predict the efficiency of any differential with better accuracy than an incomplete data set, and no additional data will need to be taken. The difference between the computer model and the first easier method is that the effects of the five parameters mentioned are not simply discarded but are considered in the computer model. A research team member on this project, PhD candidate Kyung Jin Kim, suggested a method for comparing distinct differentials with the same gear ratio but different load capacities so that both torque and speed can be accounted for. In this respect, the automotive differential out of one front-wheel-drive automobile can be compared with the automotive differential out of another front-wheel-drive automobile in the same duty class, provided the gear ratios are the same or similar. Furthermore, this model provides a method for estimating the effect of gear ratio on the construction of the differential based on an understanding of the modes of failure of differentials. All of this capability is available within the computer model, and proof-of-concept (POC) tests have validated the model. The reader should check Section C.7 for examples of this.

A basic understanding of how automotive differentials work is provided in Section C.2. Section C.3 is a general discussion regarding the modeling of a generic differential. Section C.4 provides a description of the six differential configurations of differentials that were chosen to represent the entirety of the vehicle market. The differential models and code developed for TxDOT Project 0-5974 are discussed in Section C.5. Section C.6 discusses the three different ways by which the differential model can be incorporated into a drive cycle simulation code: the fuel economy model developed during this project. Proof of concept tests that were performed to

validate the differential model are discussed in Section C.7. Section C.8 provides a summary of this appendix.

C.2. Automotive Differential Basics

It is perhaps less likely that the reader knows how a differential works or what one is than for an engine or transmission. This discussion shall begin with its purpose. The engine supplies the torque, and the transmission allows the driver to use that torque over a wide range of driving speeds. An automobile differential is an application of epicyclic gearing to address the problem of simultaneously powering two axles while allowing the axles to spin independently of one another. Before the introduction of differentials, an automobile transmission would be linked by gears or by a chain/sprocket drive or some other means to one wheel or one or both locked axles of the automobile. This difference in the number of wheels being powered represents an intrinsic trade-off. As the number of powered wheels increases, so does the maximum force that can be developed at the tire-road interface before the wheels begin to slip. The tractive limit of any tire is based on the weight placed upon it, ignoring differences in the coefficient of friction. Hence, adding more wheels is like adding more weight for the friction limit. This, in turn, allows the driver to take full advantage of the acceleration ability of the vehicle. Cornering (and likely deceleration through braking), by contrast, is handled by all of the wheels, although dominated by the outside tires (and the outside front tire if cornering while braking). However, if the powered wheels are not able to turn independently of one another, a non-ideal condition may cause one or more of the tires to slip on the road surface to accommodate this condition. A bump, for instance, would require the bumping wheel(s) to travel faster than the other wheels.

During a turn, as well, the wheels on the outside of the turn must travel faster 9and thus rotate faster) than their counterparts on the inside of the turn (unless the back is being slung outward from the tracks from the inner wheels, in which case the wheels in back travel faster than the front wheels). This phenomenon is easily observable by driving a vehicle in one complete circle on a dirt road. Four separate circles will be observed, all having a common center but each having a different radius. For each wheel to travel the circumference of its circle in the same time it takes to sweep through the entire circle, some wheels must travel faster or slower than others. Before the application of epicyclic gearing to the powertrain (i.e., the differential), axles forced to sweep in circles would have a tire digging into the road and bouncing around. That is, before the invention of the differential, cornering was unpleasant at best.

While the tires slip at the tire-road interface, the available coefficient of friction drops slightly from the static to the kinetic value. Furthermore, an initial study of tribology will elicit an understanding that the rubbing motion will produce undue wear in the tire, decreasing its life. Hence, as the number of tires that were driven increased, the worse the wear on the tires became and the more frequently tires would need to be repaired or replaced. As the number of tires that were driven decreased, the acceleration capability of a vehicle decreased near-proportionally. Performance was pitted against cost, both of which are driving factors for the consumer.

The differential allows two (or more, for more complicated configurations) wheels to be operated at different speeds while simultaneously powered. Henry Jamison Handy produced a wonderful training film for Chevrolet employees in 1937 which explained the fundamental design and operation of a differential to the layperson. That training video has been posted on YouTube and is available to the public. The film describes a mechanism which starts from two coaxial output shafts which go to the wheels. Bars are added perpendicular to these two output shafts (as a prelude to gears). A first piece is mounted on one of the shafts by a bearing so that it

is free to rotate around the shaft. A second piece is mounted at the end of the first piece such that the second piece has an axis of rotation that always intersects the axis of rotation of the coaxial shafts. A bar is added perpendicular to this second piece (as a prelude to another gear). As limitations are reached, more bars are added with the aforementioned constraints until they are replaced altogether by gears. Differential nomenclature is based on this basic understanding. The first piece is known as the carrier. The second piece and attached bar(s) are known as a spider gear; however, in epicyclic gear nomenclature, these gears would be known as planet gears. The gears on the coaxial shafts would be known in epicyclic gear set nomenclature as dual sun gears.

This configuration is a special case of epicyclic gearing. The classical case of an epicyclic gear set is a sun gear, one or more planet gears, and a star gear. The star gear is an inside-out gear (with teeth on the inside) which holds all of the planet gears against the sun gear. To ensure that the planet gear(s) do not fall out of the gear set, typically a carrier, which is free to rotate coaxially with the sun and star gears, places a shaft through the center of each planet gear. Hence, the planet gear(s) not only rotate(s) but also orbit(s) around the sun gear. The classical case of this has all of the gears in one plane. However, several designs exist for epicyclic gear sets which are not in-plane. The conventional differential design uses bevel gears which bend the planet gear(s) and star gear around until the star gear becomes a second sun gear.

Additionally, multiple types of Torsen (torque-sensing) differential gear sets exist. These Torsen differential gear sets do not require bevel gears. One type uses spur or helical gears that all have parallel axes of rotation. Another type uses worm gears, where the planet gears have axes of rotation that are perpendicular to the axes of rotation of the sun gears. These Torsen differential gear sets have an innate limited-slip capability which solves one of the issues of the conventional differential. Some conventional differentials have been designed to be actively or passively limited-slip, but conventional differentials have no innate source of slip limitation. Other limited-slip designs include electronically sensed and actuated models as well as friction disks.

While differentials nullify the trade-off between acceleration performance and tire cost for ideal road surface conditions, some non-ideal road conditions (such as water, ice, snow, or gravel) may cause one or more of the wheels to lose traction. For the conventional differential, a near-equal torque is applied to both wheels, so no mechanism exists for slowing down the slipping wheel while powering the other wheels. Limited-slip differentials have, in one way or another, added friction between the output shafts of the differential. As a result, the larger the difference in speed between the wheels connected to a limited-slip differential, the more power is being diverted from the slipping wheel to the wheel that still has traction. Now, limitation of slip counteracts the benefits of a differential. Through one means or another, a limited-slip mechanism will force the differential toward a locked-axle configuration. This forces the speeds of the wheels to be matched and is activated when the conditions favor such behavior. Hence, limited-slip differentials embody a trade-off between the ideal conventional differential and the locked axle.

Digressions aside, the way a differential works can be simple. As the carrier forces the planet gears to orbit the sun gears, in the absence of any outside forces on the sun gears from the wheels, both sun gears (and wheels) will travel at the same speed. If, however, a wheel is being forced to slow down or speed up (such as when turning a corner), that force will be transmitted through the differential in such a way that the wheels are accommodated. The planet gears begin to rotate about their axes as the speed difference develops between the sun gears (and between the wheels). Hence, when the wheels do not lose traction, it is mostly the road that determines

what the wheels will do. If the vehicle has lost traction, the road and vehicle speed no longer strictly constrain the behavior of the differential. However, they force the differential's operation toward some steady operation, whether that is that the wheels regain traction or that some other condition occurs, such as one wheel is free-wheeling. In the case of free-wheeling, the power provided upstream of the differential is being fed into the free-wheeling wheel faster than can be dissipated at the tire-road interface, and typically not enough power is being fed to the other wheel. It is this behavior that has necessitated the implementation of limited-slip mechanisms. In fact, before the implementation of limited-slip differentials in passenger vehicles, drivers were trained to demand less power from the engine in those types of situations. Now, technology is surpassing the need for such an artful touch.

With all of these improvements in mind, it can be shown that, under certain assumptions, none of these differences matter when modeling a differential. The major assumptions are straight-line driving and favorable road conditions. The former assumption eliminates turning, and the latter assumption eliminates slipping. Hence, the sun gears will always be turning at the same speed. None of the complicated motions associated with the rotation of the planet gears will occur under these assumptions. Also, the limited-slip mechanisms, whatever they may be, will never become active. Any passive losses from the simple presence of such a mechanism when disengaged are assumed to be negligible in comparison to the other losses. The model introduced in the next section will demonstrate that all that remains of a differential is a locked axle connected to the driving shaft by a gear pair. The axles are supported by bearings inside an appropriate housing and sealed from the outside environment where appropriate to retain the lubricant and seal out contaminants. The remaining differences between models are in the powertrain configuration and the weight class of the vehicle. The former determines the orientation and number of components, while the latter determines the dimensions of and relationships between components.

C.3: Fundamental Theory

The fundamental theory behind the model of a generic differential lies within the studies of mechanics, dynamics, heat transfer, and thermodynamics. The governing principles for the model are Newton's Second and Third Laws of Motion and the First Law of Thermodynamics. Newton's Second Law of Motion (e.g., Hibbeler, 2006), states that “a particle acted upon by an unbalanced force **F** experiences an acceleration **a** that has the same direction as the force and a magnitude that is directly proportional to the force.” The reader will be more familiar with the equation representation of Newton's Second Law of Motion.

$$\sum_{\text{direction x}} \vec{F}_x = m\vec{a}_x \tag{C.1}$$

This understanding is necessary to develop a relationship between the moment (or torque) of a force and the angular momentum of the system. Hibbeler writes on page 257 that the sum of moments on a system about a point is equal to the time rate of change of linear momentum, which he then decomposes into two components. If it is assumed that all of the shafts and other pieces of a differential experience negligible deflection with respect to their axes of rotation, then one of the components of angular momentum becomes negligible. The resulting equation is presented on page 385 of Hibbeler’s text:

$$\sum_{\text{axis z}} \vec{M} = \sum \vec{M}_z = I\vec{\alpha}_z \tag{C.2}$$

This rotational version of Newton's Second Law of Motion is more useful for modeling a differential. This model for the efficiency of a generic differential will presume operation at steady speed, neglecting inertial effects. The drive cycle simulator that pairs with this model estimates the inertial contribution separately over finite time steps. Use of sufficiently small time steps allows both models to maintain a fair degree of accuracy. These inertial effects are the right hand sides of the Equations C.1 and C.2; both translational and rotational acceleration are presumed to be zero.

$$\vec{v}_x = \text{const.}, \ \therefore \vec{a}_x = 0 \ \therefore \sum \vec{F}_x = 0 \tag{C.3}$$

$$\vec{\omega}_z = \text{const.}, \ \therefore \vec{\alpha}_z = 0 \ \therefore \sum \vec{M}_z = 0 \tag{C.4}$$

Each of the components of a powertrain has a mechanical efficiency, which is the ratio of power transmitted to the component downstream to power received from the component upstream. Mechanical power, p, is the product of torque, τ, and angular speed, ω.

$$\frac{dW}{dt} = p = \tau * \omega = F * v \tag{C.5}$$

While energy, and therefore power, must be conserved, torque does not have to be conserved. For instance, a gear pair may multiply or divide the torque. However, to conserve power, the speed must be adjusted accordingly, even in the absence of frictional power sinks. This is discussed in greater detail in Subsection C.5.1.2. It is useful to recall that power is simply the amount of energy, E, which is extracted, transmitted, or delivered over a given period of time, t:

$$p = \frac{dE}{dt} \tag{C.6}$$

It is perhaps easier to think of power as an energy rate, in that respect. In this respect, also, an efficiency is just as well a ratio of energies as it is a ratio of powers.

$$\eta = \frac{p_{out}}{p_{in}} = \frac{E_{out}}{E_{in}} \tag{C.7}$$

As discussed in the introduction, the efficiencies of the components are of interest in determining the fuel economy of a vehicle. The challenge is in predicting the efficiency of each component of a differential and bringing the whole differential together. As each component is encountered, it will apply a resistive torque on the powertrain. Assuming that sufficient power is supplied from the engine, this resistive torque creates an inefficiency in delivering that torque.

As previously mentioned, power is related to torque and angular velocity. Hence, the efficiency of each component can be decomposed.

$$\eta_{component} = \frac{\tau_{out} * \omega_{out}}{\tau_{in} * \omega_{in}} = \frac{\tau_{in} * \omega_{in} - \tau_{component} * \omega_{component}}{\tau_{in} * \omega_{in}} = 1 - \frac{\tau_{component} * \omega_{component}}{\tau_{in} * \omega_{in}} \quad (C.8)$$

Other than the gear pair, the speeds will be the same. However, it should be noted that the efficiency of a component has an effect on the torque that is transmitted downstream to the next component.

C.3.1. Assumptions

Under ideal conditions, everything about the differential's operation would be known every time the model runs. However, too many variables exist for the typical user to know and, thereby, be able to input. Thus, in the present model, some of these variables have been held constant. Other variables have been expressed in terms of the quantities that the user can be expected to provide.

C.3.1.1. Symmetries

The assumption of symmetry allows the model to simultaneously solve for the two or more outputs from a power splitting device. After all, the differential's purpose is to power multiple wheels simultaneously: according to the First Law of Thermodynamics, the power from the transmission must be split between the wheels so that energy can be conserved. Assuming symmetry of components entails cutting half of the components away at the split and using the mirror image of the remaining components.

C.3.1.1.A. Torque Bias and the Symmetry Assumption

Some differentials have the ability to bias torque, sending more torque to one tire than to the other. In truth, this ability is one type of limitation of slip and will only be activated when a tire is slipping. Torque biasing simply prevents the differential from passing enough power to a slipping wheel to cause it to spin up and the other wheel to stop. Because most law-abiding driving in Austin occurs with all wheels in contact with the ground, and because inclement weather conditions in Austin rarely cause this driving to include wheels slipping, the model assumes that the torque is split equally between all of the wheels.

C.3.1.1.B. The Bearing Load Symmetry Assumption

Bearing efficiency depends not only on the torque it communicates but also the axial and thrust loads it experiences. Because power is being transmitted through gear pairs from one shaft to another, the gear pairs cause the axles to have axial and thrust loads. This, in fact, is why bearings are needed in the powertrain: otherwise, the shafts would rotate about their axes without needing to be constrained by bearings.

The situation of bearings straddling the loading from a gear pair allows for simple calculation of bearing loads based on a fulcrum analysis, or a force and moment balance. This technique is covered in several undergraduate engineering classes from statics all the way to machine design. However, if the bearings are not equally spaced from the gear pair, the bearings would be supporting different loads. Different loads on the bearings would cause the efficiency

of the bearings to be different. Hence, part of the assumption of symmetry is to require that bearings are placed equidistant from the gear pair in order to assure that both bearings are loaded axially in the same way.

Furthermore, thrust loads are presumed to be split evenly between the bearings. This assumption is soundly rooted in the theory of deformable solids. As the gear pair loads the shafts with a thrust load, each shaft will compress or elongate, much like a spring. If both shafts going from the spider gears to the bearings are of equal length and cross-section, then the "springiness" of the shafts is the same, causing the thrust load to be split evenly between the bearings.

C.3.1.2. Operating Temperature Difference

In the absence of information regarding the severity of the driving being undertaken and the ambient temperature around the car, both the ambient temperature and the temperature difference between ambient and operating temperatures must be assumed. These quantities allow the calculation of the operating temperature of the differential and, more importantly, of its lubricant. The viscosity of the lubricant and its associated windage losses are highly temperature-dependent and are governed according to Walther's equation (see Subsection C.5.2.2.A). Refer to that section for more information on how viscosity is calculated. For the differential model, the ambient temperature was assumed to be 20 °C, and the temperature difference between ambient and the differential lubricant was assumed to be 50 °C.

C.3.1.3. Simplified, Laminar Flow for Windage Calculations

When fluid shears, sometimes turbulent eddies are created. The existence of these eddies complicates the calculation of shear stress and resultant windage losses from a lubricant. The Reynolds number is a quantity used to determine whether a shearing fluid will produce turbulence. This determination is based on a correlation to existing data. In fact, several correlations exist for varying enclosure geometries. However, the first attempt at modeling the windage involved the assumption that no turbulent eddies were being created within either the lubricant or the air within the differential housing. A flow free of turbulence is called a laminar flow.

C.3.1.4. Constant Speed Operation, Neglecting Inertial Effects

When trying to accelerate or decelerate a vehicle, not only do the components load the powertrain through various types of friction, but also the components apply inertial loads upon the powertrain to resist the desired acceleration. The use for which this model is intended calculates the inertial loading effects of the entire powertrain separately from the differential model. This is accomplished by assuming that the differential operates at constant speed over a short period of time. By keeping the time intervals small enough, this numerical approximation can maintain a reasonable degree of accuracy.

C.3.1.5. Smooth, Dry Pavement with No Loss of Traction

Under conditions when the coefficient of friction between the tire and the road is reduced or under periods of high acceleration demand, the driver of a vehicle can demand a motive force which exceeds the tractive limit of one or more of the drive tires. When this occurs, one of the tires will begin to freewheel. This would cause the differential to execute a complex motion and would activate any limited-slip mechanism inside the differential. Both of these effects result in

decreased differential efficiency. However, these events rarely occur in the great state of Texas, as the weather is warm and the vast majority of drivers are kind.

C.3.1.6. Straight, Level Road with No Turning

If the road were to curve, forcing the driver to turn the steering wheel, the differential would begin to execute a more complex motion than is currently modeled. This motion produces an associated decrease in the differential efficiency. A similar effect could be observed in the center differential of AWD vehicles that are traveling over hilly terrain. The vast majority of roads in Texas are sufficiently straight and flat that neglecting these effects would have only a minor effect on the efficiency calculations.

C.3.2. Torque/Energy Balance

Fuel stores chemical energy; however, converting that chemical energy to translational work is fraught with inefficiencies, as is using the work once converted. After all, the driving cycle dictates the required acceleration of the vehicle as a function of time. Acceleration is caused by an imbalance of forces, as is known from classical mechanics. These forces must occur as either body or surface forces. The force caused by gravitational acceleration is an example of a body force, as the force is distributed throughout the body. The force caused by aerodynamic drag on the outside of the chassis is an example of a surface force, as the force acts on the surface of the vehicle. Another surface force is the force action/reaction pair between the vehicle tire and the road interface. While other forces may exist, the aforementioned three forces are the only ones typically considered by this type of analysis for simplicity. It is generally assumed that forces perpendicular to the direction of travel sum to zero for a road load examination of straight-line travel. For instance, aerodynamic lift, inertial force, and the road hold the car up against gravity. Hence, only the projections of forces in the direction of travel are generally considered for driving cycles. This is good, because the driving cycle prescribes the acceleration in the direction of travel.

The way the car accelerates against aerodynamic drag is to apply a torque on the tire. That is the job of the powertrain, in fact. The road does not just keep the car from falling through the surface of the Earth, after all. Vehicles take advantage of the phenomenon of friction at the tire-road interface. The engine provides a torque to at least one tire through the rest of the powertrain, which commonly includes a transmission, some bearings, some universal or common velocity joints, and usually at least one differential. This torque from the engine is the result of liberating energy stored in chemical bonds in the fuel. During combustion, molecules of fuel and air are broken and recombined into exhaust products, which is at a lower chemical potential than the fuel and air mixture. The chemical reaction, sparked by the spark plug and encouraged by turbulence and high pressures in the combustion chamber, is therefore exothermic. The chemical-to-thermal heat release increases the temperature of the working fluid which, in turn, increases the pressure within the cylinder. The elevated pressures act on the piston top surface. This produces a force on the connecting rod which then rotates the crankshaft.

As the driving torque is transmitted through the powertrain, several phenomena cause various components of the powertrain to experience other torques. First and foremost, while the tires grip the road (and even when the tires lose traction), the road applies a force on each of the tires. While the force is balanced by the bearings such that the chassis and powertrain travel at the same speed, the road load resistive torque may only be overcome by the engine and power transmission components. The main focus of the fuel economy model developed for TxDOT

Project 0-5974 is to predict the motive force that the engine eventually produces at the tire-road interface, as the drive cycle simulator uses that force to predict the acceleration of the vehicle. However, before the driving (motive) torque is communicated to the drive wheels, other components of the powertrain generally are designed to provide a torque multiplication (although inefficient) while simultaneously decreasing the rotational speed. The sources of torque loss (inefficiency) in the transmission and differential include bearings, seals, gear tooth sliding friction, and windage. An application of Newton's Second Law of Motion for rotation to an input torque (originating from the engine) and a torque applied on an element can yield its output torque.

It is generally obvious how Newton's Second Law of Motion applies to a model of a differential. However, the First Law of Thermodynamics is also applicable for two reasons. Firstly, in the absence of either kinematic relationships or Newton's Third Law of Motion, the First Law of Thermodynamics would resolve the change in either speed or torque, respectively, for a gear pair. Secondly, however, the First Law of Thermodynamics allows an estimation of the efficiency of a differential from temperature data using a heat transfer analysis. If one can assume that all energy dissipated by the torque loss mechanisms in the powertrain become thermal energy, then, under steady operation, the differential's thermal energy loss rate (heat loss) will soon approach the total mechanical energy loss rate across all of the components of the differential. Concessions may be made for other energy inputs, such as solar radiation. Data collection procedures can control or minimize these concerns.

C.3.2.1. Strain Gauge Technique

The efficiency of a differential can be determined by connecting strain gauges to the three shafts connected to the differential. By knowing the torsional spring coefficient of the shafts, the shear strain of the shafts can be used to determine the torque being transmitted through each of the shafts. By multiplying the torque transmitted through a shaft by the speed at which it is rotating, the power delivered by each shaft can be found. As mentioned before, the efficiency of the differential is simply the sum of the power outputs divided by the power input. In order to generate a useful amount of data, both the speed of differential operation and the torque delivered to the input shaft would need to be controlled. The speed of the differential can be controlled by constraining the output shafts to operate at the speed dictated by the desired input power speed, thus developing a torque throughout the shaft.

C.3.2.2. Heat Transfer Analysis

Another method for determining the efficiency of a differential is to operate a differential for long enough for it to reach operating temperature. Sufficient knowledge of the heat transfer characteristics of the shafts and the differential housing and the temperature difference across these components would allow for an estimation of the power loss from the differential through heat. Sooner or later, all of the mechanical power that was dissipated becomes heat. Hence, knowing the heat loss at operating temperature and the power input from engine maps and transmission efficiency models would allow a reasonable estimation of efficiency without needing strain gauges.

C.3.3. Tribology

The study of tribology is dedicated to surfaces rubbing on each other, going back to the Greek root *tribos*. As surfaces rub on each other, two things occur: friction between and wear of

the surfaces. These two factors account for the energy losses associated with rubbing. When an intermediate lubricant is introduced, both friction and wear are affected. Wear is reduced because of the decreasing frequency of contact between the surfaces. Friction is also altered, but it is not necessarily reduced, depending upon the lubrication regime. The subject of tribology is mentioned as a supplement to the gear pair efficiency models.

C.4. Types of Differentials

Six differential configurations were chosen to represent the entirety of the vehicle market. These configurations span the duty classifications discussed in the following subsection.

C.4.1. Duty Classifications

According to Matthews (2011), the duty classification of a vehicle is based on its Gross Vehicle Weight Rating and/or its Loaded Vehicle Weight. As the weights increase, the duty classification will go from light-duty to medium-duty to heavy-duty. It is worth noting that EPA does not have a medium-duty vehicle classification except for medium-duty passenger vehicles. Although EPA has only this one specific type of medium-duty vehicle, truck classification schemes often include a medium-duty category.

C.4.1.1. Light-Duty

Light-duty vehicles span Gross Vehicle Weight Ratings from 0–8500 lb. LDVs are intended primarily for the transportation of people rather than cargo. Because the weight is sufficiently low that the amount of gasoline consumed is not a strong function of vehicle weight, fuel economy is generally computed in a way that ignores vehicle weight, other than indirectly through the coastdown coefficients.

C.4.1.2. Medium/Heavy-Duty

Heavy-duty vehicles have a Gross Vehicle Weight Rating floor, although the value has changed historically. These vehicles also typically have a large frontal area and are used to haul cargo instead of people. Weight becomes a significant factor in determining the cost of fuel associated with truck transportation. As a result, fuel economy for HDVs is computed in a way that accounts for vehicle weight. The present differential efficiency model treats medium-duty trucks as HDVs with the appropriate scaling.

C.4.2. Powertrain Configurations

As previously mentioned, six powertrain configurations were chosen which spanned the duty classifications. In particular, the rear-wheel drive (RWD) configuration is shared between the light- and heavy-duty classifications. The dual differential is only available for the heavy-duty classification, and the other configurations (front-wheel drive, FWD; four-wheel drive, 4WD; and all-wheel drive, AWD) are exclusive to the light-duty classification.

C.4.2.1. FWD

FWD vehicles have a transaxle in which the transmission and differential share the same housing. This provides the differential with the benefit of being exposed to a pressurized lubricant source, the oil pump, which allows less of the differential to be immersed in the more viscous differential lubricant. This cuts down on windage losses. The engine and transaxle are

typically mounted laterally across the front axle, allowing the differential to use a helical gear pair rather than a hypoid gear pair. The helical gear pair is more efficient than the hypoid gear pair.

C.4.2.2. RWD

Rear-wheel drive (RWD) vehicles have a differential on the rear axle. The engine and transmission occupy the front of the vehicle, so a long shaft must traverse the distance between the transmission and the differential. Furthermore, because that shaft is not parallel to the rear axle, the differential cannot use a helical gear pair but must use a hypoid gear pair instead.

C.4.2.3. 4WD with Transfer Case

Four-wheel drive (4WD) vehicles can operate in two modes. In the two-wheel drive mode, the transfer case is disengaged, and the vehicle behaves like a RWD vehicle. However, in 4WD mode, the transfer case engages the front differential and makes it rotate exactly as fast as the rear differential. The nature of the transfer case does not allow for operation of 4WD on pavement which is hilly or curvy, as either one will cause axle bind due to the road wanting to force one of the axles to spin faster than the other. The transfer case is typically a 1:1 chain-drive system with some sort of clutch.

C.4.2.4. AWD

All-wheel drive (AWD) vehicles address the problem of 4WD transfer cases not allowing 4WD operation on pavement. The transfer case is replaced by a center "differential" which may be anything from a conventional differential to simple loose clutch plates. When the center differential is a true conventional differential, it is similar in nature to the FWD differential, although there is no gear pair. In fact, some AWD vehicles use a transaxle to combine the transmission and center differential. The other differentials are hypoid gear differentials, similar to the RWD and 4WD vehicles.

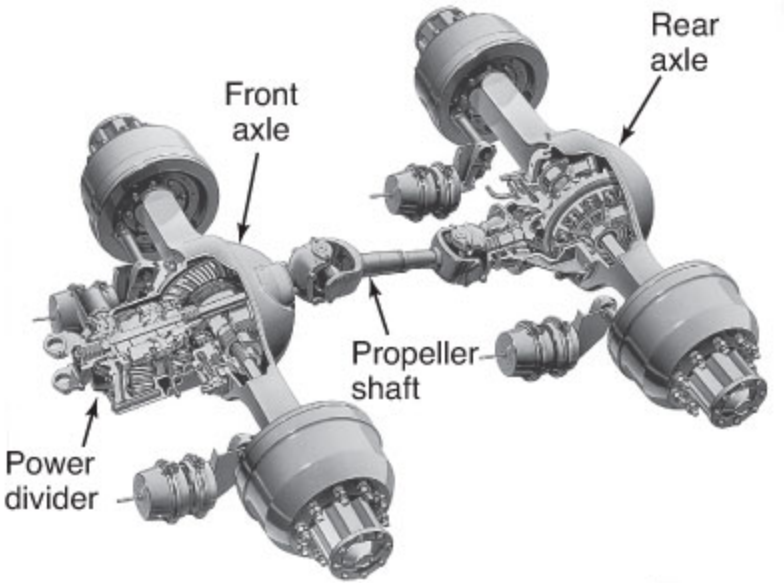

Figure C.1. A heavy-duty tandem differential (Bennett and Norman, 2011).

C.4.2.5. Heavy-Duty Differentials

A vast range of vehicles are categorized as heavy-duty: all vehicles with a Gross Vehicle Weight Rating of more than 8500 lb. Thus, many heavy-duty trucks have a single rear axle and a differential that differs from a light-duty RWD differential only in scale. Large heavy-duty trucks have two rear axles. In this case, they generally use a "tandem" differential, as illustrated in Figure C.1. In this case, torque is delivered to both rear axles, with the torque split controlled by a "power divider." However, some heavy-duty trucks have "tag axles," in which case there is a differential on only the front-most of the two rear axles. Both categories of heavy heavy-duty trucks, those with tandem axles and those with tag axles, can have a two-speed gear box in front of the first input, as discussed in the following subsection.

C.4.2.6. Heavy-Duty Dual Differentials

The dual differential is a conventional heavy-duty differential with a two-speed gearbox located directly upstream and sharing the same housing. Though most gearboxes like this are used in multi-stage transmissions, some HDVs use a dual differential instead. Dual differentials are certainly a newer addition to differential technology.

C.4.2.6.A. Low Gear Ratio

The two-speed gearbox has a low gear and a high gear. The high gear ratio is typically assumed to be unity (1.0:1). However, the low gear ratio is a required input for the model of a dual differential just like all of the transmission gear ratios are required inputs for the transmission model. The need for a low gear ratio is unique to the dual differential.

C.4.2.6.B. Gear Selection

The two-speed gearbox has the option of in which gear to operate. This shifting is controlled within the fuel economy drive cycle driver model. As a result, unlike the low gear ratio, the user has no control over the gear selection of the dual differential.

C.5. Present Differential Models with Explanation of Code

A true differential efficiency model would be excellent for the design of automotive differentials. However, most people do not want that degree of sophistication in a differential efficiency model. The modeling elements are completely fundamental; however, the differential models are all based on measurements taken from a set of differentials that were determined to be characteristic of the differential type and available for measurement by our research team at the University of Texas at Austin in a cost-effective manner. Techniques developed by several members of the research group have been employed to allow the level of sophistication that the users will want from the model while still making it user friendly.

C.5.1. Common Modeling Elements

The following sections briefly highlight the concepts used in determining the efficiencies of components that were found in all of the differentials.

C.5.1.1. Windage

Three types of geometries are of interest for determining the fluid shear drag (windage) losses of a rotating element. These geometries are spherical (because the differential carrier is typically spherical in shape), cylindrical (because shafts and some differential carriers have this geometry), and hypoid gear shapes. Hypoid gears, like bevel gears, look remarkably like frusta of right circular cones or two frusta stuck together, base to base. Hence, the remaining geometry of interest, a hypoid gear shape, is the frustum of a cone.

All of these losses require knowledge of the viscosity of the fluid in which the rotating elements are immersed, as discussed in Subsection C.5.2.2).

C.5.1.1.A. Windage Definition

Some of the energy transmitted by the gear pair is being diverted at the interface between the gears because of friction. Each of the gears is also rotating in a fluid, whether air or differential lubricant, unless the differential housing has been pumped to a perfect vacuum. This motion will cause the fluid to shear (from a continuum perspective; alternatively, one could consider the statistical particle collisions between the gas/liquid particles and the solid gear particles). Fluid shearing is a form of fluid deformation and requires an input of energy in order to do so. In any event, because of fluid shear, gears spinning in fluid also cause some of the energy transmitted to be diverted. Because two different fluids are subjected to shear, the combination of aerodynamic drag (due to the air within the differential housing) and hydrodynamic drag (due to the lubricant "gear oil," is referred to as windage.

C.5.1.1.B. Cylindrical Geometry

The losses associated with the rotation of cylindrical geometries within stationary enclosures are readily available in fluid dynamics textbooks. For example, Example 8.2 in Fox et al. (2006) calculates the torque and power dissipation at a given speed for a journal bearing using the assumption of a small gap width "so the flow may be modeled as flow between infinite parallel plates" This theory has been adapted for use in all of the powertrain configurations as appropriate.

Every rotating shaft of constant cross-section is subject to this form of windage, even if it is only in air, because even air has some viscosity. As mentioned previously, the fluid is assumed to shear with laminar behavior. The cylindrical windage torque model is based on the radii of the outside of the shaft and the inside of the enclosure, the lubricant viscosity, the rotating speed, and the length of the shaft within the enclosure.

C.5.1.1.C. Spherical Geometry

The losses associated with the rotation of spherical geometries require some calculus to determine. Similar situations are the subject of discussion on websites like Physics Forums: <http://www.physicsforums.com/printthread.php?t=427695>. The surface area of the sphere is exposed to the fluid, so the contribution of shear stress to rotational drag must be integrated over the entire surface area of the sphere; however, to track the moment that the shear stress creates when acting over the surface, the shear stress must be multiplied by the moment arm from the axis of rotation to the infinitesimal surface area element. The resulting integral formulation for fluid shear torque remains a function of the radii of the outside of the sphere and the inside of the shell (differential housing), the lubricant viscosity, and the speed of rotation.

C.5.1.1.D. Frustum Geometry

The losses associated with the rotation of the frustum of a right cone require calculations similar to those required by spherical geometries. The primary difference is in the expression for the curve that is revolved about an axis. Careful consideration of the shear stress and moment arm as integrated across the surface area of the frustum provides an equation for the torque the fluid applies on the rotating frustum. This equation is a function of frustum height, base and peak radii, clearance between frustum and shell, fluid viscosity, and rotational speed.

C.5.1.2. Gear Pair

The teeth on gears allow gears to mesh in such a way that, when one gear rotates, another is forced to rotate. When rotating gears are mated in a pair or in more complicated groups, they transmit forces between their teeth. Upon close inspection, one finds that the teeth slide past each other as the gears transmit their forces in motion. These forces impose torques, or moments, about the axis of rotation. The forces on the gears are supported by the axles they are mounted on, which themselves are mounted by bearings to the main structure. However, the slipping behavior of the teeth causes frictional losses, and the rotation of gears in viscous fluid causes windage losses.

C.5.1.2.A. Basic Gear Terms

The associated nomenclature for gears is perhaps foreign to most readers. A brief summary of important terms is given below, but more detailed information is available at the Quality Transmission Components website: <http://www.qtcgears.com/Q410/Q420cat.html>.

It bears mentioning that many types of gears exist, based on the placement of the teeth and the orientation of the gears relative to one another as a result of the tooth placement. A substantial (although by no means exhaustive) list of gear types is available in *Dudley's Gear Handbook* (Townsend, 1991). Of these dozen or so gear types, only two types are of interest in conventional differentials: helical and hypoid gears. Bevel gears also exist in conventional differentials as spider gears, but the assumption of straight-line driving negates their contribution to the efficiency of a differential.

The simplification of gears for analysis generally requires knowledge of a pitch radius/diameter which is somewhere between the radius at the tips of the teeth and the radius at the roots of the teeth. The pitch radius/diameter is the radius/diameter of the solid shape that would replace gears with teeth if one were to rely on friction rather than strict kinematics to transmit a torque and rotating speed. For instance, two spur gears could be replaced by "sticky" cylinders whose radii are the pitch radii of the spur gears. However, unlike such a configuration with cylinders, the spur gears will not slip with respect to one another unless a tooth breaks off. Gear pair efficiency models use the pitch radius instead of the outer or inner radius because the action of rubbing, sliding, and force transmission happens at or near the pitch radius regardless of the size of the teeth.

All gears have a normal pressure angle because the teeth do not jut straight out of the gear. This causes the gears to naturally repel each other through the use of inclined planes. Some gears have teeth that are angled in such a way that they develop a helix angle. This will cause the gears to pull or push on the shafts on which they are mounted, in contrast to the normal pressure angle, which causes shafts to bend. Both of these angles affect the load transmitted at the tooth-to-tooth interface, increasing the energy required to slide the teeth with respect to one another.

Two gears may mesh despite having a different number of teeth. The ratio between the number of teeth is known as the gear ratio (and is equal to the ratio of pitch radii). Due to kinematic relationships, the gear ratio from one gear to another is the inverse of the speed ratio in the same direction. Furthermore, neglecting inefficiencies, the gear ratio from one gear to another is equal to the torque ratio in the same direction.

All of these terms are quite common in gear design and are quite useful in predicting the efficiency of gear pairs. Another term is the face width of the tooth, which is related to the thickness of the gear and the helix angle. These terms will be discussed further in the following subsections.

C.5.1.2.B. Differential Gear/Final Drive/Axle Ratio

The differential gear ratio, also known as the final drive ratio or axle ratio, is the gear pair that transmits torque from the transmission to the spider gear carrier inside the differential. It is the only gear ratio of interest in the differential models.

C.5.1.2.C. Helical Gears (FWD and AWD only)

Helical gears are an improvement on spur gears because of the decrease in noise. A helical gear pair exists in the differential of a transaxle of a front-wheel-drive (FWD) passenger car. Some AWD vehicles have a transaxle as well.

Many models exist for the efficiency of a helical gear pair. *Dudley's Gear Handbook* (Townsend, 1991) is an excellent place to start. Subsection 12.3.3 of that reference, entitled "Single-Helical Gears," provides the reader with an "equation for the percent power loss." A proper understanding of the nomenclature can bridge the gap between the published equations provided or measurements collected and a real-world understanding of the significance of those quantities. In addition to Townsend's book, Appendix C in Matthews' (2011) text includes the Buckingham equation for gear pair efficiency. Another good reference is a paper by Diab and coworkers (2004).

C.5.1.2.D. Hypoid Gears (all except FWD)

Helical gears are one simple improvement descended from spur gears, the easiest gears to understand. Hypoid gears, however, are something like a cross between a helical, bevel, and worm gear pair. The teeth of a hypoid gear are beveled; that is, they are not perpendicular to any surface of a typical cylindrical disk (unlike spur, helical, and worm gears). However, the rotational axes of the hypoid gears are neither parallel nor intersecting, they are skewed. The teeth themselves of a hypoid gear are also curved like the teeth of helical gears. Handy's 1937 film ("Around the Corner," www.youtube.com/watch? V=KJY9SxDOTog, accessed 7/18/2010) also covers the improvement of hypoid gears over straight bevel gears. The film cites the reason for the use of hypoid gears, which are not as efficient as bevel gears, due to the increased leg room available to the passengers because the transverse axle could be lowered by a few inches using hypoid gears. Hypoid gears are typically more efficient than worm gears, and thus worm gears appeared less desirable. Again, a trade-off resulted in an engineering decision.

Fewer models exist for the efficiency of a hypoid gear pair when contrasted with helical gear pairs. Again, *Dudley's Gear Handbook* (Townsend, 1991) is an excellent place to start. Another good reference about hypoid gear pairs is by Hai (2005).

C.5.1.3. Bearings

Bearings are required to constrain the motion of a shaft to pure rotation while still allowing it to rotate relative to its mount. In the case of a differential, bearings force the shafts to align in such a way that the gears that should be in contact are in contact. Bearing losses occur because of friction and wear. Bearing loss calculations are also discussed very well in Khonsari and Booser (2008).

C.5.1.3.A. Types

Many types of bearings exist. Two main categories of bearings are roller element bearings and fluid film bearings. Roller element bearings are of interest for this model; and fluid film bearings are not present in automotive differentials. Roller element bearings are further categorized by the type and arrangement of rolling element. A bearing may have one or more rows of rolling elements. Furthermore, the rolling elements may take many shapes, such as spheres, cylinders, slender cylinders (or pins), cones, or barrels.

C.5.1.3.B. Types Used in the Present Differential Models

The present differential models used single-row tapered roller bearings. Tapered rollers are like truncated cones, or frusta. The moment applied by any bearing is the sum of three moments from different sources of loss. One of these moments is load-dependent, while another is speed-dependent. The moments are also functions of diameters, coefficients of friction, and lubricant viscosity.

C.5.1.4. Seals

Seals are required to keep lubricant inside with the gears and bearings while keeping contaminants out. In fact, some bearings have built-in seals; for others, this is not necessary (and is cheaper not to have). The model for seal efficiency is based on that in Appendix of Matthews' (2011) text. The seal model is based solely on geometry and an adjustable factor.

C.5.2. Common Parameters

The following sections discuss parameters that do not belong to any particular component or need further discussion.

C.5.2.1. Peak Torque

The peak torque available to the differential is a product of several factors. First, the engine produces a peak torque at its optimal range. Under the most severe conditions, the engine can supply this torque to the transmission when the transmission is in its lowest gear, or highest torque multiplication. If the transmission is an automatic, the torque converter will first multiply the torque before it reaches the transmission gearbox. Knowledge of all of these factors allows generation of a peak torque value which can be used in a method proposed by a member of this research team, PhD candidate Kyung Jin Kim, to compare the efficiency of one differential with the efficiency of another differential.

C.5.2.1.A. Kyung Jin Kim's Method

In a few words, PhD candidate Kyung Jin Kim's method scales the differential input torque by the highest possible input torque that it could see for that particular vehicle. Scaling the input torque generates a torque fraction that is halfway to converting a torque value for one vehicle's differential to the equivalent torque value for another vehicle's differential. Once the torque fraction is provided to the differential model, the torque fraction is converted back into a torque based on the torque capacity of the differential upon which the model is based (and the measurements were made).

C.5.2.1.B. Peak Engine Torque

Data will exist for the wide-open throttle (WOT) torque that an engine can produce at any speed if it was calibrated on a dynamometer. This WOT torque curve is generally not available to the user of the fuel economy model produced for TxDOT Project 0-5974. The maximum torque produced over the entire range of engine speeds at wide-open throttle is the engine's peak torque. Although this torque is often available to the user of this fuel economy model, it is not always available. Thus, the fuel economy model user is required to input the maximum brake power and the corresponding engine speed. From these, the fuel economy model calculates the corresponding WOT torque. Although this is not the peak torque, it is generally not much smaller. As the maximum torque available from the engine increases, the transmission and differential will need to be designed more robustly in order to offer the same gear ratios.

C.5.2.1.C. Maximum Torque Converter Torque Ratio

The torque converter is the component of an automatic transmission that allows the engine to idle while the wheels are stopped and the transmission is still in gear. Vehicles with manual transmissions must shift the transmission into neutral or to keep the clutch pedal depressed before coming to a stop, or the engine will stall. Torque converters are capable of immense changes in speed with more limited effects on torque. The torque ratio, the torque multiplication by an automatic transmission’s torque converter, still needs to be taken into account.

C.5.2.1.D. Maximum Transmission Gear Ratio

As mentioned previously, the transmission multiplies the torque received from the engine. For an automatic transmission, this torque multiplication occurs in both the torque converter and the gearbox. The maximum transmission gear ratio provides the maximum torque multiplication factor by the gears of the transmission.

C.5.2.2. Lubricant Type

Oil viscosity ranges are specified by their grade. Oil viscosity ranges are specified by two numbers: the first is a cold viscosity range, and the second is a hot viscosity range. Kyung Jin Kim, PhD candidate, introduced the differential model's author to Walther’s equation, which is used to calculate the viscosity of oil as a function of temperature from two points. Walther’s equation is discussed below.

C.5.2.2.A. Walther's Equation

Walther's equation relates the kinematic viscosity of a fluid to its temperature. Three constants exist within the equation that must be fit for each type of lubricant. The equation itself is (Walther, 1933)

$$\log_{10}\left(\log_{10}\left(\nu + C\right)\right) = A + B * \log_{10}\left(\mathrm{T}\right) \tag{C.9}$$

Great care must be used in determining the value of constant *C* to ensure that the sum is greater than 1. Otherwise, the equation is no longer useful. Equation C.9 uses the oil's kinematic viscosity, υ, in centistokes and temperature T, in degrees Fahrenheit.

C.5.2.2.B. Air

Air is the only fluid for which Walther's equation does not apply. Instead, the following equation was used for the kinematic viscosity of air as a function of temperature:

$$\nu_{air} = -1.1555\text{x}10^{(-14)}\text{x}T^3 + 9.5728\text{x}10^{(-11)}\text{x}T^2 + 3.7604\text{x}10^{(-8)}\text{x}T - 3.4484\text{x}10^{(-6)}$$

which yields the kinematic viscosity of air, ν_{air} in m^2/s, given the temperature in K (http://wiki.answers.com/Q/Equation_for_finding_viscosity_of_air_at_any_given_temperatures).

C.5.2.2.C. ATF

Automatic transmission fluid (ATF) is used in transaxles, so the FWD's differential and the AWD's center differential are exposed to ATF. ATF tends to be less viscous than the other gear oils examined.

C.5.2.2.D. 75W90 and 80W90

Both of these gear oils are substantially more viscous than engine oil, as denoted by the higher numbers. The nomenclature for these oils is defined by the Society of Automotive Engineers.

C.5.2.3. Immersion Fractions

Although some of the components of the drivetrain must be partially immersed in lubricant in order to protect the rubbing surfaces and reduce frictional losses, this is typically limited to the gear pairs and the spider gear carrier. Immersion fractions considered are: Fully Immersed, Halfway Immersed, Dipped, and Sprayed From Oil Pump.

C.5.3. Light-Duty FWD

The University of Texas at Austin allowed the disassembly and measurement of a spare transaxle from their 2005 Challenge X car, a Chevrolet Equinox. Because research team member Kyung Jin Kim's transmission model ends at the transmission output shaft, the first component considered in the light-duty transaxle differential model is the helical gear pair. As previously mentioned in Subsection C.5.1.2, the efficiency of a gear pair may be divided into three parts: the gear pair tooth friction follows the windage on the pinion gear, while the windage on the driven gear follows the gear pair tooth friction. After passing through the gear pair, the power transmission path flows through the spider gear carrier, which is assumed to have spherical shell

geometry and is exposed to windage. The power transmission path splits from the carrier onward as discussed in the discussion of windage on a spherical geometry. Splined shafts extend from the carrier, but the power transmission path first flows through the bearings on which the carrier is mounted. After the bearings and shaft windage, the power transmission path flows past a seal and extends through a region of shaft which may be recessed within a windage shield. Those shafts extend directly to the wheels through a couple of universal or constant velocity joints and a bearing for each wheel, but their analysis is not included in the analysis of the differential. Measurements from all of the aforementioned components that are within the bounds of consideration will follow, as will a description of the determination of the scaling parameters used for the Equinox's transaxle differential. First, however, it is important to note that, while the dimensions for other transaxle differentials may differ from those measured from the Equinox, the overall architecture is assumed not to differ substantially amongst the transaxle differentials. The scaling parameters that will follow are used to accommodate the differences in transaxle differential dimensions using the method proposed by co-investigator Kyung Jin Kim.

The following measurements were taken from the differential of the transaxle of the 2005 Chevy Equinox. For the helical gear pair, the numbers of teeth of the gears were taken and the gear ratio of 61:23 derived from them. The outer circumference of the driven helical gear was taken to be 26-7/8 inches. The tooth height was taken to be 5/16 of an inch. From those two pieces of information, the pitch radius of the driven gear, $R_{p,d}$, was inferred via the following equation.

$$R_{p,d} = \frac{1}{2}\left(d_{o,d} - \frac{h_{tooth}}{2} \right) \tag{C.10}$$

The pitch radius of the driving, or pinion, gear ($R_{p,D}$) requires only knowledge of the pitch radius of the driven gear and the gear ratio, G, via the following definition of the gear ratio.

$$G = \frac{R_{p,d}}{R_{p,D}} \tag{C.11}$$

The gear tooth face width, *FW*, and gear thickness, *GW*, were measured to be 1-3/8 inches and 1-7/32 inches, respectively. This allowed for an estimation of the helix angle, γ, of the gears using the trigonometric relationship.

$$\cos(\gamma) = \frac{GW}{FW} \tag{C.12}$$

The bearings were observed to be tapered roller bearings that had a circumference of approximately 10 inches. The diameter of the tapered rollers was on the order of 1/4 of an inch. The shafts pressed into the bearings had a circumference of 3-5/8 inches and existed inside an enclosure of diameter 2-3/8 inches between the bearings and the seals. The seals were measured as being 8 inches apart, while the diameter of the spherical spider gear carrier was measured to be 5-1/2 inches, which indicates a similar bearing spacing. The spherical spider gear carrier exists inside a spherical shell whose inner diameter was measured to be 6 inches. These

measurements are sufficient to define or reasonably approximate the missing parameters in the component models that go into the light-duty FWD differential model.

The modeling effort involves placing all of the components in series, assuming symmetry when necessary. The efficiencies of each of the components are calculated based upon values obtained from upstream components. The efficiency of the differential of the transaxle, η_{diff,LD_FWD}, is the product of the component efficiencies.

$$\eta_{diff,LD\_FWD} = \eta_{gp,hel} * \eta_{wind,sph} * \eta_{bear} * \eta_{wind,cyl,1} * \eta_{seal} * \eta_{wind,cyl,2} \quad \text{(C.13)}$$

The right-hand side of Equation C.13 must be evaluated one component at a time from left to right. Each efficiency will modify the torque as the torque travels through the powertrain before the torque gets to the next component. As such, the model works by modifying and passing the torque from component to component.

C.5.4. Light-Duty RWD

Inland Truck Parts of Austin graciously allowed the measurement of a generic 1500-series rear axle differential. The knowledge of the load capacity allowed approximation of the scaling factors that are necessary for generalization of the model. The following equation presents the efficiency calculation with the order of the components considered.

$$\eta_{diff,LD\_RWD} = \eta_{seal,1} * \eta_{bear,1} * \eta_{wind,cyl,1} * \eta_{gp,hyp} * \eta_{wind,sph} * \eta_{wind,cyl,2} * \eta_{bear,2} * \eta_{seal,2} \quad \text{(C.14)}$$

C.5.5. Light-Duty 4WD with Transfer Case

One of Jeep's powertrain configurations, called the YJ, is very popular among Jeep owners, according to a local Jiffy Lube employee. This powertrain configuration includes a transfer case. Jeep publishes specifications for all of its parts, as Jeep owners frequently break and repair their own vehicles. As such, it should be fairly easy to obtain the measurements needed to complete a future model.

A first approximation of a transfer case is a two-speed gearbox (to provide 4HI and 4LO) in front of a chain drive system. While the old method for operating 4WD systems was to connect/disconnect the front wheels to/from the hubs, the new method is to engage/disengage the chain drive system that powers the front wheels. The two-speed gearbox program developed for the heavy-duty dual differential is easily modified to suit these needs, and the chain drive system is presumed to have 97% efficiency (Steidel et al., 1996). The following equation presents the efficiency calculation with the order of the components considered and with respect to models for the other components of the differential.

$$\eta_{diff,LD\_4WD} = \eta_{gb} * \eta_{tc} * \eta_{diff,LD\_RWD} \quad \text{(C.15)}$$

where η_{gb} is the efficiency of the 2-speed gear box portion of the transfer case and η_{tc} is the efficiency of the chain drive portion of the transfer case (99%).

C.5.6. Light-Duty AWD

Recall that AWD vehicles address the problem of 4WD transfer cases not allowing 4WD operation on pavement by replacing the transfer case of 4WD drivelines with a center

"differential" which often has a center differential that is similar to the differential in a transaxle. Thus, the following equation presents the efficiency calculation for an AWD vehicle in terms of its components, the transaxle differential and two conventional RWD differentials (although one of these is the front conventional differential):

$$\eta_{diff,LD\_AWD} = \eta_{diff,LD\_FWD} * \eta_{diff,LD\_RWD} \quad \text{(C.16)}$$

Here, it must be noted that the efficiency of only one conventional differential appears in Equation C.16 because the overall AWD differential efficiency (the left hand side of Equation C.16) is used to account for the torque that actually gets transferred to the drive wheels and Equation C.16 allows this accounting for each pair of drive wheels individually.

C.5.7. Heavy-Duty Single Differential

All heavy-duty trucks are RWD. Heavy-duty trucks with only a single rear axle and those with two rear axles but the second of the two is a "tag axle" are computationally modeled exactly like a light-duty RWD vehicle. The governing equation is:

$$\eta_{diff,HD\_tag\ axle} = \eta_{seal,1} * \eta_{bear,1} * \eta_{wind,cyl,1} * \eta_{gp,hyp} * \eta_{wind,sph} * \eta_{wind,cyl,2} * \eta_{bear,2} * \eta_{seal,2} \quad \text{(C.17)}$$

C.5.8. Heavy-Duty Tandem Differential

Large heavy-duty trucks have two rear axles and generally use a "tandem" differential, as illustrated in Figure C.1. Inland Truck Parts allowed pictures to be taken of the main gear pair of a heavy-duty rear axle differential. The following equation presents the efficiency calculation with the order of the components considered.

$$\eta_{diff,HD\_tandem} = \eta_{center\ diff} * \eta_{helical\ gear\ pair} * \eta_{diff,HD\_tag\ axle} \quad \text{(C.18)}$$

C.5.9. Heavy-Duty Dual Differential

As noted above, a 2-speed gearbox can be mounted at the input to either a heavy-duty single differential or a heavy-duty tandem differential. When a single differential is modified to be a dual differential, it is assumed that the computational model behaves in much the same way as that of the heavy-duty RWD conventional differential, except that the dual differential has a two-speed gear box attached upstream in the powertrain. Fellow researcher Kyung Jin Kim developed a two-speed gear box model for use as part of some manual transmissions, some of which include a secondary two- or three-speed gear box. These calculations for 2-speed gear box performance may be calculated at the end of the transmission just as well as at the front of the differential. Mr. Kim was gracious enough to allow one of his gear boxes to be modified to suit the purposes of this HD RWD dual differential model. The following equation presents the efficiency calculation with respect to the other component models:

$$\eta_{diff,HD\_Dual\ tag\ axle} = \eta_{2speed\ gb} * \eta_{diff,HD\_tag\ axle} \quad \text{(C.19a)}$$

When a 2-speed gearbox is appended to a tandem differential, the relevant equation is:

$$\eta_{diff,HD\_Dual\ tandem} = \eta_{2speed\ gb} * \eta_{diff,HD\_tandem} \quad \text{(C.19b)}$$

C.6. Differential Model Code Running Modes

This differential model is written in such a way that it can be used several different ways conveniently. The drive cycle simulator may choose to use the model in one of these three ways to balance concerns with computational power and storage space discussed in the following subsections.

C.6.1. Run Every Time During Simulation

The first method requires the drive cycle simulator to call the appropriate differential model at each time interval with the instantaneous corrected torque input to the differential (transmission output torque), input rotation speed (transmission output speed), and gear ratio(s). With a long drive cycle, this method will be computationally demanding but requires no data storage.

C.6.2. Run Once Before Simulation

The second method requires the drive cycle simulator to call the appropriate differential model once before the drive cycle with arrays of input torque and speed and one gear ratio for each gear pair. This method requires temporary storage, but the linear interpolation algorithm is far less computationally demanding than a single input from the efficiency model. The user will notice an improvement in model performance over the first method once the number of time intervals exceeds the number of elements in the arrays by enough to offset the linear interpolations conducted up to that point.

C.6.2.1. Generate 2-D Differential Efficiency Map

With knowledge of the gear ratio of the differential used in the simulated vehicle, an efficiency map can be generated which spans the range of input torque and speed.

C.6.2.2. Interpolate Within Map When Differential Efficiency Needed

When the differential efficiency is needed for a given differential input torque and speed, an interpolation algorithm can be used to extract the needed efficiency from the efficiency map rather than directly from the differential model. The interpolation algorithm is far more efficient than the differential model, but the initial investment of time must still be made.

C.6.3. Run Once and Discard Code

The third method requires the drive cycle simulator to check for existing differential efficiency maps stored as functions of differential input torque, speed, and gear ratio. If existing maps are not found, the drive cycle simulator will call a differential model as it would in the second method. However, the drive cycle simulator will call the differential model multiple times, each time with a new gear ratio.

C.6.3.1. Generate 3-D Differential Efficiency Map

In effect, the drive cycle simulator will build a three-dimensional map of differential efficiency with respect to differential input torque, speed, and gear ratio. This will require the

most storage of these methods, but once the initial time investment is made into building these maps, the differential models will never need to be called again.

C.6.3.2. Interpolate Within Map When Differential Efficiency Needed

As a result, linear interpolations of the maps will be the only calculation required for differential efficiency. This third method would be the least computationally demanding method.

C.6.4. Examples of Inputs/Outputs for Current Differential Models

The same inputs were used for all of the models except for the dual differential, which requires more inputs. The other programs require three inputs:

- The scaled input torque to the differential, which is the scaled output torque from the transmission,
- The differential input shaft speed in rpm, and
- The differential's gear ratio.

For the other models, the following inputs were used:

Torque	0	0	0	0	0
	0.25	0.25	0.25	0.25	0.25
	0.5	0.5	0.5	0.5	0.5
	0.75	0.75	0.75	0.75	0.75
	1	1	1	1	1
Speed	0	1000	2000	3000	4000
	0	1000	2000	3000	4000
	0	1000	2000	3000	4000
	0	1000	2000	3000	4000
	0	1000	2000	3000	4000
Gear_ratio	3				

For the dual differential model, the low gear ratio and chosen gear of the two-speed gearbox also need to be set. Figures C.2–C.7 illustrate the efficiency values obtained by providing those inputs.

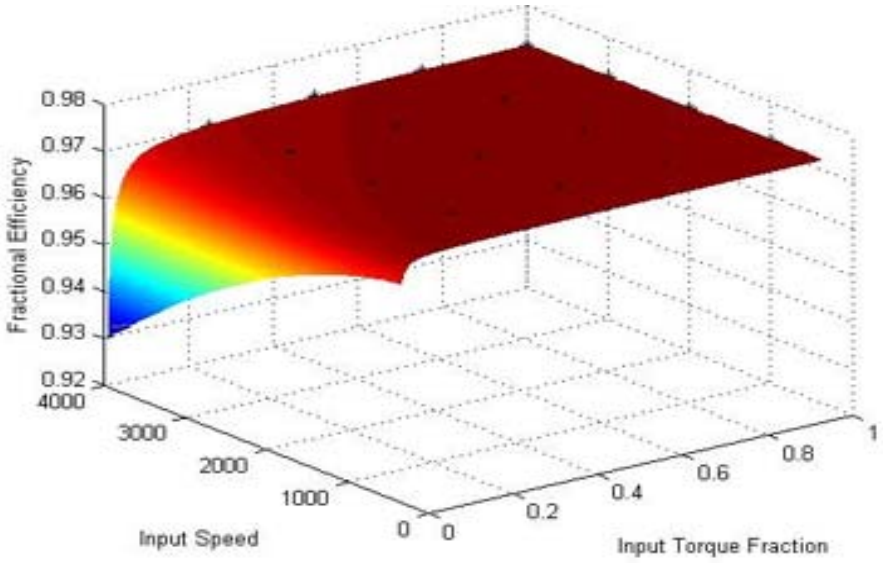

Figure C.2: Efficiency map of a light-duty FWD differential.

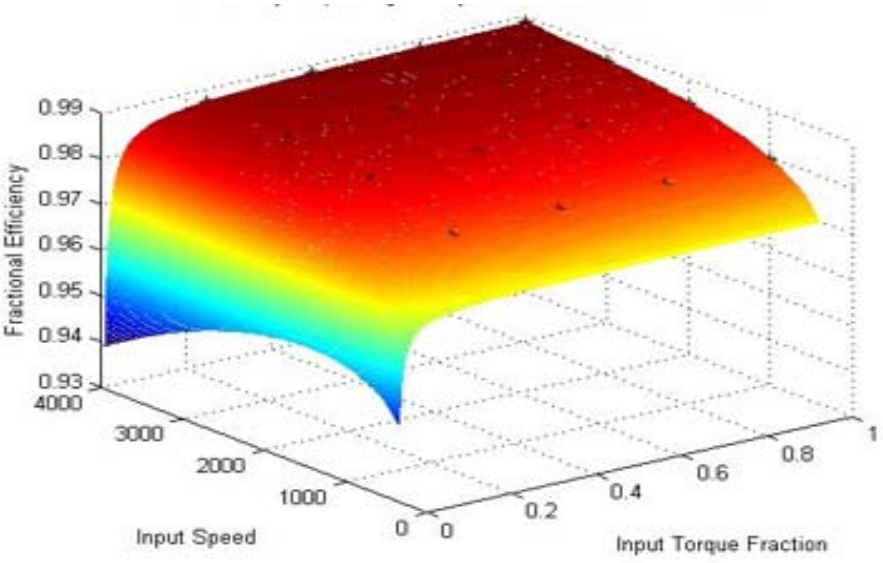

Figure C.3: Efficiency map of a light-duty RWD differential.

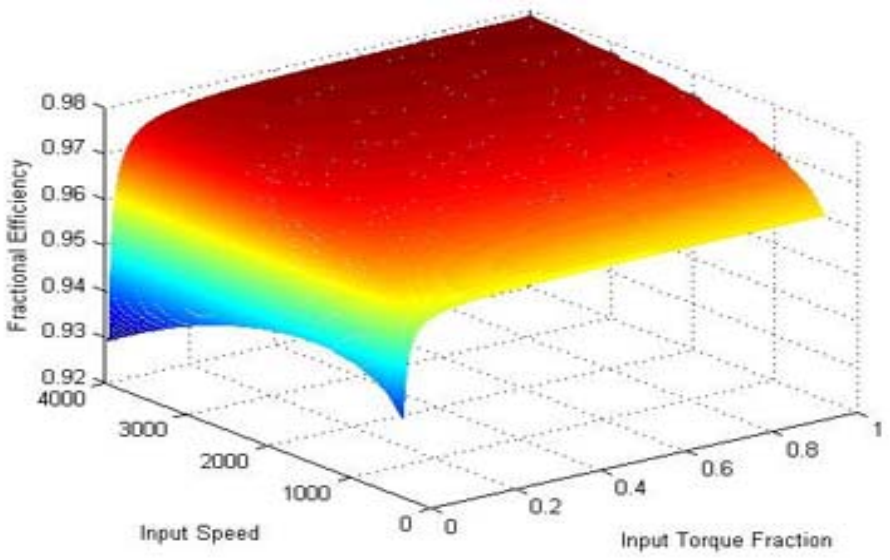

Figure C.4: Efficiency map of a light-duty 4WD differential.

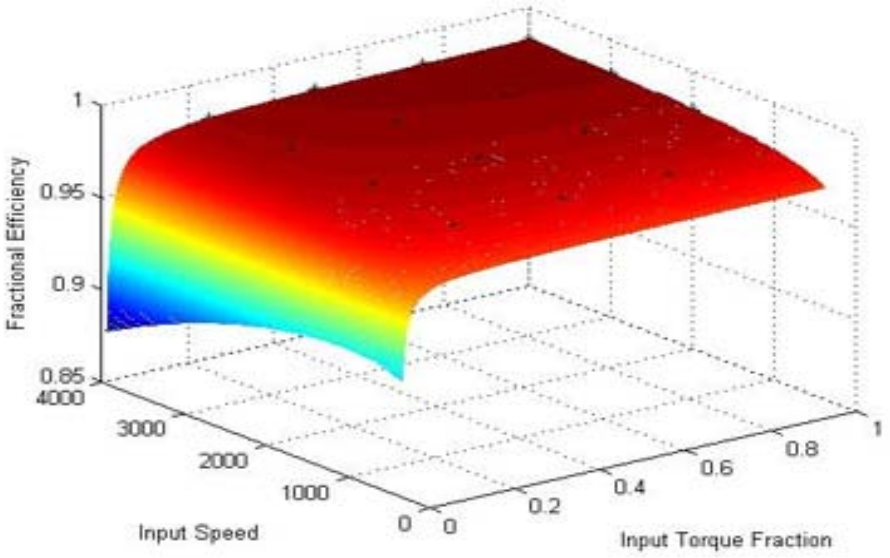

Figure C.5: Efficiency map of a light-duty AWD differential.

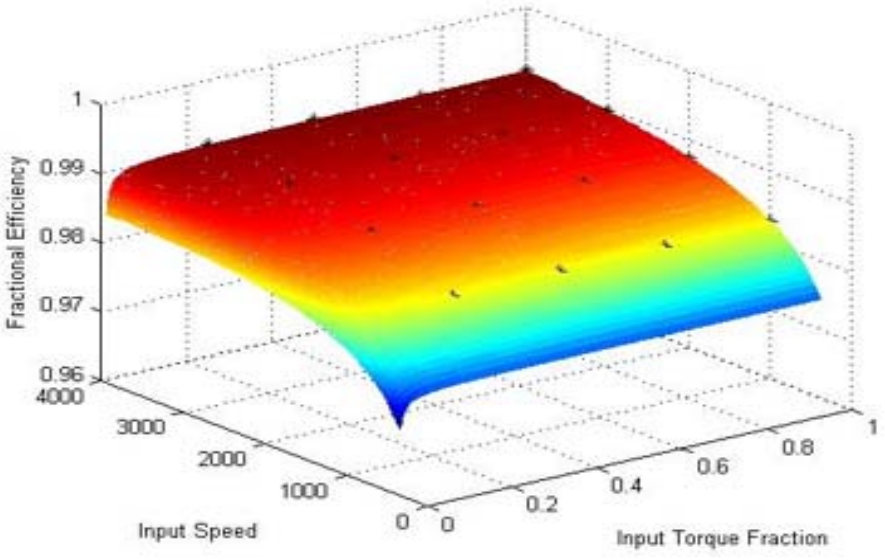

Figure C.6: Differential efficiency map for an HDV with a single rear axle or with a tag axle.

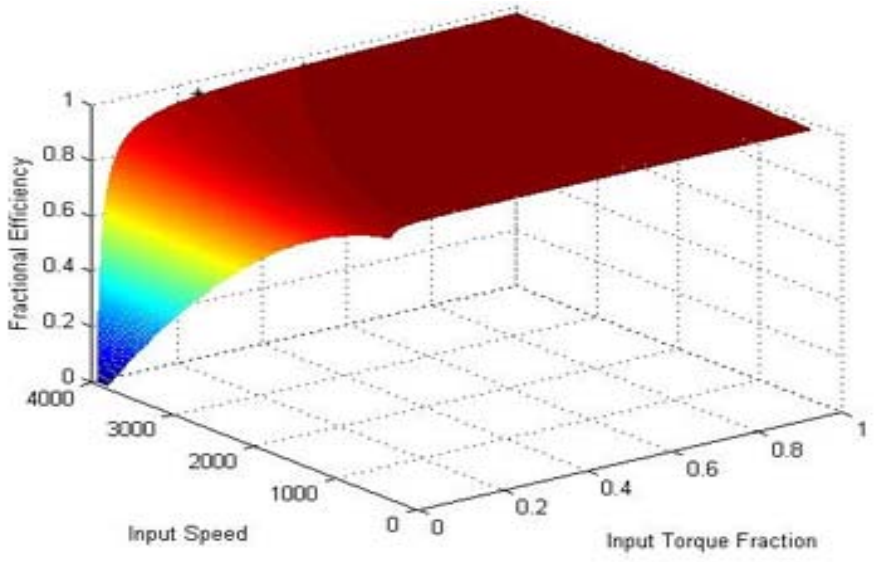

Figure C.7: Efficiency map for a heavy-duty dual differential for either a single rear axle or with a tag axle.

C.7. Proof of Concept Tests

In this section, the outputs from the models are compared with existing data and other models to determine the validity of the differential efficiency models developed as part of TxDOT Project 0-5974. Data exists for a transaxle, and a curve fit exists for a rear-wheel-drive LDV.

C.7.1. Light-Duty FWD (Manual Transaxle)

SAE Paper 820741 (van Dongen, 1982) contains graphed efficiency data for both manual and automatic transaxles from VW Rabbit vehicles circa 1980s. This paper documents the efficiency of a ~1980 Volkswagen Rabbit transaxles (FWD transmission + differential) with both a 4-speed manual and 3-speed automatic transmission. Because a transaxle assembly is a transmission and differential combined, co-investigator Kyung Jin Kim provided a model for each transmission. Figures C.8a and C.8b (part of a proof of concept test that considered all of the gears of the transmission) demonstrates the ability of the combined transmission and differential models to predict the efficiency of a light-duty FWD vehicle.

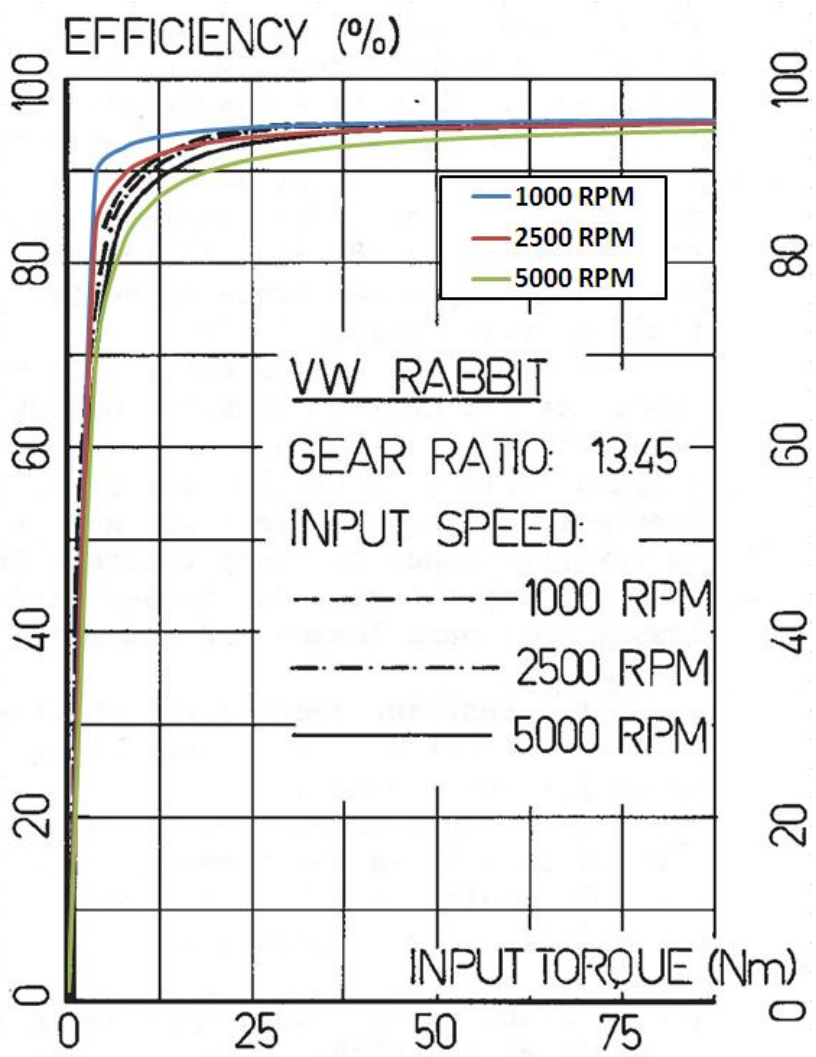

The legend (color coding) for the model predictions is provided within the box in the figure.

Figure C.8a. Comparison of the efficiency of a Volkswagen Rabbit manual transaxle in 1st gear (van Dongen, 1982) and the model predictions (combined manual transmission model plus transaxlw differential model).

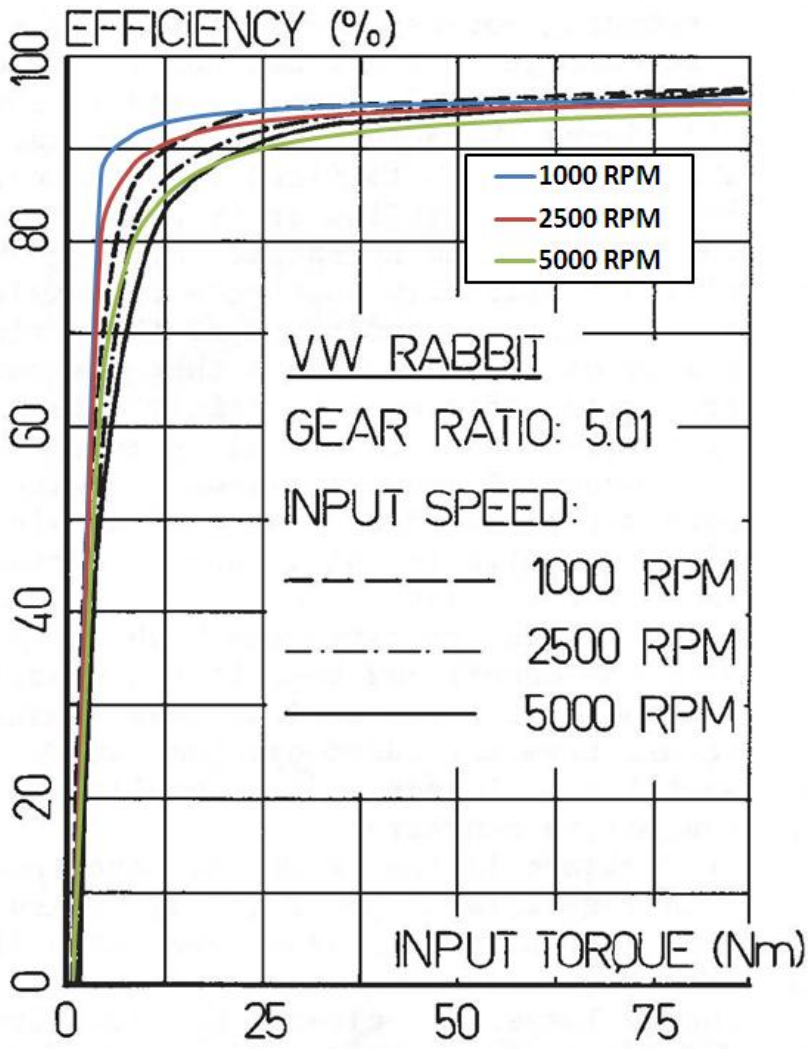

The legend (color coding) for the model predictions is provided within the box in the figure.

Figure C.8b. Comparison of the efficiency of a Volkswagen Rabbit transaxle in 3rd gear (van Dongen, 1982) and the model predictions (combined manual transmission model plus transaxle differential model).

C.7.2. Light-Duty RWD

Matthews (2011) presents a curve fit to data for the differentials of light-duty rear wheel-drive vehicles:

$$\eta_{diff,LD\_RWD} = \begin{cases} 0.6652+3.732*10^{-3}*S-1.061*10^{-5}*S^2 & ; S \le 150 \text{ kph} \\ 0.987 & ; S>150 \text{ kph} \end{cases} \quad \text{(C.20)}$$

This equation relates the efficiency of a light-duty rear-wheel-drive differential to the speed of the vehicle (S) in which it is installed. It is assumed that the curve fit data were collected in tests where vehicle speed was held constant. Extracting coastdown coefficients from the EPA website for several light-duty rear-wheel-drive vehicles (see Subsection C.7.3.2) allows

the estimation of the road load forces acting on the car as a function of vehicle speed. These road load forces must be counteracted by the torque applied by the powertrain on the wheels by acting over the moment-arm that is the rolling radius of the tire. Tire data were collected from the same EPA source for the same vehicles as the vehicles associated with the coastdown coefficients. The rolling radius was assumed to be constant, introducing a slight error in the calculation of driving force from the driving torque. Nevertheless, obtaining coastdown coefficients and tire radii allowed the estimation of differential output torque required to maintain constant vehicle speed under road load conditions.

Using the curve fit for efficiency (Equation C.20) and the calculated required differential output torque allowed for approximation of the differential input torque for the model. Because the source of the differential output torque (via the coastdown coefficients) is more reliable (EPA) than the source of the curve fit, an iterative process was used to find the predicted differential efficiency while matching the differential output torque obtained from the coastdown coefficients. In order to accomplish this, the peak torque available from each of the vehicles was estimated. Once the iterative process reached completion, the model's efficiency predictions were compared with the curve fit.

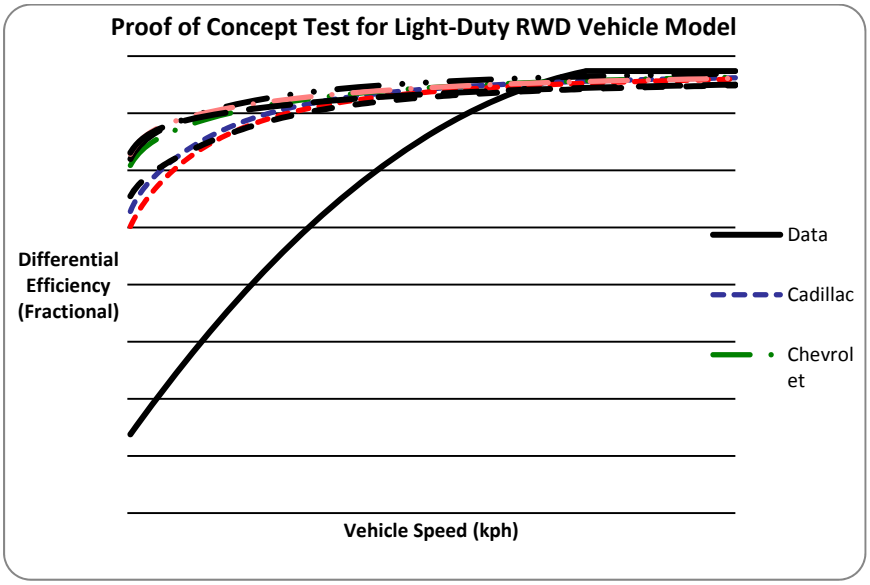

Details regarding the experimental vehicle(s) were not available.

Figure C.9. Differential efficiency as a function of vehicle speed from available data (Matthews 2011) compared to the present model predictions for a light-duty RWD vehicle.

Because the fit is so poor except at high speeds, the curve fit and the EPA information were used to compute the approximate torque losses across the differential, removing the uncertainty of the model. The resulting graph is confounding.

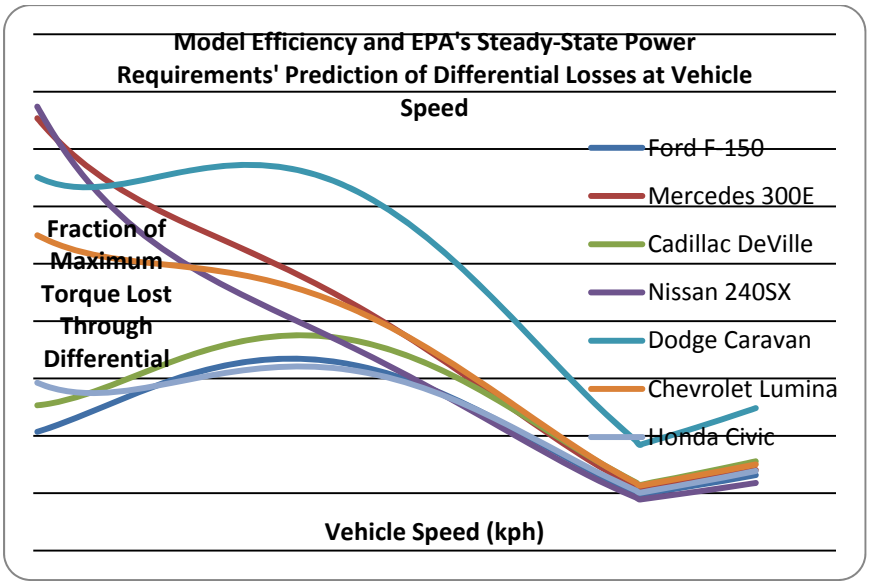

Details regarding the experimental vehicle(s) were not available.

Figure C.10. Calculated torque lost via the RWD differential as a function of speed for a light-duty RWD vehicle.

According to the EPA data and the curve fit, torque losses should be higher at low speed and high speed than at approximately highway speeds. The mechanisms for increased torque loss at high speed are windage and, to a lesser extent, bearings. One mechanism is available for increasing the torque loss at low speed, and that is the hypoid gear friction. The composite coefficient of friction is higher at low speed than at high speed for hypoid gear pairs. However, published friction coefficient data for hypoid gears are not sufficiently high at low speed to accommodate the increased torque losses predicted at low speed for light-duty rear-wheel-drive vehicles.

C.7.2.1. Tire Rolling Radius Model

The tire rolling radius was assumed to be constant at all speeds and directly dictated by the specifications of the tire. Tire manufacturers express tire size in one of a couple of different ways, but the tire diameter is always attainable.

C.7.2.2. Coastdown Coefficients and Tire Radii from EPA

The data in Table C.1 were extracted from Reineman and Nash (1995), a report by the EPA National Vehicle and Fuel Emissions Laboratory for the Dynamometer Comparison Study Task Force.

Table C.1. Coastdown Coefficients and Tire Sizes Used in the Simulations for Light-Duty RWD Vehicles.

Vehicle	A-Coefficient	B-Coefficient	C-Coefficient	Tire Size
Ford F-150	21.8	0.9315	0.03266	P235/75R15
Mercedes 300E	40.4	0.3529	0.01636	195/65VR16
Cadillac DeVille	15.9	0.4716	0.02444	P205/70R15
Nissan 240SX	48.1	0.0096	0.01809	195/60R15
Dodge Caravan	27.1	0.4804	0.02494	P205/70R15
Chevrolet Lumina	26.9	0.4216	0.01637	P215/60R16
Honda Civic	15.4	0.1384	0.01960	P175/70R13

C.8. Summary and Conclusions: Differential Models

The basis for a model for the efficiency of an automotive differential has been provided. The results from proof of concept tests were analyzed to determine the validity of the model.

While the proof of concept tests seem to demonstrate that the model leaves the user wanting for accuracy, the reader is reminded that the fundamental model could very well have been a step back. Instead, the fundamental model is, in both cases of proof of concept, an improvement over the assumption of constant efficiency. Further, no extra data collection aside from what is already available was necessary to create this code. Finally, further improvements to the model could bring the model's results much closer to the accepted values.

Appendix D. Light-Duty Hybrid Electric Vehicle Model

The number of LDVs is expected to triple by 2050, and the most rapid growth will take place in developing countries. In order to control exhaust emissions from these vehicle, efficient steps must be taken to control the vehicle fleet sizes and composition in the long term. Therefore, some cleaner vehicle technologies, such as hybrid electric vehicles (HEVs) and CNG vehicles, have been receiving recent attention.

The Toyota Prius was the first mass-produced HEV. It was also the first HEV with an engine that was optimized for this type of operation; the Prius engine operates over the Miller cycle rather than the traditional Otto cycle that most spark ignition engine ideally operate over. The Toyota Synergy Drive, the drivetrain used in the Prius, is also unique.

Categories of HEVs are discussed in Section D.1. The drivetrain of the Toyota Prius is discussed in Section D.2. Our method for modeling the main components of the Prius drivetrain is discussed in Section D.3. The Prius hybrid system control strategy model is discussed in Section D.4. Example results from the light-duty HEV model are presented in Section D.5.

D.1. Introduction

Hybrid electric vehicles can be subdivided into three types: Series HEVs, Parallel HEVs, and Series-Parallel Combination HEVs.

The dominant light-duty hybrid system is the Series–Parallel (torque and speed coupling) hybrid drivetrain. The Toyota "Synergy Drive," used in the Prius and several other hybrid cars, is a typical series–parallel hybrid vehicle. Its series–parallel hybrid drive train is composed of a planetary gear set as a speed-coupling device. The series-parallel HEV has an internal combustion engine (ICE) and two electric motors, both of which can act as either motors or generators and are often referred to as MG sets. These three components are coupled with a combination of clutches. Its torque and speed coupling mode frees the engine from the driven wheels in the torque and speed constraints. Consequently, the instantaneous engine torque and speed can be independent of the load torque and speed of the vehicle. Therefore, the engine can be operated in its high efficiency region in a similar way as that of the series (electrical coupling) drive train, and on the other hand, part of the engine power is directly delivered to the driven wheels without experiencing multiform conversion.

The Toyota Prius was introduced in Japan in model year 1998 and became the first modern mass-produced hybrid electric vehicle. The Toyota Prius is considered a "grid independent" or also "charge-sustaining" HEV design because it does not require electric power from an off-board source. That is, it is not a plug-in hybrid.

D.2. Toyota Prius Drivetrain Configuration

The Toyota Prius series–parallel hybrid drivetrain is formed by using both torque and speed coupling through a planetary gear set, as shown in Figure D.1.

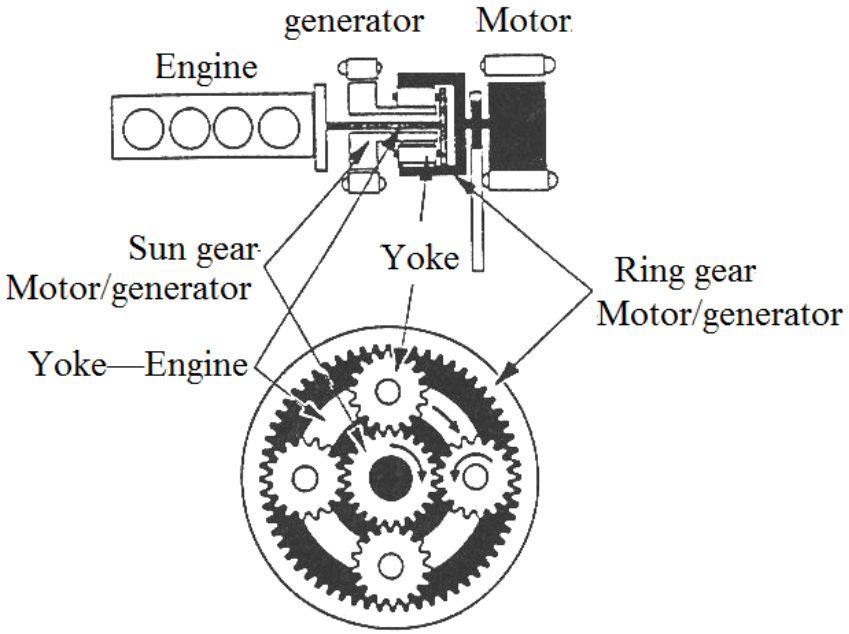

Figure D.1. Toyota Prius series—parallel hybrid system.

The Toyota Prius uses two electric motor/generators and an engine all coupled to a passive "power split" planetary gear set. The control of the generator and/or motor enables the system to act in a similar fashion to a constantly variable transmission (CVT). The engine output shaft is connected to the planet carrier (the "yoke"), the generator is connected to the sun gear, and the motor is connected to the ring gear. The ring gear is also connected to the wheels through the final drive: a differential that is similar to that in a transaxle. The planetary gear set allows part of the engine torque to flow directly to the wheels, and the remaining fraction can go to the generator to recharge the battery pack.

In this configuration, one clutch and two locks (e.g., band brakes) are used. The clutch serves for connecting or disconnecting the engine to or from the yoke of the planetary gear unit. One lock is used to lock or release the sun gear and the other lock to lock or release the shaft of the ring gear.

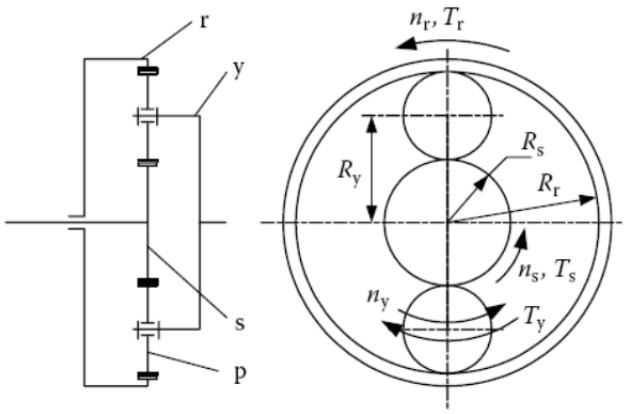

Figure D.2. Planetary gear set as used for speed coupling.

The operating characteristics of planetary gear functioning as a speed-coupling device are discussed in detail below.

A mechanical planetary gear set has the structure shown in Figure D.2. It consists of a sun gear labeled "s," a ring gear labeled "r," several planetary gears labeled "p" (usually three or four for force balance), and a yoke labeled "y," which is attached to the centers of the planetary gears. The rotational speeds (e.g., in rpm) of the sun gear, N_s, ring gear, N_r, and yoke, N_y, have the relationship

$$N_y = \frac{N_s}{1+r_g} + \frac{N_r \times r_g}{1+r_g} \tag{D.1}$$

where r_g is the gear ratio defined as the ratio of the radii of the ring gear to the sun gear, R_r/R_s, as shown in Figure D.2. The speeds N_s, N_r, and N_y are defined as positive in the direction shown in Figure D.2.

Defining $k_{ys} = (1+r_g)$ and $k_{yr} = (1+r_g)/r_g$, Equation D.1 can be further expressed as:

$$N_y = N_s/k_{ys} + N_r/k_{yr} \tag{D.2}$$

Neglecting the energy losses during steady-state operation, if the yoke drives, and the sun gear and ring gear are driven, the torques acting on the sun gear, ring gear, and yoke have the relationship:

$$\tau_y = -k_{ys}\tau_s = -k_{yr}\tau_r \tag{D.3}$$

Equation D.3 also indicates that with $r_g > 1$, which is the general case because $R_r > R_s$, τ_s is the smallest, τ_y is the largest, and τ_r is in between. This means that the torque acting on the yoke is balanced by torques acting on the sun gear and ring gear.

When one element among the sun gear, ring gear, and yoke is locked to the vehicle frame, that is, one degree of freedom of the planetary gear set is constrained, the unit becomes a single-gear transmission (one input and one output). In this case; the speed and torque relationship, with one element fixed, is shown in Table D.1.

Table D.1 Speed and Torque Relationships while One Element Is Fixed.

Element fixed	Speed	Torque
Sun gear	$N_y = N_r/k_{yr}$	$\tau_y = -k_{yr}\tau_r$
Ring gear	$N_y = N_s/k_{ys}$	$\tau_y = -k_{ys}\tau_s$
Yoke	$N_s = -k_{ys} * N_r/k_{yr}$	$\tau_s = k_{yr} * \tau_r/k_{ys}$

D.3. HEV Main Components Modeling and Input Parameters

The light-duty HEV model was initially developed as a stand-alone program to ensure that the development of this model did not conflict with the on-going development of the fuel economy model for conventional LDVs. Although this involved some duplication of effort, it is believed that it resulted in faster model development.

The vehicle submodel used for the initial development of the light-duty HEV model is discussed in Subsection D.3.1. This submodel was later replaced with the similar vehicle submodel used as a key component of the overall fuel economy model. The engine submodel used for the development of the light-duty HEV model is discussed in Subsection D.3.2. Unlike the engines that were used to develop the engine submodels discussed in Appendix A, the Prius engine operates on the Miller cycle. Therefore, the light-duty HEV engine model discussed in Subsection D.3.2 was not replaced after initial development of the light-duty HEV model. The transmission submodel used for the development of the light-duty HEV model is discussed in Subsection D.3.3. Like the engine in the Prius, the transmission in the Prius is also unique to light-duty HEVs and, thus, was not later replaced with a more generic transmission submodel. The differential submodel used for the initial development of the light-duty HEV model is discussed in Subsection D.3.4. This submodel was also later replaced with the similar differential submodel used as a key component of the overall fuel economy model. The "axle and brakes" submodel is discussed in Subsection D.3.5. The submodels developed for the electric components of the drivetrain are the subject of Subsection D.3.6.

D.3.1. The Initial Vehicle Model

The initial vehicle model was based on the force balance at the drive tire contact patch. Given the vehicle speed required at the end of the current time step, the motive force and required speed averaged over the time step are calculated. Then, given the available motive force and speed, the actual/achieved speed is computed.

The classic equation for longitudinal vehicle dynamics—Newton's Second Law of Motion—is implemented in this block: $\Sigma F_x=ma_x$, where among the forces acting in the longitudinal direction (x) are rolling resistance, aerodynamic drag, and the force of gravity that must be overcome to climb a grade. This equation is first used to compute the required motive force given the required acceleration, and then used to compute the achievable acceleration given the available motive force. The average speed over the time step is taken to be the average of the speed at the beginning of the time step (a.k.a. the speed at the end of the previous time step) and the speed required at the end of the time step.

The main input variables for the vehicle definition are listed in Table D.2. The Vehicle_Mass input for the Toyota Prius is 1368 kg, including a vehicle mass of 1332 kg and a cargo mass of 136 kg, the Frontal_Area input for the Toyota Prius is 1.746 m^2, and the tire size is 165/65R15.

Table D.2. Input Variables for the Initial Light-Duty Vehicle Definition.

Name	Type	Units	Value	Description
driving cycle	scalar	--	All	desired vehicle speed vs time, and grade vs distance
C_D	scalar	--	All	coefficient of aerodynamic drag
Frontal_Area	scalar	m^2	All	vehicle frontal area 80% of height*Width*length
veh_front_wt_frac	scalar	--	All	fraction of total vehicle mass supported by front axle when vehicle is not moving
Tire_Dia	scalar	m	All	tire diameter
Vehicle_Mass	scalar	kg	All	test mass, including fluids, passengers, and cargo
Rolling_Ressistance_Coefficient	scalar	--	All	coefficient of rolling resistance force
amb_temp	scalar	C	All	ambient temperature
veh_air_density	scalar	kg/m^3	All	density of air
veh_gravity	scalar	m/s^2	All	gravitational acceleration

D.3.2. The Engine Model

The Toyota Prius engine is a 1.5-L, in-line 4 cylinder, DOHC, 4-valve engine that operates on the Miller cycle. Its peak power is 43 kW at 4000 rpm and the peak torque is 75 lb-ft at 4000 rpm, which is also the peak engine speed. Engine control is completely computerized. The ignition system is coil-on-plug, the fueling is sequential port injection, and the throttle is motor actuated. The engine mechanicals have also been optimized for operation at less than 4000 rpm by using components with less reciprocating mass and lower friction. The overall result of these improvements is a claimed engine efficiency of about 37%.

In our model, the internal combustion engine is defined as a "fuel converter" (to allow easy expansion in the future to fuel cell vehicles, if they ever become available), and its normal operating speed and torque ranges need to be input by the user. These values are also used to determine the fuel use for each time step from a look-up table indexed by fuel converter speed and torque (look-up- tables for engine-out emissions can also be added in the future). Table D.3 presents the input variables for the fuel converter model.

Table D.3. Input Variables for the "Fuel Converter" (Engine) Model.

Name	Type	Units	Vehicle Type	Description
fc_fuel_type	char	--	All	description of fuel type
fc_disp	scalar	L	All	engine size (cyl displacement)
fc_emis	boolean	--	All	0= no emissions data available 1= emissions data available
fc_map_spd	vector	rad/s	all(~fuel cell)	engine speed range
fc_map_trq	vector	N-m	all(~fuel cell)	engine torque range
fc_fuel_map	matrix	g/s	All	fuel use indexed by fc_map_spd and fc_map_trq
fc_ct_trq	vector	N-m	all(~fuel cell)	closed throttle torque indexed by fc_map_spd
Fuel_Sp_Gravity	scalar	g/L	All	fuel specific gravity
fc_fuel_lhv	scalar	J/g	All	Lower Heating Value of the fuel
fc_max_trq	vector	N-m	all(~fuel cell)	maximum torque output indexed by fc_map_spd
fc_spd_scale	scalar	--	All	scaling factor for speed range
fc_trq_scale	scalar	--	All	scaling factor for torque range

D.3.3. The Transmission Model

For the Toyota Prius hybrid system, the clutch serves for connecting or disconnecting the engine to or from the yoke of the planetary gear set, cutting off or providing the engine torque to the driveline.

The Toyota Prius uses a planetary gear set configuration, which we call the "power split device." It acts in a similar fashion to a constantly variable transmission (CVT). The input parameters for the transmission are shown in Table D.4. The number of teeth on the sun gear and ring gear are 30 and 78, respectively. For the initial simulations, a constant efficiency was assumed.

Table D.4. Input Variables for the "Power Split Device" (Transmission) Model.

Name	Type	Units	Vehicle Type	Description
tx_pg_s	scalar	--	all	number of teeth in sun gear
tx_pg_r	scalar	-	all	number of teeth in ring gear
CVT_Transmission_Efficiency	scalar	-	all	Toyota Prius planetary gear unit transmission efficiency

D.3.4. The Differential Model

The differential model includes the effects of losses, inertia, and gear ratio. The torque loss in the differential can be calculated by the differential model discussed in another section of this report. For the initial development of the model for the fuel economy of a light-duty hybrid, it was assumed that the efficiency of the differential is constant. The main input variables for the differential model are listed in Table D.5. For the Toyota Prius hybrid system, the Differential_Ratio is 3.93.

Table D.5. Input Variables of the Differential Model.

Name	Type	Units	Vehicle Type	Description
Differential_Ratio	scalar	--	All	gear ratio of final drive
Differential_Efficiency	scalar	--	All	final drive efficiency

D.3.5. Axle and Brakes

The drive axle transmits actual torque and rotational speed from the differential to the drive tire contact patch. In the light-duty HEV fuel economy model, the engine generates torque and rotational speed. Depending upon the "mode" of operation of the HEV, this torque may then multiplied inefficiently in the planetary gear set and delivered to the differential input gear. The transmission output torque may then be multiplied inefficiently by the differential and delivered to the drive axle. Simultaneously, the rotational speed of the engine is reduced in both the transmission and differential to yield the rotational speed of the drive axle and tires. Thus, other than the electric components of the HEV drivetrain, all of the elements are now in the light-duty HEV model to predict fuel economy, at least when the HEV is in "engine only" mode.

A second mode for the Toyota Synergy drive is regenerative braking. However, the regenerative braking mode cannot be covered until after the electric components of the drivetrain have been discussed in Subsection D.3.6. However, conventional braking is also a required feature of the simulation. Braking control ensures that the vehicle slows down when deceleration is encountered during the driving cycle. In the model, the brakes are applied based on the error between the actual vehicle speed and the desired speed. There is an upper limit to the value of the brake force based on the locked wheel braking limit. The friction coefficient is assumed 0.9.

The main parameters needed as input for the brake model are listed in Table D.6.

Table D.6. Main Input Parameters for the Mechanical Brake Model.

Throttle_Position Threshold for braking	scalar	--	all	Throttle_Position Threshold under which braking begins to function
Thresholds for error between the actual vehicle speed and desired speed	scalar	mph	all	Different thresholds of error between the actual vehicle speed and desired speed for braking control choice
Step values for the Braking force increment or decrease	vector	--	all	Different step values for the Braking force increment or decrease
Braking_Limit	scalar	--	all	0.9*Vehicle_Mass*0.8, wh_slip_force_coeff is 0.9

D3.6. Toyota Prius Drivetrain Electric Components

The main electric components of the Toyota Prius hybrid system include a generator (which can also act as a motor), an electric motor (which can also act as a generator), a battery pack, and their related control modules.

D.3.6.1. Generator

The Toyota Prius hybrid car has a 15-kW permanent magnet generator/motor. For the generator model, the normal operating speed and torque ranges of the generator are required inputs (the default values are those for the Prius). The generator model also includes the effects of losses in the generator and controller, the generator's speed-dependent torque capability, and the controller's electric current limit. Power losses are considered by a 2-D efficiency lookup table indexed by rotor speed and input torque. The generator's maximum torque is enforced using a lookup table indexed by rotor speed, and this limits the maximum electric power output of the generator. The main input variables for the generator model are listed in Table D.7.

Table D.7. Input Variables for the Generator Model.

Name	Type	Units	Vehicle Type	Description
gc_map_spd	vector	rad/s	Ser/par	speed range of the generator
gc_map_trq	vector	N*m	ser/par	torque range of the generator
gc_eff_map	matrix	--	ser/par	generator efficiency map indexed by gc_map_spd and gc_map_trq
gc_max_crrnt	scalar	A	ser/par	max. current allowed in generator/controller
gc_max_trq	vector	N*m	ser/par	maximum torque output of the generator indexed by gc_map_spd
gc_min_volts	scalar	V	ser/par	min. voltage allowed in generator/controller
gc_overtrq_factor	scalar	--	ser/par	factor by which absorbed input torque can exceed max continuous for short periods
gc_spd_scale	scalar	--	ser/par	speed scaling factor
gc_trq_scale	scalar	--	ser/par	torque scaling factor

D.3.6.2. Electric Motor

The electric motor of the Toyota Prius hybrid system is a 30-kW permanent magnet motor /generator.

The electric motor model provides the motor torque and speed operating ranges, and also describes the effects of losses in the motor and controller. The power losses of the electric motor are also considered by the motor efficiency map, which is handled as a 2-D lookup table indexed by rotor speed and output torque. The motor's maximum torque is obtained using a lookup table indexed by rotor speed.

The main input variables for the motor model are listed in Table D.8.

Table D.8. Main Input Variables for the Motor Model.

Name	Type	Units	Vehicle Type	Description
mc_description	char	--	par/ser	text string description of the motor/controller
mc_map_spd	vector	rad/s	par/ser	speed range of the motor
mc_map_trq	vector	N*m	par/ser	torque range of the motor
mc_eff_map	matrix	--	par/ser	efficiency map of the motor indexed by mc_map_spd and mc_map_trq
mc_inertia	scalar	kg*m^2	par/ser	rotational inertia of the motor
mc_max_crrnt	scalar	A	par/ser	max. current allowed in motor/controller
mc_max_trq	vector	N*m	par/ser	maximum torque curve of the motor indexed by mc_map_spd
mc_max_gen_trq	vector	N*m	par/ser	maximum torque curve of the motor acting as a generator, indexed by mc_map_spd
mc_min_volts	scalar	V	par/ser	min. voltage allowed in motor/controller
mc_overtrq_factor	scalar	--	par/ser	factor by which output torque can exceed max continuous for short periods
mc_spd_scale	scalar	--	par/ser	speed scaling factor
mc_trq_scale	scalar	--	par/ser	torque scaling factor
tc_description	char	--	par	text string description of the torque coupler
tc_mc_to_fc_ratio	scalar	--	par	constant ratio of speed at motor torque input to speed at engine torque input
tc_eff	scalar	--	par/ser	Mechanical efficiency of the torque coupler

D.3.6.3. Energy Storage System

Nickel-Metal Hydride (NiMH) batteries are used in the Toyota Prius hybrid car. The nominal cell voltage is 1.2 V and there are 240 total cells (6 cells x 40 modules). The NiMH battery is environmentally friendly and quickly rechargeable. It is composed of a hydrogen storage metal alloy, a nickel oxide cathode, and a potassium hydroxide electrolyte.

Generally, a battery is difficult to simulate because the main variables that characterize battery operation, i.e., state of charge (SOC), voltage, current, and temperature, are dynamically related to each other in a highly non-linear fashion. Batteries seem to act like simple electrical energy storage devices, when they deliver and accept energy, but they actually undergo thermally-dependent electrochemical processes that make them difficult to model. For this reason, a lot of battery models have been developed in the past, ranging from very basic and simple models to empirical models to highly complex models based on fundamental electrochemical processes.

For the present research, a **Power and Energy Model** was chosen to calculate the SOC of the battery pack, as discussed below.

For simulation purposes, it is necessary to define some design variables for the battery. A battery pack is composed of *modules* that are, in turn, composed of *cells*. The battery module voltage may be different for different battery types.

The battery module has two internal resistances: the charging resistance (R_c) representing the energy losses while charging and the discharging resistance (R_d) representing the energy losses while discharging. R_c and R_d can be calculated by interpolation based on the R_c and R_d 2-D lookup tables indexed by the battery SOC and temperature. I represents the current and V_{cell} the module voltage. Battery voltage V and battery capacity Q are assumed equal for different battery modules.

If all the battery modules are connected in series, then the battery pack voltage and the total capacity can be calculated via:

$$V_{batt} = \mathrm{n} \cdot V_{module} \tag{D.4}$$

$$Q_{batt} = Q_{module} \tag{D.5}$$

where V_{batt} is the battery pack voltage, V_{module} is the battery module voltage, n is the number of battery modules, Q_{batt} is the battery pack total capacity, and Q_{module} is the battery module capacity.

Otherwise, if all the battery modules are connected in parallel, then the battery pack voltage and the total capacity are calculated by:

$$V_{batt} = V_{module} \tag{D.6}$$

$$Q_{batt} = \mathrm{n} \times Q_{module} \tag{D.7}$$

The total energy capacity of the battery pack is defined as:

$$E_{max} = V_{batt} \cdot Q_{max} \tag{D.8}$$

where Q_{max} is the battery capacity (the discharge current depleting the battery in 1 hr in units of A-hr) and E_{max} is the battery capacity [W-hr]. The power P_{batt} of the battery can be calculated in each time step by considering the motor power, brake regenerating power and generator power. The current I of the battery can be calculated in each time step via:

$$I = P_{batt} / V_{oc} \tag{D.9}$$

where V_{oc} is the battery open cell voltage that can be calculated by interpolation from the battery voltage 2-D lookup table indexed by the battery SOC and temperature.

The rate of energy loss from the battery due to the internal resistance is calculated by:

$$P_{loss} = \mathrm{n} \cdot I^2 R \tag{D.10}$$

Of course, this power loss always has a negative effect on the overall efficiency of the battery. Also, to minimize power losses generally, the current I should be as low as possible and, therefore, the voltage V_{batt} is preferably high (thus the need for a high voltage electric circuit between the battery and motor).

When the battery is charged, the SOC of a battery under working conditions can be calculated by:

$$\text{SOC}_t = \text{SOC}_{t-1} + \frac{\Delta t \cdot \left(\text{abs}\left(P_{\text{batt}}\right) - P_{\text{loss}}\right)}{E_{\text{max}}} \tag{D.11}$$

where SOC_t and $\text{SOC}_{t\text{-}1}$ are the SOC of the battery pack at time steps t and t-1 , Δt is the calculation time step, and E_{max} is the total energy capacity [in W-s].

Otherwise, when the battery is discharged, the SOC of a battery under working conditions can be calculated by

$$\text{SOC}_t = \text{SOC}_{t-1} - \frac{\Delta t \cdot \left(\text{abs}\left(P_{\text{batt}}\right) + P_{\text{loss}}\right)}{E_{\text{max}}} \tag{D.12}$$

The main input variables for the battery model are listed in Table D.9.

Table D.9. Main Input Variables for the Battery Model.

Name	Type	Units	Vehicle Type	Description
ess_description	char	--	par/ser	text string description of the ESS
ess_coulombic_eff	scalar	--	par/ser	average Coulombic efficiency of the energy storage system (ESS)
ess_init_soc	scalar	--	par/ser	initial state of charge of the ESS
ess_max_ah_cap	scalar	Ah	par/ser	maximum A-h capacity the ESS can have, no matter how slowly it is drained
ess_module_mass	scalar	kg	par/ser	mass of one energy storage module
ess_module_num	scalar	--	par/ser	number of modules in a pack; ASSUMED TO BE STRUNG IN SERIES
ess_min_volts	scalar	V	par/ser	minimum battery operating voltage, not to be exceeded during discharge
ess_max_volts	scalar	V	par/ser	maximum battery operating voltage, not to be exceeded during charge
ess_r_chg	matrix	ohms	par/ser	module's resistance to being charged; indexed by ess_soc and ess_tmp
ess_r_dis	matrix	ohms	par/ser	module's resistance to being discharged; indexed by ess_soc and ess_tmp
ess_soc	vector	--	par/ser	vector of SOCs used to index other ESS variables
ess_tmp	vector	C	par/ser	vector of temperatures used to index other ESS variables
ess_voc	matrix	volts	par/ser	module's open-circuit voltage; indexed by ess_soc and ess_tmp

D.4. Toyota Prius Hybrid System Control Strategies

The Toyota Prius hybrid system uses a series–parallel hybrid configuration that has many operation modes, but the motor speed is determined by the vehicle speed. The remaining two degrees of freedom (engine and generator) interact by splitting the engine torque and power, depending upon the speed of the generator. The control strategy keeps the engine operating in the most efficient manner and shuts down the engine during driving when the load demand is low. The Toyota hybrid system (THS) allows the engine to operate independently of road speed and

demand. The generator speed set point determines the engine speed, and the generator absorbs engine torque. If excess torque is sent to the generator, this electrical power can go to either the batteries or to the motor that is powering the wheels.

In the following subsections, the Toyota Prius hybrid operation modes in response to different driving conditions will be analyzed, and their control strategies will be discussed: The operation modes of the engine, MG1 (Motor Generator 1, the generator), and MG2 (Traction Motor - Generator) are depicted as follows.

D.4.1. Vehicle Stopped

If the HEV battery pack is fully charged and the vehicle is not moving, the engine may stop. However, if the HEV battery needs charging, the engine will start up automatically. In this case,

$$N_r = 0 \tag{D.13}$$

$$N_y = N_s / k_{ys} \quad \text{and} \quad N_s \le 5500 \tag{D.14}$$

where N_s, N_r, and N_y are the rotational speeds of the sun gear, ring gear, and yoke, and as previously defined $k_{ys} = (1 + r_g)$. Also:

$$\tau_s = \eta_{cvt} \tau_y / k_{ys} \tag{D.15}$$

where η_{cvt} is the planetary gear system efficiency.

D.4.2. Starting Out

When starting out under light load and light throttle, only MG2 turns to provide torque. The engine does not run and the vehicle runs on electric power only. MG1 rotates backwards and just idles. It does not generate electricity. In this case,

$$N_y = 0 \tag{D.16}$$

$$N_s = -N_r k_{ys} / k_{yr} \tag{D.17}$$

$$\tau_y = 0 \tag{D.18}$$

$$\tau_s = 0 \tag{D.19}$$

$$\tau_r = \tau_v \tag{D.20}$$

where τ_v is the required torque to propel the vehicle.

D.4.3. Engine Starting

As the speed increases above 24 km/h to 32 km/h (15–20 mph), the engine starts. The engine is started by MG1. The relationship of the engine, MG1, and MG2 are, functionally:

$$N_y = N_s / k_{ys} + N_r / k_{yr} \tag{D.21}$$

$$\tau_s = \tau_y \eta_{cvt} / k_{ys} \tag{D.22}$$

$$\tau_r = \tau_v \tag{D.23}$$

D.4.4. Low-Speed Cruising

In this mode, the engine's power is divided into two paths: a portion drives the wheels and a portion drives MG1 to produce electricity. The HEV ECU controls the energy distribution ratio for maximum efficiency.

$$N_y = N_s / k_{ys} + N_r / k_{yr} \tag{D.24}$$

$$\tau_s = \tau_y \eta_{cvt} / k_{ys} \tag{D.25}$$

$$\tau_r = \tau_y \eta_{cvt} / k_{yr} \tag{D.26}$$

$$\tau_r = \tau_v \tag{D.27}$$

D.4.5. Light Acceleration with Engine

This mode is similar to the mode of low-speed cruising. In this mode, the engine delivers its power to the driven wheels and MG1, which is generating electricity. When the required torque is increased, MG2 may assist the engine for propulsion if required, depending on the engine power and the requested driving power. In this mode, the energy generated by MG1 may be equal to the energy delivered to MG2.

$$N_y = N_s / k_{ys} + N_r / k_{yr} \tag{D.28}$$

$$\tau_s = \tau_y \eta_{cvt} / k_{ys} \tag{D.29}$$

$$\tau_v = \tau_r + \tau_y \eta_{cvt} / k_{yr} \tag{D.30}$$

where $\tau_r > 0$ if MG2 assists the engine for propulsion, if required. Otherwise, $\tau_r = 0$.

D.4.6. Full Acceleration

In this mode, the engine delivers its power to the wheels and to MG1, which is in the generating mode. MG2 adds its power to the engine power and is delivered to the wheels. The power drawn by MG2 from the high voltage (HV) battery power is greater than the power generated by MG1. Thus, the HV battery pack contributes energy to the drive train and its SOC drops.

$$N_y = N_s / k_{ys} + N_r / k_{yr} \tag{D.31}$$

$$\tau_s = \tau_y \eta_{cvt} / k_{ys} \tag{D.32}$$

$$\tau_v = \tau_r + \tau_y \eta_{cvt} / k_{yr} \tag{D.33}$$

D.4.7. High-Speed Cruising

In this mode, the shaft of MG1 is fixed to the stationary vehicle frame and the drive train is operated in pure torque-coupling mode. Both the engine and MG2 propel the vehicle.

$$N_s = 0 \tag{D.34}$$

$$N_y = N_r / k_{yr} \tag{D.35}$$

$$\tau_v = \tau_r + \tau_y \eta_{cvt} / k_{yr} \tag{D.36}$$

D.4.8. Driving with Maximum Speed

In this mode, both MG1 and MG2 receive power from the HV battery pack and deliver their mechanical power to the drive train. In this case, MG1 turns in the opposite direction.

$$N_y = N_s / k_{ys} + N_r / k_{yr} \tag{D.37}$$

where if $N_s > 5500$, then $N_s = 5500$.

$$\tau_v = \tau_r + \tau_y \eta_{cvt} / k_{yr} + \tau_s \eta_{cvt} k_{ys} / k_{yr} \tag{D.38}$$

D.4.9. Deceleration or Braking

During deceleration or braking, the wheels drive MG2. MG2 acts as a generator for regenerative energy recovery. The recovered energy from braking is stored in the HV battery pack.

$$N_y = 0 \tag{D.39}$$

$$N_s = -N_r k_{ys} / k_{yr} \tag{D.40}$$

$$\tau_y = 0 \tag{D.41}$$

$$\tau_s = 0 \tag{D.42}$$

$$\tau_r = \tau_v \tag{D.43}$$

where, again, if $N_s > 5500$, then $N_s = 5500$.

$$N_y = N_s / k_{ys} + N_r / k_{yr} \tag{D.44}$$

D.5. Toyota Prius Hybrid Simulation and Results

The Driving_Cycle input into the vehicle model is the desired vehicle speed vs. time, and the "actual" vehicle speed will be calculated and compared with the desired instantaneous speed from the driving cycle. The simulation is carried out from the throttle pedal position down to the wheels for a selected driving cycle.

If the user selects FTP_Driving_Cycle as the input Driving_Cycle, the simulation results are 1) the average gas mileage: Avg_MPG: 59.41 and average fuel consumption: L/100km: 3.9545.

Figures D.3–D.12 provide graphical representations regarding the details that can be extracted from this model, such as the desired speed and the simulated speed vs. time over the cycle, the fuel consumption (g/s, gram per second) profile, the battery power history, etc.

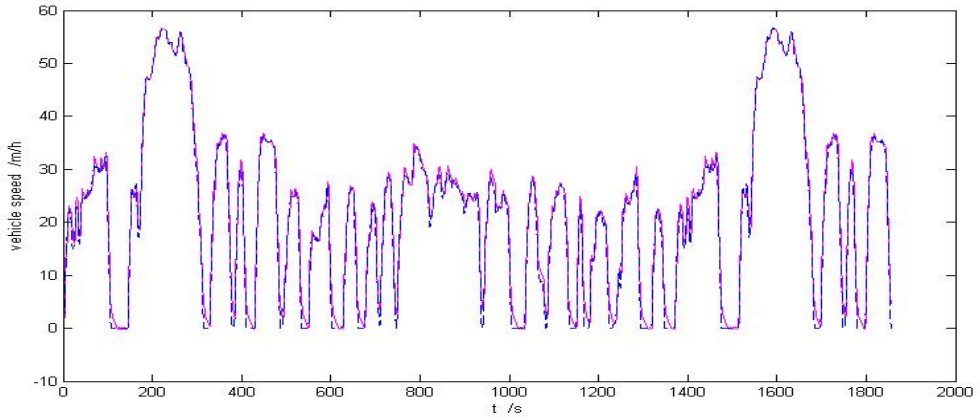

Figure D.3. The desired vehicle speed and the simulated speed vs. time profile.

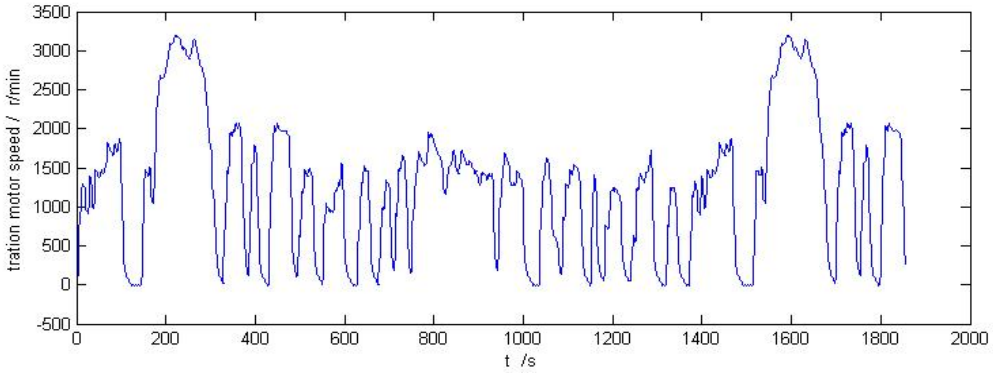

Figure D.4. Simulated traction motor speed vs. time profile.

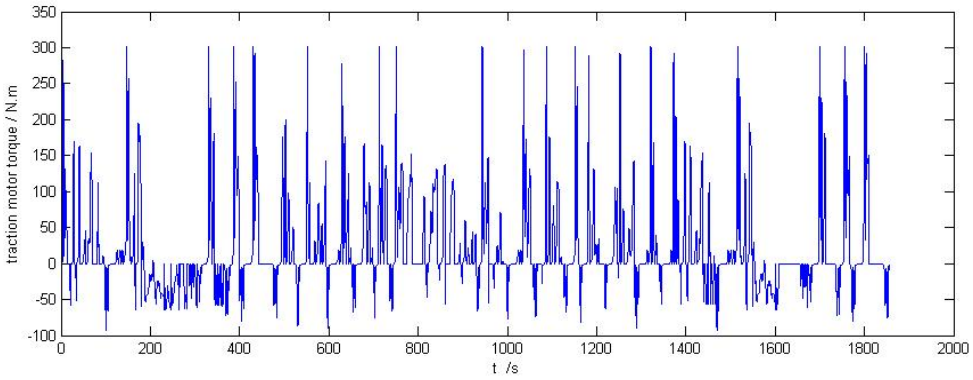

Figure D.5. Simulated traction motor torque vs. time profile.

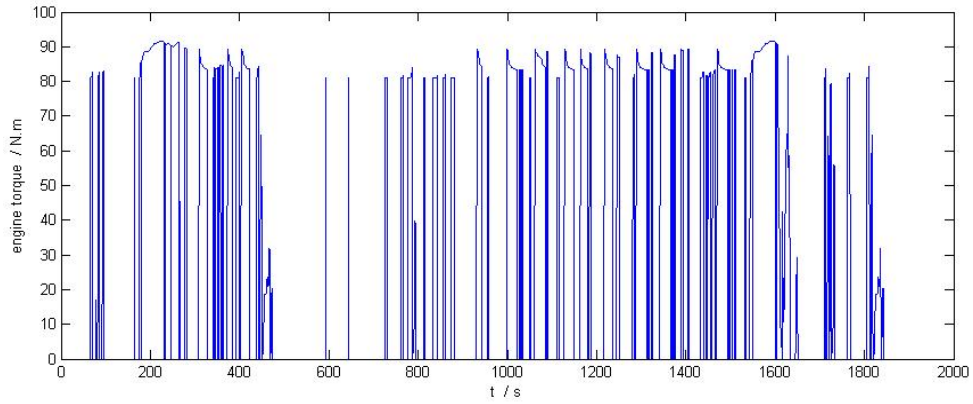

Figure D.6. Simulated engine torque vs. time profile.

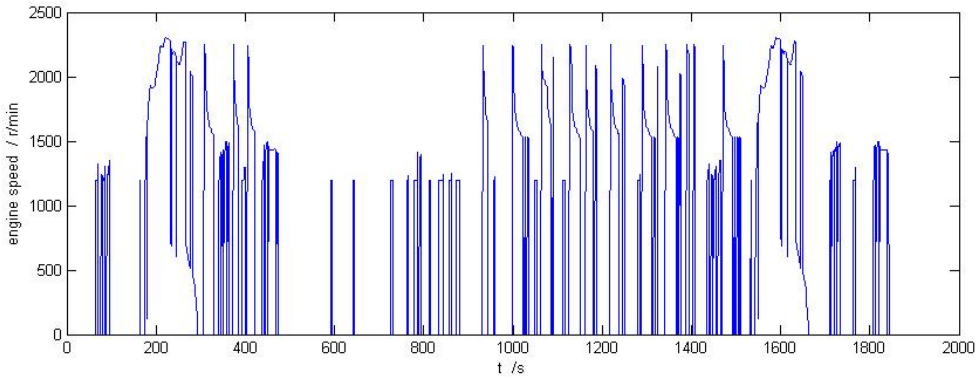

Figure D.7. Simulated engine speed vs. time profile.

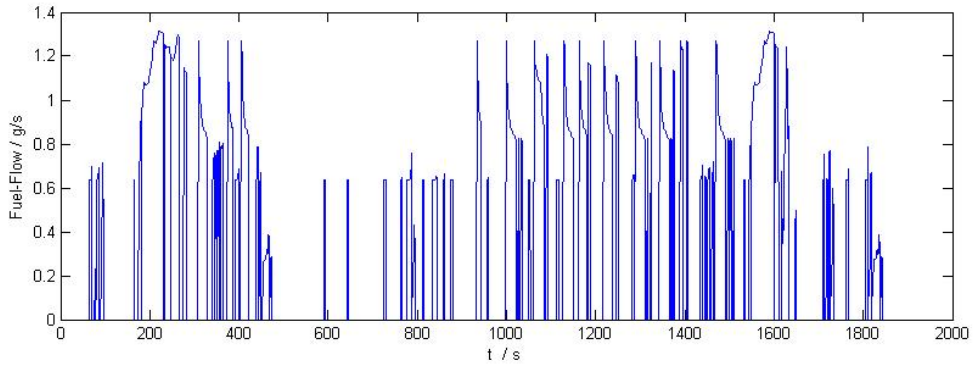

Figure D.8. Simulated engine fuel consumption vs. time profile.

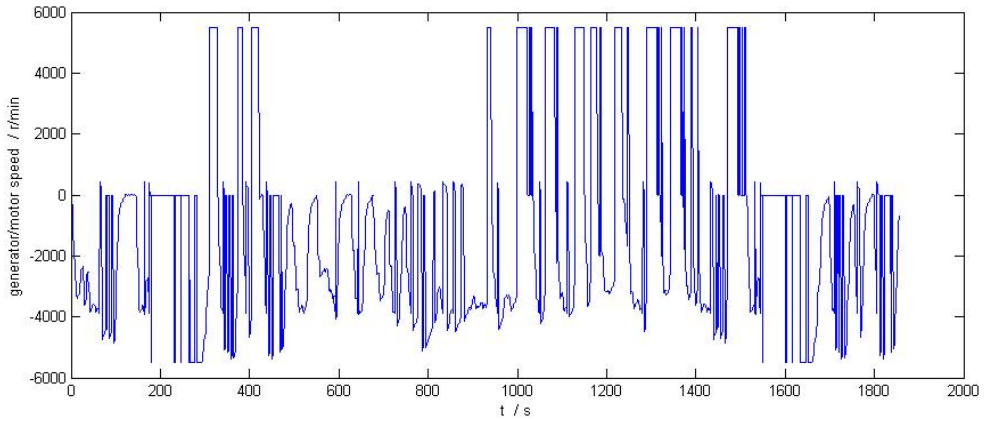

Figure D.9. Simulated generator speed vs. time profile.

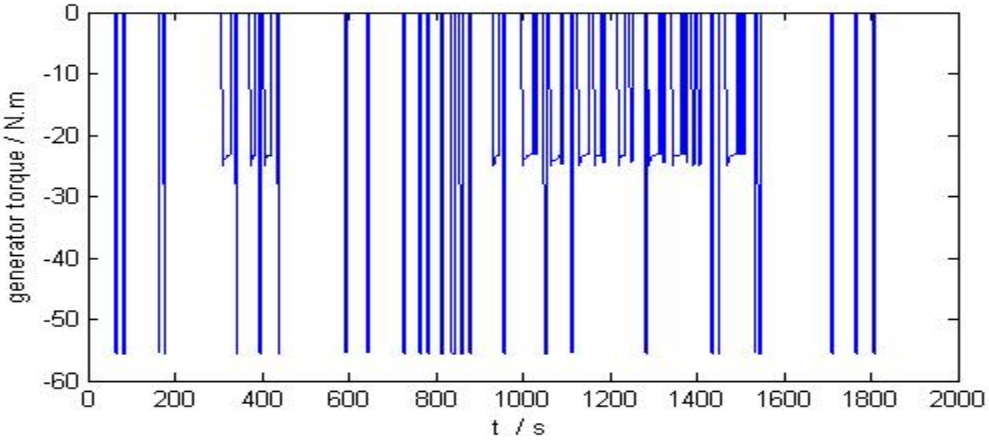

Figure D.10. Simulated generator torque vs. time profile.

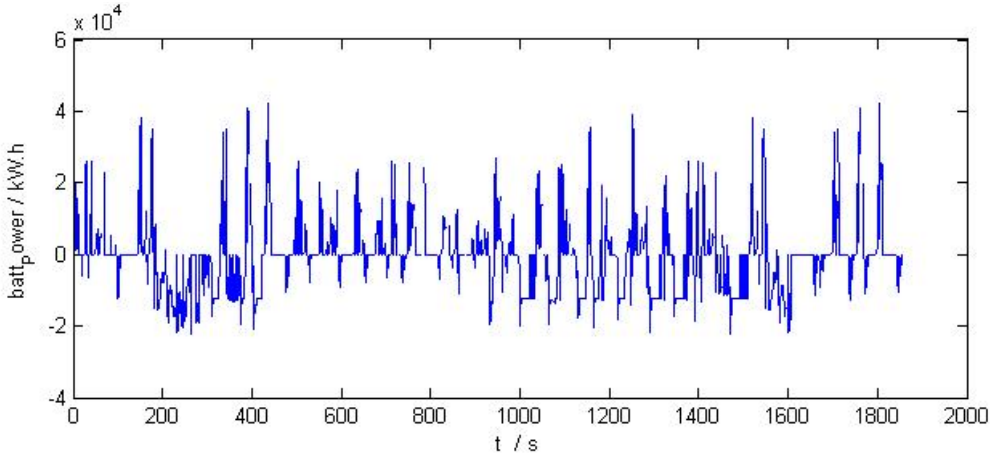

Figure D.11. Simulated battery power vs. time profile.

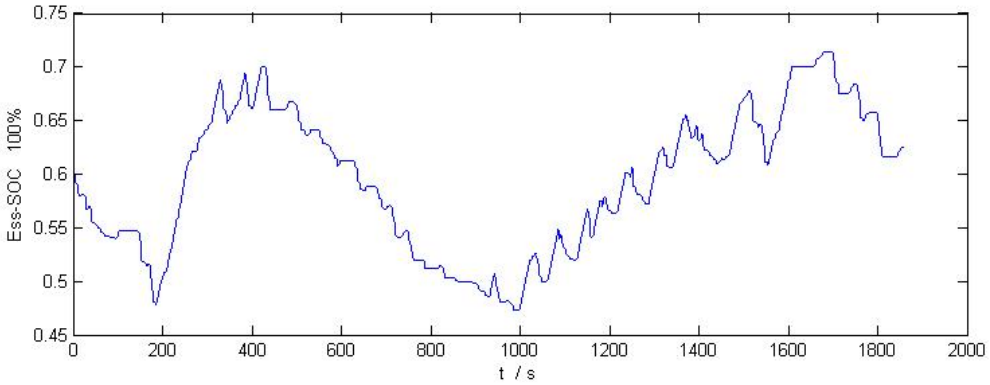

Figure D.12. Simulated battery SOC vs. time profile.

Appendix E. Heavy-Duty Hybrid Electric Vehicle Models

E.1. Introduction

Hybrid electric vehicles have gained much attention due to increased concerns about fuel economy and emissions from the vehicles. Though hybrids also rely on the usage of fuels derived from crude oil, they reduce fuel consumption to a considerable extent.

A typical hybrid electric drive system provides a buffer between the torque and speed requirements of the final drive by adding an electric motor and battery system between the combustion engine and the drive wheels. By buffering the system, the combustion engine can run in more efficient speed and torque ranges, and thereby improve the fuel efficiency and decrease the emissions from the vehicle. Hybrid systems with sufficient energy storage can also recapture energy through regenerative braking systems. Hybrids can use diesel, gasoline, or natural gas engines. Additionally, hybrids are quieter than conventional vehicles and have higher torque and better performance at low speeds.

Hybrid electric vehicles (HEVs) show great potential for use in a wide variety of driving situations, especially for the urban transit buses, courier trucks, and refuse trucks, which operate predominantly under stop-and-go conditions. Such service takes advantage of the electric drive's efficiency at acceleration from a dead stop to low city traffic speeds. However, the optimization of components and control strategies for HEVs is more complex.

The goals of this appendix are to provide an overview of the architecture and basic working principles of heavy-duty HEVs, to set up the simulation models for different kinds of heavy-duty HEVs, to simulate the HEV fuel consumption, and to analyze other important working parameters of HEVs during the driving process. The categories into which heavy-duty HEVs can be subdivided are discussed in Section E.2. Modeling the main components of an HEV is discussed in Section E.3. Section E.4. provides a description of the model for the HEV control system. Section E.5 is a discussion of the results from the simulations of heavy-duty HEVs.

E.2. Types of Heavy-Duty Hybrid Electric Vehicle Layouts

Hybrid electric vehicles can be subdivided into three types: Series HEVs, Parallel HEVs, and Series-Parallel HEVs. Each of these is briefly discussed in the following three subsections.

E.2.1. The Series Hybrid Electric Vehicle

Figure E.1 shows a typical series HEV layout. In a series HEV, an internal combustion engine (ICE) is used to produce electrical energy that is sent to the battery pack and electric motor. The electric motor supplies all of the power required to drive the vehicle. In series HEVs there is no physical coupling between the engine and the transaxle or transmission. This can reduce the transient operation of the ICE that is especially helpful from an emissions standpoint, allowing optimal fueling and combustion control. Disadvantages in current series HEVs include losses during changing energy from chemical to mechanical, mechanical to electrical, and electrical to mechanical forms, and the need for costly, heavy battery packs and electric motors. Series HEVs typically show substantial fuel economy improvements in highly transient driving in urban situations due to recovery of large amounts of regenerative braking energy. However,

the efficiency benefit can be negligible for less transient operation such as highway driving, where there is less available regenerative braking energy.

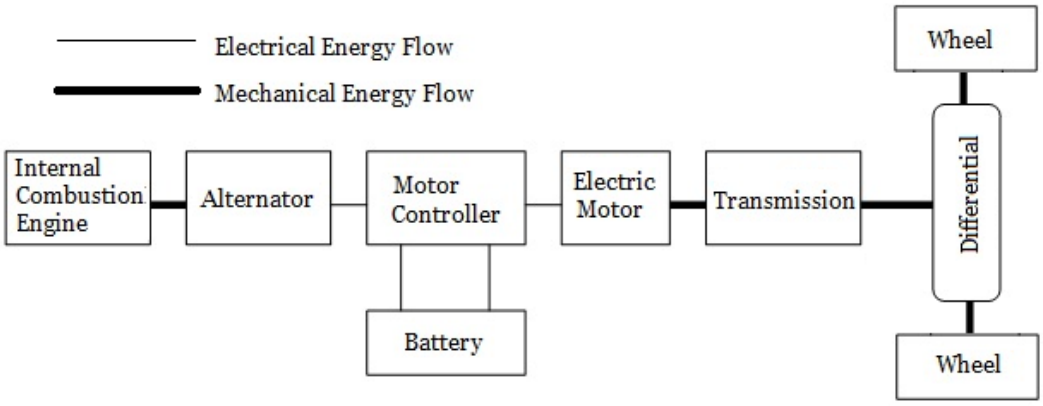

Figure E.1. Schematic of a Series HEV.

The series configuration is the simplest architecture and is very suitable for plug-in hybrid vehicles. The series architecture delivers excellent fuel economy in urban driving conditions. The drivetrain uses an engine/generator set to extend the travel range of the vehicle. The primary drawback of this configuration is the size of the electrical traction motor, which must be rated for the maximum power requirement of the vehicle.

E.2.2. The Parallel Hybrid Electric Vehicle

In a parallel HEV, there is a direct connection between both the ICE and the electric motor with the wheels, as shown in Figure E.2. This configuration allows a wide variety of control strategies to be employed. When high torque is demanded, such as for hard acceleration, both the ICE and the electric motor deliver power to the wheels. In less demanding situations, the ICE can be operated at a higher power, more than is required to drive the vehicle, and the excess power is stored in the batteries for later use. Alternatively, the electric motor alone can be used to drive the vehicle when relatively little torque is required by the driver. . This has the advantage of operating the ICE in a more efficient mode or not at all. During long, steady state cruises, the ICE alone can drive the vehicle avoiding the inherent inefficiency of the batteries. The main advantage of parallel HEVs is improved dynamic performance due to the direct coupling between the ICE, electric motor, and the wheels. The disadvantage with the ICE being directly coupled to the wheels is that there is more transient speed operation than in a series HEV. This tends to result in poorer fuel efficiency and increased emissions.

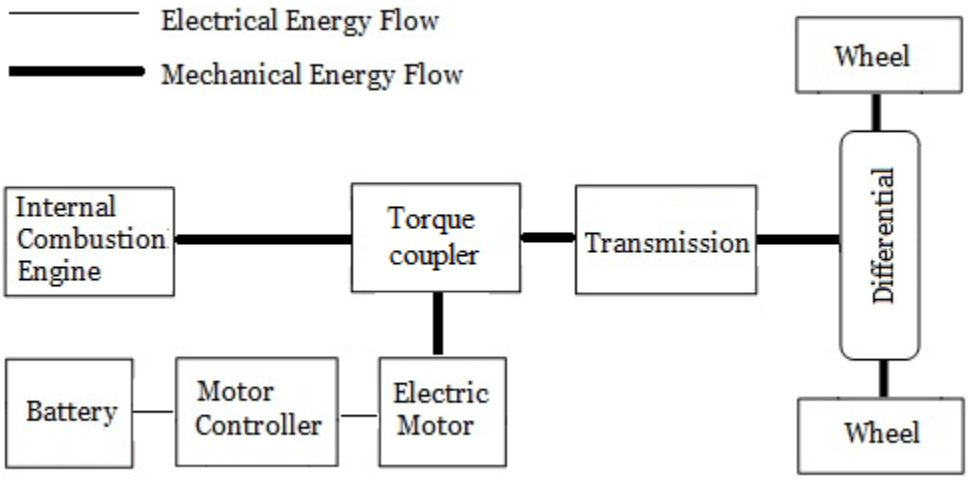

Figure E.2. Schematic of a parallel HEV.

E.2.3. The Series-Parallel HEV

The series-parallel HEV operates as a series HEV at one instant and as a parallel HEV at another. The series-parallel HEV has two electric motors and an ICE coupled with a combination of clutches. As might be expected, the control system for these vehicles is more complex than those for either series HEVs or parallel HEVs. Figure E.3 shows the layout of a series-parallel HEV.

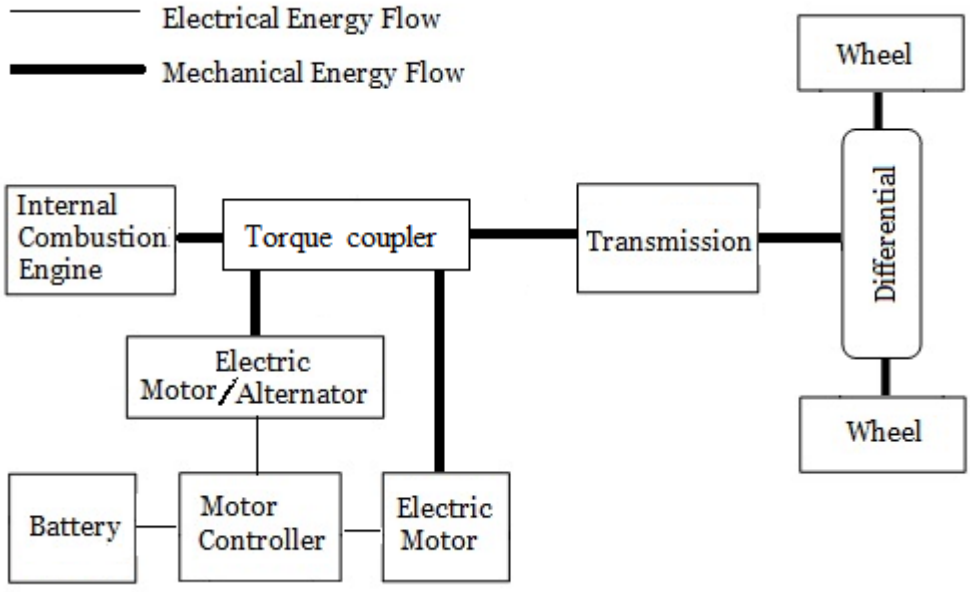

Figure E.3. Schematic of a Series-Parallel HEV.

E.3. HEV Main Components Modeling and Input Parameters

From the perspective of the drivetrain, an HEV can be subdivided into six components: the vehicle itself, the engine, the transmission, the differential, the wheels and brakes (coupled into a single component for convenience), and the electric components of the HEV drivetrain. Each of these is discussed in the following subsections.

E.3.1. Vehicle

Equation 3.6b was presented in Chapter 3 of this report as a fundamental relationship between the forces resisting motion of the vehicle (in the denominator), the fuel economy of the vehicle under conditions for which the wind is negligible, two properties of the fuel, three efficiencies related to the engine, and two efficiencies for the remainder of the driveline (the transmission and the differential):

$$FE_{no\ wind} = \frac{(\eta_{ti}\eta_c\eta_m)\eta_T\eta_D[\rho_f LHV_P]}{m_e\frac{dV}{dt} + f_0 + f_1 V + f_2 V^2 \pm W_{tot}\sin\theta} \tag{3.6b}$$

This relationship can also be posed in Equation E.1 as a function of the BSFC of the engine, $bsfc_e$:

$$FE_{no\ wind} = \frac{\eta_T\eta_D[\rho_f]}{bsfc_e\left\{m_e\frac{dV}{dt} + f_0 + f_1 V + f_2 V^2 \pm W_{tot}\sin\theta\right\}} \tag{E.1}$$

One advantage of a hybrid is that the control system can be used to keep the engine operating near its most efficient speed and load (lowest $bsfc_e$) much more often than would be possible if the engine were the sole power source. Another advantage is that the vehicle can sometimes operate solely on electricity.

The driver submodel algorithm, which will be discussed in Subsection E.4.1, monitors the error between the desired vehicle speed and the actual (calculated) speed (both the value of the speed error and the rate of change of the error), and controls the throttle pedal position and the braking action in order for the vehicle speed to track the desired speed as closely as possible. Simultaneously, the shift strategy submodel that will be discussed in Subsection E.4.2, controls the selection of the appropriate transmission gear ratio depending on vehicle speed and load. The rotational speed of the power plant (the engine or the electric motor or their combination), N_{pp}, can be calculated via Equation E.2:

$$N_{pp} = \frac{r_T r_D V}{2\pi R_t} \tag{E.2}$$

where r_T is the gear ratio of the transmission, r_D is the gear ratio of the differential (final drive), R_t is the rolling radius of the tires, V is the instantaneous vehicle speed, and it is assumed that there is no slip in the clutch or torque converter of the transmission.

Given the instantaneous speed of the power plant, the maximum torque that the power plant can deliver at this speed, $\tau_{max}(N_{pp})$, is determined from the full load torque map to allow determination of the instantaneous torque via Equation E.3:

$$\tau_{req,pp} = \tau_{max}(N_{pp})\theta \tag{E.3}$$

where $\tau_{req,pp}$ is the instantaneous torque required from the power source and θ is the accelerator pedal position.

Next, the motive force (or tractive force) on the driven wheels is calculated using Equation E.4:

$$F_{mot} = \frac{\tau_{req,pp}\eta_T r_T \eta_D r_D}{R_t} \tag{E.4}$$

where F_{mot} is the motive force delivered to the tire-road interface, η_T is the transmission efficiency, and η_D is the differential efficiency.

Finally, we apply Newton's Second Law of Motion in two different ways. First, it is used to compute the required motive force given the required acceleration, using Equation 3.1 from Chapter 3 to reach Equation E.5:

$$F_{mot} - F_{res} = m_e \frac{dV}{dt} \tag{3.1}$$

$$F_{mot,req} - \left(f_0 + f_1 V + f_2 V^2 \pm W_{tot}\sin\theta\right) = m_e \left.\frac{dV}{dt}\right|_{req} \tag{E.5}$$

Second, Equation E.4 is used for the motive force and the consequent acceleration is calculated to yield Equation E.6:

$$\frac{\frac{\tau_{req,pp}\eta_T r_T \eta_D r_D}{R_t} - \left(f_0 + f_1 V + f_2 V^2 \pm W_{tot}\sin\theta\right)}{m_e} = \left.\frac{dV}{dt}\right|_{actual} \tag{E.6}$$

Additionally, the actual vehicle speed is calculated by rearranging Equation E.2 to yield Equation E.7:

$$V_{act} = \frac{2\pi R_t N_{pp}}{r_T r_D} \tag{E.7}$$

The average speed over the time step is taken to be the average of the speed at the beginning of the time step, which is the speed at the end of the previous time step, and the speed will be updated at the end of each time step.

The main input variables for the vehicle definition are listed in Table E.1. Some of these variables were only used for the initial development of the heavy-duty battery-electric hybrid vehicle model: C_D, Frontal_Area, veh_front_wt_frac, and Rolling_Resistance_Coefficient. After the heavy-duty battery-electric hybrid vehicle model was determined to produce correct results, these parameters were replaced by coastdown coefficients.

Table E.1. Input Variables for the Vehicle Definition.

Name	Type	Units	Vehicle Type	Description
driving cycle	scalar	-	all	Desired vehicle speed vs time, and grade vs distance
C_D	scalar	--	all	coefficient of aerodynamic drag
Frontal_Area	scalar	m^2	all	vehicle frontal area 80% of height*Width*length
veh_front_wt_frac	scalar	--	all	fraction of total vehicle mass supported by front axle when vehicle is not moving
Tire_Dia	scalar	m	all	Tire diameter
Vehicle_Mass	scalar	kg	all	test mass, including fluids, passengers, and cargo
Rolling_Resistance_Coefficient	scalar	--	all	coefficient of rolling resistance force
amb_temp	scalar	C	all	ambient temperature
veh_air_density	scalar	kg/m^3	all	density of air
veh_gravity	scalar	m/s^2	all	gravitational acceleration

E.3.2 Engine

The internal combustion engine is defined in the program as a "fuel converter" that can be incorporated into various vehicle configurations including, series HEVs, parallel HEVs, and conventional vehicles but could be used for fuel cell vehicles in the future, and thus the term "fuel converter."

The fuel converter model determines the engine's normal operating speed and torque ranges. Once the achievable speed and torque have been determined, these values are passed back to the rest of the vehicle model. These values are also used to determine the fuel use (and can be used for emissions calculations) for each time step. The fuel use and "engine-out" (pre-catalyst) emissions values are stored in tables indexed by engine speed and torque. Temperature correction factors can be incorporated to scale the fuel use and emissions for cold starts. Table E.2 provides the input variables for the engine submodel.

Table E.2. Input Variables for the Engine Submodel.

Name	Type	Units	Vehicle Type	Description
fc_fuel_type	char	--	all	description of fuel type
fc_disp	scalar	L	all(~fuel cell)	engine size (displacement)
fc_emis	boolean	--	all	0= no emissions data available 1= emissions data available
fc_map_spd	vector	rad/s	all(~fuel cell)	engine speed range
fc_map_trq	vector	N*m	all(~fuel cell)	engine torque range
fc_fuel_map	matrix	g/s	all	fuel use indexed by fc_map_spd and fc_map_trq
fc_co_map	matrix	g/s	all	engine out CO indexed by fc_map_spd and fc_map_trq
fc_hc_map	matrix	g/s	all	engine out HC indexed by fc_map_spd and fc_map_trq
fc_nox_map	matrix	g/s	all	engine out NOx indexed by fc_map_spd and fc_map_trq
fc_pm_map	matrix	g/s	all	engine out PM indexed by fc_map_spd and fc_map_trq
fc_ct_trq	vector	N-m	all(~fuel cell)	closed throttle torque indexed by fc_map_spd
Fuel_Sp_Gravity	scalar	g/L	all	fuel specific gravity
fc_fuel_lhv	scalar	J/g	all	Lower Heating Value of the fuel
fc_max_trq	vector	N-m	all(~fuel cell)	maximum torque output indexed by fc_map_spd
fc_spd_scale	scalar	--	all	scaling factor for speed range
fc_trq_scale	scalar	--	all	scaling factor for torque range

E.3.3. Transmission

The transmission submodel can be subdivided into two components: the clutch and the gearbox.

For manual transmissions, a clutch is needed to transmit torque and rotational speed from the 'ICE fuel converter' to the 'gearbox' or 'torque coupler'. In the clutch simulation submodel, the clutch also transmits torque and speed requests from the 'gearbox'. The clutch is useful whenever the vehicle control needs to interrupt torque transmission from the engine to the transmission, such as during a gear shift.

The clutch has three states: disengaged, slipping, and fully engaged. When disengaged, the clutch requests and transmits no torque. For HEVs, the engine can run at idle speed or can stop completely. When slipping, the clutch requests that the output torque be the same as the input torque, and passes the actual input torque as the actual output torque even though the

output speed is not equal to the input speed. When engaged, the clutch passes the torque and speed unchanged.

For the clutch submodel, the input variables are listed in Table E.3.

Table E.3. Input Variables for the Clutch Submodel.

Name	Type	Units	Vehicle Type	Description
Clutch_Speed	scalar	--	par/ser	Clutch fully engaged speed
Idle_Speed	scalar	--	par/ser	Engine idle speed

The gearbox of a multi-speed transmission houses gear pairs with various gear ratios that are used to transmit torque from the engine or traction motor to the final drive and on to the wheels. It thereby allows a number of discrete speed reduction and torque multiplication factors. Inclusion of a gearbox is critical to the drivetrain of conventional and parallel hybrid vehicles, and generally less important for series hybrids.

The main effects of the gearbox on torque and speed include torque multiplication and speed reduction via the gear ratio, and also cause torque loss due to the acceleration of rotational inertia, friction of the turning gear pairs, windage losses, bearing losses, and seal losses.

These effects are modeled empirically in the gearbox submodel. The input variables used for the gearbox are listed in Table E.4. This gearbox submodel was used for the initial development of the heavy-duty battery-electric hybrid model. However, after successful development, the transmission model discussed in Appendix B was used to more accurately reflect the effects of torque and speed on the efficiency of the transmission.

Table E.4. Input Variables for the Gearbox Submodel.

Name	Type	Units	Vehicle Type	Description
Transmission _description	char	--	all	text description of the transmission
Transmission_Ratio	vector	-	all	available gear ratios of the gearbox
Transmission_Efficiency	vector	-	all	an array indexing columns of tx_eff_map with transmission output torque

E.3.4. Differential

The differential refers to the ‘final drive’ block in the code, which transmits torque and speed requests from the ‘wheel and axle’ upstream to the ‘gearbox’, and also transmits the actual torque and speed from the ‘gearbox’ back to the ‘wheel and axle’.

The differential submodel includes the effects of gear pair, windage, bearing, and seal losses, inertia, and gear ratio. Torque loss can be calculated by the differential model that was discussed in Appendix C. However, for the initial development of the heavy-duty battery-electric hybrid model, the differential efficiency was assumed to be constant. The gear ratio reduces the speed input from the ‘gearbox’ and increases the torque delivered to the axle.

The main input variables for the differential submodel are listed in Table E.5.

Table E.5. Input Variables for the Differential Submodel.

Name	Type	Units	Vehicle Type	Description
Differential_Ratio	scalar	--	all	gear ratio of final drive
Differential_Efficiency	scalar	--	all	final drive efficiency

E.3.5. Axle and Brakes

The wheel transmits actual torque and speed from the final drive to the axle and then to the tire contact patch, and in this submodel also returns the actual (as calculated by the code) torque and speed back to the final drive.

Braking control ensures that the vehicle slows down when deceleration is encountered during the driving cycle. The brakes are applied based on the error between the actual vehicle speed (calculated after working downstream in the code from the "power source" rpm) and the desired speed (from the driving cycle). There is an upper limit to the value of the brake force based on the tractive limit. The friction coefficient between the tires and the road surface during braking is assumed to be 0.9.

The main input parameters for the brake submodel are listed in Table E.6.

Table E.6. Main Input Parameters for the Brake Submodel.

Throttle_Position threshold for braking	scalar	--	all	Throttle_Position Threshold under which braking begins to function
Thresholds for error between the actual vehicle speed and desired speed	scalar	mph	all	Different thresholds of error between the actual vehicle speed and desired speed for braking control choice
Step values for the Braking force increment or decrease	vector	--	all	Different step values for the Braking force increment or decrease
Braking_Limit	scalar	--	all	0.9*Vehicle_Mass*9.8, wh_slip_force_coeff is 0.9

E.3.6. HEV Drivetrain Electric Components

The main electric components of HEV drivetrain include the generator, electric motor, battery pack, and their related control modules**.** The first three of these submodels are discussed in the following three subsections. HEV control systems are the subject of the Subsection E.4.

E.3.6.1. Generator

The generator submodel determines its normal operating speed and torque ranges of the generator. Once the achievable speed and torque have been determined, these values are used to calculate the electric power production that will be supplied to the electric bus. The generator submodel also includes the effects of losses in the generator and controller, the generator's speed-dependent torque capability, and the controller's electric current limit. Power losses are considered via a 2-D efficiency lookup table indexed by rotor speed and input torque. The generator's maximum torque is enforced using a lookup table indexed by rotor speed, and this limits the maximum electric power output from the generator.

If the generator's normal operating speed and torque ranges are not matching with the engine's operating ranges, the code can use a speed/torque coupler, and utilize the generating system in the most efficient way.

The main input variables for the generator submodel are listed in Table E.7.

Table E.7. Input Variables for the Generator Submodel.

Name	Type	Units	Vehicle Type	Description
gc_map_spd	vector	rad/s	Ser/par	speed range of the generator
gc_map_trq	vector	N*m	ser/par	torque range of the generator
gc_eff_map	matrix	--	ser/par	generator efficiency map indexed by gc_map_spd and gc_map_trq
gc_max_crrnt	scalar	A	ser/par	max. current allowed in generator/controller
gc_max_trq	vector	N*m	ser/par	maximum torque output of the generator indexed by gc_map_spd
gc_min_volts	scalar	V	ser/par	min. voltage allowed in generator/controller
gc_overtrq_factor	scalar	--	ser/par	factor by which absorbed input torque can exceed max continuous for short periods
gc_spd_scale	scalar	--	ser/par	speed scaling factor
gc_trq_scale	scalar	--	ser/par	torque scaling factor
Spd_coup_ratio	scalar	--	ser/par	speed coupling factor of the torque coupler
Torq_coup_ratio	scalar	--	ser/par	torque coupling factor of the torque coupler
Coupling_eff	scalar	--	ser/par	speed /torque coupler efficiency

E.3.6.2. Electric Motor

The electric motor submodel provides the motor torque and speed operating ranges, and also describes the effects of losses in the motor and motor controller. The power losses of the electric motor are also considered via the motor efficiency map, which is handled as a 2-D lookup table indexed by rotor speed and output torque. The motor's maximum torque is determined using a lookup table indexed by rotor speed.

The electric motor controller's maximum current is not allowed to exceed the highest current limit threshold, and the motor can shut down when it is not needed or if the gearbox is in the process of changing gears.

If the electric motor's normal operating speed and torque ranges are not matching with the engine's speed and torque operating ranges, a speed/torque coupler can also be invoked in order to match the motor with the transmission.

The main input variables for the motor submodel are listed in Table E.8.

Table E.8. Main Input Variables for the Motor Submodel.

Name	Type	Units	Vehicle Type	Description
mc_description	char	--	par/ser	text string description of the motor/controller
mc_map_spd	vector	rad/s	par/ser	speed range of the motor
mc_map_trq	vector	N*m	par/ser	torque range of the motor
mc_eff_map	matrix	--	par/ser	efficiency map of the motor indexed by mc_map_spd and mc_map_trq
mc_inertia	scalar	kg*m^2	par/ser	rotational inertia of the motor
mc_max_crrnt	scalar	A	par/ser	max. current allowed in motor/controller
mc_max_trq	vector	N*m	par/ser	maximum torque curve of the motor indexed by mc_map_spd
mc_max_gen_trq	vector	N*m	par/ser	maximum torque curve of the motor acting as a generator, indexed by mc_map_spd
mc_min_volts	scalar	V	par/ser	min. voltage allowed in motor/controller
mc_overtrq_factor	scalar	--	par/ser	factor by which output torque can exceed max continuous for short periods
mc_spd_scale	scalar	--	par/ser	speed scaling factor
mc_trq_scale	scalar	--	par/ser	torque scaling factor
tc_description	char	--	par	text string description of the torque coupler
tc_mc_to_fc_ratio	scalar	--	par	constant ratio of speed at motor torque input to speed at engine torque input
tc_eff	scalar	--	par/ser	Mechanical efficiency of the torque coupler

E.3.6.3. Energy Storage System

The main component of the Energy Storage System is the battery. Different types of batteries are currently used in HEVs and "pure electric vehicles, as discussed below.

Lead-Acid battery (VRLA). The lead acid battery is composed of lead plates of grids suspended in an electrolyte solution of sulphuric acid and water. These batteries can be ruined by completely discharging them. Thus, it is necessary to set a lower charge limit. The advanced lead-acid battery, such as the Valve-Regulated Lead Acid (VRLA) battery, has a longer cycle life.

Nickel-Cadmium battery. The nickel-cadmium battery is composed of a nickel hydroxide cathode and a cadmium anode in an alkaline electrolyte solution. Batteries made from Ni-Cd cells offer high currents at relatively constant voltage and they are tolerant to physical abuse.

Nickel-Metal Hydride battery. Environmentally friendly and quickly rechargeable, the Ni-MH battery is composed of a hydrogen storage metal alloy, a nickel oxide cathode, and a potassium hydroxide electrolyte. This type of battery has been used in the Honda Civic IMA and the Toyota Prius.

Lithium-Ion. Lithium is the lightest metal having the highest electric potential of all metals, making it ideal for HEV applications. Li-ion batteries have no memory effect and are environmentally friendly.

Generally, a battery is difficult to simulate because the main variables that characterize battery operation, i.e., state-of-charge (SOC), voltage, current, and temperature, are dynamically related to each other in a highly non-linear fashion. Batteries seem to act like simple electrical energy storage devices, when they deliver and accept energy, but they actually undergo thermally-dependent electrochemical processes that make them difficult to model. For this reason, a lot of battery models have been developed in the past, ranging from very basic and simple models to empirical models to highly complex models based on fundamental electrochemical processes.

In general, the objective of the battery submodel in a vehicle simulator is to predict the change in SOC given the electrical load. The dependence on aging does not affect battery performance in the short term, but it is possible to evaluate the effect of an aged battery by reducing the value of its capacity.

For this project, two fairly simple battery models were chosen to calculate the SOC of the battery pack, as described in the following two subsections.

E.3.6.3.A. Power and Energy Model

A battery pack is composed of *modules* that are composed of *cells* themselves. The battery module voltage may be different for different battery types. For simulation purposes, we must define some design variables for the battery.

The battery module has two internal resistances, being the charging resistance (R_c) representing the energy losses while charging and the discharging resistance (R_d) representing the energy losses while discharging. I represents the current and V_{cell} the module voltage. Battery voltage V and battery capacity Q are assumed equal for different battery modules.

If all the battery modules are connected in series, then the battery pack voltage and the total capacity are calculated with Equations E.8 and E.9:

$$V_{batt} = n * V_{module} \tag{E.8}$$

$$Q_{batt} = Q_{module} \tag{E.9}$$

where V_{batt} is the battery pack voltage, V_{module} is the battery module voltage, n is the number of battery modules, Q_{batt} is the battery pack total capacity and Q_{module} is the battery module capacity.

Otherwise, if all the battery modules are connected in parallel, then the battery pack voltage and the total capacity are calculated with Equations E.10 and E.11:

$$V_{batt} = V_{module} \tag{E.10}$$

$$Q_{batt} = n * Q_{module} \tag{E.11}$$

The total energy capacity of the battery pack is defined with Equation E.12:

$$E_{max} = V_{batt} \cdot Q_{max} \tag{E.12}$$

where Q_{max} is the battery capacity [in units of amp-hours, A-h], the discharge current depleting the battery in 1 hour, and E_{max} is the battery energy capacity [in units of Watt-hours, W-h].

The power of the battery pack, P_{batt}, can be calculated in each time step by considering the motor power, brake regenerating power, and the generator power. The current I of the battery pack can be calculated in each time step with Equation E.13:

$$I = P_{batt} / V_{oc} \tag{E.13}$$

where V_{oc} is the open circuit battery voltage that can be calculated by interpolation from the battery voltage 2-D lookup table indexed by the battery SOC and temperature. *Rc* and *Rd* can also be calculated by interpolation based on R_c and R_d 2-D lookup tables indexed by the battery SOC and temperature.

The rate of energy loss from the battery pack because of the internal resistances is calculated with Equation E.14:

$$P_{loss} = nI^2R \tag{E.14}$$

This power loss always has a negative effect on the overall efficiency of the battery pack. Also, to minimize power losses, generally the current I should be as low as possible and the battery pack voltage V_{batt} is preferably high (thus the need for a high voltage electric circuit between the battery and the motor).

The SOC of a battery under working conditions can be calculated with Equation E.15:

$$\mathrm{SOC_t} = \mathrm{SOC_{t-1}} + (\mathrm{t} * (\mathrm{abs}(P_{batt}) - P_{loss})) / (E_{max}) \tag{E.15}$$

where SOC_t and SOC_{t-1} are the SOC of the battery pack at time step t and t-1, t is the calculation time step, and E_{max} is the total energy capacity of the battery pack [in units of Watt-seconds, W-s]. Otherwise, when the battery is discharged, the SOC of a battery under working conditions can be calculated with Equation E.16:

$$\mathrm{SOC_t} = \mathrm{SOC_{t-1}} - (\mathrm{t} * (\mathrm{abs}(P_{batt}) + P_{loss})) / (E_{max}) \tag{E.16}$$

The difference in signs between Equations E.16 and E.17 should be noted by the reader.

E.3.6.3.B SOC Model Based on the Average Charge/Discharge Current

The state of charge (SOC) is defined as the amount of charge stored in the battery. To determine the State of Charge of a battery, consider a completely discharged battery. With a charging current I, the charge delivered to the battery (Equation E.18) is

$$\int_{t_0}^{t} I(\mathrm{t})\mathrm{dt} \quad \text{when } t_0=0$$

and

$$Q_{max} = \int_{t_0}^{\infty} I(\mathrm{t})\mathrm{dt} \tag{E.17}$$

where Q_{max} is the total amount of charge that the battery can accept, i.e., its charge capacity or simply capacity Q_{batt}, and $\int_{t_0}^{t} I(t)dt$ is the amount of charge actually stored in the battery when charged from time t_0 to time t. The SOC of the battery is defined relative to the total charge capacity (Equation E.18):

$$SOC(t) = \xi(t) = \frac{\int_{t_0}^{t} I(t)dt}{Q_{batt}} \tag{E.18}$$

where Q_{batt} is the total amount of charge of the battery when fully charged (i.e., $Q_{batt} = Q_{max}$).

Calculating the SOC given the current is relatively straightforward, if the capacity is assumed to be a constant, known parameter. In reality, the battery capacity changes according to several parameters, mainly the magnitude of current and the age of the battery, but both of these effects can be neglected for a model used for driving cycle simulations, because this does not introduce any modeling error, but simply implies a slightly different definition of SOC, given in terms of nominal capacity rather than actual capacity.

When a battery is depleted by discharging current, it will need more charge than was taken out to fill it back up to its starting point. Coulombic efficiency is defined as the total charge removed divided by the total charge added to replenish the charge removed. Thus, when the battery is charged with a charging current *I*, one should consider the Coulombic efficiency when calculating the charge delivered to the battery. Thus, in our code, when the battery is charged from time t-1 to time t, the battery SOC is calculated using Equation E.19.

$$SOC(t) = SOC(t) \;=\; SOC(t-1) + \frac{I \cdot t \cdot \eta_{coulomb}}{Q_{batt}} \tag{E.19}$$

where t is the simulation time step, SOC(t) and SOC(t-1) are the SOC values of the battery at time t and t-1 separately, and $\eta_{coulomb}$ is the coulombic efficiency when calculating the charge delivered to the battery.

When the battery is discharged (Equation E.20):

$$SOC(t) = SOC(t) \;=\; SOC(t-1) - \frac{I \cdot t}{Q_{batt}} \tag{E.20}$$

Typically, the SOC of a battery is held strictly between certain operating limits (SOC= 0.4 ~0.7) to optimize the performance, efficiency, and lifespan of the battery.

The main input variables for the battery submodel are listed in Table E.9.

Table E.9. Main Input Variables for the Battery Submodel.

Name	Type	Units	Vehicle Type	Description
ess_description	char	--	par/ser	text string description of the energy storage system (ESS)
ess_coulombic_eff	scalar	--	par/ser	average Coulombic efficiency of the ESS
ess_init_soc	scalar	--	par/ser	initial state of charge of the ESS
ess_max_ah_cap	scalar	Ah	par/ser	maximum A-h capacity the ESS can have, no matter how slowly it is drained
ess_module_mass	scalar	kg	par/ser	mass of one energy storage module
ess_module_num	scalar	--	par/ser	number of modules in a pack; ASSUMED TO BE STRUNG IN SERIES
ess_min_volts	scalar	V	par/ser	minimum battery operating voltage, not to be exceeded during discharge
ess_max_volts	scalar	V	par/ser	maximum battery operating voltage, not to be exceeded during charge
ess_r_chg	matrix	ohms	par/ser	module's resistance to being charged; indexed by ess_soc and ess_tmp
ess_r_dis	matrix	ohms	par/ser	module's resistance to being discharged; indexed by ess_soc and ess_tmp
ess_soc	vector	--	par/ser	vector of SOCs used to index other ESS variables
ess_tmp	vector	C	par/ser	vector of temperatures used to index other ESS variables
ess_voc	matrix	volts	par/ser	module's open-circuit voltage; indexed by ess_soc and ess_tmp

E.4. The HEV Control Model

As was done for our model of a conventional vehicle, the heavy-duty HEV vehicle simulation is carried out from the throttle pedal position through the powertrain down to the wheels based on the specific driving cycle chosen by the user, which is the desired speed vs. time profile. One of the inputs to the vehicle model is the desired vehicle speed (from the driving cycle), and one of the outputs is the actual vehicle speed (calculated by the model). A driver model is needed to control the throttle pedal and brake pedal based on the error between the actual vehicle speed and the desired speed. A shift control model is also important for the best match between the power system, transmission, and the vehicle driving condition.

For a conventional vehicle an internal combustion engine drives a transmission that drives the differential, which in turn drives the wheels. However, the HEV powertrain is more complex. In addition to the engine, the electric motor is another power source. In order to let the engine operate at more efficient speed and torque ranges, to improve the fuel consumption and decrease the emissions, the power distribution between the internal combustion engine, electric motor, generator and battery system needs to be controlled and optimized. Also, when the HEV

decelerates, the regenerative braking system must be engaged to recapture the vehicle dynamic energy (to recharge the battery pack rather than using excess engine output) and improve the HEV fuel efficiency and extend the vehicle travelling distance.

The HEV control system model is the subject of this section of the Final Report for TxDOT Project 0-5974. The driver submodel is discussed in Subsection E.4.1. The gear shift strategy submodel is the subject of Subsection E.4.2. The control strategies for the various types of hybrids are discussed in Subsection E.4.3. Braking control, including regenerative braking, is discussed in Subsection E.4.4.

E.4.1. Driver Submodel

This algorithm determines the throttle position and the braking action in order for the vehicle speed to track the desired speed as closely as possible. This throttle position parameter is used by the shift algorithm as well as the engine model.

The driver submodel algorithm monitors the error between the desired vehicle speed and the actual speed (both the value of the error and the rate of change of the error). If the error is or is becoming large, the throttle position is adjusted up and down accordingly. In the driver submodel, some control strategies, such as PID control and adaptive control, can be applied.

During the driving cycle, rates of deceleration are often encountered that are much larger than coasting (engine compression braking in addition to the normal resistive forces) can accomplish. When this happens, the brakes are applied, controlled in a similar way to the throttle position. There is an upper limit to the value of the brake force based on the tractive limit. The friction coefficient is assumed to be 0.90.

E.4.2. Shift Submodel

The transmission shift pattern depends on input (engine) speed and load. The basic logic behind the shift pattern, however, is that the higher the throttle position, the longer the lower gear remains. At full throttle, the lower gear is maintained all the way to the upper speed limit of the engine, assuming that maximum acceleration is required. As the throttle position is relaxed, the speed at which a higher gear ratio is selected is reduced. The selection of up-shift or down-shift vs. speed and load is shown in Figure E.4, which is the transmission shift scheme for a conventional vehicle with a piston engine (rather than a hybrid). However, the speed and load selection for up-shift or down-shift is arbitrary, and should be designed specifically for different vehicles.

Two lines in Figure E.4 indicate upshift and downshift lines in engine torque and speed space. The black curve near the top of this figure indicates the engine's maximum torque envelope. The numbered curves are efficiency contours. The transmission shift model chooses the shift command (up, down, or no shift) based upon the current gear, engine speed, and engine load assuming the current gear is maintained.

Note that although the plot's y-axis is engine torque, the elbow points are in fact defined in terms of percent engine load, which is defined here as the torque at a given speed divided by its maximum torque at that speed. However, in our code percent engine load is indicated by throttle position.

For a hybrid vehicle, the load definition is the same, and indexed by the throttle position. The motor speed or the speed of the power system that is composed of the motor and the engine is considered by the shift strategy.

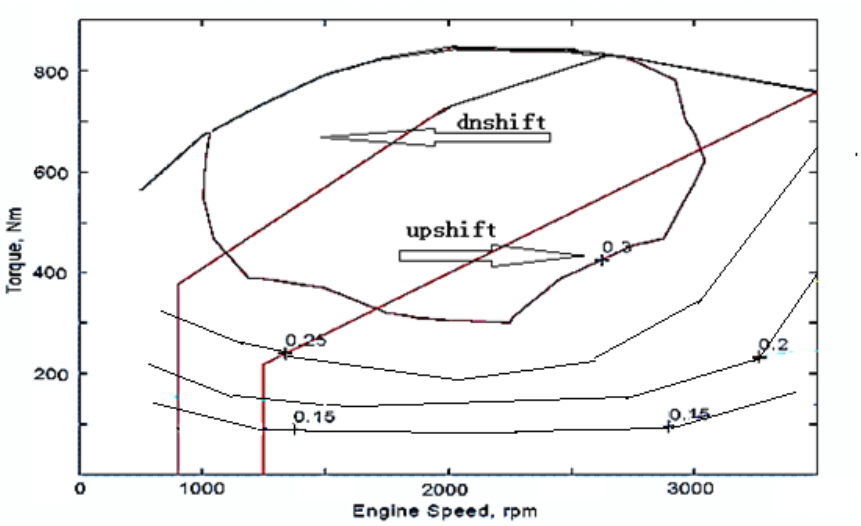

Figure E.4. Upshift and downshift based on the power source load and speed.

There are two types of down shifting. One is as the vehicle speed slows down due to desired vehicle speed demands, the engine speed gets too close to its idle speed, and then a down shift is selected. Second, if the throttle position exceeds a certain percentage and the engine speed is below a certain threshold, a down shift command is executed.

Also, if the vehicle accelerates in 1st gear from a complete stop or from very low vehicle speed, the clutch is allowed to slip. Therefore, if the engine speed is less than the "clutch speed," it is assumed that the driver slips the clutch. This allows the engine speed to operate at a more favorable speed to accelerate the vehicle.

The shift algorithm also includes a shift delay. The shift delay (set at 0.3 seconds) eliminates any engine motive force for the shift delay period after a shift has been ordered. This may be a larger factor for HDVs that take longer to shift and have many more gear ratios that they have to go through.

E.4.3. Hybrid Control Strategies

Control strategies for series hybrids are discussed in Subsection E.4.3.1.

E.4.3.1. Series Hybrid Control Strategies

The series HEV drivetrain components include a "fuel converter" (the engine), a generator, batteries, and a motor. The fuel converter does not drive the vehicle shaft directly. Instead, it converts mechanical energy directly into electrical energy via the generator. All torque used to move the vehicle comes from the motor. The default speed ratio of the speed/torque coupler between the internal combustion engine and the generator is one, just a one speed axle.

The series HEV control strategy determines at what torque and speed the engine should operate to generate electric power via the generator, given the conditions of the motor, battery, and/or the engine/fuel converter itself, and usually is designed to minimize fuel use or emissions or maximize battery pack life. Series HEV control strategies can be divided into 'thermostat' and 'power follower' categories, each of which is discussed below.

E.4.3.1.A. The "Thermostat" Control Strategy

When the battery reaches a threshold selected by the user, cs_lo_soc, the engine begins to work at a desired operating point where it can achieve the highest efficiency or lowest emissions, and drive the generator to generate electricity to supply to the electric motor or to charge the battery. The engine is turned off when the battery reaches another threshold, cs_hi_soc, and the cycle continues. When the SOC of the battery is between cs_lo_soc and cs_hi_soc, the engine remains at its previous working state until the SOC of the battery reaches cs_lo_soc or cs_hi_soc.

The engine on–off or thermostat control strategy is appropriate for plug-in HEVs. This control strategy is illustrated in Figure E.5. The operation of the engine/generator is completely controlled by the SOC of the battery pack. When the SOC of the battery pack reaches its top line, the engine/generator is turned off and the vehicle is propelled only by the motor and the battery pack. On the other hand, when the SOC of the battery pack reaches its bottom line, the engine/generator is turned on and the battery pack gets its charging from the engine. In this way, the engine can be always operated within its optimal efficiency region.

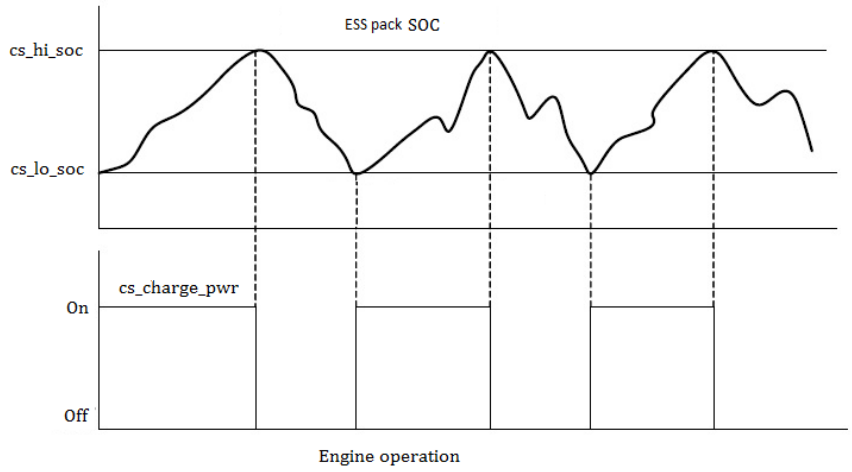

Figure E.5. Illustration of the thermostat control strategy.

Series hybrid systems benefit by operating the engine at a desired operating point where they can achieve the highest efficiency or lowest emissions of a selected type. The series hybrid can also allow engine designers to design an engine such that the emissions at the highest efficiency are as low as possible without regard to other operating points of the engine.

The output power designed for the IC engine is characterized by torque and speed, and calculated and selected before the simulation is run. The locus of highest efficiency torque/speed points is computed over the range of genset (the combination of the engine and mated generator) powers. The control strategy keeps the IC engine torque and speed on this locus using a lookup table defined by cs_pwr and cs_spd.

E.4.3.1.B. The "Power Follower" Control Strategy

The target of this control strategy is to meet the power demand required by the vehicle, and maintain the SOC of the battery at its highest efficiency level at the same time. The engine/generator power is sufficient to provide electric power to the electric bus, and the battery can be taken as an auxiliary power source. That is, both the motor and the engine/generator should

be able to produce power equal to the vehicle's demanded power, and the engine/generator is much larger than the plug-in engine/generator, and the vehicle's cost and weight increase accordingly.

The power follower control strategy is depicted in Figure E.6, which indicates the engine operating state as a function of engine power, battery pack SOC, and the engine's previous state. The cs_min_pwr refers to the minimum power requirement to cause the engine to turn on when it was previously off in order to let the engine operate within its optimal efficiency region. According to cs_min_pwr, we can divide the whole engine working range into two parts. When the engine output power is larger than cs_min_pwr, the engine keeps on working and supplies the electric power to the motor directly in order to reduce the energy conversion loss of the battery. Otherwise, when the engine's power is less than cs_min_pwr, the engine operating state depends on the battery SOC. In fact, even though the engine output power is less than cs_min_pwr, if the engine was last on and the SOC less than cs_hi_soc or the SOC is less than cs_lo_soc, the engine will stay on regardless of power command.

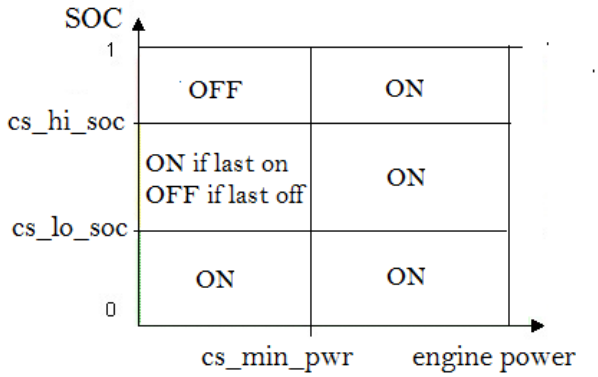

Figure E.6. Illustration of the power follower control strategy.

Finally, regardless of all other conditions, if the power required by the bus is greater than the ESS pack capability, the engine will turn on and stay running.

For the 'power follower' control strategy, the engine/generator output power will try to fulfill the vehicle power requirement, and the battery acts as a load-leveling device with the battery SOC around a high efficiency SOC level. And the FC power command will increase no faster than cs_max_pwr_rise rate and decrease no faster than cs_max_pwr_fall_rate in order to improve the IC engine economic and emissions performance. The engine working state is also characterized by cs_pwr and cs_spd.

The main input variables for the series hybrid control strategy are shown in Table E.10.

Table E.10 Main Input Variables for the Series Hybrid Control Strategy.

Variable	Units	Description
cs_hi_soc	--	highest desired battery state of charge
cs_lo_soc	--	lowest desired battery state of charge
cs_charge_pwr	W	the engine/generator Output Power needed for SOC-stabilizing adjustment and the bus power requirement
cs_fc_init_state	--	1=>fuel converter (FC) is initially on; 0=>FC initially off
cs_max_pwr	W	the maximum charging power output of the fuel converter
cs_min_pwr	W	the minimum charging power output of the fuel converter
cs_max_pwr_fall_rate	W/s	the fastest the fuel converter power command can decrease
cs_max_pwr_rise_rate	W/s	the fastest the fuel converter power command can increase
cs_min_off_time	s	the shortest allowed duration of a FC-off period; after this time has passed, the FC may restart if high enough powers are required by the bus
cs_pwr	W	IC engine powers that define the locus of best efficiency points throughout the genset map
cs_spd	rad/s	IC engine speeds in locus of best efficiency points, indexed by cs_pwr*fc_spd_scale*fc_trq_scale

E.4.3.2. Parallel Hybrid Control Strategies

The parallel HEV components include the engine, electric motor/generator, and batteries. In a parallel design, both the motor and the engine can apply torque to move the vehicle. The electric motor also acts as a generator during vehicle braking, and recaptures the vehicle's kinetic and/or potential energy.

The power management strategy refers to the control algorithm that determines the proper power (torque) level to be generated, and its split between the motor and the engine in order to satisfy the power (torque) demand from the vehicle/driver and maintains adequate energy in the battery. It should be noted that the power management could be either a torque-based or a power-based strategy depending on the application. In this study, we selected the torque-based strategy. Figure E.7 shows the motor and engine working state for a parallel HEV, and a parallel HEV control strategy can realize the following features.

E.4.3.2.A Pure electric traction mode

The motor can be used for all driving torque commands below a certain minimum vehicle speed or engine speed with the engine turned off, and the vehicle is propelled only from the batteries. In other words, when a small torque is required, the engine would run inefficiently, and the engine will shut off and the motor will produce the required torque.

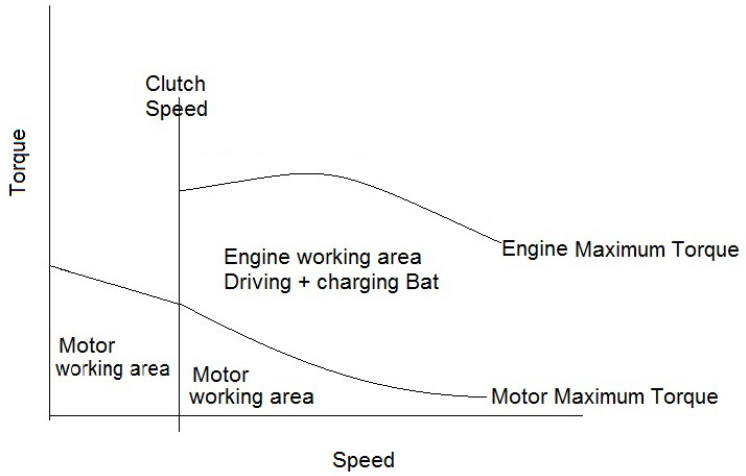

(a) Engine power can meet the vehicle traction requirement.

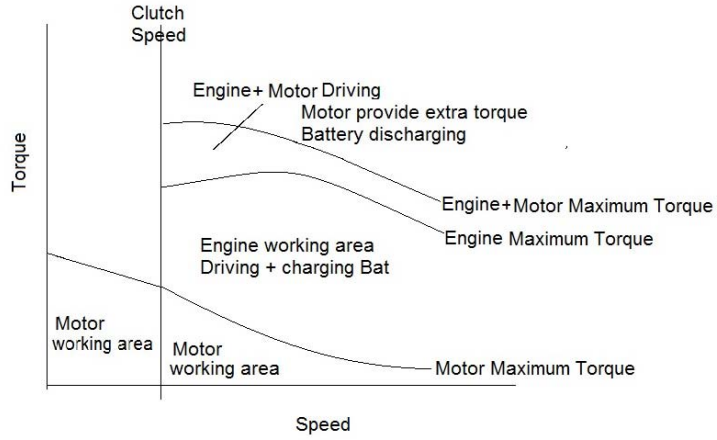

(b) Hybrid traction to meet the vehicle traction power requirement.

Figure E.7. Working range distribution of the motor and engine for a parallel HEV.

E.4.3.2.B Pure engine traction mode

The vehicle traction torque comes only from the engine, while the batteries neither supply power nor accept any power from the drivetrain. In other words, the engine provides all of the power needed to propel the vehicle.

E.4.3.2.C Hybrid traction mode

The traction torque is drawn from both the engine and the batteries, and the motor is used for torque assist if the required torque is greater than the maximum producible by the engine at the engine's operating speed.

E.4.3.2.D Engine traction with battery charging mode

The engine supplies power to charge the batteries and to propel the vehicle simultaneously.

E.4.3.2.E Regenerative braking mode

The traction motor is operated as a generator powered by the vehicle's kinetic or potential energy. The power generated is used to charge the batteries, which are later reused in propelling the vehicle.

E.4.3.2.F Battery charging mode

When the battery reaches cs_lo_soc, while the vehicle is coasting, the traction motor will be driven by the engine and operates as a generator to charge the battery pack.

Table E.11 shows the main input variables for the parallel hybrid control strategy.

E.4.3.3. Series-Parallel Hybrid Control Strategies

The series-parallel HEV components include an engine, batteries, a generator, and a motor. It is named "series-parallel HEV" just because the series-parallel combination can operate as a series HEV at one instance and as parallel HEV at another instance. The series-parallel combination has two electric motors and an engine coupled with a combination of clutches. Although the control of these kind of vehicles is more complex than either series HEVs or parallel HEVs, the control strategies for series HEVs and parallel HEVs that were discussed in Subsections 4.3.1 and 4.3.2 are also applicable to the series-parallel HEV.

Table E.11. Main Input Variables for the Parallel Control Strategy.

Name	Type	Units	Vehicle Type	Description
cs_charge_trq	scalar	N*m	par	an alternator-like torque loading on the engine to recharge the battery pack
Clutch_Speed	scalar	m/s	par	engine speed threshold; below this speed, the fuel converter is turned off
cs_min_trq_frac	scalar	--	par	cs_min_trq_frac*(torque capability of engine at current speed) = minimum torque threshold; when commanded at a lower torque, the engine will operate at the threshold torque and the motor acts as a generator
cs_off_trq_frac	scalar	--	par	cs_off_trq_frac*(torque capability of engine at current speed) = minimum torque threshold; when commanded at a lower torque, the engine will SHUT OFF
cs_fc_init_state	scalar	Boolean	ser	1=fuel converter (FC) is initially on; 0=FC initially off
cs_charge_pwr	scalar	W	ser	cs_charge_pwr produced to meet the bus power requirement
cs_max_pwr	scalar	W	ser	the maximum charging power produced by the fuel converter
cs_min_pwr	scalar	W	ser	the minimum power produced by the fuel converter
cs_max_pwr_fall_rate	scalar	W/s	ser	the fastest the fuel converter power command can decrease
cs_max_pwr_rise_rate	scalar	W/s	ser	the fastest the fuel converter power command can increase
cs_min_off_time	scalar	s	ser	the shortest allowed duration of a FC-off period; after this time has passed, the FC may restart if high enough powers are required by the bus
cs_pwr	vector	W	ser	IC engine power
cs_spd	vector	rad/s	ser	IC engine speeds
cs_hi_soc	scalar	--	par/ser	highest state of charge allowed
cs_lo_soc	scalar	--	par/ser	lowest state of charge allowed
cs_fc_init_state	scalar	--	EV	initial FC state; 1=> on, 0=> off

E.4.4. Vehicle Braking and Regenerative Braking

Vehicle braking can be carried out by driveline braking (engine compression braking) and friction braking, and the friction braking is the main braking method in a traditional vehicle**.** For hybrid vehicles, regenerative braking is one of the key advantages. The kinetic energy normally dissipated during braking can be recaptured by applying negative torque to the electric motor to generate electricity to recharge the battery pack.

The amount of regenerative braking torque that can be added to the friction braking torque is calculated by considering the electric motor torque characteristics and vehicle speed.

The automotive "brake-force distribution" is limited by the front and rear wheel braking force distribution relationship, which in turn depends upon the dynamic normal load on the front and rear tire pairs. Either front-wheel drive or rear-wheel drive can recapture braking energy by applying negative torque to the drive-axle by the electric motor. However, regenerative braking alone is insufficient for most circumstances, and the conventional friction braking is also required, which plays a key role especially when in an emergency braking situation.

Within the desired total braking force, assume that X% of the braking force is provided by the regenerative braking, with the remaining (100-X)% of the braking force provided by the friction brakes. Drive-wheel regenerative braking coefficient X is a function of the vehicle speed, and the regenerative braking force is also related to the motor parameters.

Figure E.8 shows the braking force distribution scheme. The regenerative braking force distribution coefficient can be determined from a look-up table based on the current brake wheel speed, the variable called wh_fa_dl_brake_frac. This parameter can be modified to achieve a different form of distribution. After the drive-wheel brake-force distribution has been determined, the remaining braking force must be provided by the drive wheel friction brakes.

At low vehicle speeds, typically below 10 mph, the braking primarily depends on the friction brakes.

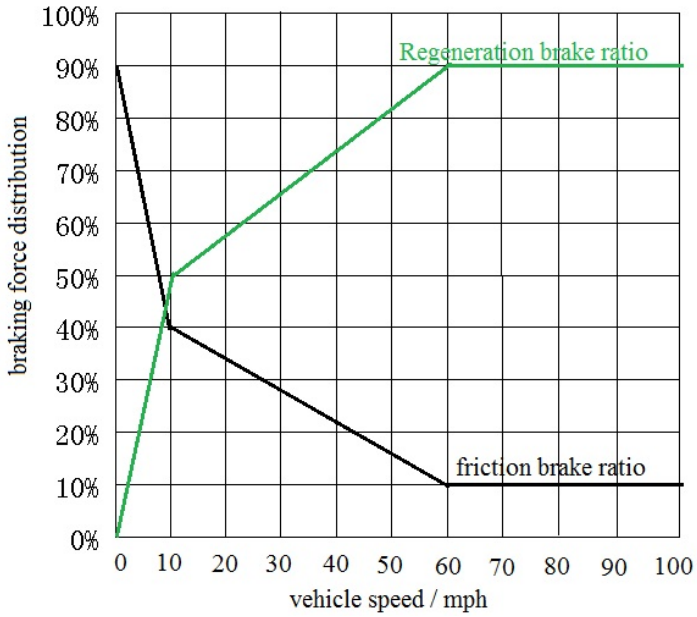

Figure E.8. Braking force distribution scheme.

Table E.12 shows the main input variables for the regenerative braking control strategy.

Table E.12. Main Input Variables for the Regenerative Braking Control Strategy.

Name	Type	Units	Vehicle Type	Description
veh_front_wt_frac	scalar	--	all	fraction of total vehicle mass supported by front axle when vehicle is not moving
wh_fa_dl_brake_frac	vector	--	all	fraction of braking done by driveline via front axle
wh_fa_dl_brake_mph	vector	mph	all	vehicle speed, used to index wh_fa_dl_brake_frac
wh_fa_fric_brake_frac	vector	--	all	fraction of braking done by front axle friction brakes
wh_fa_fric_brake_mph	vector	mph	all	vehicle speed, used to index wh_fa_fric_brake_frac
wh_inertia	scalar	kg*m^2	all	rotational inertia of the wheels
wh_mass	scalar	kg	all	total mass of all wheels
wh_radius	scalar	m	all	rolling radius of the drive tire
wh_slip	vector	--	all	wheel slip of drive wheels
wh_slip_force_coeff	vector	--	all	(tractive force on front tires)/(vehicle weight on front tires), used to index wh_slip

E.5. Vehicle Simulation and Results

As mentioned above, for the hybrid vehicle simulation, one of the main input parameters to the vehicle model is the desired vehicle speed, and the actual vehicle speed will be calculated and compared with the input desired vehicle speed. The simulation is carried out from the throttle pedal position down to the wheels for a selected driving cycle, which is the desired speed vs. time profile.

One of the most important output parameters is the fuel economy of the vehicle, which can be calculated by two methods. One method calculates the power required from the engine and uses the apparent thermal efficiency of the engine to convert that amount of energy to an equivalent volume of a given fuel using the energy of that fuel. The equations used (Equation E.21a-b) are

$$\frac{\dot{m}_f}{bp} = bsfc = \frac{1}{\eta_{ti}\eta_c\eta_m LHV_p} \tag{E.21a}$$

Therefore:

$$\dot{m}_f = \frac{bp}{\eta_{ti}\eta_c\eta_m LHV_p} \tag{E.21b}$$

where LHV_p is the constant pressure Lower Heating Value of the fuel, $\dot{m}_f$ is the fuel mass consumption rate, and bp is the brake power required. Equation E.22 follows:

$$FE = \frac{d\rho_f}{\dot{m}_f t} \tag{E.22}$$

where FE is the fuel economy, d is the distance traveled during the driving cycle, ρ_f is the density of the fuel (in kg/gal), and t is the duration of the driving cycle.

In our research, we use the engine instantaneous engine torque and speed to interpolate in the BSFC map to calculate the instantaneous fuel consumption rate. The cumulative fuel mass during each time step is used to calculate the average gas mileage. The cumulative fuel mass is calculated using Equation E.23:

$$m_{f,tot} = \sum(\dot{m}_f t) \tag{E.23}$$

where $m_{f,tot}$ is the cumulative fuel mass during time step t in g, $\dot{m}_f$ is the fuel mass consumption rate in g/s during time step t, and t is the simulation time step. The fuel economy during time step t is calculated via Equation E.22.

Besides the average fuel economy, many other parameters can be obtained from the vehicle simulation. Table E.13 shows only a few output parameters from the heavy-duty HEV simulation.

Table E.13. Output Parameters of the Hybrid Vehicle Simulation.

Name	Type	Units	Vehicle Type	Description
Avg_MPG	scalar	mile/gal	all	average gas mileage
Lper100km	scalar	L/100km	all	fuel economy of the vehicle
Desired_Speed	vector	m/s	all	requested vehicle speed
Vehicle_Speed	vector	m/s	all	real vehicle speed
t	vector	s	all	time vector defining the drive cycle
Vehicle_Travel	vector	m	all	Vehicle travel distance
Motive_Force	scalar	N	all	Vehicle Motive_Force
Engine_Torque	vector	N.m	all	Engine Instant Operating Torque
Motor_Torque	vector	N.m	all	Motor Instant Operating Torque
Gear	scalar	--	all	Shift number
ess_eff	scalar	--	vehicles with ess	round-trip efficiency
ess_soc	scalar	--	vehicles with ess	Soc of energy storage system
fc_trq_ out	vector	N*m	all(-fuel cell)	torque output achieved by the engine
fc_speed_ out_r	vector	N*m	all(-fuel cell)	torque output requested of the engine

Appendix F. Heavy-Duty Hydraulic Hybrid Vehicle Model

A hydraulic hybrid powertrain is an alternative type of hybrid that has gained interest within the last decade. Hydraulic hybrids have the benefit of a very high power density and the ability to use many "off the shelf" hydraulic components. The drawback to this technology is that it has a much lower energy density when compared to an electric hybrid. Two of the main applications are refuse trucks and delivery trucks. Both of these applications exhibit duty cycles that involve a great deal of starting and stopping. However, this interest is not limited to HDVs. In January 2011, Chrysler and the EPA announced that a feasibility study would be conducted to evaluate the potential of a hydraulic hybrid system for a large passenger car or LDV.

The following sections describe the basic structure of hydraulics hybrids and the development of the model. Section F.1 is a brief overview of the structure of typical hydraulic hybrids, followed by two sections describing the hydraulic components (Section F.2) and their models (Section F.3) in detail. Section F.4 discusses the development of the controller for the two hybrid systems. Section F.6 provides a discussion of the simulation results for the two hybrid drivetrains.

F.1. Hydraulic Hybrid Technology

Just as with an electric hybrid, the hydraulic hybrid is available in several configurations. The two configurations that have seen the most interest are the parallel and the series hydraulic hybrid configurations.

The hydraulic parallel configuration typically differs from that of the electric hybrids that are commercially available in how the two powertrains are joined together. The typical heavy-duty electric hybrid places the motor/generator between the engine and transmission while the hydraulic hybrid ties the two powertrains together through a transfer case between the transmission and differential. The transfer case also contains a clutch to enable the pump/motor to be disengaged at higher speeds. This configuration is illustrated in Figure F.1.

The hydraulic series configuration is much like the electric hybrid series configuration. There is a pump mounted directly to the engine which is connected to a high pressure accumulator and hydraulic motor. This configuration is illustrated in Figure F.2.

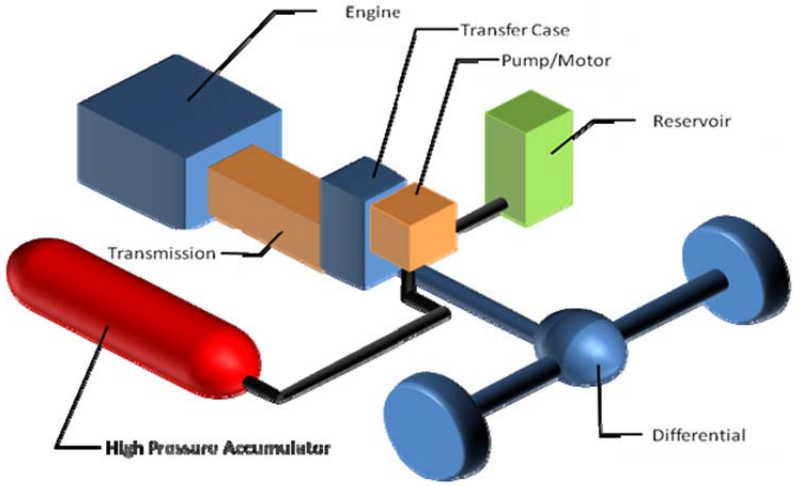

Figure F.1. Basic representation of typical hydraulic parallel hybrid.

Figure F.1. Basic representation of typical hydraulic parallel hybrid.

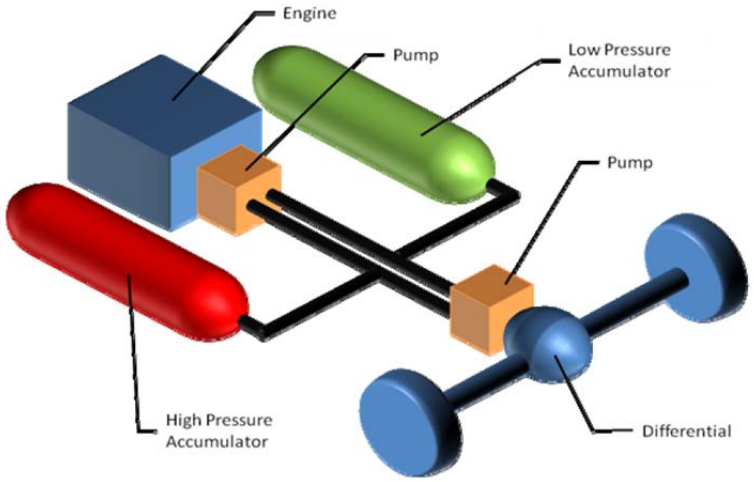

Figure F.2. Basic representation of typical series hydraulic hybrid.

F.2. Hydraulic Energy Storage

The hydraulic component used to store energy is an accumulator. Accumulators offer a very high power density over batteries and typically do not use materials that are expensive or pose a severe environmental risk. Most accumulators use compressed nitrogen to store energy. Because of this, most accumulators must be serviced as the nitrogen charge is lost slowly over time (US EPA, 2010). The disadvantages are that they are large, can be heavy, the compressed fluid can be dangerous, the energy density is much lower than batteries, and certain types of hydraulic fluid can pose an environmental risk if spilled (Eaton, 2006). Figure F.3 is an example of a bladder-type accumulator.

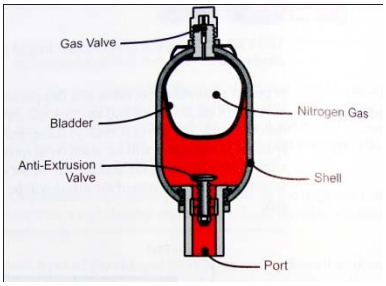

Figure F.3. Cross-section of bladder-type accumulator with anti-extrusion valve to protect bladder (Eaton, 2006).

To model this component the gas expansion and compression was assumed to be isentropic. This results in the following equation (Karnopp, et al., 2006) where P_{acc} is the pressure exerted by the compressed gas in the accumulator. P_{chg} is the precharge of the nitrogen gas contained in the accumulator. V_{acc} is the total volume of the accumulator, and V_{oil} is the volume of oil that has been pumped into the accumulator (Equation F.1).

$$P_{acc} = P_{chg} \times \left(\frac{V_{acc}}{V_{acc} - V_{oil}} \right)^{\gamma} \quad \text{(F.1)}$$

In the UT CTR Fuel Economy model, the volume of the accumulator assumed for the parallel hybrid was 25 gallons. This was done to closely match the Eaton Hydraulic Launch Assist system that is commercially available. The precharge was estimated to be 1585 psi (109 bar) based on information from the Eaton service manual (Eaton, 2011). The specific heat ratio of nitrogen gas was assumed to be 1.4 (Cengel, 2001). With these assumptions, Figure F.4 was generated showing the accumulator pressure as a function of oil volume that it contains. It should be noted that the accumulator only reaches an oil volume about 1/2 of the total volume before the maximum system pressure of 5000 psi is reached.

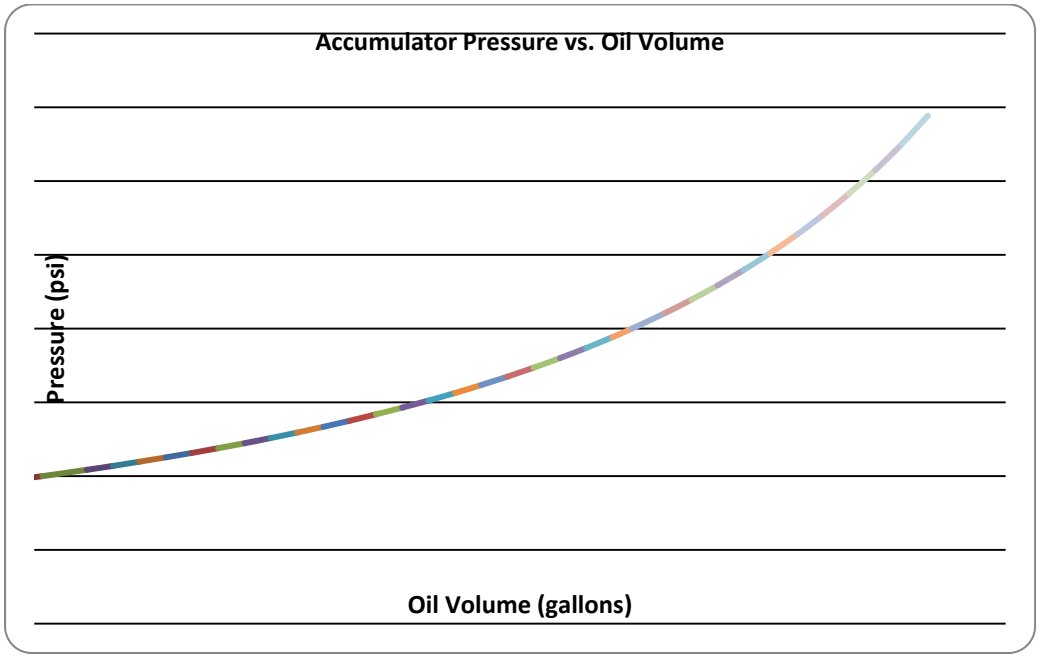

Figure F.4. Accumulator pressure as a function of oil volume for a 25-gallon accumulator with a precharge of 1585 psi.

F.3. Hydraulic Energy Conversion

A hydraulic pump or motor is used for the conversion between fluid energy storage and rotational mechanical energy. There are several common types of hydraulic pumps and motors that exist. These include gear, vane, and piston pumps. However, piston pumps are the primary type of pump that is used in hydraulic hybrids because of their high efficiency, high pressure capability, and their commonly available with a variable displacement.

Two types of piston pumps are commonly used in hydraulic hybrids. These two types are a “bent axis” piston pump, shown in Figure F.5, and the “axial” piston pump shown in Figure F.6. The axial piston pump is used in systems available from Eaton and Bosch Rexroth, while the bent axis type pump has been extensively used in research conducted by the EPA.

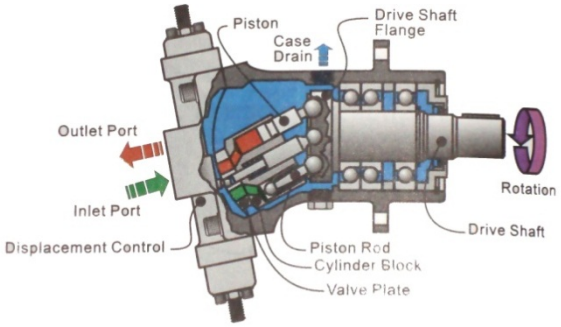

Figure F.5. Basic variable displacement bent axis piston pump design (Eaton, 2006).

Within each of these pump designs are many interfaces that cause losses through either friction or leakage that decrease the efficiency of the pump. While there is a great deal of information available for modeling the various aspects of these pumps, it would very difficult to tie all of them into a model to accurately predict pump performance.

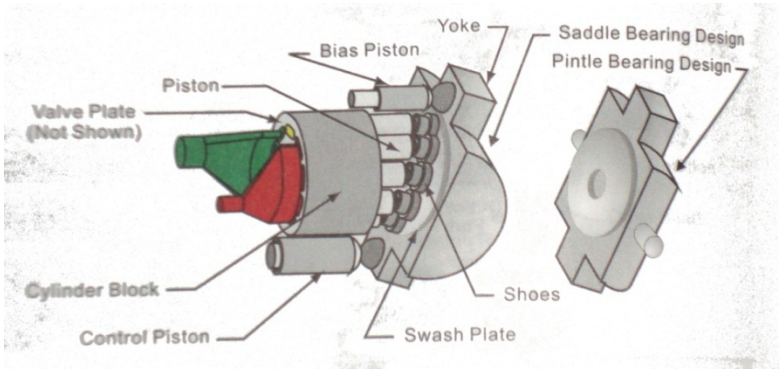

Figure F.6. Basic variable displacement axial piston pump design (Eaton, 2006).

Because of the complexity, another method was chosen to predict pump efficiency where the losses within the pump are accounted for at the system level. However, this model still attempts to recognize that the behavior of these losses may change with speed, pressure, and displacement. This model was originally presented in 1946 (Wilson, 1946). Since then others have sought improve the model, and it has recently been used by others to model hydraulic hybrid systems (Wilson and Lemme, 1968; Pourmovahed et al., 1992; Wu et al., 2004; Shan, 2009).

Because of the way in which the volumetric and mechanical efficiencies are calculated for pump motors, two separate sets of equations were created to effectively predict their values: Equations F.2 through F.3 and Equations F.4 through F.7. These equations are shown below.

Pump Efficiencies

$$\eta_v = 1 - \frac{C_s}{|x|S} - \frac{\Delta P}{\beta} - \frac{C_{st}}{|x|\sigma} \tag{F.2}$$

$$\eta_m = \frac{1}{1 + \frac{C_v S}{|x|} + \frac{C_f}{|x|} + C_h x^2 \sigma^2} \tag{F.3}$$

Motor Efficiencies

$$\eta_v = \frac{1}{1 + \frac{C_s}{xS} + \frac{\Delta p}{\beta} + \frac{C_{st}}{x\sigma}} \tag{F.4}$$

$$\eta_m = 1 - \frac{C_v S}{x} - \frac{C_f}{x} - C_h x^2 \sigma^2 \tag{F.5}$$

$$S = \frac{\mu \omega}{\Delta p} \tag{F.6}$$

$$\sigma = \frac{\omega \sqrt[3]{D}}{\sqrt{\frac{2\Delta p}{\rho}}} \tag{F.7}$$

With Equations F.2–F.7 and the values presented in Table F.1, the efficiencies for the pump were predicted at 2000 and 5000 psi for a wide range of displacement and speed. These efficiency maps are presented in Figure F.7.

Table F.1. Table of Parameters Used for Modeling of Pump/Motor Efficiencies (Shan, 2009).

Variable	Parameter	Value
Beta	Bulk Modulus (MPa)	1660
mu	Dynamic Viscocity (N-s/m^2)	0.034
rho	Fluid Density (kg/m^3)	850
Cs	Laminar Leakage Coefficient	2.63E-09
Cst	Turbulent Leakage Coefficient	1.33E-07
Cv	Viscous Loss Coefficient	1.20E-04
Cf	Friction Loss Coefficient	1.01E-02
Ch	Hydrodynamic Coefficient	1.98E+01
S	Dimensionless number	
Sigma	Dimensionless number	
omega	Pump Speed (rad/s)	
D	Maximum Pump Displacement (m^3/rad)	
x	Percent of Maximum Displacement	

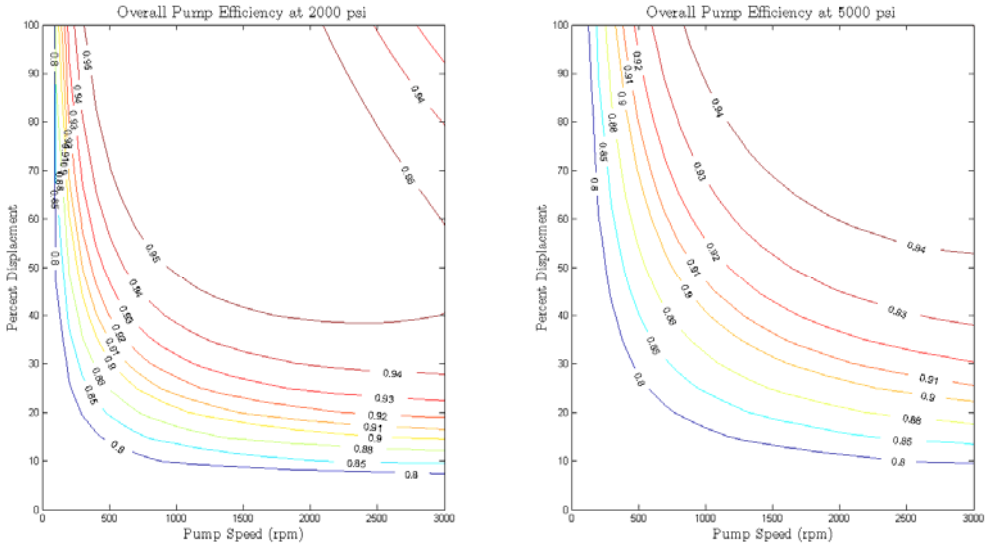

Figure F.7. Estimated pump efficiency as a function of pressure, speed, and percent displacement.

F.4. Power Management Controller

The power management controller is the portion of the system that determines how much power is supplied by the hydraulic system and the engine. There are many alternatives available to determine how the system functions. These alternatives fit into two main categories that are "Rule Based" and "Optimization Based" strategies (Desai and Williamson, 2009).

Rule based strategies typically involve "if-then" type logic. The two methods mentioned in Appendix E are both rule based strategies. While these strategies do yield good results they typically optimize the operation of the system for that instant in time (Lin et al., 2003b).

Optimization based strategies seek to optimize the system operation with respect to the time horizon. Two methods that have been used are deterministic and stochastic dynamic programming (Lin et al., 2003b; 2004). Both of these strategies have yielded good results, but they are more difficult to develop and are more computationally intense. The drawback to the deterministic dynamic programming method is that a surface must be fit to the resulting data to derive a control law. However, the stochastic dynamic programming strategy eliminates this step. Therefore, this method was chosen because of its consideration for time and its direct calculation of an implementable control law.

F.4.1. Controller Development

The stochastic control strategy that was chosen seeks to optimize the control strategy of the vehicle based on the most statistically probable future operation of the vehicle. The use of this information attempts to account for future behavior of the driver.

The first step is to model the driver behavior as series of power demand/wheel speed combinations. A Markov chain is used to model this behavior. A Markov chain is represented by a square matrix that contains the probability of the transitions from the current state to the next state. This matrix is referred to as a transition probability matrix. Because of the nature of the data, all rows must sum to 1 and all elements must be positive. Figure F.8 is a hypothetical

transition probability matrix for daily temperature. The Markov chain has two discrete states that are "Hot" and "Cold." The labels for the rows on the side represent the current temperature today, and the labels on the top represent the potential states for tomorrow. Based on the data presented below there is a 90% chance that it will be hot tomorrow if it is hot today.

$$\begin{array}{c} \\ Hot \\ Cold \end{array} \begin{array}{c} \begin{array}{cc} Hot & Cold \end{array} \\ \begin{bmatrix} 0.90 & 0.10 \\ 0.15 & 0.85 \end{bmatrix} \end{array}$$

Figure F.8. Hypothetical transition probability matrix for daily temperature.

To generate the Markov chain to model the driver behavior, a basic model was created to represent the vehicle to estimate the power requirement while operating in a given drive cycle. Because the power requirement is what must be calculated, the vehicle model uses the vehicle acceleration as an input which then estimates the required torque at the rear wheel. Equation F.8 was used to calculate this torque. It includes the effective mass of the vehicle (m_{eff}), vehicle acceleration (a), aerodynamic drag (F_{drag}), and rolling resistance (F_{roll}) of the tires.

$$\tau_{wheel} = \frac{m_{eff} a + F_{drag} + F_{roll}}{R_{tire}} \tag{F.8}$$

Using Equation F.8, the power can then be calculated using the corresponding wheel speed. This data must then be further processed to create the transition probability matrix. The next step of the process is to discretize the values of power demand (P_{dem}) and wheel speed (ω_{wheel}). Then a set of states is generated by creating all possible power demand/wheel speed combinations. The simulation data was then placed into the corresponding state that matched it closest. When selecting the step size of the discretization it is important to select a small enough size to capture the detail of the data, but it is also important to keep it large enough to keep the size of the problem small enough to execute without exceeding the memory limit of the computer. The sequence of these states is then used to generate the transition probability matrix. For each transition from state to state the corresponding matrix element is incremented to document the occurrence. Then each row is summed to find the total number of occurrences in each state. Each element is then divided by the summation of its row to find the correct probabilities. The resulting probability matrix can be seen in Figure F.9. It should be noted that the states along the X and Y axes are simply labeled 0 to 500.

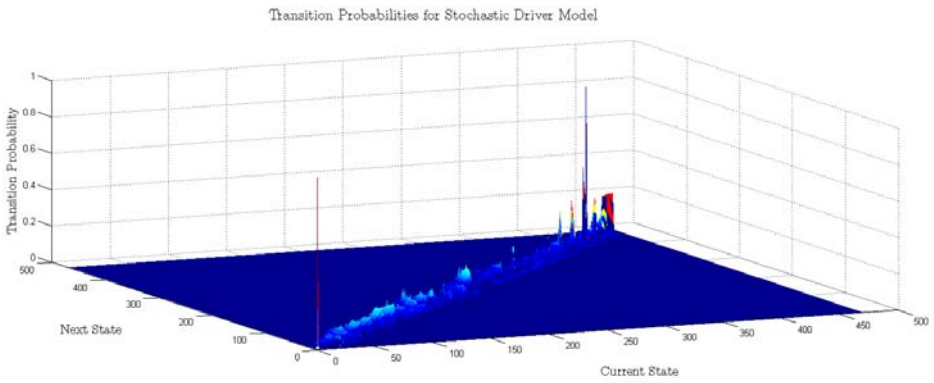

Figure F.9. Transition probability matrix for stochastic driver model represented as a surface.

The next step in the problem formulation is to add yet another state to the system. This additional state is the pressure of the accumulator, which is equivalent to the state of charge of the system in an electric hybrid. Because the driver behavior is not dependent on the state of the hydraulic system, it was assumed that the distribution of probabilities of power demand and wheel speed would remain constant based on this pressure. Therefore, the matrix generated in the previous step was repeated for each level of pressure. However, when the pressure is added to the state combination, the problem becomes more complex because the transition probability distributions are based on the control action taken by the vehicle controller in each given state. This aspect makes the problem a Markov Decision Process (Sutton and Barto, 1998).

The solution to this problem was found through an iterative process known as policy evaluation. There are several solution methods for this type of problem (Bertsekas, 1995; Sutton and Barto, 1998). Policy evaluation was chosen as the solution method because it was used in the literature to solve this problem previously for an electric hybrid (Lin et al., 2004). The next information that is needed is a set of possible control actions that the system can execute for each given state and an equation to determine the cost for each action and state is also needed.

The set of possible actions was created in a similar manner to the set of states by first discretizing the power split ratio (PSR). Each possible action consists of a combination PSR, transmission gear, and pump clutch state. With these control actions, vehicle states, and cost function, an optimal control policy can then be calculated. Figure F.10 displays a portion of the resulting policy. In addition to this surface are more data that correspond to various vehicle speeds.

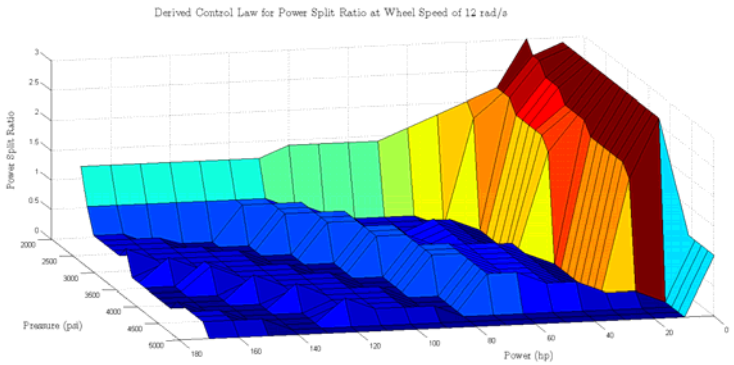

Figure F.10. Optimal control policy for power split ratio at a wheel speed of 12 rad/s.

In addition to the control laws that were developed with the prior calculation, some logic was also developed to handle various modes of operation. The two modes of operation were "with the pump engaged" and "with the pump disengaged." This was done to ensure that the pump would be disengaged above a vehicle speed threshold (25 mph in the present model) and avoid possible pump damage. Within these two modes of operation were positive and negative torque demands. During positive torque demands with the pump engaged the control laws developed in the prior steps are used. During periods of negative torque demand the controller must determine the correct split between the brakes and pump based on the maximum torque that the pump can produce.

A similar strategy was followed for the series hybrid. The difference was that the possible control actions were combinations of engine speed and torque. The state combinations that defined the vehicle were torque demand, vehicle speed, and the high pressure accumulator pressure. Other than these differences, the same process was followed. The torque demand was used rather than the power demand because of issues at a wheel speed of 0.

F.4.2. Accessory Loads

In addition to the required torque to drive the vehicle are the accessory loads. These loads can include but are not limited to a power steering pump, an air conditioning compressor, an air brake compressor, and a cooling (radiator) fan. The estimated power requirements for these loads were taken from SAE Specification J1343. This specification contains estimates for the power requirements of these types of loads under various applications. The values used for this model can be found in Table F.2. While most of these loads will be intermittent, they were considered to be on continually with the torque varying with engine speed to maintain a constant power.

Table F.2. Average Accessory Power Requirements for Local Haul Applications [18].

	Average Load (hp)
Air Brake Compressor	4.6
A/C Compressor	3.0
Engine Fan	4.0
Power Steering Pump	9.0

The model for the refuse truck included all of these loads, but the delivery truck did not. The loads for the air brake compressor and the air conditioning compressor were omitted because these trucks typically are not configured with these items.

F.5. Target Vehicles and Simulation Results

Two vehicles of interest were modeled as hydraulic hybrids based on current usage and testing that has been publicized. These vehicles are a refuse truck and a package delivery truck. The refuse truck was modeled as a parallel hybrid, and the delivery truck was modeled as a series hybrid. This selection was based on current usage.

F.5.1. Driver Model

The driver model used for this simulation was different from the model used for the other HDVs. The driver model used for the hydraulic hybrid simulations was a much simpler design based on a non-linear control. A feedback linearization was used in conjunction with a PI (proportional integral) controller. The feedback linearization utilizes nominal parameters from the vehicle to account for the nonlinearities of the vehicle model. The parameters needed to implement this controller were vehicle mass, frontal area, aerodynamic drag coefficient, and coefficient of rolling resistance. The derived control law in Equation F.9 is:

$$\text{u=control signal=}F_{mot} = \frac{F_{drag} + F_{roll} + m_{eff} a}{R_{tire}} \tag{F.9}$$

The use of the feedback linearization then allowed for classical linear control design procedures to be used (Slotine and Li, 1991).

F.5.2. Parallel Hydraulic Hybrid

The base vehicle chosen for the refuse truck was a Peterbilt 320, as illustrated in Figure F.11. This vehicle is commercially available as a hydraulic hybrid and is frequently used as a refuse truck. Several other manufacturers offer trucks that are similar to this model.

*Figure F.*11. *Image of Peterbilt 320 hydraulic hybrid refuse truck (Peterbilt, 2010).*

Because the configuration and loading of this truck can vary greatly, the weight varies as well. The weight also varies a great deal depending on how much cargo the truck is carrying. The estimated curb weight for an empty refuse truck was estimated to be about 33,000 lb (15,000 kg). The hybrid system was assumed to add 1,350 lb (600 kg) to the weight of the vehicle. When

fully loaded the vehicle was estimated to weigh 60,000 lb (27,200 kg). The fully loaded vehicle weight was used for the present simulations to represent a worst case scenario.

The parallel hydraulic hybrid system requires an extra transfer case between the transmission and the differential to transmit power to and from the hydraulic system. This location is depicted in Figure F.4; a basic schematic of the transfer case is shown in Figure F.12.

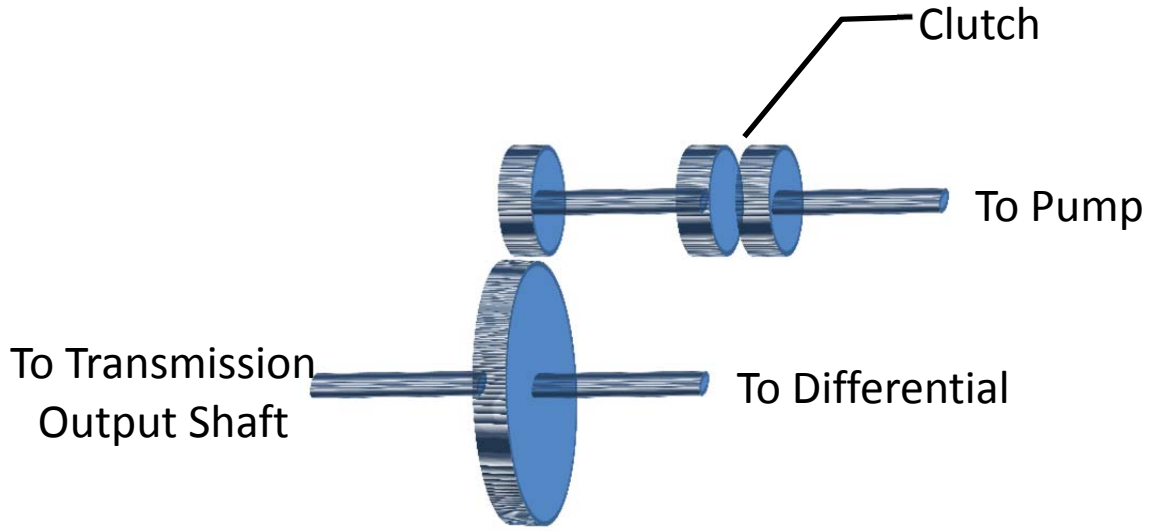

Figure F.12. Basic schematic of a transfer case to join a hydraulic pump and a conventional drivetrain.

There is not a great deal of information available on this extra transfer case. It is mentioned in the service manual that it contains a clutch that disengages the pump at 24 to 26 mph (Eaton, 2011a). However, little additional information is provided. Based on the information given, the gear ratio of the transfer case (r_{tc}) was estimated using Equation F.10. It should be noted that units of vehicle speed (V) should be in the correct units of ft/s or m/s which are compatible with the tire radius (R_{tire}), and the maximum pump speed ($\omega_{max\ pump}$) should be specified in radians per second. The last value required is the gear ratio of the differential (r_{diff}).

$$r_{tc} = \frac{R_{tire}\omega_{max\ pump}}{r_{diff}V} \tag{F.10}$$

It was decided that when accounting for the losses through this component, that only losses to and from the pump would be considered. Therefore the power from the engine that is transmitted to the rear axle is not reduced, but the energy that is transferred to the pump is reduced. The efficiency of the gear pair (η_{tc}) was assumed to be 95% (a more accurate model for this gear pair efficiency could be extracted from the model for the efficiency of a manual transmission). Equation F.11 was used to calculate the torque input to the differential ($\tau_{diff\ in}$).

$$\tau_{diff\ in} = \tau_{trans} + \tau_{pump} R_{tc} \eta_{tc}^{sgn(\tau_{pump}\omega_{pump})} \tag{F.11}$$

where "sgn($\tau_{pump}\omega_{pump}$)" is the "signum" of the product of the pump torque and its rotational frequency (sgn(A)=1.0 when A is positive and sgn(A)=-1.0 when A is negative). When the pump is acting as a motor (the pump torque is positive), it produces positive torque that adds to the torque from the transmission, increasing the torque input to the differential. When the pump is acting as a pump (the pump torque is negative), it uses some of the torque output from the transmission, thereby decreasing the torque delivered to the differential.

Because coastdown data was not available for this type of truck, parameters for aerodynamic drag and rolling resistance were estimated. The drag coefficient was assumed to be 0.8. This value was the upper limit specified by Wong (2008) for vans and buses. The coefficient of rolling resistance was calculated as a function of vehicle speed using the following correlation (Equation F.12) where vehicle speed is specified in kph Wong (2008):

$$f_{roll}=0.006+0.23\times10^{-6}V^2 \tag{F.12}$$

A major deviation from the production vehicle that was made in the model was the transmission type. To maintain consistency between the two hybrid models developed for this project, a similar method was used that assumes the transmission is essentially an automated manual. The production vehicle is actually available with either a manual transmission or a torque converter type automatic transmission. Therefore, the gear ratios used were for an Eaton 10 speed, UltraShift transmission (Eaton, 2011b), which is an automated manual.

Many other specifications were used for modeling the parallel hydraulic hybrid refuse truck, as shown in Table F.3. The constant values for the transmission and differential efficiencies were used only for the initial development of the model but were later replaced with the transmission and differential submodels discussed in Appendices B and C.

Table F.3. Parameters Used for Modeling a Parallel Hydraulic Hybrid Refuse Truck.

Parameter	Value
Height (in)	150
Weight (in)	90
Tire Diameter (in)	40
Differential Gear Ratio	5.714
Transmission Gear Ratios (Eaton 2011b)	12.8, 9.25, 6.76, 4.90, 3.58, 2.61, 1.89, 1.38, 1.00, 0.73
Transmission Efficiency	95%
Differential Efficiency	95%
Accumulator Precharge (psi)	1985
Accumulator Volume (gallons)	25
Pump Displacement (in^3/rev)	10.98
Maximum Pump Speed (rpm)	3000
Transfer Case Ratio	2.76
Transfer Case Efficiency	95%

The parallel hydraulic hybrid refuse truck was evaluated through several standard driving cycles:

- New York Truck Cycle
- Central Business District Cycle
- Orange County Bus Cycle
- Heavy Duty Urban Dynamometer Driving Schedule
- West Virginia University City Cycle

As would be expected, the hybrid system exhibited a range of fuel economies over the various driving cycles. The results of the simulations are provided in Table F.4. The driving cycles that had less idling and more frequent stops yielded the best fuel economy for the hybrid system. A control strategy that turned the engine off when not needed for propulsion ("start/stop") could help. to improve the fuel economy further.

Table F.4. Estimated Fuel Economy of a Parallel Hydraulic Hybrid Refuse Truck.

	New York Truck Cycle	Heavy Duty Urban Dynamometer Driving Schedule	Orange County Bus Cycle	West Virginia University City Cycle	Central Business District Cycle
Conventional (mpg)	3.06	6.29	4.53	3.77	4.68
Hybrid (mpg)	3.38	6.71	5.22	4.16	5.91
Improvement	9%	6%	13%	9%	21%

F.5.3. Series Hydraulic Hybrid

The series hybrid has been tested by UPS on actual routes and is shown in Figure F.13. A basic representation of this hybrid architecture can be seen in Figure F.2. This type of vehicle is commonly used in many delivery applications and has seen much interest for various types of hybrids because of the characteristics of its operation.

Figure F.13. Image of a series hydraulic hybrid being evaluated by UPS (Barry, 2008).

The specifications for this type of vehicle have a great deal of variation due to the way in which they are manufactured. Typically, the chassis is purchased from a truck manufacturer and a different company constructs and installs the body. Because of this variation, specifications from a study conducted by the NREL and UPS were used (Lammert, 2009). These base values are in Table F.5 and were used for sizing of the other components for the hybrid system.

Table F.5. Basic Parameters for Step Van Used as a Basis for Series Hybrid (Lammert, (2009).

Parameter	Value
Vehicle Weight	17,500 lb
GVWR	23,500 lb
Engine	VT275
Transmission	Allison automatic

To begin the design process, a pump was selected for the engine to drive. In the literature (Kim and Filipi, 2007; Shan, 2009), the displacement of the pump was selected to enable the pump to absorb the entire power of the engine even when the pressure of the system was at a very low threshold or 1000 to 1500 psi. This leads to the selection of a very large pump which may have a limited speed capability. The chart shown in Figure F.14 depicts the relation between pump displacement and maximum speed for a series of Eaton bent axis piston pumps. Because of this aspect of the pump behavior, the selection of the pump was a tradeoff between the maximum speed and the displacement.

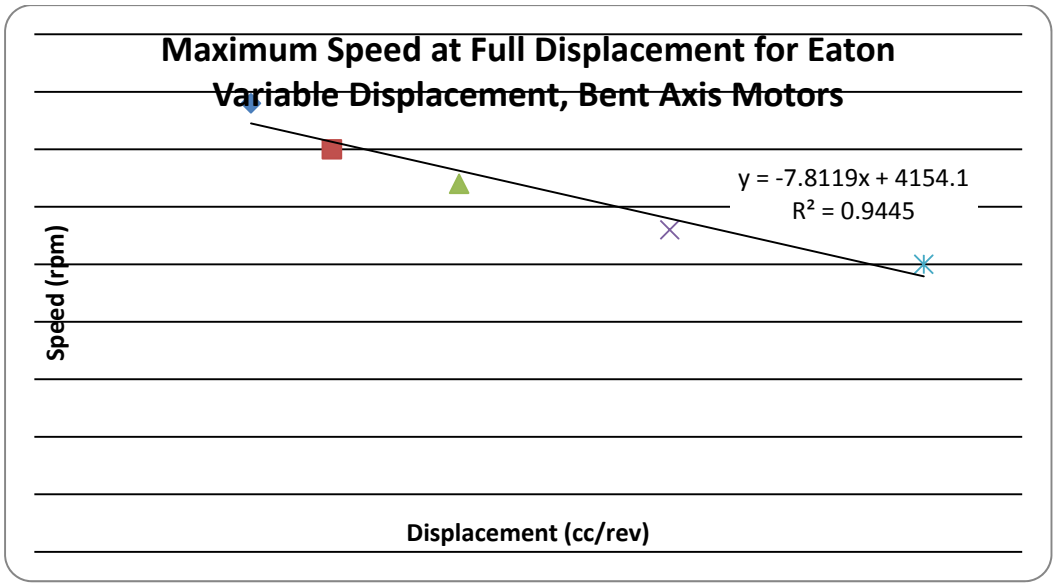

Figure F.14. Relationship between maximum operating speed and pump displacement for Eaton bent-axis hydraulic motors.

The final pump selected was a bent axis piston pump, which had a displacement of 160 cc/rev (9.76 in^3/rev). This specific size was one mentioned in the EPA report as an initial selection for another design. It was assumed that the maximum speed of the pump would be rated close to the 130 cc/rev pump. The efficiency maps presented in Appendix F of a 2004 Report published by the EPA on advanced technology were also assumed to be valid (Alson et al., 2004). Choosing two smaller pumps in tandem with a through shaft was not an option because of the bent axis design. The design of the selected pump is shown in Figure F.15.

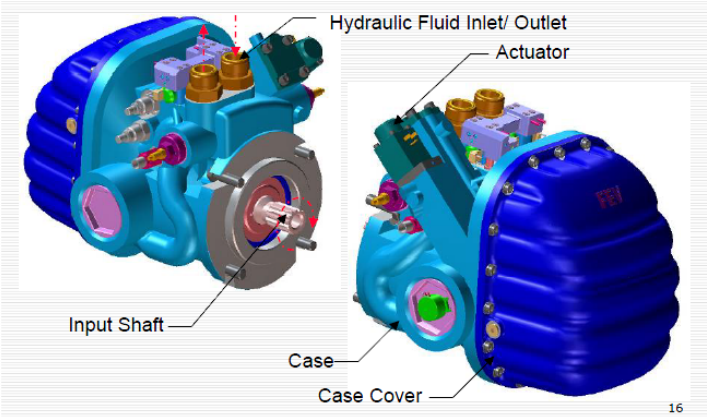

Figure F.15. Image of the EPA Gen 2 bent axis pump/motor (Gray, 2006).

A similar tradeoff was faced when selecting an appropriately sized motor to drive the vehicle. However, in this case the selection of two pumps was possible. The method discussed in U.S. Patent 7374005 allows for the mounting of two opposing pumps to cancel loads on bearings to increase the overall efficiency of the system as shown in Figure F.16. This also allowed for the selection of two smaller pumps capable of operating at higher sustained speeds than a single

large pump. The UPS hybrid constructed by the EPA used this method of pump mounting (Gray, 2006). The final displacement selected was 110 cc/rev (6.71 in^3/rev) for both pumps.

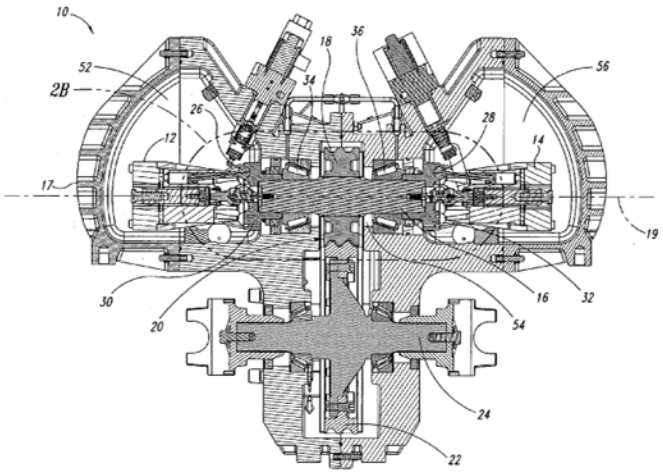

Figure F.16. Opposing pump/motor mounting mentioned in U.S. Patent 7374005 (Gray, 2008).

When selecting a differential gear ratio, the maximum speed of the pump was used to ensure that the vehicle could reach highway speeds. The efficiency of the pump was also considered so that it would be able to operate at highway speeds efficiently. While studying the efficiency map of the pump, it was noted that the efficiency begins to drop past 3500 rpm. This pump speed was then set to occur at 70 mph which yields a differential gear ratio of 4.61 assuming a tire radius of 15.5 inches. Because this may not be a standard ratio, a stand ratio of 4.63 was selected from the Dana catalog (Dana Corp. 2007).

The last hydraulic components that must be sized for the vehicle are the hydraulic accumulators. Little information was found on how these accumulators were sized, but a size range of 34–54 gallons was mentioned in a presentation given by the EPA (Gray, 2006). The size specified for the model was 50 gallons for the high pressure accumulator and 50 gallons for the low pressure accumulator. A special design of the pump allows for the usage of a low pressure accumulator charged to about 70 psi. The EPA bent axis pumps are specially designed to withstand case pressures of up to 200 psi, eliminating the need for a case drain to a low pressure reservoir (Also et al., 2004).

The same drive cycles used for the refuse truck were used to simulate the delivery trucks. However, a conventional truck was not simulated for comparison because chassis dyno test data was available for a subset of these cycles for comparison for both a conventional truck and a parallel electric hybrid. Those test results are compared to the present predictions for a series hydraulic hybrid (Table F.6). There is some variance between the performance of the actual electric hybrid and the simulated hydraulic hybrid. A portion of this can be attributed to the engine on/off ("stop/start") operation that was not incorporated in the hydraulic hybrid's simulated control system. This still does not fully account for the performance of the hydraulic hybrid on the WVU City cycle. It should also be noted that the test weight of the NREL trucks was 17,500 lb while the simulated truck was 23,000 lb. This was done to eliminate any bias that may be present from the heavier hydraulic system.

Table F.6. Estimated Fuel Economy of a Series Hydraulic Hybrid Delivery Truck Compared to Experimental Data for a Conventional Truck and a Parallel Electric Hybrid.

	New York Truck Cycle	Heavy Duty Urban Dynamometer Driving Schedule	Orange County Bus Cycle	West Virginia University City Cycle	Central Business District Cycle
Conventional truck (mpg)				6.87	6.83
Parallel electric hybrid (mpg)				9.38	9.16
Series hydraulic hybrid (mpg)	6.06	14.90	9.13	6.73	9.39

F.6. Future Work

Several potential sources of error and more detail could be added to this model for a heavy-duty hydraulic hybrid truck:

1. The current parallel model does not include the power requirements to run the secondary functions of the garbage truck. Specifications for the pump installed on many garbage trucks were gear pumps capable of 42 gpm @ 2500 rpm. The pressure rating of these pumps was 2500 psi. At full pressure this pump would have a power requirement of at least 61 hp. This pump is typically mounted directly to the engine and cannot be disengaged. When not being used, this pump would still require some amount of power depending on the standby pressure of the system. Defining the duty cycle and loads presented by the system could add more detail for the refuse truck application. However, the omission of this load does not destroy the validity of the model in general, but this should be considered when evaluating a refuse truck.
2. The brake wear was not considered for this model. In previous studies it has been found that the reduction in brake wear can be a large cost savings. The city of Denver estimates that it costs $2,000 to service the brakes on a refuse truck, and they conduct this service about every 3 to 4 months Eaton (2009).
3. Losses within the hydraulic system through valves and hoses were not accounted for. This additional piece of information would reduce the fuel savings by the hybrid system if it were included, but the degree to which this would occur is unknown. To add this into the system, assumptions would need to be made about hose lengths, hose sizes, and valve sizes. However, valves and other components are sized to reduce the losses when designing the hydraulic system.
4. A more detailed accumulator model could also add to the accuracy of the model. The current model does account for the heat transfer between the nitrogen, ambient air, and hydraulic fluid.

5. Configuring the parallel model with a 6 speed automatic transmission with a torque converter would also be beneficial to investigate. This configuration is very common among refuse trucks.
6. A key factor in the performance of the hybrid vehicle is the quality of the control strategy. Improvements could be made to allow for the engine to be turned off and on during operation. This would improve the fuel economy of the vehicle where there are large amounts of idling.

References

AAA (2011) Your Driving Costs—How much are you really paying to drive? Available at http://www.aaaexchange.com/Assets/Files/201145734460.DrivingCosts2011.pdf

Alson, J., D. Barba, J. Bryson, M. Doorlag, D. Haugen, J. Kargul, J. McDonald, K. Newman, L. Platte, and M. Wolcott (2004), *Progress Report on Clean and Efficient Automotive Technologies Under Development at EPA: Interim Technical Report*. APA Report No. EPA420-R-04-002.

American Transportation Research Institute (ATRI), An Analysis of the Operational Costs of Trucking: A 2011 Update. Prepared by the American Transportation Research Institute, June 2011.

Anderson, N.E., and S.H. Loewenthal (1980), "Spur-gear-system efficiency at part and full load," NASA Technical Paper 1622.

Barry, K. (2008), "UPS to roll out hydraulic hybrids." *Conde Nast Digital*, 28-Oct-2008.

Bennett, S., and I.A. Norman (2011), *Heavy Duty Truck Systems*, Fifth Edition, Delmar Cengage Learning, Clifton Park, NY

Bertsekas, D.P. (1995), *Dynamic Programming and Optimal Control*. Athena Scientific.

Buckingham, E. (1949), *Analytical Mechanics of Gears*, 1st edition, McGraw-Hill, pp. 395-406

Capps, Gary, Oscar Franzese, Bill Knee, M.B. Lascurain, and Pedro Otaduy. Class-8 Heavy Truck Duty Cycle Project Final Report, ORNL/TM-2008/122, Oak Ridge National Laboratory, Oak Ridge, TN, December 2008.

Cengel, Y. (2001), Selected Material from Fundamentals of Thermal-Fluid Sciences. McGraw-Hill Primis Custom Publishing.

Dana Corporation (2007), "Spicer® Single Reduction Single Axles," specification brochure.

Dawson, P. (1984), "Windage loss in larger high speed gears," *Proc. Inst. Mech. Eng.*, 198A(1):51-59.

Dawson, P. (1988), "High speed gear windage," *GEC Review*, 4(3):164-167.

Desai, C., and S.S. Williamson (2009), "Comparative study of hybrid electric vehicle control strategies for improved drivetrain efficiency analysis," in the proceedings of the *2009 IEEE Electrical Power & Energy Conference (EPEC)*, pp. 1-6.

Diab, Y., F. Ville, P. Velex, and C. Changenet (2004), "Windage losses in high speed gears – preliminary experimental and theoretical results." *ASME Journal of Mechanical Design*,**126**:903-908.

Eaton (2006), *Mobile Hydraulics Manual*, 2nd ed., Eaton Hydraulics Training, Eaton Corporation, Eden Prairie, MN.

Eaton (2009), "Success Story: City of Denver Colorado." Apr.

Eaton (2011a), "Service Manual: Eaton Hydraulic Launch Assist (HLA)." Eaton Corporation, Eden Prairie, MN.

Eaton (2011b), "UltraShift LST," 2011. [Online]. Available at: http://www.roadranger.com/Roadranger/productssolutions/transmissions/UltraShiftLST/index.htm. [Accessed: 10-Aug-2011].

Fox, R.W., A.T. McDonald, and P.J. Pritchard (2006). *Introduction to Fluid Dynamics*, 6th edition, John Wiley & Sons.

Gray Jr., C. (2006), "Hydraulic Hybrids: EPA Hybrid Truck Initiative," presentation to HARC, 17-Oct-2006.

Gray Jr., C.L. (2008), "Opposing pump/motors," U.S. Patent 7374005.

Greenbaum, J.J., M.A. Kluger, and B.E. Westmoreland (1994), "Manual transmission efficiency trends and characteristics," SAE Paper 942274.

Hibbeler, R.C. (2006), *Engineering Mechanics: Dynamics*, 11th Edition, Prentice Hall.

Höhn, B., K. Michaelis, and A. Wimmer (2007), "Low Loss Gears," *Gear Technology*, June.

HSH® Associates, Financial Publishers, http://www.hsh.com/autosample.html retrieved July 24, 2011.

Ivanič, Ž. (2007), "Data collection and development of New York City Refuse Truck Duty Cycle," SAE Paper 2007-01-4118.

Karnopp, D.C., D.L. Margolis, and R.C. Rosenberg (2006), *System Dynamics: Modeling and Simulation of Mechatronic Systems*, 4th ed., Wiley.

Khonsari, M.M., and E.R. Booser (2008), Applied Tribology: Bearing Design and Lubrication, 2nd ed., John Wiley and Sons.

Kim, Y.J., and Z. Filipi (2007), "Simulation study of a series hydraulic hybrid propulsion system for a light truck," SAE Paper 2007-01-4151.

Kluger, M., and J. Greenbaum (1993), "Automatic transmission efficiency characteristics and gearbox torque loss data regression technique," SAE Paper 930907.

Kluger, M.A., J.J. Greenbaum, and D.R. Mairet (1995), "Proposed efficiency guidelines for manual transmissions for the year 2000," SAE Paper 950892.

Kluger, M.A., D.R. Fussner, and B. Roethler (1996), "A performance comparison of various automatic transmission pumping systems," SAE Paper 960424.

Krstich, A.M. (1987), "Determination of the general equation of the gear efficiency of planetary gear trains," International Journal of Vehicle Design, 8(3):365-374.

Kuromachi, K., K. Shindo, S. Kubo, and M. Miura (1984), "Toyota new four-speed automatic transmission for front wheel drive vehicles," SAE Paper 840049.

Lammert, M. (2009), *Twelve-Month Evaluation of UPS Diesel Hybrid Electric Delivery Vans*. National Renewable Energy Laboratory, Technical Report NREL/TP-540-44134.

Lin, C-C., H. Peng, J.W. Grizzle, J. Liu, and M. Busdiecker (2003). "Control system development for an advanced-technology medium-duty hybrid electric truck," SAE Paper 2003-01-3369.

Lin, C-C., H. Peng, J.W. Grizzle, and J.-M. Kang (2003b), "Power management strategy for a parallel hybrid electric truck," *IEEE Transactions on Control Systems Technology*, **11**(6):839- 849.

Lin, C-C., H. Peng, and J.W. Grizzle (2004), "A stochastic control strategy for hybrid electric vehicles," *Proceedings of the 2004 American Control Conference,*, **5**:4710-4715.

Matthews, R.D. (2011), *Internal Combustion Engines and Automotive Engineering*, draft textbook, to be published by SAE International.

Merritt, H.E. (1946), *Gears*, Sir Isaac Pitman & Sons, pp.238-246

Meuller, H.K., and B.S. Nau (1998), *Fluid Sealing Technology: Principles and Applications*, pp. 73-94 and 101-110, Marcel Dekker, Inc., New York.

Nam, E.K., and R. Giannelli (2005), "Fuel consumption modeling of conventional and advanced technology vehicles in the Physical Emission Rate Estimator (PERE)," EPA draft report EPA420-P-05-001, February.

Naunheimer, H., B. Bertsche, J. Ryborz, and W. Novak (2010), *Automotive Transmissions: Fundamentals, Selection, Design and Application*, 2nd edition, Springer.

National Association of Insurance Commissioners (NAIC) (2007), taken from CompuQuoutes.com. Available at http://www.compuquotes.com/average-costs-of-insurance.html

Niemann, G., and H. Winter (1983), *Mascinelemente*, Bd. 2, pp.220, 276-278, Springer

Numazawa, A., F. Ushijima, K. Fukumura, T. Ishihara (1983), "An experimental analysis of fluid flow in a torque converter," SAE Paper 830571.

Nunney, M.J, (2010), *Light and Heavy Vehicle Technology*, 4th edition, Butterworth-Heinemann.

Park, D.H., T.S. Seo, D.G. Lim, and H.B. Choi (1996), "Theoretical investigation on automatic transmission efficiency," SAE Paper 960426.

Peterbilt Motors Company (2010), "Peterbilt Green Technologies." http://www-cert.peterbilt.com/eco/ReadyTrucks-HeavyDutyHybrids.htm

Petrushov, V.A. (1997), "Coast down method in time-distance variables," SAE Paper 970408.

Petrushov, V.A. (1998), "Improvement in vehicle aerodynamic drag and rolling resistance determination from coast-down tests," *Proceedings of the Institution of Mechanical Engineers*, **212**(D):369-380.

Petrushov, V.A. (2009), "Coast down method in time and distance variables for tire rolling resistance determination," SAE Paper 2009-01-0072.

Pourmovahed, A., N.H. Beachley, and F.J. Fronczak (1992), "Modeling of a hydraulic energy regeneration system: Part I—analytical treatment," *Journal of dynamic systems, measurement, and control*, **114**:155.

Reineman, M., and R. Nash (1995), "EPA/industry dynamometer comparison study: nine vehicle fleet," a report by from the US EPA National Vehicle and Fuel Emissions Laboratory for the Dynamometer Comparison Study Task Force, available at: http://www.epa.gov/nscep/index.html

SAE International (2000), "Information Relating to Duty Cycles and Average Power Requirements of Truck and Bus Engine Accessories," SAE Standard J1343.

Shan, M. (2009), "Modeling and control strategy for series hydraulic hybrid vehicles," PhD Dissertation, Dept. of Electrical Engineering, The University of Toledo.

Slotine, J.J.E., and W. Li (1991), Applied Nonlinear Control, Prentice Hall, 1991.

Steidel, R.F., V. Castelli, J.W. Murdock, and L. Meirovitch (1996), "Mechanics of Solids and Fluids," Chapter 3 in Mark's Standard Handbook for Mechanical Engineers, 10th Edition, E.A. Avalonne, and T. Baumeister III (editors), McGraw Hill.

Sutton, R.S., and A.G. Barto (1998), Reinforcement Learning: An Introduction. The MIT Press.

Townsend, D.P. (1991), Dudley's Gear Handbook, Second Edition, McGraw-Hill.

U.S. Environmental Protection Agency, Detailed Test Information. Available at http://www.fueleconomy.gov/feg/fe_test_schedules.shtml. Accessed July 2011.

U.S. Department of Energy, Transportation Energy Data Book, 30th Edition. Chapter 8. Available at http://cta.ornl.gov/data/tedb30/Edition30_Chapter08.pdf

van Dongen, L.A. (1982), "Efficiency Characteristics of Manual and Automatic Passenger Car Transaxles," SAE Paper 820741.

Walther, C. (1933), "Kennzeichnung der Schmieröle durch die Viskositäts-Pol-Höhe", *Proc. World Petroleum Congress* **2**:419-421.

Welter, D., M. Ates, L. Loftus-Otway, R. Matthews, R. Harrison (2009), *Estimating Texas Motor Vehicle Operating Costs*, Texas Department of Transportation Report No. 5974-1, FHWA/TX-11/0-5974-1, The University of Texas at Austin, Center for Transportation Research.

West, B.H., R.N. McGill, J.W. Hodgson, S.S. Sluder, D.E. Smith, Development and Verification of Light-Duty Modal Emissions and Fuel Consumption Values for Traffic Models, Washington, DC, April 1997, and additional project data, April 1998.

Wilson, W. E. (1946), "Rotary-pump theory," *Trans. ASME*, **68**(4):371–384.

Wilson, W.E., and C.D. Lemme (1968), "The hydromechanical transmission—ideal and real," SAE Paper 680605.

Wipke, K., M. Cuddy, D. Bharathan, S. Burch, V. Johnson, A. Markel, and S. Sprik (1999), "Advisor 2.0: a second generation advanced vehicle simulator for systems analysis," NREL Technical Report NREL/TP-540-25928; National Renewable Energy Laboratory, last modified: April 30, 2002 [version 2002].

Wu, B., C.C. Lin, Z. Filipi, H. Peng, and D. Assanis (2004), "Optimal power management for a hydraulic hybrid delivery truck," *Vehicle System Dynamics*, **42**(1-2):23–40.

Yada, T., "Review of Gear Pair Efficiency Equation and Force Treatment," *JSME International Journal*, 1997, Series C., Vol. 40, No.1

Zaabar, I., and K. Chatti (2010), "Calibration of HDM-4 models for Estimating the Effect of Pavement Roughness on Fuel Consumptions for US Conditions," *Transportation Research Record: Journal of the Transportation Research Board. No. 2155,* Washington D.C., 2010, pp. 105-116.